MSc Thesis Report

Design a complete active heave system based on an existing concept

Daniel Yang Nielsen

TU Delft
Delft University of Technology

JUMBO

Faculty of Mechanical, Maritime, and Materials Engineering

Design a complete active heave system based on an existing concept

by

Daniel Yang Nielsen

Student number: 4421957
Graduation date: 13th September 2016

in partial fulfillment of the requirements for the degree of

Master of Science
in Offshore and Dredging Engineering

at the Delft University of Technology

in cooperation with
Jumbo Maritime

Graduation committee

Graduation professor:	Prof. dr. A.V. Metrikine, TU Delft
Company daily supervisor:	Ir. K.T. van der Heiden, Jumbo Maritime
University daily supervisor:	Ir. A.J. Laguna, TU Delft
Member:	Dr. ir. K.N. van Dalen, TU Delft

Preface

I would first like to thank Jumbo Maritime for offering me the opportunity to carry out my thesis with them. I would like to thank my company supervisor Ir. K.T. van der Heiden from Jumbo Maritime and my daily supervisor Ir. A.J. Laguna from the Delft University of Technology for their advice and support. I would also like to thank Prof. dr. A. V. Metrikine for the guidance and the other members of my graduation committee for providing me with the opportunity to graduate. I would also like to thank my colleagues at Jumbo Maritime for supplying company information and the positive working environment. Finally, I am grateful to my family for their support during my studies.

Daniel Yang Nielsen

Abstract

Jumbo Maritime has worked in the offshore market where it has installed equipment using offshore cranes. The heave motion of the vessel results in relative motion between the payload and the crane-tip which limits the conditions the vessel can operate in. A passive heave compensation system has been used but clients desire an active heave compensation system to be used to award certain work to Jumbo. This project investigates a system that combines passive and active heave compensation systems to form a hybrid heave compensation system. The result is a numerical time-domain model of a hybrid heave compensation system coupled with an existing vessel model.

The problem investigated is introduced. The design operating conditions are significant wave height of 2.5m, peak period of 8s, beam waves, and a water depth of 2500m. The crane can take a maximum of 900t static load and a maximum of 650t dynamic load. Using the model of the coupled system the main research question to answer is: How important is the change in natural period from when the active heave compensation system is disabled to when the active heave compensation is enabled on resonance?

The methodology is discussed. The starting point is three concepts for an active heave compensation system from Jumbo Maritime. The concepts are evaluated and a concept chosen. This project uses a numerical approach to the investigation. A numerical crane-tip motion model is derived. The passive heave compensation system is designed and put into a numerical model and the natural frequencies determined. The frequency and time responses of the system are analyzed to verify the natural frequencies. The crane-tip model is combined with the passive heave compensation system to see the performance of the system in the design sea-state and other sea-states. This is coupled with an existing vessel model to see the effect of the coupling. The active heave compensation system is designed and combined with the passive heave compensation system, crane-tip model, and vessel model. This forms the final model which is assessed on performance and the main research question mentioned in the second paragraph is answered. Furthermore, a sensitivity study is done to see the effect of considering the Dyneema rope as a continuous structural element with coupled axial and transverse motion. Previously the Dyneema rope was discretized as a discrete mass with springs. The continuous model of the Dyneema rope takes into account the damping and added mass from water at the large water depths considered, such as 2500m.

The main results are summarized. The passive heave compensation system by itself is effective in the design operating conditions with rms reduction ratio of 0.137 (closer to zero is better), compensation rate of 83% (closer to 100% is better), and significant double amplitude of 0.38m (closer to zero is better). Coupling this system with the vessel model produces no remarkable behavior. The performance is essentially the same with a 2.2%, 1.7%, 9.5% difference in the rms reduction ratio, compensation rate and significant double amplitude respectively. The inclusion of the active system results in worse performance than either the passive system by itself or coupled with the vessel. The reason for this is that the controller design is done in a relatively simple manner. To achieve better performance more advanced control design is needed. To answer the main research question mentioned in the second paragraph, activating the AHCS does not lead to a change in natural period that influences the resonance behavior. What is found is that the controller design is a key part of any adverse effects when using the active part. Additionally, from the sensitivity study of the continuous Dyneema rope the main effect is that the motions of the hook/payload are reduced.

The main contribution of the project is a numerical time-domain model of a hybrid heave compensation system coupled with a crane-tip and vessel model. An additional model is the passive heave compensation system using a continuous Dyneema rope model instead of a discrete Dyneema rope model.

Contents

List of Acronyms **vi**

1 Introduction **1**
1.1 Problem description . . . 1
1.2 Research objective . . . 3
1.3 Research questions . . . 3
1.4 Structure of report . . . 4

2 Literature review **5**
2.1 Introduction . . . 5
2.2 Background . . . 5
2.3 State-of-the-art . . . 10
2.4 Conclusion . . . 15

3 Design requirements and approach **16**
3.1 Introduction . . . 16
3.2 Design requirements . . . 16
3.3 Methodology . . . 18
3.4 Existing concepts . . . 19
3.5 Multi-criteria analysis . . . 21
3.6 Conclusion . . . 21

4 Vessel motion model **22**
4.1 Introduction . . . 22
4.2 Equations of motion . . . 22
4.3 Time domain . . . 23
4.4 Degrees of freedom . . . 24
4.5 Choice of domain . . . 24
4.6 Applying the equations of motion . . . 25
4.7 Conclusion . . . 27

5 Crane-tip motion model **28**
5.1 Introduction . . . 28
5.2 Degrees of freedom investigated . . . 28
5.3 Frequency of encounter . . . 29
5.4 Vertical motion, $z_P = h$ . . . 29

5.5 Applying the equations . . . 31
5.6 Conclusion . . . 32

6 Passive heave compensation cylinder **33**
6.1 Introduction . . . 33
6.2 Model . . . 33
6.3 Size the piston-head area . . . 37
6.4 Conclusion . . . 37

7 Passive heave compensation system **38**
7.1 Introduction . . . 38
7.2 PHCS design: one accumulator . . . 38
7.3 PHCS design: two accumulators . . . 40
7.4 Forces to consider when lifting . . . 41
7.5 PHCS equations of motion . . . 41
7.6 Cylinder and accumulator equations . . . 44
7.7 Pressure equations . . . 46
7.8 Solving the equations . . . 48
7.9 Various design iterations . . . 54
7.10 Adding fluid inertia . . . 56
7.11 Conclusion . . . 59

8 Sizing of pressure system **61**
8.1 Introduction . . . 61
8.2 Sizing of the pressure system . . . 61
8.3 Conclusion . . . 70

9 Natural frequencies of PHCS **71**
9.1 Introduction . . . 71
9.2 Natural frequencies of the LAM . . . 73
9.3 Natural frequencies of the RLAM . . . 74
9.4 Natural frequencies of the ORLAM . . . 75
9.5 Conclusion . . . 78

10 Frequency and time responses of PHCS **79**
10.1 Introduction . . . 79
10.2 Frequency response of pressures . . . 79
10.3 Time response of pressures . . . 80
10.4 Frequency response of hook/payload motion . . . 82
10.5 Time response of hook/payload motion . . . 83
10.6 Verifying Simulink results . . . 85
10.7 Conclusion . . . 85

11 Performance of the PHCS **87**
11.1 Introduction . . . 87
11.2 Number of wave frequency components . . . 87
11.3 Parameters of performance . . . 89
11.4 Obtaining results . . . 90
11.5 Results irregular and regular input: various periods and wave heights . . . 91
11.6 Results irregular and regular input: natural periods and Hs/H=2.5m . . . 106
11.7 Time domain results . . . 111
11.8 Conclusion . . . 118

12 C-PHCS **119**
12.1 Introduction . . . 119
12.2 Time-domain results . . . 119
12.3 Conclusion . . . 123

13 C-HHCS **124**
13.1 Introduction . . . 124
13.2 Research question . . . 124
13.3 AHC design . . . 125
13.4 Equations of motion . . . 129
13.5 PI controller, open-loop model . . . 134
13.6 HHCS equations . . . 135
13.7 Non-linear HHCS state-space equations . . . 135
13.8 Linear HHCS state-space equations . . . 135
13.9 Response . . . 135
13.10Conclusion . . . 143

14 Sensitivity study: continuous rope model **144**
14.1 Introduction . . . 144
14.2 Steel rope versus Dyneema rope . . . 144
14.3 String . . . 144
14.4 Rod . . . 145
14.5 Coupling terms . . . 146
14.6 Boundary conditions . . . 147
14.7 Initial conditions . . . 148
14.8 Solution . . . 148
14.9 Results . . . 150
14.10Conclusion . . . 151

15 Conclusion **152**
15.1 Summary . . . 152
15.2 Results . . . 153
15.3 Discussion . . . 154
15.4 Recommendations . . . 155
15.5 Contributions . . . 155

List of Figures **156**

List of Tables **159**

References **160**

A Appendices **166**
A.1 Euler-Lagrange method . . . 167
A.2 Derivation of equation (7.36) . . . 169
A.3 Derivation of linearized state-space equations . . . 171
A.4 Throttle . . . 179
A.5 Throttle again . . . 182
A.6 Bottom accumulator . . . 184
A.7 Upper accumulator . . . 186
A.8 Non-linear equations . . . 188
A.9 Non-linear state-space equations . . . 189
A.10 Non-linear state-space equations simplified . . . 191
A.11 Linearized state-space equations . . . 194

A.12 Resulting linear state-space equations . . . 198
A.13 Equations of motion for the LAM . . . 203
A.14 Working out upper/lower case initial conditions for section 8.2 . . . 205
A.15 Natural frequencies, the RLAM . . . 210
A.16 Upper/lower case for the ORLAM . . . 214
A.17 Frequency response of pressures, upper/lower case initial conditions . . . 216
A.18 Time response of pressures, upper/lower case initial conditions . . . 218
A.19 Frequency response of hook/payload motion, upper/lower case initial conditions . . . 219
A.20 Time response of hook/payload motion, upper/lower case initial conditions . . . 221
A.21 HHCS equations . . . 224
A.22 Non-linear HHCS state-space equations . . . 225
A.23 Linear HHCS state-space equations . . . 228
A.24 Verifying Simulink results with MATLAB results . . . 238

List of Acronyms

- **AHC** Active Heave Compensation
- **AHCS** Active Heave Compensation System(s)
- **HCS** Heave Compensation System(s)
- **HHC** Hybrid Heave Compensation
- **HHCS** Hybrid Heave Compensation System(s)
- **PHC** Passive Heave Compensation
- **PHCS** Passive Heave Compensation System(s)

1 Introduction

1.1 Problem description

The handling of payloads by cranes at sea poses numerous logistical and technical challenges. One of the key technical challenges is the constant movement of the vessel due to the hydrodynamic forces exerted by the waves. The resulting heave, pitch, and roll of the vessel results in significant crane-tip motion that needs to be reduced for safe handling of the payload. One way to do this is through heave compensation. Active heave compensation (AHC) and passive heave compensation (PHC) can be distinguished. AHC refers to a system that uses energy external to the system to compensate heave motion. PHC refers to a system that uses only the energy within the system to compensate heave motion. A system that combines AHC and PHC is known as a hybrid heave compensation (HHC) system.

The relevance of the work at an industry level is that the work is being performed for a commercial company, Jumbo Maritime, who would like more information on using an AHC system on their existing vessels. Jumbo Maritime would like to use an active heave compensation system (AHCS) on the 900t cranes on their J-type vessels. The compensation requirements are compensation for 2.5m of heave within 8 seconds. Potential clients of Jumbo Maritime desire an AHC system to be used otherwise they will not award certain work to Jumbo Maritime. Jumbo Maritime has used PHC systems in the past and found them to be good enough for most applications such as seabed landing. There are many companies that are already using AHC systems on their cranes. For example, Big Lift, a competitor of Jumbo Maritime, has an AHC system on their Happy-D type vessels [1]. Bourbon Subsea Services has at least 22 AHC systems for offshore cranes varying from 10t to 250t [2]. Other shipping companies with AHC systems for offshore cranes in their fleet include:

Ceona Offshore	Deep Ocean	EMAS AMC	Ensco	Fincantieri Offshore
Fugro-tsm	Harkand	Island Offshore	Kreuz Subsea	McDermott
Oceaneering	Saipem	Subsea 7	Tasik Subsea	Zafiro Marine

Furthermore, there are many equipment suppliers highlighting AHC systems for offshore cranes as important and they are developing innovations in this application. Some 40 examples of companies that supply AHC systems for offshore crane/winch applications are:

AHC Cranes	Allied Marine Crane
Axtech	Bargemaster
Bosch Rexroth	Bourbon Subsea Services
Cargotec	EMS Energy
Favelle Favco	GustoMSC
Heila Cranes	Huisman Equipment
Hydramarine	IHC Hytop
IHC Motion Control and Automation	International Offshore Equipments
Jebsen and Jessen Offshore	Karmoy Winch
Lidan Marine	Liebherr
Macgregor	Melcal Marine
National Oilwell Varco	Norwegian Deck Machinery
Optilift	Palfinger
Pellegrini Marine Equipments	Preferred Marine
Promac	Raoul Engineering
Rapp Marine	Rolls-Royce
Scantrol	SIM Crane Singapore
SMI Offshore	Sormec
Technical and Maritime Services	TTS
Ulstein Equipment	West Marine

Many of the companies listed above also produce a passive heave compensation system (PHCS). Specialist suppliers of PHC systems are:

Cranemaster	Innovative Input

Considering the large number of suppliers of AHC systems as well as the number of shipping/offshore companies with AHC systems for cranes it is clear that having an AHC system for cranes is an important competitive advantage.

Since August 2014 Jumbo Maritime has investigated adapting an AHC system to its cranes. This investigation included concepts for purely active heave compensation systems and hybrid heave compensation systems. Jumbo Maritime worked with Bosch Rexroth, the world leader in active heave compensation systems, to develop eight concepts. The main requirements for the concepts were that they are efficient, compact, state-of-the-art, and provide compensation for 2.5m of heave within 8 seconds. Following this, work was done by Jumbo Maritime to narrow the concepts down to those that fit Jumbo Maritime's requirements better. This means the starting point of this investigation is three concepts. From these three concepts one will be chosen that fits the design criteria set for this project.

The relevance of this work at an academic level is that the project investigates a design for a hybrid heave compensation system and develops a detailed design from this. The hybrid heave compensation system is assembled from passive and active heave compensation systems. The design is implemented in a time-domain numerical model. This numerical model is coupled to an existing vessel motion numerical model. The result is a coupled dynamical model of a heavy lift monohull vessel with a deep-water hybrid heave compensation system. The coupled dynamical model is implemented in a commercial software package. The software used is Simulink. Simulink provides a block diagram environment for multi-domain simulation and model-based design. The reason to use Simulink is that the existing vessel motion model given as a starting point for the thesis was made in Simulink. Simulink is integrated with MATLAB, a numerical computing environment. Within MATLAB the post-processing of the model simulation results is done. The research objective is given in section 1.2 and the research questions are given in section 1.3.

1.2 Research objective

Based on the issues described in the section above, the main research objective is given as:

The main research objective is to make a design of a modular and removable deep-water hybrid heave compensation system for an offshore crane installed on a monohull heavy lift vessel. This is accomplished by identifying and then assessing designs of heave compensation systems and selecting a design. The hybrid heave compensation system is modelled as a numerical time-domain model.

To achieved the main research objective several sub-objectives are defined.

- The selected hybrid heave compensation system design is composed of active and passive systems. The passive system is analyzed and the heave reduction performance is assessed.
- An existing numerical time-domain model of a monohull heavy lift vessel is coupled to the passive system. This coupled model is assessed to determine the performance of the passive system coupled with the vessel.
- The active system is combined with the passive system (to form the hybrid system) and the vessel. This coupled model is assessed to determine the performance of the hybrid system coupled with the vessel.
- An investigation is made about the effect of the hybrid system relative to the passive system, to see the effect of activating the active system.

1.3 Research questions

The main research objective and sub-objectives were given in section 1.2. Research questions are written to achieve the main research objective and sub-objectives. These research questions are used to guide the modelling and analysis of the hybrid heave compensation system and are not answered explicitly. These research questions are used to come to the hybrid heave compensation system combined with the vessel model to form the coupled dynamical model of the vessel and the hybrid heave compensation system. This constitutes the main achievement of the project. With this model, a further question to answer is:

How important is the change in natural period from when the active heave compensation system is disabled to when the active heave compensation is enabled on resonance?

This is based on work by Mannigel from Subsea 7 [3] which claimed activating the AHC system resulted in auto-excitation of the vessel and load. This is further explained in section 13.2.

1. The 'basic concept' is the selected design for the hybrid heave compensation system. What level of detail in the model of the 'basic concept' is required?
   (a) How detailed are existing models?
   (b) What physical coupling is there between the hook and the active heave compensation system?
2. What methods of analysis should be used to analyze the model of the 'basic concept'?
   (a) What are applicable methods of analysis?
3. To what extent does the model of the 'basic concept' satisfy the criteria of performance?
   (a) What are the criteria of performance used to measure the performance of AHC systems?
   (b) How does the model perform using the criteria of performance?

(c) What tests can be done on the model to derive data that is assessed by the criteria of performance?

4. To what extent do the assumptions behind the model of the 'basic concept' affect the accuracy of the model?

   (a) What assumptions are made in creating the model of the 'basic concept'?

1.4 Structure of report

An overview of the structure of the report is given:

- In chapter 1, the introduction to the report is given.
- In chapter 2, the literature review is given.
- In chapter 3, the design requirements and approach of the thesis are given.
- In chapter 4, the existing numerical time-domain vessel motion model of a monohull heavy lift vessel is described.
- In chapter 5, the crane-tip motion model is described.
- In chapter 6, the passive heave compensation system is introduced by discussing the principle of operation of the passive heave compensation cylinder.
- In chapter 7, the passive heave compensation system is developed.
- In chapter 8, more detailed design of the passive heave compensation system is done.
- In chapter 9, the passive heave compensation system is analyzed to obtain more insight into the system. This is done by investigating the natural frequencies of the passive heave compensation system.
- In chapter 10, the frequency and time responses of the passive heave compensation system are investigated.
- In chapter 11, the passive heave compensation system is combined with the crane-tip model and the performance is assessed.
- In chapter 12, the passive heave compensation system is coupled with the vessel model and the performance discussed.
- In chapter 13, the active heave compensation system is included to form the hybrid heave compensation system which is coupled to the vessel. The performance is discussed.
- In chapter 14, a sensitivity study is done to see the effect of using a continuous rope model which takes into account water damping and coupled axial/transverse motion of the rope, rather than the discrete mass model used in previous chapters.
- In chapter 15, the conclusion to the report is given.
- In chapter A, the appendices are given. The structure of the appendices is as follows. Each appendix is labelled as A followed with a number for example, A.1 is the first appendix. The other appendices follow in numerical order such as A.2, A.3, etc.

Literature review 2

2.1 Introduction

This literature review relies much on the review done by Woodacre et al. published in June 2015 [4]. The field of heave compensation on cranes has existed for decades. One of the first investigations into heave compensation was by Southerland [5] in 1970 who examined passive and active methods of heave motion compensation. Today, there are numerous existing systems that vary in payload capacity. For example, AHC systems by Bosch Rexroth have been specified for 5t to 40,000t systems [6]. From the 40 suppliers of active heave compensation systems found in the introduction it has been discovered that the most common type of system uses a winch.

This literature review will deal with passive heave compensation systems, active heave compensation systems, and some control theory related to active heave compensation systems.

The main aims of the review are to:

- Provide an overview of active heave compensation systems and passive heave compensation systems
- Review different methods for an active heave compensation system
- Review different methods to model the ropes and payload
- Review control theory

The rest of the review will start with some background information. Then a review of the literature on active heave compensation systems will be done. The reviewed literature will then be analyzed. Conclusions will then be made.

2.2 Background

2.2.1 Types of AHCS

Most heave compensation systems have been found to combine a passive and active heave compensation system. One approach, by IHC Hytop, is to use the passive part to balance the force due to the pressure of the hydraulic oil and nitrogen gas with the force of the payload [7]. The active part changes the position of the cylinder in response to the motion of the crane or vessel with these motions being measured by a motion reference unit (MRU) [7]. This enables the passive part to take most of the force and the active part takes a smaller part of the force. Since the active part handless less force it requires

less actuation power and so can be physically smaller than the passive part [4], a key advantage of this hybrid system on a ship where space is limited.

Various types of current AHC systems exist with the primary designs being primary controlled rotary AHC (hydraulic), secondary controlled rotary AHC (hydraulic), electric rotary AHC, and linear AHC (hydraulic/pneumatic) as defined by Bosch Rexroth [6]. These are elaborated upon below to show what is being commonly used today.

2.2.1.1 Rotary AHC (RAHC)

A rotary AHC system uses energy generated from the movement of the vessel to compensate for heave. When the vessel heaves upwards, the drive unwinds the rope and the drive is acting as a pump, storing energy. When the vessel then heaves downwards the drive pulls in the rope by acting as a motor, using the stored energy to partially power the system [8]. Two variations of this design, the primary and secondary RAHC systems, are elaborated on below.

2.2.1.2 Primary controlled rotary AHC

The primary controlled rotary AHC system works as follows. The motion reference unit (MRU) inputs a signal to the controller which then controls a hydraulic motor connected to a pump. The winch is powered by the pump to keep the load stationary [9]. The mechanics are that to rotate the winch drum the hydraulic pump builds pressure on one side of the winch drum which creates torque in one direction and rotation. When the controller requires the winch drum to rotate in the other direction the pump reduces pressure on one side and increases the pressure on the other side. The inherent lag in having the pump work against the hydraulic spring lowers the speed of response. This leads to the disadvantage that to rotate the winch drum by an arbitrary angle a fixed amount of flow is needed which requires over-dimensioning of the pumps if high speed at low load is desired [10]. See Figure 2.1 for a schematic of the primary control method. Advantages of this system [9]:

- The system is integrated fully into the winch requiring little space on deck.
- The system recovers energy either by returning it to the electric grid or storing the energy in capacitors or fly-wheels (Kinetic Energy Recovery System, KERS).
- The system can be integrated into already installed winches and cranes, enabling an expanded operating window at small cost and effort.

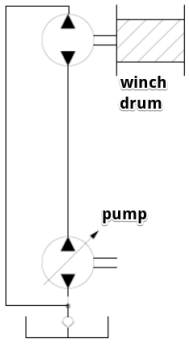

Figure 2.1: A schematic of the primary control method [10]

2.2.1.3 Secondary controlled rotary AHC

The secondary controlled rotary AHC system works as follows. The MRU inputs a signal to the controller which then controls a secondary regulated motor connected to the winch directly [6]. The motor is controlled using an actuator on the motor which controls the swash-plate angle of the motor [10]. The

swash-plate angle determines the direction of torque of the motor allowing the winch to be driven in two directions. This differs from the primary controlled system since the winch is controlled directly by the motor rather than by a pump. The key advantage of the secondary system is it responds very fast, has low power consumption [11], and is energy efficient since there is less movement of fluid and associated losses [10]. Since the motor is connected directly to the winch it is reasonable to say it is faster than the primary system where the motor is connected to a pump and the pump is connected to the winch. See Figure 2.2 for a schematic of the secondary control method. Other advantages of the secondary system [8]:

- Accurate
- High repeatability
- Possibility to store and recover energy
- Safe system
- High responsiveness
- Flexible operation
- Compact system so small deck footprint
- No extra operators required

A supplier, Bosch Rexroth, claims that its secondary-controlled drives are able to compensate for up to 95% percent of heave. The energy generated from the upward motion of the vessel is fed back into the hydraulic system with up to 70% of the energy being recovered [12].

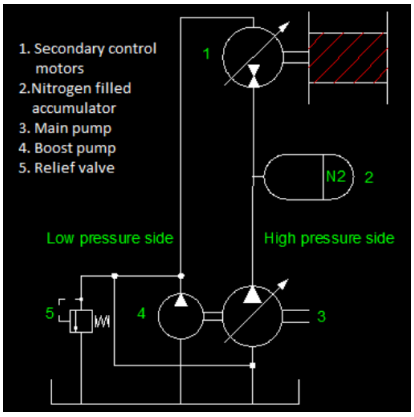

Figure 2.2: A schematic of the secondary control method [10]

2.2.1.4 Electric rotary AHC

The electric rotary AHC system works like the rotary AHC systems since it stores recovered energy and reuses the energy. The main difference is that the system uses electric motors. The hardware control interfaces are the same as for the hydraulic AHC systems [6]. This makes the use of electric and hydraulic systems in one company simple since some parts can be interchanged.

2.2.1.5 Linear AHC

A linear AHC system (LAHCS) differs from the rotary systems in the components and how the components are controlled. A linear system is such that the stroke of the cylinder sizes the winch rope length and therefore the load position [6]. The principle of operation of the LAHCS is that an MRU inputs a signal to the controller that controls a cylinder which combines active and passive compensation abilities.

The cylinder pays out wire when the vessel heaves up and hauls in wire then the vessel heaves down. The combination of passive and active compensation into one system lowers the required power. The average load is compensated by the passive part and the wave-induced load changes are compensated by the active part [13]. Bosch Rexroth claims a 90% compensation of heave motion. See Figure 2.3 for a schematic of the LAHCS method. Some advantages of the linear AHC system [13]:

- Reduced power consumption relative to alternative AHC controlled winches
- Accurate
- Easy integration into any existing winch system
- Modular option transported in containers enables use on multiple similar vessels
- The modular design enables flexibility on a vessel arrangement
- The LAHCS is based on a closed force loop which means it requires a simple mechanical interface to the vessel's structure

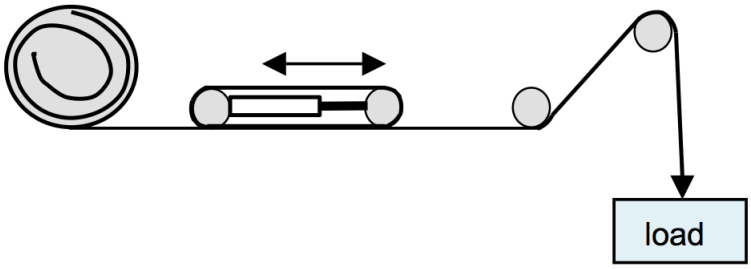

Figure 2.3: A schematic of the LAHCS [14]

2.2.2 Operating modes of active heave compensation systems

The operating mode of an AHCS is an important consideration to show the capabilities of an AHCS. In this thesis, the heave compensation mode is of most interest. This is because the seabed-landing phase of the lift is of most interest and the heave compensation mode is most relevant for this.

2.2.2.1 Constant tension

The constant tension (CT) mode is when the load in the wire is kept at a constant tension value so that any snap-load is reduced. The advantage of a reduced snap-load is less crane fatigue. The CT mode works for a supported or fixed load. This mode is usually available on any AHC system. Another use of the CT mode is that when a load is pulled from the seabed there may be suction which can cause the load to be stuck. The high tension in the wire would counteract this suction force. For example, the CT mode is used to counteract the weight of a mudmat. The tension will be adjusted as the mudmat is lifted from the seabed by paying in/out wire to maintain the reference load. Once the 'break' suction force is reached the mudmat will be lifted from the seabed and then the crane can switch to AHC mode. Without the CT mode, the wire tension would vary largely increasing the chance of exceeding the crane's safe working load (SWL) and generating a snap-load [2].

2.2.2.2 Heave compensation

In general, the purpose of this mode is to decouple the load's movement from the boom tip's movement. This is important for subsea operations to reduce the landing speed and lower re-bouncing effects. Similarly, when the load is lowered through the air and through the splash-zone the heave compensation mode is active. Heave compensation is also used in transfer lifts done entirely in air, for resonance avoidance during the lowering phase of a lift, and for subsea shock absorption due to overcoming the suction force when lifting objects off the seabed [15].

2.2.2.3 Other modes

Other modes are the empty hook mode, when there is no load attached to the crane and the mode where no heave compensation is used.

2.2.3 The cylinder-type PHCS

PHCS are relatively simple compared to AHCS. The working principle of the most commonly used PHCS design, the cylinder-type PHCS, is described since this type is used in the thesis.

The cylinder-type PHCS consists of a piston inside a cylinder attached to the payload, and the internal chamber of the cylinder is attached to an accumulator. The extension of the piston rod causes hydraulic fluid to flow through orifices which causes a floating piston to compress gas (usually nitrogen). This results in a spring-damper unit. The spring part comes from the compressed gas and the damping part comes from the restricted flow through the orifices. The hydraulic fluid in the cylinder is pushed through an orifice into the accumulator when the payload heaves. This results in damping by flowing through the orifice and storage of energy by compressing the nitrogen in the accumulator. The device operates as a low stiffness spring [16]. The spring and damping parameters are adapted to each lifting operation by specifying the hydraulic fluid volume and gas pressure [17]. This still allows relative motion but the load variations in the wires are reduced which keeps the load suspended in tolerable limits. PHC systems are useful to remove or significantly reduce the slamming forces and snap loads that can occur during the splash-zone crossing [18]. PHC systems require no power for operation. Main applications of PHC systems are subsea operations where the load is on the seabed and the drill string compensators in riser systems and dredging systems [16].

The passive heave compensation system of Cranemaster has been modeled by Nam et al. [19]. The system was modeled as a spring-damper system. This is too simplistic however since it does not take into account the gas pressure in the accumulator, which is an important parameter.

The main differences between AHC and PHC systems can be summarized as [16]:

- PHC systems use a spring principle whereas AHC systems use an MRU
- PHC systems are powerless whereas AHC systems require power

See Figure 2.4 for key differences between AHC and PHC systems.

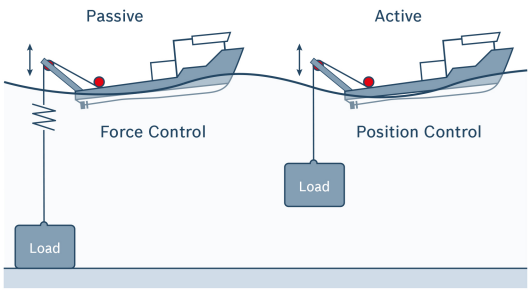

Figure 2.4: A diagram from Bosch Rexroth showing the key differences between PHC and AHC systems [16]

Generally, passive systems cannot deliver greater than 80% heave compensation. To get higher heave compensation an active or hybrid system should be used [4].

2.2.4 Hybrid system

A hybrid system includes an active and a passive system to form a hybrid heave compensation system (HHCS). A hybrid system is usually more efficient since it can have reduced power requirements compared to a purely active system [4]. In this thesis it is desired to use a HHCS system since this is more efficient and is commonly used by shipping companies today.

2.2.5 Electric system

Nearly all early active heave compensation systems were hydraulic powered, electric powered systems are becoming more popular due to their higher efficiency. According to Angelis [20], hydraulic drive winches have efficiencies of 45-70% and electric drive winches have efficiencies of 70-85%. The higher efficiencies are due to energy recovery through regenerative braking and winch efficiency. Challenges with electric systems are their high cost and greater difficulty to troubleshoot when not working. Other key advantages of an electric winch system over a hydraulic winch are [21]:

- Lower power consumption, for example a 400t, all-electrical driven AHC winch system has 7720kW power consumption whereas an equivalent electrical-hydraulic system has 9400kW.
- Takes less space, although a hydraulic motor has a higher power density than an electric motor the hydraulic motor needs an external hydraulic power unit whereas the electric motor just needs an electric cable for power. This hydraulic power unit is large which means the overall hydraulic system of a hydraulic motor and power unit takes more space than an electric system.
- Additionally, the hydraulic power unit is continuously running whereas an electric system is only running when needed, thus the electric system is more efficient.

2.3 State-of-the-art

2.3.1 Previous work on AHCS

Some articles on AHCS that are relevant to the thesis and are well-referenced within the literature are discussed. This is done to give an over-view of techniques that have been investigated for heave compensation systems (HCS).

2.3.1.1 AHCS on drill-ships

Actuated harmonic absorber (drillship): Korde [22]
An example of an AHC system for a drill-pipe system on a drill-ship is given by Korde [22]. Korde assumes small oscillations in environmental loads allowing the use of linear differential equations. Korde used the idea from Ogata [23] and Meirovitch [24] that if there is an undamped spring-mass system that is coupled with a second oscillating system excited by a sinusoidal external force then there is an excitation frequency where the second mass will remain stationary for any excitation magnitude. Korde used this type of behavior to stabilize an oscillator in a system of three coupled oscillators. Korde also used active control to enable this behavior over a range of excitation frequencies. The three oscillators consist of a spring-supported block M_c (to be kept stationary) from where the drill-pipe is driven, a drill-ship with mass M_s, and a third oscillator of undamped mass M_m. See Figure 2.5 for a schematic diagram of the system. The three masses are assumed to move in the vertical direction. Active control was applied to mass M_m such that mass M_c remains stationary over a large frequency range. The masses are coupled by mass M_m being spring-supported and controlled from M_c by a linear actuator. The drill-pipe is rotated from mass M_c and M_c is supported on spring-loaded vertical guides and is driven from the derrick by linear actuators. The damping on M_m should be minimized and the damping force on M_c can be non-zero. The input actuation is achieved using linear motors or hydraulic rams. Li and Liu [25] have also used a dynamic vibration absorber, similar in principle to Korde's system, to form an AHCS for the lift pipe of a deep-sea mining system. Li and Liu's system achieved a theoretical 84% reduction in heave motion.

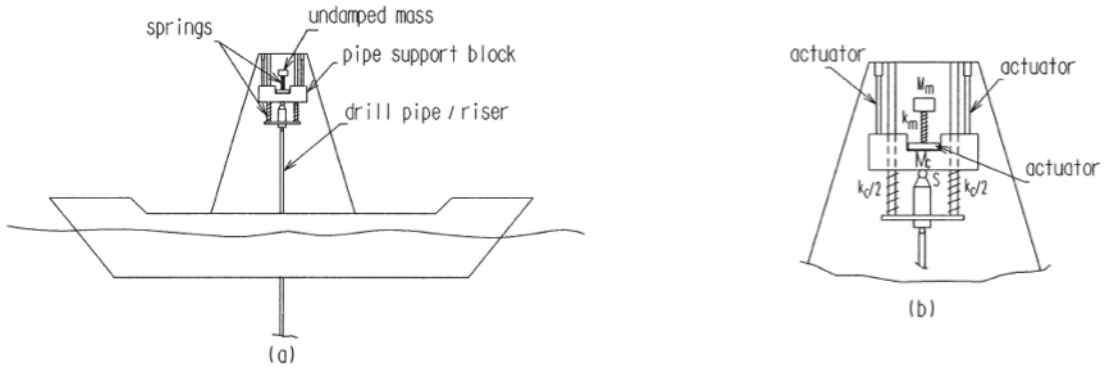

Figure 2.5: A diagram of the three coupled masses, for definitions of the variables see the paper by Korde [22]

Nonlinear controller double rod actuator (drillship): Do and Pan [26]
Another method for heave compensation on a drill-pipe was developed by Do and Pan [26] who designed a nonlinear controller for an AHCS that uses an electro-hydraulic system to drive a double rod actuator. Do and Pan have worked with AHC systems for drilling vessels. Do and Pan have stated that an AHCS is often used with a passive riser compensator to stabilize the crown block relative to the seabed. The system can keep the crown block position constant relative to the seabed within (0.1-0.5)m with vessel heave up to (4-5)m. See Figure 2.6 for a schematic of their system. A disturbance observer is included to estimate the force on the piston of the hydraulic system and the vessel's heave acceleration. The inclusion of the disturbance observer results in a high performance control system. Do and Pan used Lyapunov's direct method for the control development and stability analysis.

2.3.1.2 Splash-zone crossing

Feedforward control through wave synchronization: Johansen et al. [27]
Johansen et al. have investigated a AHCS for a crane during the water entry phase (splash-zone crossing) for a subsea installation [27]. The paper introduced the idea of wave synchronization where the purpose is to use a free surface elevation measurement to compensate directly for the water motion due to waves inside a moonpool. This means the system uses feedforward control to have wave-synchronized motion of the load through the splash-zone. This is achieved using feedforward with an estimate of the vessel's vertical velocity. The heave compensator makes the payload track a given trajectory in an Earth-fixed reference frame. The objective is to minimize variations in the hydrodynamic forces on the payload. Furthermore, this applies only during the water-entry phase, thus a blending factor is used to couple the wave synchronization and regular heave compensation. The experimental tests (in regular waves) show that this method can reduce the standard deviation of the wire tension up to 50%. In other words wave synchronization combined with heave compensation reduces the wire-tension variability. The system also reduced peak wire-tension. Effects from the vessels roll and pitch motion were neglected.

Feedforward control through wave synchronization: Skaare et al. [28]
Skaare and Egeland [29] discussed Johansen et al. [30] and Johansen et al. [27] as introducing the concept of wave synchronization where the load was lowered through the splash-zone with a constant speed relative to the waves in order to minimize the hydrodynamic forces on the load. This work was furthered by Skaare et al. [28] who have investigated wave synchronization obtained from feedforward control from a wave observer using measurements of the vessel and load accelerations and wire-tension, thus avoiding wave-amplitude measurements. One advantage is that there is less noise in the processed data since numerical differentiation of the wave amplitude to obtain the wave amplitude velocity is not required. The wave synchronization reduces hydrodynamic forces but the consequent inertial forces of the load give large oscillations in the wire-tension if the load is massive and wave large.

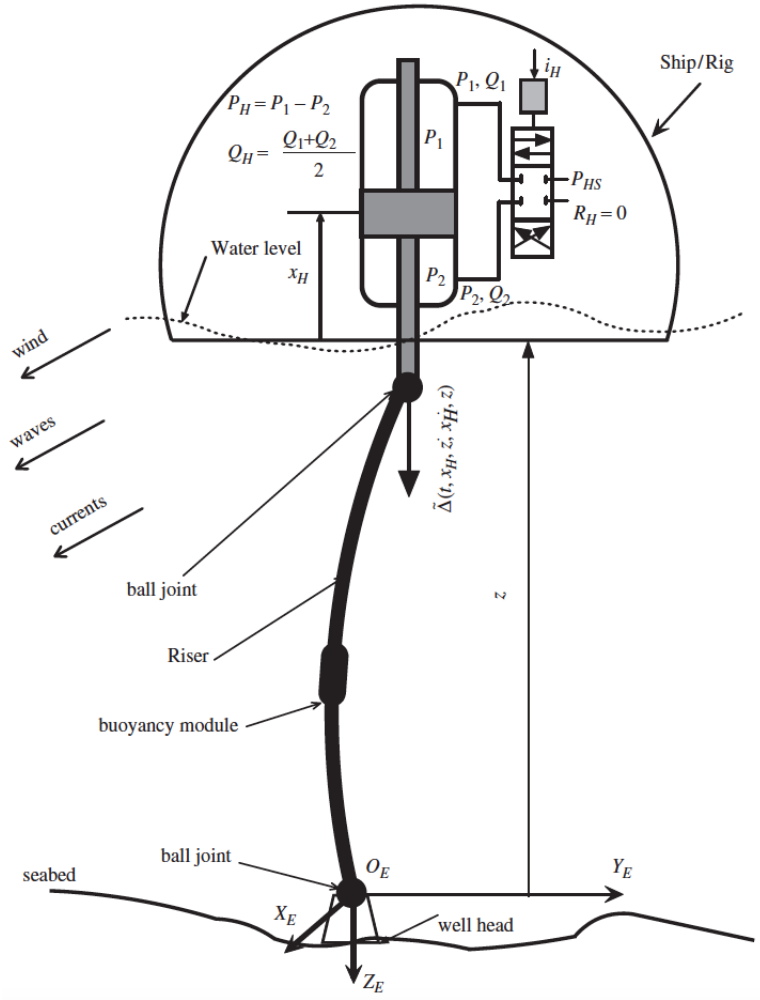

Figure 2.6: A schematic of an AHCS using an electro-hydraulic system being driven by a double rod actuator, for definitions of the variables see the paper by Do and Pan [26]

Parallel force/position controller: Skaare and Egeland [29]
Skaare and Egeland [29] discussed a parallel force/position controller for controlling loads through the splash-zone. The controller had a large improvement of the minimum value of the wire-tension compared to the wave synchronization approach used by Johansen et al. [27].

The method of force and position control is a well-developed field. The parallel force/position control of a load through the splash-zone has been investigated using a simulation study by Skaare and Egeland [31]. Skaare and Egeland [29] obtained results with a parallel force/position controller from model scale experiments of a crane vessel with a moonpool. Three control methods were used by Skaare and Egeland; parallel force/position control, AHC, and wave synchronization. The parallel force/position control method had the best average performance for wire tension and payload acceleration compared to the other methods tested of AHC and wave-synchronization. Improvements in the tests with regular waves ranged from 51% to 1061% which means the operational weather window is increased. Skaare and Egeland suggest the performance of the parallel force/position control method can be improved by combining it with a PHCS that shifts the resonance frequency of the wire away from the frequency area of the measurement noise. Skaare and Egeland have suggested to use position control instead of speed control in the wave-synchronization method since differentiation of the free surface elevation measurements is avoided. Combining the parallel force/position controller with an AHCS is simple since the wire tension measurement is usually available. Thus, it would seem best to use the parallel force/position control method.

Although the wave synchronization method provides good results, it is considered too complex by the author for this thesis.

Inertance control: Sagatun et al. [32]
Skaare and Egeland [29] have mentioned that an "augmented impedance control scheme denoted as inertance control was introduced for crane control of loads" through the splash-zone crossing by Sagatun et al. [32] and Sagatun [33]. Sagatun et al. [32] investigated a modified impedance controller with feedforward corrections and acceleration feed-back. The acceleration feed-back leads to a frequency dependent virtual mass which provides additional flexibility to the user in tuning the system performance.

These methods seem quite advanced and although provide good accuracy are considered too complex for this thesis.

2.3.2 Rope and payload

The situation considered for the payload is when the payload is in the water, close to the sea-bed and about to make the sea-bed landing. This means the forces on the payload when it is in the air are not considered.

2.3.2.1 Sawodny et al. [34]

Sawodny et al. [34] made a model for an AHCS that takes into account the time-delay between the winch acting and having an effect on the payload for very long rope lengths used in deep water. This delay is due to the finite speed of longitudinal pressure waves in ropes. Horizontal forces acting on the payload and rope due to current are neglected. The system is shown in Figure 2.7. The vertical motion of the payload is described by combining the rope and payload as a spring-mass-damper system. The forces acting on a payload submerged in water were given as the self-weight, hydrodynamic forces, and the rope force. The disadvantage of combining the payload and rope as a spring-mass-damper system is that is provides less flexibility in modelling the payload. Since this thesis aims to include a PHCS there needs to be flexibility in separating the rope and payload. Thus, this approach of combining the payload and rope will likely not be used.

The hydrodynamic forces for a product submerged in water or lowered through the wave zone may be written as the sum of forces from potential theory and viscous forces. The added mass term at infinite frequency was used. The added mass term can be determined as:

$$A_{33} = \rho_{\mathrm{w}} C_a \nabla \tag{2.1}$$

where C_a is the added mass coefficient and depends on the shape of the object, ρ_{w} is the density of water, and ∇ is the displaced volume. The rope is assumed to only transmit tension. The winch dynamics were approximated by a first order system.

2.3.2.2 Yuan [35]

Yuan [35] investigated an actively damped heave compensation control method. The relevant part to this thesis is the way used to model the rope-payload dynamics using a mass-less rope plus an equivalent spring where the equivalent spring coefficient $k(z_{\mathrm{l}})$ is:

$$k(z_{\mathrm{l}}) = \frac{z_{\mathrm{l}}}{E A_{\mathrm{c}}} \tag{2.2}$$

where E is the elastic modulus, A_{c} is the cross-sectional area of the rope, and z_1 is the length of the rope. This is similar to modeling the payload and rope as a pendulum. This is an effective model for a purely active heave compensation system since there is no other system, such as a passive HCS interacting with the payload. However, since this thesis will design a hybrid HCS it is preferred not to model the rope

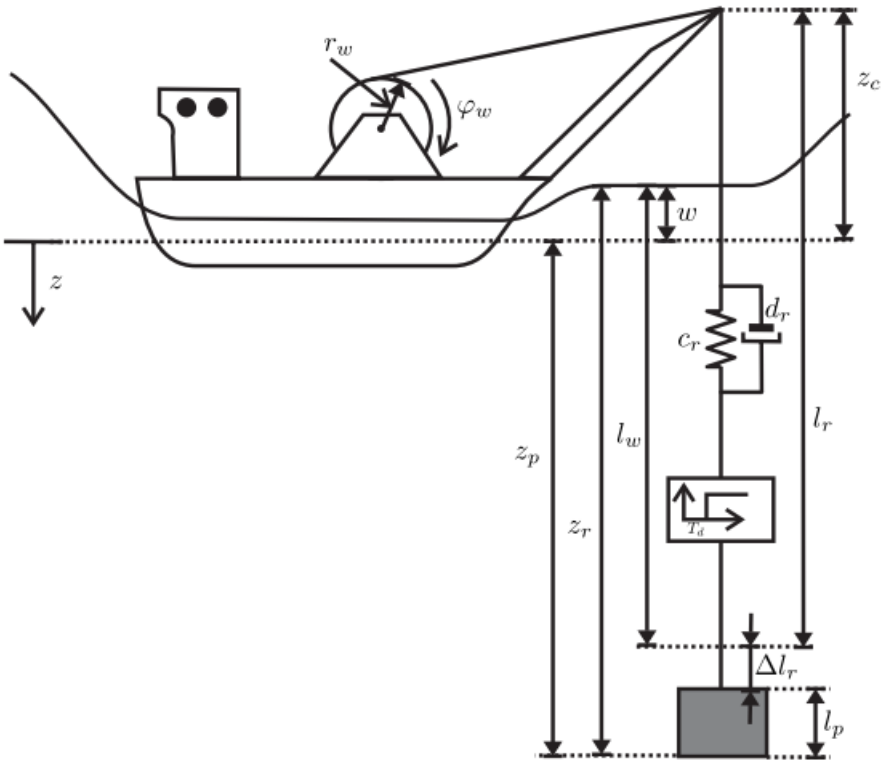

Figure 2.7: Crane model from Sawodny et al., for definitions of the variables see the paper by Sawodny et al. [34]

and payload in this way. The equation to model the rope in (2.2) is a reasonable relationship that is believed to capture the physics well, so it is used in this project.

2.3.2.3 Johansen et al. [27]

As mentioned earlier, Johansen et al. [27] investigated a purely active HCS that uses wave synchronization. The method used in this paper to model the rope and payload is similar to that of Yuan [35]. However, there is no stiffness within the rope. This is not suitable for this thesis since the water depths are significant so the stiffness of the rope becomes important. This is especially the case for synthetic rope such as Dyneema which acts as a soft spring.

2.3.3 PID control

PID control is widely used in many offshore applications. A few examples are highlighted here.

Nicoll et al. [36] investigated a winch-controlled active heave compensator for a remotely operated vehicle cage. A P controller was used to control dynamic tension in the rope and a PD controller was used to control the depth of the cage. This use of PID control proved effective. This is similar to the use of PID control in the work of Skaare and Egeland [29] in section 2.3.1.2 who used a parallel force/position controller for controlling loads through the splash-zone.

2.3.4 Analysis

The current understanding of AHCS for use on drill-ships and the splash-zone crossing is well developed. This is shown by the many examples of investigations into these areas described above. In contrast, there have been very little articles dealing with the seabed landing. It could be said placing equipment

on the seabed using AHC is easier than going through the splash-zone so less research has been done on that, explaining the lack of articles. There have been good experiences in practice using AHC to place equipment on the seabed [37]. The sea-bed landing phase is also an important part of an offshore lifting operation. Thus, the sea-bed landing phase is a worthwhile area to investigate.

Furthermore, from the above descriptions it is apparent that much work has been done on AHCS with various existing models. These systems have primarily been hydraulic systems. To explore the area of AHCS further it is desirable to investigate electric-driven systems. Modeling of the electric system based on similar methods presented in the articles reviewed should be possible.

PID control is relatively simple compared to some of the more complex methods described above but provides effective control. Woodacre et al. [4] have stated that using PID control is the simplest control algorithm for an AHCS [4]. A more complex method has the potential to provide more effective control but this is unnecessary since PID can work well enough and is relatively simple. This thesis will use a PID controller since it showed sufficient effectiveness and is simple.

The approach taken by Sawodny et al. [34] in section 2.3.2.1 of combining the payload and rope as a spring-mass-damper system is not used since there needs to be flexibility in separating the rope and payload. Instead, the rope and payload are discretized as separate masses.

Yuan [35] in section 2.3.2.2 modelled the rope stiffness as dependent on the rope length. This approach will be used since Dyneema rope will likely be used and for this the length should have a strong effect on the stiffness.

2.4 Conclusion

This thesis will address the seabed landing phase of a payload controlled by a hybrid heave compensation system. Based on the literature read by the author, all of which is not included in the review, a hybrid heave compensation system coupled with the vessel for the seabed-landing phase has not been investigated before. Most papers focus on the splash-zone crossing instead of the seabed-landing phase. Papers most commonly deal with either a purely active system or a purely passive system, with the purely active system being most common, although there are examples of hybrid heave compensation systems being investigated. Few papers couple the heave compensation system with the vessel in order to provide feed-back to the vessel. Thus, this work is different from previous literature since it combines three parts; firstly it investigates a hybrid heave compensation system, secondly it examines the seabed-landing phase, and thirdly it couples the heave compensation system with the vessel. Furthermore, most active heave compensation systems investigated previously used hydraulic or electric-hydraulic systems. This work is different since it will use a purely electric-driven system. Additionally, PID control will be used as the control method. The rope and payload will be modelled as discrete masses.

Design requirements and approach 3

3.1 Introduction

The design requirements are given in section 3.2, followed by the methodology in section 3.3. The existing concepts are discussed in section 3.4 and evaluated in section 3.5.

3.2 Design requirements

The main design requirements were given for the thesis by Jumbo Maritime. The compensation requirements for the heave compensation system are:

- Compensation for 2.5m of heave motion within 8 seconds, this means a heave amplitude of 1.25m

Jumbo Maritime would like to operate the heave compensation system and vessel for offshore operations in offshore Brazil. This gives the environmental conditions as:

- Significant wave height of H_s=2.5m and peak period of T_p=8s
- Operating at water depth of 2500m
- Beam waves, which means a wave heading of μ=90°

The heave compensation system is adapted to a 900t crane. There are two 900t cranes on the J-type vessel used in the investigation. These two cranes can be operated in dual-lift mode. This gives a limitation on the maximum payload that can be lifted. These are given as:

- Single lift maximum load of 150t at 2500m
- Dual lift maximum load of 300t at 2500m

See Figure 3.1 for an ideal modelling and simulation process given by Birta and Arbez [38]. This flowchart is used as guide to the modelling and simulation process of this thesis.

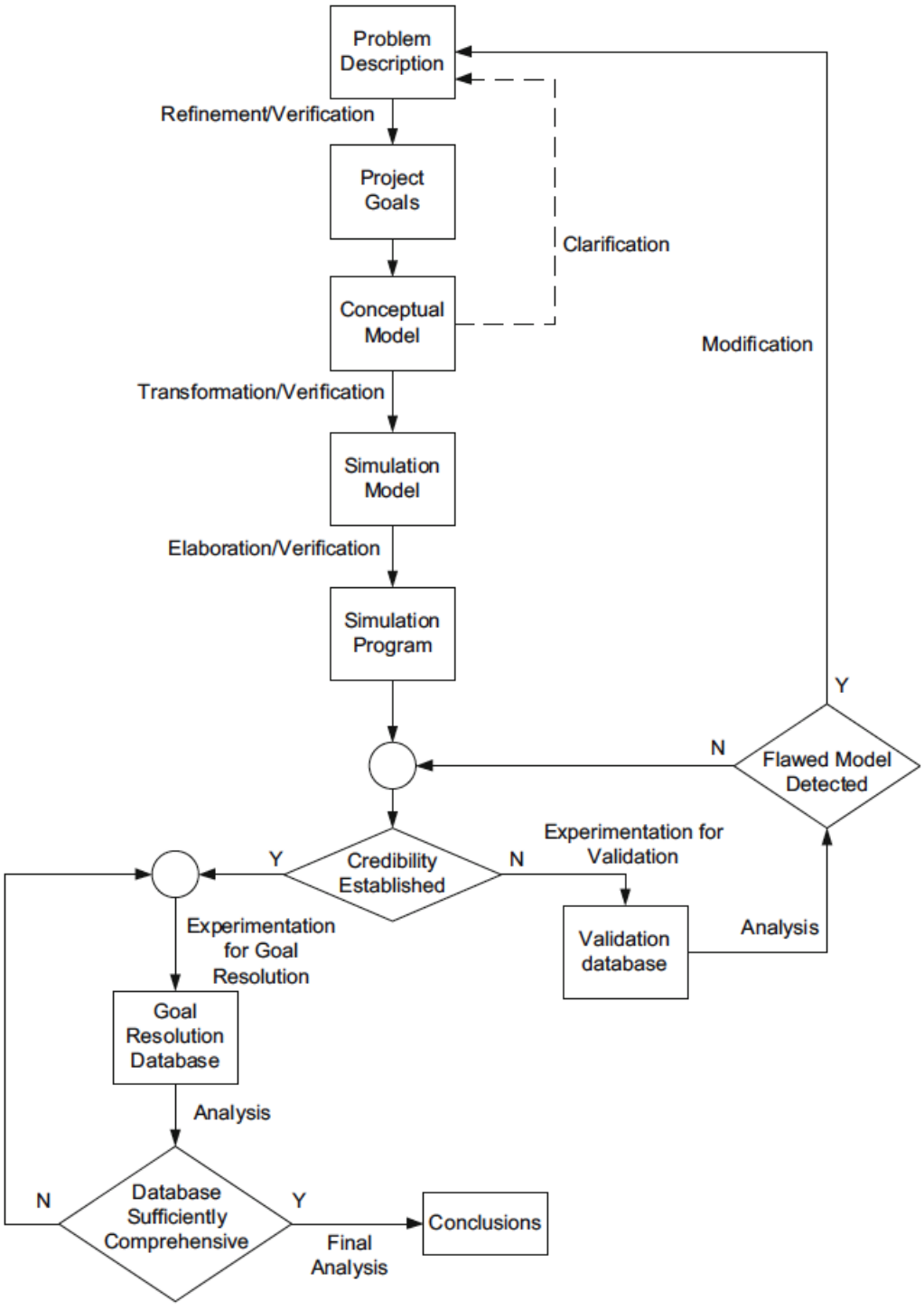

Figure 3.1: Ideal modelling and simulation process [38]

3.3 Methodology

The end goal is to have a hybrid heave compensation system. To do this a methodology based on Figure 3.1 is followed that is shown below.

1. The starting point for the investigation is three concepts from Jumbo Maritime. Evaluate the three concepts.
2. Determine a 'basic concept' derived from the evaluation of the three concepts.
3. Using the 'basic concept', build a numerical model of the PHCS
    - An existing numerical vessel motion model from Jumbo Maritime, developed by Jasper van Heijst for his MSc thesis [39] was given as a starting point for this thesis. This existing model will be built upon.
    - Build a numerical model of the crane-tip motion
    - Model the rope compliance since this is significant in deep water
    - Build a numerical model of the PHCS
    - The PHCS is not yet providing feed-back to the vessel model, the vessel model and crane-tip model are used to generate the crane-tip motion as an input to the PHCS. This is done to see the performance of the PHCS itself.
    - Analyze the PHCS by determining the natural frequencies and looking at the frequency and time responses of the system.
    - The PHCS is assessed on how well it can reduce heave motion, quantified with the criteria of performance.
4. Couple the PHCS, crane, and vessel models so that the PHCS gives feed-back to the vessel model, this gives the coupled PHCS model (henceforth called C-PHCS), analyze the C-PHCS model
    - The C-PHCS model will be assessed on how well the system can reduce heave motion, quantified with the criteria of performance.
    - The model will also be assessed on if its natural frequencies coincide with the design wave frequency
5. Using the 'basic concept' make a model of the AHCS combined with the PHCS, giving the HHCS model. Combine the HHCS, crane, and vessel models, this results in the coupled HHCS model (henceforth called C-HHCS)
    - Build a numerical model of the AHCS.
    - Couple the AHCS with the PHCS to form the HHCS
    - Couple the HHCS, crane, and vessel models
    - The C-HHCS will be assessed on how well the system can reduce heave motion, quantified with the criteria of performance.
    - The effect of the C-HHCS on the vessel's motion will be assessed.
6. Draw conclusions

3.4 Existing concepts

The first step in the methodology in section 3.3 is performed.

The AHCS concept, concept 1, is shown in Figure 3.2. This uses a purely active system where a roll reduction system is used to control roll of the vessel which controls the crane's movement. Since the crane is extended from the vessel the vessel roll generates reasonable heave motion of the crane. This leads to an active heave reduction capability.

Concept 2 is a HHCS concept, shown in Figure 3.3. This is referred to as a linear active heave compensation system. The system works by having a motion reference unit measure heave motion at the location where the winch rope leaves the vessel. The system compensates heave motion with a cylinder combining active and passive capabilities. This dual-purpose cylinder saves power since the passive part takes most of the load (the average load) and the active part takes the wave-induced load variations. This system uses hydraulic power and a wet hand-shake is used.

Jumbo's existing HHCS concept, concept 3, is shown in Figure 3.4. This uses an active traction winch attached to the crane. The hook is integrated with a passive heave compensation cylinder. The top of the piston in the passive heave compensation cylinder is attached to the active traction winch via Dyneema rope. The bottom of the piston is rigidly connected to the hook. The outer surface of the passive heave compensation cylinder is connected to the main winch of the crane using steel rope.

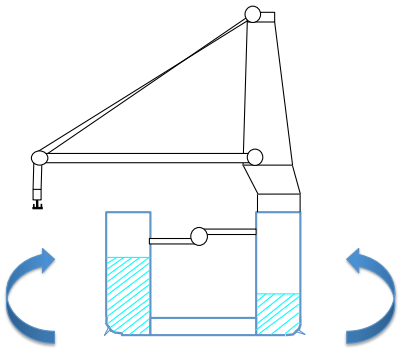

Figure 3.2: Concept 1: using a roll reduction system

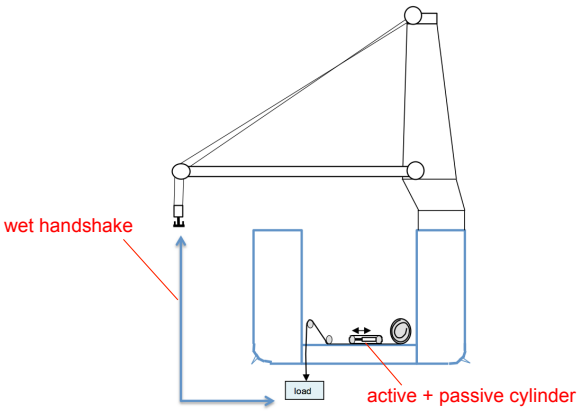

Figure 3.3: Concept 2: the linear active heave compensation system

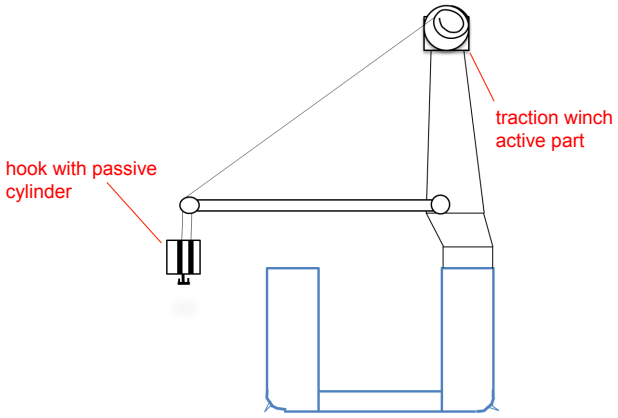

Figure 3.4: Concept 3: electric winch at the top of the crane and a passive cylinder integrated with the hook

3.5 Multi-criteria analysis

The main criteria of interest are:

1. The efficiency of the system
    - Higher efficiency is better
2. The space taken by the system
    - Less space is better
3. The transportability of the system
    - It is better if the system is more transportable
4. The cost of the system
    - Lower cost is better

Using the criteria above each concept is discussed.

Concept 1 is not considered very efficient due to the large volumes of water that need to be moved but it is integrated with existing ballast tanks so takes little space. Concept 1 is not transportable since it needs to connect to the ballast tanks which are deep inside the vessel. However, Concept 1 is relatively low cost since only a limited amount of additional equipment is necessary and the ballast tanks already exist.

Concept 2 is not that efficient since it uses a hydraulic power unit that is constantly running and this unit takes up a large amount of space. Concept 2 also requires a moon-pool for the wet handshake but it is highly transportable since the system is available in a containerized form. Concept 2 is easy to integrate into an existing winch system and is effective at compensation with compensation of 90% of heave. It is an existing design used by Bosch Rexroth so it is known that it works. Nevertheless, Concept 2 is expensive.

Concept 3 is highly efficient since the active traction winch is electric-driven, and it does not take a lot of space since a hydraulic power unit on deck is not required. Concept 3 is not very transportable since the winch is integrated into the crane but the small size of the system and relatively small number of parts contributes to making it relatively inexpensive.

Based on this discussion the multi-criteria analysis was performed in Table 3.1. Plus signs indicate the concept performs well under the specific criteria and minus signs indicate the concept performs poorly. It can be seen from Table 3.1 that concept 3 is the best concept among the three. Therefore, concept 3 is the chosen design, the 'basic concept'.

Table 3.1: The multi-criteria analysis

	efficiency	space	transportable	cost	**Total**
concept 1	−	++	−−	+	**0**
concept 2	−−	−	++	−	−−
concept 3	++	+	−	++	++++

3.6 Conclusion

This concludes step 1 and 2 in the methodology in section 3.3. In chapter 4, step 3 in the methodology is started with the ship model.

4 Vessel motion model

4.1 Introduction

The vessel model developed by van Heijst [39] was used to predict ship motions. This model was used since it was given as a starting point for this thesis. Furthermore, this available model is a model of the J-type vessel of Jumbo and this thesis is investigating a HHCS for the J-type vessel. The ship model predicts sway, heave, and roll motions of the vessel. The main changes to the model was adding a spring in the sway direction to prevent excessive sway motion and to add roll moment to account for the HHCS exerting a force on the crane-tip, which produces a moment.

The model was made in Simulink and MATLAB by van Heijst. Since the vessel model was given as a starting point for this thesis the model was kept in Simulink and MATLAB. To couple with the vessel model, the model of the HHCS was made in Simulink and MATLAB. This was done so that the work of this thesis would be ensured to be compatible with the vessel model.

4.2 Equations of motion

Newton's second law:

$$F = Ma \tag{4.1}$$

is used to derive the equations of motion of the ship. A ship has six degrees of freedom thus Newton's second law must be applied to each degree of freedom. Writing Newton's second law using the conventional notation:

$$\sum_{k=1}^{6} M_{jk} \cdot \ddot{q}_k(t) = \sum F_j \quad : j = 1...6 \tag{4.2}$$

The frequency and time domain models are based on Newton's second law in (4.2). The degrees of freedom are given by the vector q_k with $k = 1, 2, 3$ being the translations surge, sway, and heave respectively and $k = 4, 5, 6$ are the rotations roll, pitch, and yaw respectively. $\sum F_j$ represents the sum of forces and moments (collectively called loads) acting on the vessel. Only the time domain model is discussed below since this will be used in this thesis, with the reason for selecting the time domain model given in section 4.5. The time domain model is discussed in section 4.3.

4.3 Time domain

The time domain equations are based on (4.2). By expanding $\sum F_j$, which represents summation of forces and moments, the following equation is obtained [39]:

$$\sum_{k=1}^{6} M_{jk} \cdot \ddot{q}_k(t) = F_j^{\mathrm{HD}} + F_j^{\mathrm{HS}} + F_j^{\mathrm{D}} + F_j^{\mathrm{A}} + F_j^{\mathrm{E}} \quad : j = 1...6 \tag{4.3}$$

where $F_j^{\mathrm{HD}} + F_j^{\mathrm{HS}} + F_j^{\mathrm{D}} + F_j^{\mathrm{A}} + F_j^{\mathrm{E}}$ represent the hydrodynamic, hydrostatic, diffraction, actuator, and environmental loads. M_{jk} is the 6x6 mass matrix of the ship.

The hydrostatic load F_j^{HS} is proportional to displacement q with the proportionality factor being the hydrostatic coefficient C_{jk}, where C_{jk} is the 6x6 frequency independent hydrostatic restoring coefficient matrix. The hydrostatic load is given by:

$$-F_j^{\mathrm{HS}} = \sum_{k=1}^{6} C_{jk} \cdot q_k(t) \quad : j = 1...6 \tag{4.4}$$

The hydrodynamic load F_j^{HD} is given by:

$$-F_j^{\mathrm{HD}} = A_{\infty,jk} \cdot \ddot{q}_k(t) + \int_{-\infty}^{t} K_{jk}(t-\tau) \cdot \dot{q}_k(\tau) d\tau \quad : j = 1...6 \tag{4.5}$$

where $A_{\infty,jk}$ is the 6x6 frequency independent added mass matrix. $K(\tau)$ is the retardation function. The convolution integral in the hydrodynamic load gives the radiation load which is the damping due to waves generated by the vessel's motion. The retardation function $K(\tau)$ is given by:

$$K(\tau) = \frac{2}{\pi} \cdot \int_0^{\infty} b(\omega) \cdot \cos(\omega\tau) d\omega \tag{4.6}$$

where $b(\omega)$ is the frequency-dependent hydrodynamic damping coefficient.

A is given using the retardation function $K(\tau)$ from (4.6):

$$A = a(\omega) + \frac{1}{\omega} \cdot \int_0^{\infty} K(\tau) \cdot \sin(\omega\tau) d\tau \tag{4.7}$$

where $a(\omega)$ is the frequency-dependent hydrodynamic mass coefficient. Since (4.7) is valid for any value of ω then it is valid for $\omega = \infty$. Thus, $A_{\infty,jk}$ is obtained from (4.7) by evaluating it at $\omega = \infty$
Substituting (4.4) and (4.5) into (4.3) and replacing τ with $t - \tau$ to give more convenient integration limits gives the Cummins equation [39]:

$$\sum_{k=1}^{6} (M_{jk} + A_{\infty,jk}) \cdot \ddot{q}_k(t) + \int_0^{\infty} K_{jk}(\tau) \cdot \dot{q}_k(t-\tau) d\tau + C_{jk} \cdot q_k(t) = F_j^{\mathrm{D}} + F_j^{\mathrm{A}} + F_j^{\mathrm{E}} \quad : j = 1...6 \tag{4.8}$$

The added mass matrix was calculated by van Heijst using WAMIT. WAMIT is described in section 4.3.1.

4.3.1 WAMIT

WAMIT is a program that uses the panel method to solve the velocity potential and fluid pressure on the submerged surfaces of bodies such as ships, semi-submersibles, and other floating structures [40]. WAMIT is based on the linear and second-order potential theory.

4.4 Degrees of freedom

For a vessel there are six degrees of freedom these are three translations and three rotations, see Figure 4.1. The three translations are:

- Surge- x, motion in the longitudinal x direction, the motion in direction 1
- Sway- y, motion in the lateral y direction, the motion in direction 2
- Heave- z, motion in the vertical z direction, the motion in direction 3

The three rotations are:

- Roll- ϕ, motion about the x axis, the motion in direction 4
- Pitch- θ, motion about the y axis, the motion in direction 5
- Yaw- ψ, motion about the z axis, the motion in direction 6

The number of degrees of freedom was limited to three to make the model simple and not too time-consuming to make [39]. The heave motion was included to account for mass changing over time due to a roll reduction system. The sway and roll motions are coupled so one cannot be included without the other. In summary, the heave, sway, and roll are considered. This captures all the degrees of freedom in the $y-z$ plane shown in Figure 4.1.

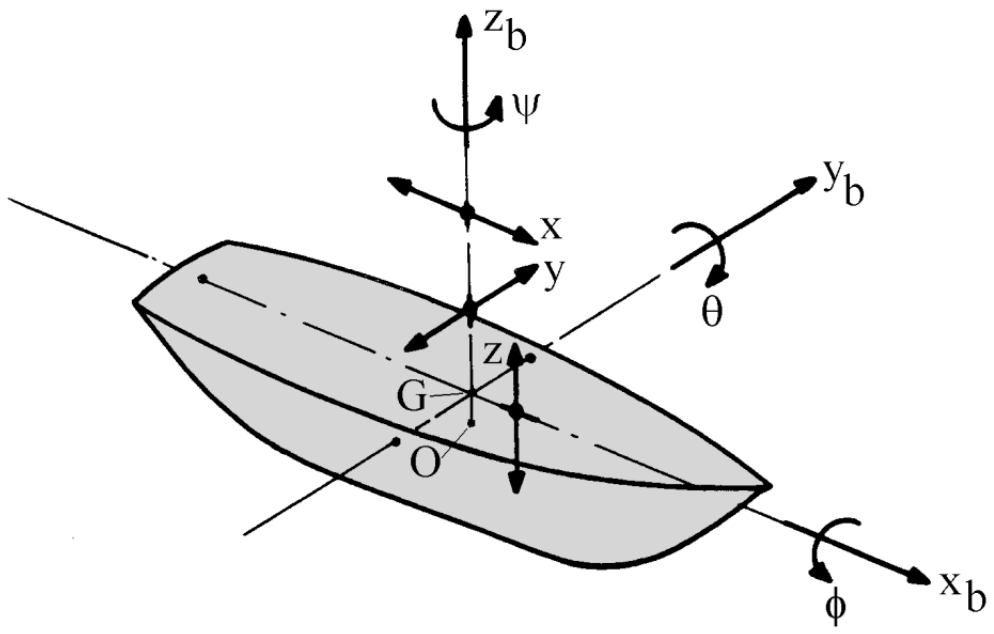

Figure 4.1: Six degrees of freedom for three axes with the origin at the center of gravity [41]

4.5 Choice of domain

The frequency domain model is less computationally expensive to solve than the time domain model. However, the frequency domain model has more limitations. The vessel model can be made with the wave exciting it being a regular wave with frequency ω and for which the vessel characteristics are known. Alternatively the wave can be a summation of waves with different amplitudes, phases, and frequencies for which the vessel characteristics are known. These vessel characteristics can be calculated using potential theory software such as WAMIT. The main limitation of the frequency domain model is that it applies only to linear systems [39] since in non-linear systems the superposition principle is not

applicable. The model of van Heijst is in the time-domain since van Heijst investigated a roll reduction system which introduced non-linearities meaning the frequency domain model could not be used [39]. Since this thesis uses van Heijst's model as a starting point the time domain model of van Heijst is used. Furthermore, the HHCS will use non-linear accumulators, a key reason to keep the vessel model in the time domain.

4.6 Applying the equations of motion

4.6.1 Coupling of degrees of freedom

The J-type vessel is considered a slender vessel. This means the movements in directions 2-4-6 and 1-3-5 are uncoupled from each other [39]. The vessel is assumed to have lateral symmetry (symmetry about the $x-z$ plane, called port-starboard symmetry) and the center of gravity is assumed to be at the origin of the axes. The generalized mass matrix with these assumptions is (4.9):

$$M_{jk} = \begin{bmatrix} M & 0 & 0 & 0 & 0 & 0 \\ 0 & M & 0 & 0 & 0 & 0 \\ 0 & 0 & M & 0 & 0 & 0 \\ 0 & 0 & 0 & I_{xx} & 0 & I_{46} \\ 0 & 0 & 0 & 0 & I_{yy} & 0 \\ 0 & 0 & 0 & I_{46} & 0 & I_{zz} \end{bmatrix} \tag{4.9}$$

Where M is the mass of the ship, I_{jk} is the inertia in the j direction from the contribution in the k direction. I_{46} is the roll-yaw inertia. Continuing with the lateral symmetry assumption, the added mass terms are (4.10):

$$A_{jk} = \begin{bmatrix} A_{11} & 0 & A_{13} & 0 & A_{15} & 0 \\ 0 & A_{22} & 0 & A_{24} & 0 & A_{26} \\ A_{31} & 0 & A_{33} & 0 & A_{35} & 0 \\ 0 & A_{42} & 0 & A_{44} & 0 & A_{46} \\ A_{51} & 0 & A_{53} & 0 & A_{55} & 0 \\ 0 & A_{62} & 0 & A_{64} & 0 & A_{66} \end{bmatrix} \tag{4.10}$$

A_{jk} is frequency dependent so can be written as $A_{jk}(\omega)$. There is coupling of added mass between different motion directions. For example, A_{13} means the added mass in the 1 direction contributed from motion in the 3 direction. The port-starboard symmetry assumption means the matrix in (4.10) is symmetric. The C_{jk} matrix is diagonally symmetric, it is given by (4.11):

$$C_{jk} = \begin{bmatrix} 0 & 0 & 0 & 0 & 0 & 0 \\ 0 & 0 & 0 & 0 & 0 & 0 \\ 0 & 0 & C_{33} & 0 & C_{35} & 0 \\ 0 & 0 & 0 & C_{44} & 0 & 0 \\ 0 & 0 & C_{53} & 0 & C_{55} & 0 \\ 0 & 0 & 0 & 0 & 0 & 0 \end{bmatrix} \tag{4.11}$$

As mentioned in section 4.4 only heave, sway, and roll of the vessel are considered. This means the only non-zero values in C_{jk} are C_{33} and C_{44}. Thus (4.11) can be written as (4.12):

$$C_{jk} = \begin{bmatrix} 0 & 0 & 0 & 0 & 0 & 0 \\ 0 & 0 & 0 & 0 & 0 & 0 \\ 0 & 0 & C_{33} & 0 & 0 & 0 \\ 0 & 0 & 0 & C_{44} & 0 & 0 \\ 0 & 0 & 0 & 0 & 0 & 0 \\ 0 & 0 & 0 & 0 & 0 & 0 \end{bmatrix} \tag{4.12}$$

where:

$$C_{33} = \rho g A_{\text{wl}} \tag{4.13}$$

$$C_{44} = \rho g \text{GM} \tag{4.14}$$

where ρ is the density of water, g is the gravitational acceleration, A_{wl} is the area at the waterline, and GM is the metacentric height. C_{33} is constant by the assumption that the walls of the vessel remain vertical over the range of the heave motion.

4.6.2 Calculation of M, A, and C coefficients

The values of the coefficient matrix A_{jk} were calculated by van Heijst using WAMIT. The matrix is frequency dependent. Using the choice of degrees of freedom in section 4.4 some of the coefficients found in the coefficient matrices in section 4.6.1 are neglected, resulting in the coefficient matrices:

$$M_{jk} = \begin{bmatrix} M & 0 & 0 \\ 0 & M & 0 \\ 0 & 0 & I_{xx} \end{bmatrix} \tag{4.15}$$

$$A_{jk} = \begin{bmatrix} A_{22} & 0 & A_{24} \\ 0 & A_{33} & 0 \\ A_{42} & 0 & A_{44} \end{bmatrix} \tag{4.16}$$

$$C_{jk} = \begin{bmatrix} 0 & 0 & 0 \\ 0 & C_{33} & 0 \\ 0 & 0 & C_{44} \end{bmatrix} \tag{4.17}$$

4.6.3 Diffraction load

The loads on the right-hand side of (4.8) are described. The diffraction loads are first described. The diffraction loads F_j^{D} were modelled as sinusoidal functions with amplitudes, frequencies, and phase angles. To model a regular beam sea a single sine wave is used and to model a complex sea state a superposition of multiple sine waves is used to give irregular waves [39]. A single sine wave is given as:

$$\mu(t, y) = A\sin(\omega t - ky\sin(\theta)) \tag{4.18}$$

The diffraction load for the sway, heave, roll directions shown by j is:

$$F_j^{\text{D}}(t, y) = R_j^{\text{D}} A\sin(\omega t - ky\sin(\theta) + \phi_j) \tag{4.19}$$

where R_j^{D} is the load response amplitude operator calculated by WAMIT for various frequencies and headings, ϕ_j is the phase in the j direction, the amplitude of the wave is A, θ is the heading of the wave, t is time, and y is location. The wave number k is related to the wave frequency ω via the dispersion relationship:

$$\omega^2 = gk\tanh(kd) \tag{4.20}$$

Where d is water depth, for deep water which is a reasonable assumption for this thesis $\tanh(kd) = 1$, this gives the deep water dispersion relationship:

$$\omega^2 = gk \tag{4.21}$$

This gives a water depth independent wave number:

$$k = \frac{\omega^2}{g} \tag{4.22}$$

The load response amplitude operator R_j^{D} measures the amount of force or moment as a function of the relative wave height for each motion direction. It was found using WAMIT and depends on frequency and heading.

4.6.3.1 Wave spectrum

To represent the sea state in the frequency domain a wave spectrum is used. Various wave spectra are available for example the Pierson-Moskowitz spectrum. The main parameters for the Pierson-Moskowitz spectrum are the peak period, T_p, and the significant wave height H_s. The spectrum is represented by the spectral density function given by:

$$S(f) = \lim_{\Delta f \to 0} \frac{1}{\Delta f} \frac{1}{2} \bar{a^2} \tag{4.23}$$

where a is wave amplitude and f is frequency.

4.6.3.2 Irregular waves

A single sine wave is not a realistic representation of a sea state. Instead an irregular sea state is more realistic. This means a linear superposition of sine waves is used with each sine wave having an amplitude, phase, and frequency. To obtain these parameters the wave spectrum is used. If an irregular sea state has n sine waves then the frequency range is divided into n bins. For each bin the value of $S(\omega)$ is calculated at the center of the bin. This is used to find the amplitude of a wave i through:

$$A_i = \sqrt{2S(\omega_i)\Delta\omega} \tag{4.24}$$

When creating the spectral density function the phase of the wave is lost. Thus, a uniformly distributed random phase is added to each wave. Re-writing (4.18) gives:

$$\mu(t, y) = \sum A_i \mathrm{sin}(\omega t - k_i y \mathrm{sin}(\theta_i) - \epsilon_i) \tag{4.25}$$

where ϵ_i is the phase for each wave. Using (4.19) the diffraction loads are found:

$$F_j^\mathrm{D} = \sum_i R_{j,i}^\mathrm{D} A_i \mathrm{sin}(\omega_i t - k_i y \mathrm{sin}(\theta_i) + \phi_{j,i} - \epsilon_i) \tag{4.26}$$

4.6.4 Other loads

Wind and current loads are neglected. This is because it is assumed the workability of the vessel is limited by wave loads and not wind or current loads. This means F_j^E is removed from (4.8).

The actuator load F_j^A is used to account for the roll moment due to the payload on the crane. A simple dynamic positioning system in the form of a spring is used to control the sway motion. This is to keep the vessel from drifting off since without a sway restoring force the vessel will be free to sway unlimited.

4.6.5 Assumptions of model

The assumptions for the vessel model are summarized below [39]:

- 3 degree of freedom model
- Heave uncoupled
- Inviscid, irrotational fluid
- Viscous loads only modelled in roll
- No wind/current
- Dynamic positioning system is a soft spring

4.7 Conclusion

Now that a vessel model is available the crane-tip motion model can be obtained. In chapter 5, step 3 of the methodology in section 3.3 is continued with the crane-tip model.

Crane-tip motion model 5

5.1 Introduction

The equations to obtain the transformation of the vessel motion to crane-tip motion are described. The motion of a fixed point on the vessel corresponds to the motion of the crane tip since it is assumed the crane is sufficiently stiff to hold a fixed position on the vessel.

5.2 Degrees of freedom investigated

To obtain a fully accurate model of the motion $(x_{\mathrm{P}}, y_{\mathrm{P}}, z_{\mathrm{P}})$ of a fixed point on the vessel (5.1) (5.2) (5.3) should be used [41]:

$$x_{\mathrm{P}} = x - y_{\mathrm{b}}\psi + z_{\mathrm{b}}\theta \tag{5.1}$$

$$y_{\mathrm{P}} = y + x_{\mathrm{b}}\psi - z_{\mathrm{b}}\phi \tag{5.2}$$

$$z_{\mathrm{P}} = z - x_{\mathrm{b}}\theta + y_{\mathrm{b}}\phi \tag{5.3}$$

where x, y, z, ϕ, θ, and ψ are surge, sway, heave, roll, pitch, and yaw, respectively, of the vessel about the center of gravity of the vessel and $x_{\mathrm{b}}, y_{\mathrm{b}}$, and z_{b} are the coordinates of the crane-tip. In this thesis, the motion transformation is only done to obtain the vertical motion:

$$z_{\mathrm{P}} = h \tag{5.4}$$

where h is the vertical motion of the crane-tip. This is because this is the desired motion to compensate for and adding more motion directions would add unnecessary complexity. Furthermore, the x, y, ψ, and θ motions of the vessel are deemed neglectable. Why this is the case will become clear below. For Jumbo, the AHCS will always be fitted to a vessel that has a dynamic positioning (DP) system. Therefore, one can assume the DP system works well enough to remove nearly all vessel motion in the horizontal plane. Thus x, y, and ψ motions of the vessel can be neglected. Since the crane is near the middle of the vessel, the effect of vessel pitch θ motion is negligible. Thus, it has been justified why the x, y, ψ, and θ motions of the vessel can be neglected.

The ship-motion-predicting model of van Heijst outputs heave z, sway y, and roll ϕ. Since the sway y is neglected only the heave z and roll ϕ of the vessel are used for the crane-tip model.

5.3 Frequency of encounter

The frequency at which the vessel encounters waves is:

$$\omega_e = \omega - kV\cos(\mu) \tag{5.5}$$

where ω is the wave frequency, k is the wave number, V is the ship's speed vector, and μ is the wave direction angle. The wave number is obtained using the dispersion relationship. Assuming deep water simplifies the dispersion relationship to:

$$\omega^2 = kg \tag{5.6}$$

$$k = \frac{\omega^2}{g} \tag{5.7}$$

this gives the frequency at which the vessel encounters waves as:

$$\omega_e = \omega - \frac{\omega^2}{g}V\cos(\mu) \tag{5.8}$$

When the vessel is performing lifting operations the vessel will not be moving which means vessel velocity $V = 0$. This gives:

$$\omega_e = \omega \tag{5.9}$$

the frequency of encounter is the same as the frequency of waves. Since the waves are irregular there is not one frequency to describe the waves. An approximation is found using the peak period. The peak period is used since at this period the maximum power in the spectrum occurs so the most energetic waves occur at this period so these waves are more dominant. Since the frequency of encounter is the same as the wave frequency then:

$$\omega_e = \frac{2\pi}{T_p} \tag{5.10}$$

5.4 Vertical motion, $z_P = h$

The equation for the absolute harmonic vertical motion of a fixed point $P(x_b, y_b, z_b)$ on the vessel is given below [41]:

$$h(\omega_e, t) = z + y_b\phi = z_a\cos(\omega_e t + \epsilon_{z\zeta}) + y_b\phi_a\cos(\omega_e t + \epsilon_{\phi\zeta}) \tag{5.11}$$

Where the variables are defined in Table 5.1. The coordinate system is defined in Figure 5.1.

Table 5.1: Definitions of variables

Variable	Definition
z	Heave
y_b	y coordinate of point P in the body-bound coordinate system
ϕ	Roll angle of vessel in steadily translating $O(x, y, z)$ coordinate system
z_a	Heave amplitude
ω_e	$\omega_e = \omega$
$\epsilon_{z\zeta}$	Heave phase shift with respect to the harmonic wave elevation at the origin of the steadily translating $O(x, y, z)$ coordinate system
$\epsilon_{\phi\zeta}$	Roll phase shift with respect to the harmonic wave elevation at the origin of the steadily translating $O(x, y, z)$ coordinate system
ϕ_a	Roll amplitude of vessel in the steadily translating $O(x, y, z)$ coordinate system

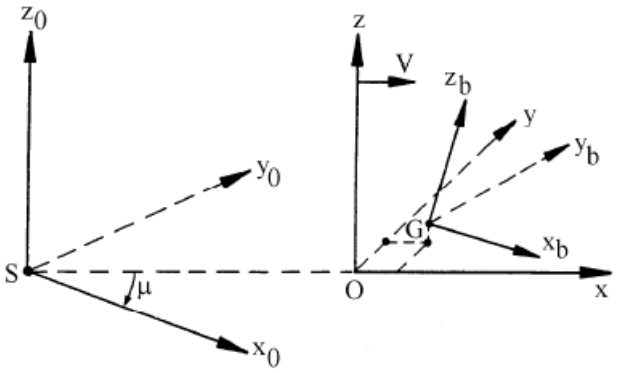

Figure 5.1: Coordinate system [41]

$$\cos(\alpha+\beta) = \cos(\alpha)\cos(\beta) - \sin(\alpha)\sin(\beta) \tag{5.12}$$

Using the identity (5.12) to expand (5.11):

$$h(\omega_e, t) = z_a\Big[\cos(\omega_e t)\cos(\epsilon_{z\zeta}) - \sin(\omega_e t)\sin(\epsilon_{z\zeta})\Big] + y_b\phi_a\Big[\cos(\omega_e t)\cos(\epsilon_{\phi\zeta}) - \sin(\omega_e t)\sin(\epsilon_{\phi\zeta})\Big] \tag{5.13}$$

Further simplification of (5.13):

$$h(\omega_e, t) = \cos(\omega_e t)\Big[z_a\cos(\epsilon_{z\zeta}) + y_b\phi_a\cos(\epsilon_{\phi\zeta})\Big] - \sin(\omega_e t)\Big[z_a\sin(\epsilon_{z\zeta}) + y_b\phi_a\sin(\epsilon_{\phi\zeta})\Big] \tag{5.14}$$

Since $h(\omega_e, t)$ was obtained from a linear superposition of two harmonic motions then $h(\omega_e, t)$ must be harmonic:

$$h(\omega_e, t) = h_a\cos(\omega_e t + \epsilon_{h\zeta}) = [h_a\cos(\epsilon_{h\zeta})]\cos(\omega_e t) - [h_a\sin(\epsilon_{h\zeta})]\sin(\omega_e t) \tag{5.15}$$

Where h_a is the motion amplitude and $\epsilon_{h\zeta}$ is the phase lag of the motion with respect to the wave elevation at the origin of the body-bound coordinate system (the ship's center of gravity). Equating the terms with $\cos(\omega_e t)$ in (5.15) and (5.14) gives $h_a\cos(\epsilon_{h\zeta})$. Equating the terms with $\sin(\omega_e t)$ in (5.15) and (5.14) gives $h_a\sin(\epsilon_{h\zeta})$:

$$h_a\cos(\epsilon_{h\zeta}) = z_a\cos(\epsilon_{z\zeta}) + y_b\phi_a\cos(\epsilon_{\phi\zeta}) \tag{5.16}$$

$$h_a\sin(\epsilon_{h\zeta}) = z_a\sin(\epsilon_{z\zeta}) + y_b\phi_a\sin(\epsilon_{\phi\zeta}) \tag{5.17}$$

The right hand sides of (5.16) and (5.17) are known from the model of the vessel motions. Thus the amplitude h_a and phase shift $\epsilon_{h\zeta}$ can be determined by combining (5.16) and (5.17) and solving for h_a and phase shift $\epsilon_{h\zeta}$:

$$h_a = \sqrt{(h_a\cos(\epsilon_{h\zeta}))^2 + (h_a\sin(\epsilon_{h\zeta}))^2} \tag{5.18}$$

$$h_a = \sqrt{(z_a\cos(\epsilon_{z\zeta}) + y_b\phi_a\cos(\epsilon_{\phi\zeta}))^2 + (z_a\sin(\epsilon_{z\zeta}) + y_b\phi_a\sin(\epsilon_{\phi\zeta}))^2} \tag{5.19}$$

$$\epsilon_{h\zeta} = \arctan\Big[\frac{h_a\sin(\epsilon_{h\zeta})}{h_a\cos(\epsilon_{h\zeta})}\Big] \tag{5.20}$$

$$\epsilon_{h\zeta} = \arctan\Big[\frac{\sin(\epsilon_{h\zeta})}{\cos(\epsilon_{h\zeta})}\Big] \tag{5.21}$$

$$\epsilon_{h\zeta} = \arctan\Big[\frac{z_a\sin(\epsilon_{z\zeta}) + y_b\phi_a\sin(\epsilon_{\phi\zeta})}{z_a\cos(\epsilon_{z\zeta}) + y_b\phi_a\cos(\epsilon_{\phi\zeta})}\Big] \tag{5.22}$$

The vertical motion of the crane-tip is given by:

$$h(\omega_e, t) = h_a\cos(\omega_e t + \epsilon_{h\zeta}) \tag{5.23}$$

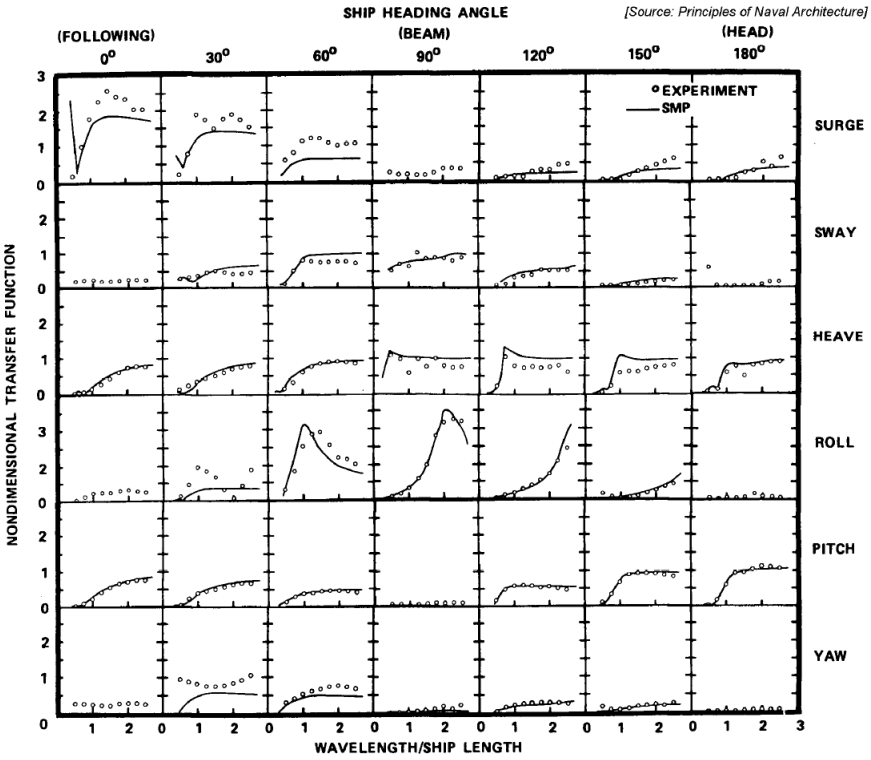

Figure 5.2: RAO for 6 degrees of freedom [41]

with h_a given by (5.19) and $\epsilon_{h\zeta}$ given by (5.22). The required inputs and outputs are listed in Table 5.2

Table 5.2: Inputs and outputs of the crane model

Inputs	Outputs
z_a	h_a
y_b	$\epsilon_{h\zeta}$
ϕ_a	
$\epsilon_{z\zeta}$	
$\epsilon_{\phi\zeta}$	

5.5 Applying the equations

5.5.1 Vertical motion, $z_P = h$

The metocean conditions are significant wave height $H_\mathrm{s} = 2.5$m and peak period $T_\mathrm{p} = 8$s. Beam waves are used, this means the waves have a heading of $\mu = 90°$. This is because the RAOs of a vessel in roll and heave for beam waves are generally greatest compared to other wave headings, see Figure 5.2. The figure shows that the pitch RAO is negligible for beam waves. The figure shows RAOs for an aircraft carrier which is assumed valid for the J-type vessel since both are relatively slender structures.

The equations of motion have been described in section 5.4. The equations are now applied to the vessel. See Figure 5.3 for an example of the motions of the crane-tip.

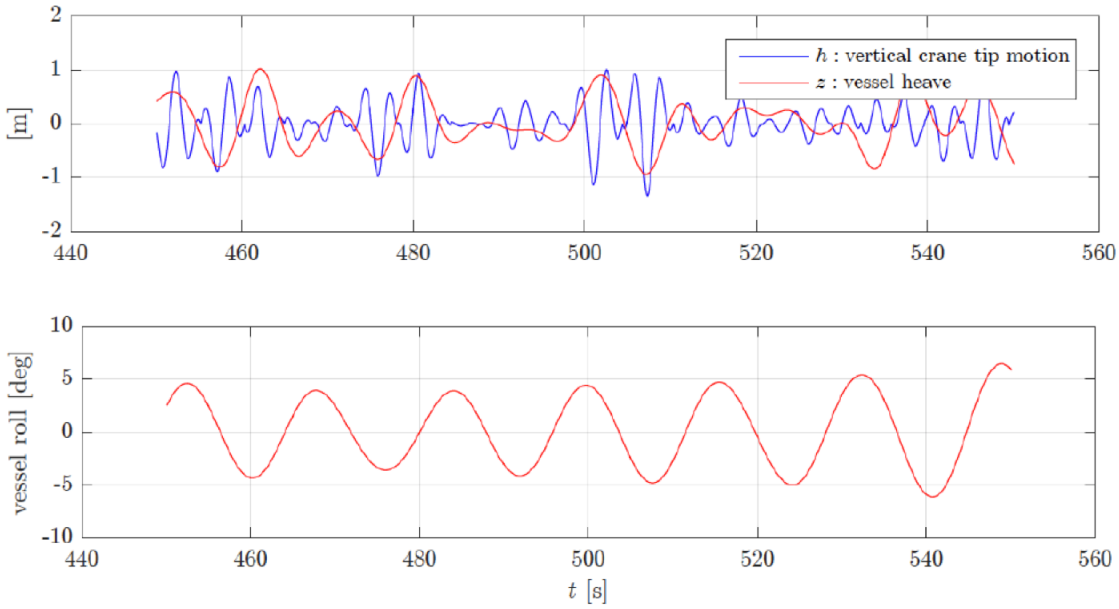

Figure 5.3: Vertical crane-tip motion in the top sub-plot in blue with vessel heave in red, in the bottom sub-plot the vessel roll is shown

5.6 Conclusion

In chapter 6, step 4 of the methodology in section 3.3 is continued with the model of the PHCS.

Passive heave compensation cylinder

6

6.1 Introduction

This chapter discusses the principle of the passive heave compensation cylinder.

6.2 Model

To model the cylinder the approach taken was to use the ideal gas law under the assumption of an isentropic process (adiabatic and reversible), similar to Sverdrup-Thygeson [42]. A diagram of this system is shown in Figure 6.1.

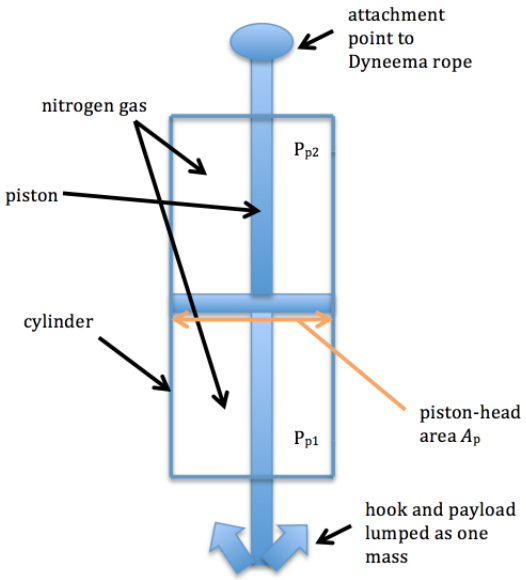

Figure 6.1: Schematic of the system

The following key assumptions are made (for all simulations):

- Environment

  - $g = 9.81\text{m/s}^2$
  - $\rho_{\text{water}} = 1025\frac{\text{kg}}{\text{m}^3}$
  - Water depth of 2500m assumed
  - Water temperature at operating depth is 4° Celsius

- Rope
  - $d_{\text{c}} = 0.05\text{m}$ is the diameter of the steel rope and A_{c} is the cross-sectional area
  - $d_{\text{Dyneema}} = 0.052\text{m}$ is the diameter of the Dyneema rope and A_{Dyneema} is the cross-sectional area
  - $E_{\text{c}} = 1.96e9(\frac{\text{N}}{\text{m}^2})$ [43], modulus of steel rope
  - $E_{\text{Dyneema}} = 6.75e8(\frac{\text{N}}{\text{m}^2})$, modulus of Dyneema rope
  - L_{c} length of steel rope and L_{Dyneema} length of Dyneema rope is the same as the water depth
  - The steel rope has stiffness, $k_{\text{c}} = \frac{E_{\text{c}}A_{\text{c}}}{L_{\text{c}}}$
  - The Dyneema rope has stiffness, $k_{\text{d}} = \frac{E_{\text{Dyneema}}A_{\text{Dyneema}}}{L_{\text{Dyneema}}}$
  - The mass of a meter of Dyneema rope is $5.3\frac{\text{kg}}{\text{m}}$, this is for LankoDeep, a Dyneema rope designed for deep-water applications
  - The mass of the Dyneema rope is M_{Dyneema}, mass per meter times length
  - The mass of a meter of steel rope is $15.3\frac{\text{kg}}{\text{m}}$, for high-tensile steel
  - The mass of the steel rope is M_{c}, mass per meter times length
  - Several steel ropes are used to connect the PHCS cylinder to the crane. The interaction of the steel ropes which each other is neglected so it is decided to combine the steel ropes into one rope, to simplify the model.
  - One Dyneema rope is used to connect the hook/payload mass to the crane.

- Payload and PHCS
  - The dimensions of the PHCS are (L,W,H) (1m, 2.3m, 5.9m).
  - The PHC cylinder, accumulators, pressure vessel and link frame have a mass M_{phc}=10e3kg
  - The mass of the hook is M_{hook}=2e3kg
  - The mass of the payload, M_{payload} =150e3kg, is rigidly attached to the hook, so they are a rigid mass, the combined mass of the payload and the hook is $M_{\text{hook,payload}} = M_{\text{payload}} + M_{\text{hook}}$
  - The water drag force on the PHC system is given using the quadratic drag equation, $\frac{1}{2}\rho_{\text{water}}C_{\text{d,phc}}D_{\text{phc}}|\dot{z}_{\text{phc}}|\dot{z}_{\text{phc}}$. The PHCS is modelled as a square rod. This is because the shape of PHC systems such as the Cranemaster system approximate a square rod so it is reasonable to use the same shape for this PHCS. Using data for a square rod from DNV-RP-H103 [44], the drag coefficient is $C_{\text{d,phc}} = 0.90$. D_{phc} is the bottom-view area of the PHCS.
  - As mentioned, the PHCS is modelled as a square rod. Added mass is a function of wave frequency. Using DNV-RP-H103 [44], the added mass of a square rod at infinite wave frequency is obtained. The added mass at infinite wave frequency is used to simplify the situation. When the wave frequency increases the added mass coefficient increases and converges to a constant value [45], so it is reasonable to use the added mass at infinite frequency.
  - The water drag force on the payload and hook is included in a similar way as for the PHCS. The drag force is given by $\frac{1}{2}\rho_{\text{water}}C_{\text{d,hook,payload}}D_{\text{hook,payload}}|\dot{z}_1|\dot{z}_1$. The hook is neglected since it has a small size relative to the payload. The payload is modelled as a circular cylinder. The reason to use a circular cylinder shape is that it provides an approximation for shapes of common subsea equipment. Some common subsea equipment better approximates a rectangular plate.

However, not all types of subsea equipment can be considered so a decision was made to use a circular cylinder shape. Using data for a circular cylinder from DNV-RP-H103 [44], the drag coefficient is $C_{\mathrm{d,hook,payload}} = 0.88$. $D_{\mathrm{hook,payload}}$ is two times the cylinder radius times the cylinder length.

- As mentioned, the payload is modelled as a circular cylinder and the hook is neglected. Using DNV-RP-H103 [44], the added mass of a circular cylinder at infinite wave frequency is obtained. The reason to use added mass at infinite frequency was given above.
- The crane-tip motion is z_{in}

- Pressure system
  - $n = 1.4$ is the specific heat ratio of nitrogen gas [46]
  - The maximum stroke of the piston is $L_{\mathrm{max,stroke}}$ =3m, based on a Cranemaster system sized for a maximum 600t payload [47]
  - The internal stopper spring length is $L_{\mathrm{s,phc}}$ =0.2m
  - The length of the lower chamber and upper chamber of the cylinder is $L_{\mathrm{m,phc}} = L_{\mathrm{max,stroke}} * 0.5 + L_{\mathrm{s,phc}}$, these are the same since the piston-head is assumed to be in the middle of the cylinder at equilibrium
  - The area the pressure in the lower chamber and upper chamber acts on is the effective piston-head area A_{p}
  - The initial volume of the upper chamber of the cylinder $V_{\mathrm{p2,1}} = A_{\mathrm{p}} * L_{\mathrm{m,phc}}$
  - The initial volume of the lower chamber of the cylinder $V_{\mathrm{p1,1}} = A_{\mathrm{p}} * L_{\mathrm{m,phc}}$
  - Kinematic viscosity of hydraulic fluid, ν =40e-6 m^2/s
  - Density of hydraulic fluid, $\rho_{\mathrm{fluid}} = 859\mathrm{kg}/\mathrm{m}^3$

The mass of the system components is shown in Table 6.1. The total mass is less than the maximum dynamic load of the crane, 650t. This is to provide for a dynamic amplification factor for safety. Thus, this constrains the mass of the payload to 150t.

Table 6.1: Mass data

Variable	Value [kg]	Description
M_{phc}	10e3	mass of the PHC cylinder, accumulators, pressure vessel and link frame
M_{payload}	150e3	mass of payload
M_{hook}	2e3	mass of hook
M_{d}	13.25e3	mass of Dyneema rope
M_{c}	153.2e3	mass of steel rope
Total	328.4e3	$M_{\mathrm{phc}} + M_{\mathrm{payload}} + M_{\mathrm{hook}} + M_{\mathrm{d}} + M_{\mathrm{c}}$

It is desired to have equations for P_{p1} and P_{p2}. Where P_{p1} is the pressure in the lower part of the cylinder and P_{p2} is the pressure in the upper part of the cylinder, shown in Figure 6.1. The subscript p1 indicates the lower part of the cylinder and the subscript p2 indicates the upper part of the cylinder. The pressures P_{p1} and P_{p2} act on the piston-head area, A_{p}, to produce forces on the piston-head. Since the pressures act on opposite sides of the piston-head the forces they produce are opposite in sign. This is because P_{p2} acts in the upper part of the cylinder so a downwards force results and P_{p1} acts in the lower part so an upward force results. The difference between the forces produces the resultant force acting on the piston-head by the passive heave compensation cylinder. Since the piston-head is rigidly attached to the hook and payload, this is the force acting to accelerate the hook and payload, F_{phc}:

$$F_{\mathrm{phc}} = P_{\mathrm{p1}}A_{\mathrm{p}} - P_{\mathrm{p2}}A_{\mathrm{p}} \tag{6.1}$$

For an ideal gas, the equation of state is:

$$PV = NRT \tag{6.2}$$

where P is pressure, V is volume, N is the amount of gas in moles, R is the ideal gas constant, and T is temperature. For an isentropic process one can derive the isentropic relations using the equation of state:

$$\frac{T2}{T1} = \left(\frac{V1}{V2}\right)^{n-1} = \left(\frac{P2}{P1}\right)^{\frac{n-1}{n}} \tag{6.3}$$

where n is the specific heat ratio. The number 1 refers to the state at the initial condition and 2 refers to the state at a time after the initial condition. Using (6.3) gives:

$$\left(\frac{V1}{V2}\right)^{n-1} = \left(\frac{P2}{P1}\right)^{\frac{n-1}{n}} \tag{6.4}$$

$$\frac{P2}{P1} = \left(\frac{V1}{V2}\right)^{n} \tag{6.5}$$

The pressure $P2$ at a time after the initial condition is a function of the volume $V2$ at this time, this is shown by:

$$P2 = P1\left(\frac{V1}{V2}\right)^{n} \tag{6.6}$$

The relationship between pressure and volume from (6.6) is used. This gives the pressure in the lower part of the cylinder, P_{p1}:

$$P_{\mathrm{p1}} = P_{\mathrm{p1,1}}\left(\frac{V_{\mathrm{p1,1}}}{V_{\mathrm{p1}}}\right)^{n} \tag{6.7}$$

where $P_{\mathrm{p1,1}}$ is the initial pressure and $V_{\mathrm{p1,1}}$ is the initial volume.
Using (6.6), the pressure in the upper part of the cylinder, P_{p2}, is given by:

$$P_{\mathrm{p2}} = P_{\mathrm{p2,1}}\left(\frac{V_{\mathrm{p2,1}}}{V_{\mathrm{p2}}}\right)^{n} \tag{6.8}$$

where $P_{\mathrm{p2,1}}$ is the initial pressure and $V_{\mathrm{p2,1}}$ is the initial volume.

Substituting (6.7) and (6.8) into (6.1) gives:

$$F_{\mathrm{phc}} = \left[P_{\mathrm{p1,1}}\left(\frac{V_{\mathrm{p1,1}}}{V_{\mathrm{p1}}}\right)^{n}\right]A_{\mathrm{p}} - \left[P_{\mathrm{p2,1}}\left(\frac{V_{\mathrm{p2,1}}}{V_{\mathrm{p2}}}\right)^{n}\right]A_{\mathrm{p}} \tag{6.9}$$

6.2.1 Initial pressure across the piston-head

Static dimensioning of the initial pressures $P_{\mathrm{p1,1}}$ and $P_{\mathrm{p2,1}}$ is done. The initial pressure in the cylinders is set to support the wet weight of the hook and payload. This means $P_{\mathrm{p1,1}}$ and $P_{\mathrm{p2,1}}$ cannot be the same since this would result in no support. Instead it is necessary that $P_{\mathrm{p1,1}} > P_{\mathrm{p2,1}}$ so there is a net force upwards. The static relation for supporting the wet weight of the hook and payload by the pressure difference across the piston-head is:

$$(M_{\mathrm{hook,payload}} - \rho_{\mathrm{water}}V_{\mathrm{d}})g = (P_{\mathrm{p1,1}} - P_{\mathrm{p2,1}})A_{\mathrm{p}} \tag{6.10}$$

where V_{d} is the displaced volume of the payload (since the hook is neglected due to its small size), ρ_{water} is water density, and g is gravitational acceleration. For clarity, the variable $P_{\Delta\mathrm{p}}$ is defined as:

$$P_{\Delta\mathrm{p}} = P_{\mathrm{p1,1}} - P_{\mathrm{p2,1}} \tag{6.11}$$

substituting $P_{\Delta\mathrm{p}}$ from (6.11) into (6.10) and solving for $P_{\Delta\mathrm{p}}$ gives:

$$P_{\Delta\mathrm{p}} = \frac{(M_{\mathrm{hook,payload}} - \rho_{\mathrm{water}}V_{\mathrm{d}})g}{A_{\mathrm{p}}} \tag{6.12}$$

6.3 Size the piston-head area

The maximum load on the piston-head is used to size the area of the piston-head. The maximum load is the load due to the maximum permissible mass suspended from the crane tip, 650t. To size the piston-head (6.13) is used. This sizes the piston-head for the largest load it is designed to take:

$$A_{\mathrm{p}} = \frac{F_{\max}}{p_{\mathrm{L}}\eta_{\mathrm{c}}} \tag{6.13}$$

where $F_{\max}$ is the maximum force on the piston-head, p_{L} is the difference in pressure across the piston, and η_{c} is the coefficient of efficiency of the cylinder (this includes losses due to internal friction in the cylinder) [42]. The internal friction is ignored so $\eta_{\mathrm{c}} = 1$.

6.3.1 Model damping

To model viscous damping the approach of having the damping as a dash-pot modeled by the product of a constant and a velocity was considered. This would give damping such as $F_{\mathrm{damping}} = C * \dot{x}$. This was tried initially but does not provide a useful model since the actual damping mechanism is more complex. This is because in PHC systems the damping arises normally from a flow restrictor obstructing the flow of hydraulic fluid such as done by Ni et al. [48]. This would be used in combination with an accumulator. The flow restrictor has dynamics connected with the gas pressure and volume in the accumulator. From the literature review, for PHC systems it was more common to use a flow restrictor type damping mechanism. For these reasons a flow restrictor is used for the damping.

6.3.2 Dyneema selection

Two ropes manufactured by Lankhorst are considered for the Dyneema rope, the LankoDeep rope [49] and the LankoForce rope [50]. The LankoDeep has a higher mass per meter which means it provides a more conservative estimate of the Dyneema mass, so this is used.

6.4 Conclusion

In this chapter the principle of the passive heave compensation cylinder was discussed. This is part of step 3 of the methodology which is continued in chapter 7. In chapter 7, the equations of motion for the system are developed and three flow restrictors investigated, the throttle, orifice, and Darcy-Weisbach system.

Passive heave compensation system

7

7.1 Introduction

In this chapter, the equations of motion for the PHCS are developed and three flow restrictors investigated, the throttle, orifice, and Darcy-Weisbach system. Two PHC systems were considered, the first with one accumulator and the second with two accumulators. The PHCS with one accumulator was first used to determine which flow restrictor to proceed with. The PHCS with one accumulator is briefly discussed in section 7.2 and the PHCS with two accumulators, discussed in section 7.3, is focused on since it is used in further analysis.

7.2 PHCS design: one accumulator

Using work done in chapter 6, the rest of the system is added. The steel rope, Dyneema rope, the hook and payload mass, the flow restrictor, and the accumulator are added. The pressure distribution around the cylinder means that depth-compensation is automatic. A schematic of the system is shown in Figure 7.1. There is only an accumulator connected to the lower chamber of the cylinder. In the literature, this is called a plunger cylinder with a schematic from Bauer [51] shown in Figure 7.2.

For the system shown in Figure 7.1 three types of flow restrictors were used, the throttle, the orifice, and the Darcy-Weisbach equation that governs pipe volume flow. These three restrictors were used while the rest of the system is kept the same. The Darcy-Weisbach type system provided poor performance so was discontinued. The orifice and throttle are investigated further.

It was found that the overall design, despite which flow restrictor was used, had some issues. Firstly, there is a large difference in amplitude between the pressures P_{p1} and P_{p2}. Secondly, the pressures P_{p1} and P_{a1} were not out of phase significantly. These two issues were thought to occur because there is only one accumulator. Thirdly, volume flow rate Q_{r} has large amplitude and unrealistically high frequency, this is due to there being no fluid inertia included in the model. In section 7.3, another accumulator was added and the throttle and orifice systems further investigated.

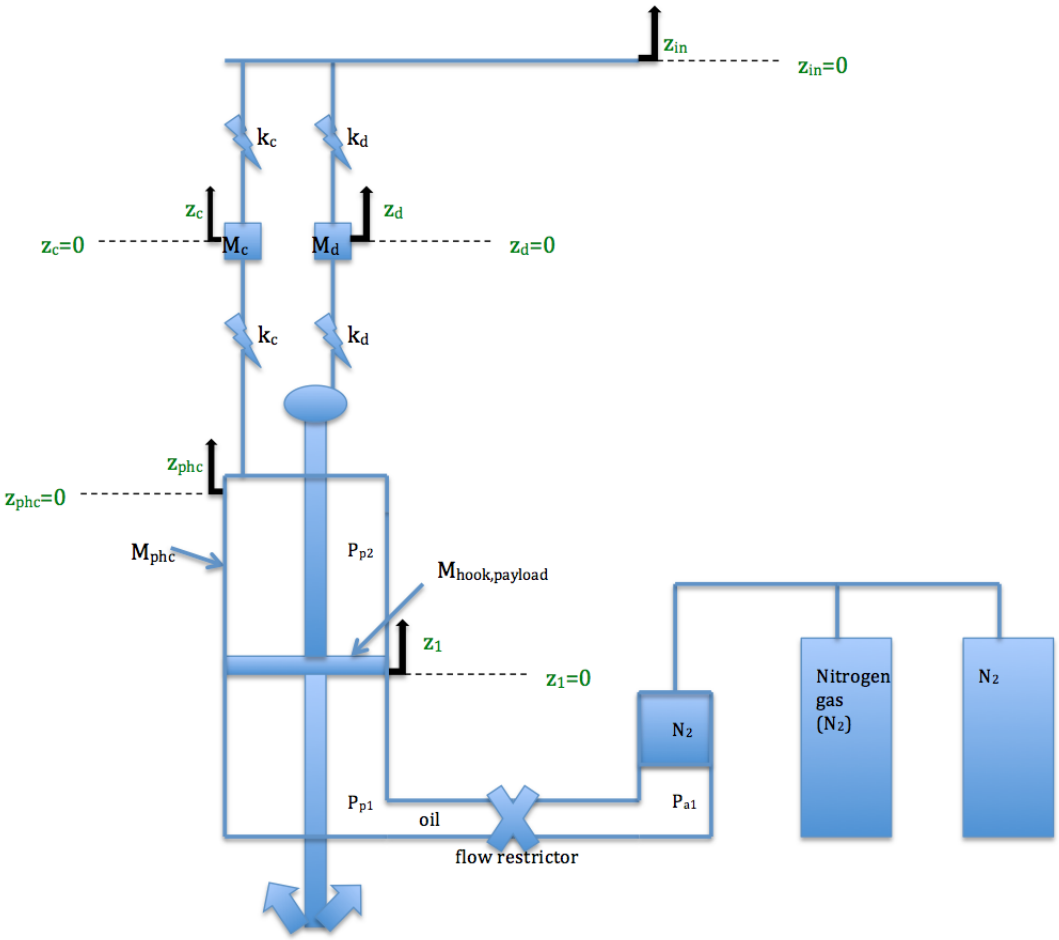

Figure 7.1: Schematic of the PHCS

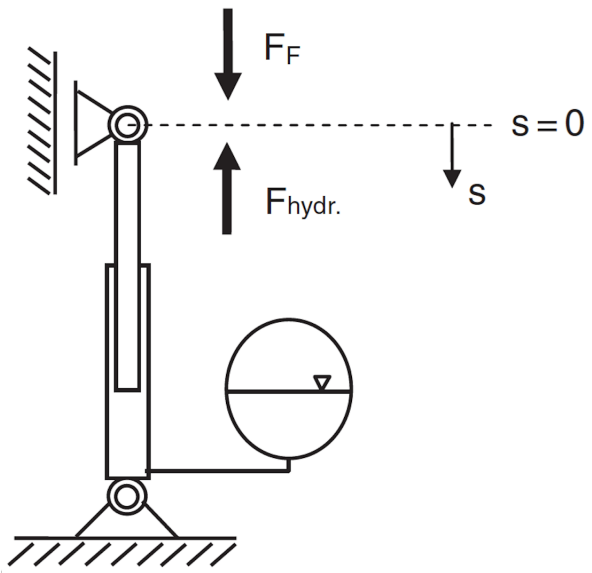

Figure 7.2: In the literature this system is referred to as the plunger cylinder [51]

7.3 PHCS design: two accumulators

As discussed in section 7.2 the PHCS with one accumulator had three issues. The volume flow rate Q_r issue is solved by adding fluid inertia. For the two other issues, two hypotheses are made:

1. The lack of an accumulator at the top of the cylinder is hypothesized to contribute to there being a large difference in amplitude between the pressures P_{p1} and P_{p2}. It is hypothesized that the amplitudes will be more similar with the new design. This is because the accumulator acts as a spring so having an accumulator at the top and bottom should provide a more balanced system leading to more balanced pressures P_{p1} and P_{p2}.

2. The lack of an accumulator at the top is hypothesized to contribute to the pressures P_{p1} and P_{a1} not being out of phase significantly. It is hypothesized that they will be more out of phase. Again, this is because of the reason above where the accumulator acts as a spring.

The new design is shown in Figure 7.3. In the literature, this is called a double-acting cylinder with a schematic from Bauer [51] shown in Figure 7.4. In the following sections, the model is discussed and equations of motion derived. Fluid inertia is not added immediately but is added in section 7.10.

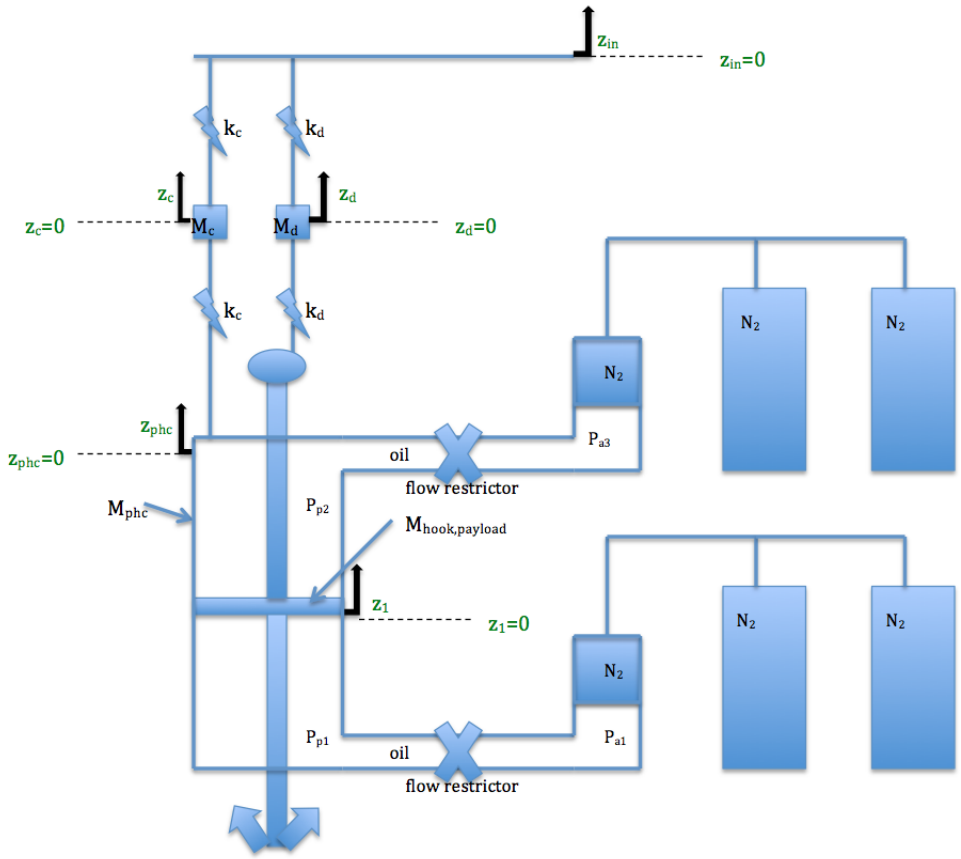

Figure 7.3: Schematic of the PHCS with two accumulators

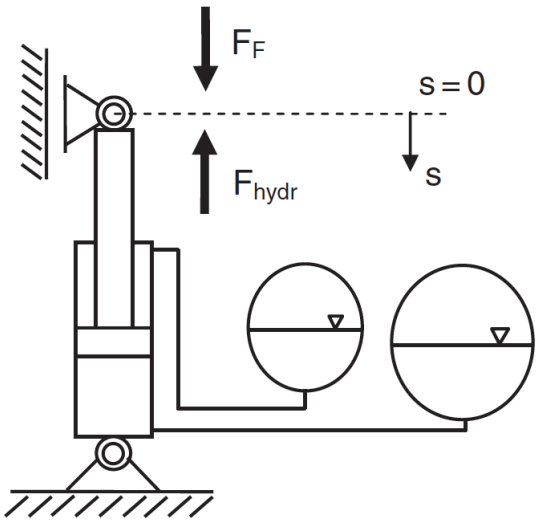

Figure 7.4: In the literature this system is referred to as the double-acting cylinder [51]

7.4 Forces to consider when lifting

The scenario being investigated is a load already through the splash-zone and being lowered to the seabed. From DNV recommended practice RP-H103 [44], the main forces to consider are shown below:

- W_0, weight of the object in air
- F_{B}, buoyancy force
- F_{d}, drag force

7.5 PHCS equations of motion

The equations of motion are obtained by using Newton's second law $F = Ma$. This is done by obtaining a free-body diagram for each mass $M_{\mathrm{hook,payload}}$, M_{phc}, M_{c}, and M_{d}.

7.5.1 Added mass of payload and PHCS

The added mass is associated with the hydrodynamic force which is in phase with the acceleration of the body. This means any body accelerating in water will have added mass. Furthermore, the added mass depends on the direction of the body's motion. For a non-symmetrical body there are cross-coupling terms $M_{1,2}$, $M_{1,3}$, and $M_{2,3}$ which mean the hydrodynamic force is in a different direction than the acceleration [52].

To simplify the model only the added mass of the payload and passive heave compensation cylinder is considered. These objects are bluff bodies in the sense that their shapes are not stream-lined and would have significant added mass. The cross-coupling terms are ignored since it is assumed they are symmetrical shapes. The added mass of the hook is neglected since the hook has a small profile compared to the payload so the added mass is relatively small compared to that of the payload.

From DNV recommended practice DNV-RP-H103 [44] various added mass values for 3D bodies are shown in Table 7.1. As mentioned earlier, the square rod was chosen for the PHCS and the circular cylinder for the payload. The passive heave compensation cylinder dimensions are taken as the same as shipping dimensions of the Cranemaster system to be conservative, L=1m, W=2.3m, H=5.9m with a height of b=5.9m and width of a=2.3m.

Table 7.1: Added mass $A = \rho C_A V_R$ for vertical direction of motion

Variable	Flat rectangular plate	Square rod	Circular cylinder
V_R	$\frac{\pi}{4}a^2b$	a^2b	$\pi a^2 b$
C_A	$f(a,b)$	$f(a,b)$	$f(a,b)$

7.5.2 Hook and payload equation of motion

The mass of the hook and the payload are lumped together in $M_{\text{hook,payload}}$. The forces acting on the hook/payload are described. The buoyancy force F_b and gravity force F_m are included. The damping force due to the movement through water is F_d. The force from the spring in the Dyneema is F_s. The force generated by the pressure difference across the piston-head inside the cylinder is included as F_{phc}. The initial pressure at the bottom of the piston-head, $P_{\text{p1,1}}$ is greater than the initial pressure at the top of the piston-head, $P_{\text{p2,1}}$. In the static case this balances the buoyancy and gravity force. F_{water} is the force due to water pressure on the outside surface of the PHCS cylinder which cancels out since it acts on both top and bottom. The damping of the piston-head against the cylinder is neglected since this is likely to be small relative to the damping caused by the hydraulic fluid. Applying Newton's second law gives:

$$(M_{\text{hook,payload}} + A_{\text{hook,payload}})\ddot{z}_1 = F_{\text{phc}} + F_{\text{water}} - F_{\text{water}} + F_b - F_m - F_d - F_s \tag{7.1}$$

where $A_{\text{hook,payload}}$ is the added mass of the hook and payload.

$$F_{\text{phc}} = P_{\text{p1}}A_p - P_{\text{p2}}A_p \tag{7.2}$$

$$F_b = \rho_{\text{water}} V_d g \tag{7.3}$$

$$V_d = 0.5\pi R^2_{\text{cylinder}} L_{\text{cylinder}} + L_{\text{phc}} W_{\text{phc}} H_{\text{phc}} \tag{7.4}$$

$$F_m = M_{\text{hook,payload}} g \tag{7.5}$$

$$F_d = \frac{1}{2}\rho_{\text{water}} C_{\text{d,hook,payload}} D_{\text{hook,payload}} |\dot{z}_1| \dot{z}_1 \tag{7.6}$$

$$F_s = k_d(z_1 - z_d) \tag{7.7}$$

$$\begin{aligned}(M_{\text{hook,payload}} + A_{\text{hook,payload}})\ddot{z}_1 = {} & P_{\text{p1}}A_p - P_{\text{p2}}A_p + F_{\text{water}} - F_{\text{water}} + \rho_{\text{water}} V_d g \\ & - M_{\text{hook,payload}} g - \frac{1}{2}\rho_{\text{water}} C_{\text{d,hook,payload}} D_{\text{hook,payload}} |\dot{z}_1| \dot{z}_1 - k_d(z_1 - z_d)\end{aligned} \tag{7.8}$$

(7.8) was verified by taking the Euler-Lagrange approach in appendix A.1.

7.5.3 PHCS equation of motion

z_{phc} is the movement of the PHCS:

$$(M_{\text{phc}} + A_{\text{phc}})\ddot{z}_{\text{phc}} = -F_s - F_d \tag{7.9}$$

$$F_s = k_c(z_{\text{phc}} - z_c) \tag{7.10}$$

$$F_d = \frac{1}{2}\rho_{\text{water}} C_{\text{d,phc}} D_{\text{phc}} |\dot{z}_{\text{phc}}| \dot{z}_{\text{phc}} \tag{7.11}$$

$$(M_{\text{phc}} + A_{\text{phc}})\ddot{z}_{\text{phc}} = -k_{\text{c}}(z_{\text{phc}} - z_{\text{c}}) - \frac{1}{2}\rho_{\text{water}} C_{\text{d,phc}} D_{\text{phc}} |\dot{z}_{\text{phc}}| \dot{z}_{\text{phc}} \tag{7.12}$$

(7.12) was verified by taking the Euler-Lagrange approach in appendix A.1.

7.5.4 Movement of steel/Dyneema rope

According to Purcell and Forrester [53], assuming no current, the lateral motion of the steel or Dyneema rope can be ignored for deep water since in depths exceeding 100m the lateral motions of the rope are rapidly damped by the water drag on the rope. Thus, the steel and Dyneema rope are assumed to not have any transverse motion but only longitudinal motion, heave. In chapter 14 a sensitivity study is done to include the damping effect of water for deep water. This is done by modelling the Dyneema rope as a continuous element with coupled axial and transverse motion and taking into account added mass and water drag.

7.5.5 Added mass and drag of steel/Dyneema rope

The steel rope and Dyneema rope are very slender and since only vertical motion of the ropes is assumed the added mass is neglected. If they are allowed to sway or move transversely then added mass is more important. The added mass coefficient varies for a given rope depending on the rope length and mode of movement [54]. The ratio $\rho_{\text{water}}/\rho_{\text{rope}}$ is an important parameter with a relationship with the influence of added mass [54]. For a steel rope this ratio is low which means the added mass influence is low whereas for the Dyneema rope the ratio is high so added mass has a stronger effect. This should be kept in mind since this is a limitation of the assumption that the steel/Dyneema ropes only move vertically. The drag in the longitudinal direction of the steel and Dyneema rope is neglected. This is because the steel and Dyneema ropes have small cross-sectional areas.

7.5.6 Steel rope equation of motion

z_{c} is the movement of the steel rope, discretized as a mass. Quadratic damping of water and added mass are neglected, as explained in section 7.5.5. The steel rope is assumed to only move in the vertical direction, the reason for this was given in section 7.5.4. The reason to discretize the steel rope as one mass was to simplify the dynamics of the system. Applying Newton's second law:

$$(M_{\text{c}})\ddot{z}_{\text{c}} = -F_{\text{s}} \tag{7.13}$$

$$F_{\text{s}} = k_{\text{c}}(z_{\text{c}} - z_{\text{in}}) + k_{\text{c}}(z_{\text{c}} - z_{\text{phc}}) \tag{7.14}$$

$$(M_{\text{c}})\ddot{z}_{\text{c}} = -k_{\text{c}}(z_{\text{c}} - z_{\text{in}}) - k_{\text{c}}(z_{\text{c}} - z_{\text{phc}}) \tag{7.15}$$

(7.15) was verified by taking the Euler-Lagrange approach in appendix A.1.

7.5.7 Dyneema rope equation of motion

z_{d} is the movement of the Dyneema, discretized as a mass. For the same reasons as for the steel rope, the quadratic damping of water and added mass are neglected and the rope is assumed to only move in the vertical direction. Applying Newton's second law:

$$(M_{\text{d}})\ddot{z}_{\text{d}} = -F_{\text{s}} \tag{7.16}$$

$$F_{\text{s}} = k_{\text{d}}(z_{\text{d}} - z_{\text{in}}) + k_{\text{d}}(z_{\text{d}} - z_{1}) \tag{7.17}$$

$$(M_{\text{d}})\ddot{z}_{\text{d}} = -k_{\text{d}}(z_{\text{d}} - z_{\text{in}}) - k_{\text{d}}(z_{\text{d}} - z_{1}) \tag{7.18}$$

(7.18) was verified by taking the Euler-Lagrange approach in appendix A.1.

7.6 Cylinder and accumulator equations

Expressions for the masses in the system have been obtained; the hook and payload, the PHCS, the steel rope and the Dyneema rope. The next step is to model the cylinder and accumulators shown in Figure 7.3. The type of damping in the system was considered in section 6.3.1 and was decided to be a flow restrictor. The flow restrictor is in the hydraulic fluid flow-line connecting the cylinder to an accumulator. The volume flow rate of hydraulic fluid is always a function of the pressure difference across the flow-line containing the hydraulic fluid. There are several ways to model this. The main ways found from the literature are the Darcy-Weisbach equation, the throttle (which is a special case of the Darcy-Weisbach equation), and the orifice. The Darcy-Weisbach equation is first described since it is the most general equation.

7.6.1 Darcy-Weisbach equation

The Darcy-Weisbach equation gives a volume-flow-rate-pressure relationship commonly used for flow-line resistance. This gives volume flow rate for a flow-line with a friction factor influencing the volume flow rate. The Darcy-Weisbach equation is given by:

$$\Delta P = f\frac{L}{D}\frac{\rho V^2}{2} \tag{7.19}$$

where f is friction factor, L is the pipe length, D is the flow-line diameter, ρ is the fluid density, V is the fluid velocity, re-arranging for velocity:

$$V = \sqrt{\frac{2D\Delta P}{Lf\rho}} \tag{7.20}$$

Multiplying with the flow-line cross-sectional area to get volume flow rate

$$Q = \sqrt{\frac{2D\Delta P}{Lf\rho}}A = Q_{\mathrm{r}} \tag{7.21}$$

Since ΔP can be negative or positive the absolute value is taken and the Q term is multiplied with sign(ΔP) so the direction of flow corresponds with the pressure gradient:

$$Q = \mathrm{sign}(\Delta P)\sqrt{\frac{2D|\Delta P|}{Lf\rho}}A = Q_{\mathrm{r}} \tag{7.22}$$

It is important to note that this equation is applicable to laminar and turbulent flows with the friction factor f governing whether the flow is laminar or turbulent. The Darcy-Weisbach equation was used in simulations with the flow being checked if it was in the laminar or turbulent regime and then applying the correct friction factor. Although this is the more accurate approach it was judged not necessary to take such an accurate approach. This is because this adds more variables to the system (such as pipe roughness to calculate the friction factor) which will make it harder to see what part of the system is causing what effect. Thus, it was decided to simplify the system by only assuming laminar flow. This leads to the special case of the Darcy-Weisbach equation, the throttle.

7.6.2 Throttle equation

The equation for the throttle is obtained using the laminar friction factor:

$$f = \frac{64}{\mathrm{Re}} \tag{7.23}$$

Substituting (7.23) into the Darcy-Weisbach relation (7.19) gives:

$$\Delta P = Q\nu\rho\frac{128l_{\mathrm{D}}}{\pi d_{\mathrm{D}}^4} \tag{7.24}$$

where ν is the fluid kinematic viscosity, ρ is the fluid density, Q is the volume flow rate, ΔP is the pressure difference, d_{D} is the diameter of the flow-line, and l_{D} is the length of the flow-line. Re-arranging for volume flow-rate as a function of pressure drop in (7.25):

$$Q = \Delta P \frac{\pi d_{\mathrm{D}}^4}{128 l_{\mathrm{D}} \nu \rho} \tag{7.25}$$

Substituting in the relationship between kinematic and dynamic viscosity gives:

$$Q = \Delta P \frac{\pi d_{\mathrm{D}}^4}{128 l_{\mathrm{D}} \mu} \tag{7.26}$$

The characteristics of the throttle can be altered by changing the flow-line diameter and flow-line length. The dependence on dynamic viscosity gives the throttle a linear flow resistor characteristic. As mentioned the throttle equation assumes laminar flow and assumes a no-slip condition with the wall which means the fluid's viscosity develops the velocity profile. In turn, high shear forces are made and high pressure losses are generated. These energy losses gives a damping effect in the PHCS. This throttle type system has been used for a PHCS by Ni et al. [48].

Lower chamber of cylinder and lower accumulator

Applying (7.26) to the system in Figure 7.3 for the lower chamber of the cylinder and accumulator gives (7.27):

$$Q_{\mathrm{r}} = \frac{\pi d_{\mathrm{f}}^4}{128 \mu l} (P_{\mathrm{p1}} - P_{\mathrm{a1}}) \tag{7.27}$$

where d_{f} is the diameter of the flow-line, μ is the dynamic viscosity, l is the length of the flow-line, P_{p1} is the pressure in the lower chamber of the cylinder, and P_{a1} is the pressure in the accumulator, and to simplify the equation a variable is defined:

$$C_{\mathrm{q,r}} = \frac{\pi d_{\mathrm{f}}^4}{128 \mu l} \tag{7.28}$$

giving:

$$Q_{\mathrm{r}} = C_{\mathrm{q,r}} (P_{\mathrm{p1}} - P_{\mathrm{a1}}) \tag{7.29}$$

Upper chamber of cylinder and upper accumulator

Applying (7.26) to the system in Figure 7.3 for the upper chamber of the cylinder and accumulator gives (7.30):

$$Q_{\mathrm{r,2}} = \frac{\pi d_{\mathrm{f,2}}^4}{128 \mu l_2} (P_{\mathrm{p2}} - P_{\mathrm{a3}}) \tag{7.30}$$

To simplify the equation a variable is defined:

$$C_{\mathrm{q,r,2}} = \frac{\pi d_{\mathrm{f,2}}^4}{128 \mu l_2} \tag{7.31}$$

giving:

$$Q_{\mathrm{r,2}} = C_{\mathrm{q,r,2}} (P_{\mathrm{p2}} - P_{\mathrm{a3}}) \tag{7.32}$$

7.6.3 Orifice equation

To further explore options for the flow-line another flow resistor, the orifice is considered. The working principle of an orifice is that the fluid experiences a sudden transition from a wide to narrow or narrow to wide stream tube [51]. This sudden change in geometry leads to turbulence which gives internal fluid friction and conversion of kinetic energy to heat which manifests as damping in the system [51].

Furthermore, the orifice causes a pressure increase upstream of the orifice, relative to the case if there was no orifice. This pressure increase acts on the piston-head which creates a retarding force or damping force.

An advantage of using the orifice is that it has a stronger effect on a system, relative to the throttle, due to the quadratic relationship between pressure drop and volume flow-rate [51]. A throttle creates a slow transition of the stream tube from wide to narrow and back to wide which is a soft version of an orifice [51]. The throttle characterizes flow-lines and flow-lines are used in this hydraulic system. This means in reality throttle and orifice characteristics apply. Bauer [51] states that when throttle and orifice characteristics exist in parallel it is better to use the prevailing character. It is expected that the orifice character is dominant so only the orifice is used. Assuming an incompressible steady-state flow (Bernoulli's energy equation is used) the volume-flow-rate-pressure equation for an orifice is [55]:

$$Q = C_{\text{discharge}} A \sqrt{\frac{2}{\rho}|\Delta P|}\text{sign}(\Delta P) \tag{7.33}$$

Lower chamber of cylinder and lower accumulator

$$Q_{\text{r}} = C_{\text{discharge}} A \sqrt{\frac{2}{\rho}|\Delta P|}\text{sign}(\Delta P) \tag{7.34}$$

Upper chamber of cylinder and upper accumulator

$$Q_{\text{r,2}} = C_{\text{discharge}} A \sqrt{\frac{2}{\rho}|\Delta P_2|}\text{sign}(\Delta P_2) \tag{7.35}$$

Where $C_{\text{discharge}}$ is the discharge coefficient (0.61) [55], A is the cross-sectional area of the orifice, ΔP is the pressure drop across the orifice, ρ is the density of the hydraulic fluid, and sign(ΔP) is included so that a positive pressure drop corresponds to positive flow (from left to right, from the bottom of the cylinder to accumulator) and vice versa for a negative pressure drop.

The discharge coefficient $C_{\text{discharge}}$ is a function of the Reynolds number [55]. For turbulent flow and increasing Reynolds number $C_{\text{discharge}}$ is relatively constant [55]. To simplify the system, the flow is assumed turbulent which means that a constant value of $C_{\text{discharge}}$ is assumed.

7.7 Pressure equations

7.7.1 Lower chamber of cylinder

The convention for Q is that it is positive from left to right (from cylinder to accumulator) and negative vice versa. This means that if $\Delta P = P_{\text{p1}} - P_{\text{a1}}$ is positive then Q is positive and if ΔP is negative then Q is negative.

The governing equation for P_{p1} is given by (7.36):

$$\dot{P}_{\text{p1}} = \frac{K}{V_{\text{p1,1}}}\Big[- A_{\text{p}}(\dot{z}_1 - \dot{z}_{\text{phc}}) - Q_{\text{r}}\Big] \tag{7.36}$$

The steps to derive (7.36) are described in appendix A.2.

Throttle
(7.36) is adapted to the throttle system using (7.29):

$$\dot{P}_{\text{p1}} = \frac{K}{V_{\text{p1,1}}}\Big[- A_{\text{p}}(\dot{z}_1 - \dot{z}_{\text{phc}}) - C_{\text{q,r}}(\Delta P)\Big] \tag{7.37}$$

Orifice
(7.36) is adapted to the orifice system using (7.34):

$$\dot{P}_{\mathrm{p1}} = \frac{K}{V_{\mathrm{p1,1}}}\Big[- A_{\mathrm{p}}(\dot{z}_1 - \dot{z}_{\mathrm{phc}}) - C_{\mathrm{discharge}} A \sqrt{\frac{2}{\rho}|\Delta P|}\mathrm{sign}(\Delta P)\Big] \tag{7.38}$$

where:

$$\Delta P = P_{\mathrm{p1}} - P_{\mathrm{a1}} \tag{7.39}$$

Since (7.36) is an equation for P_{p1} an initial condition is needed, this is $P_{\mathrm{p1,1}}$. This is defined using the charge pressure $\mathrm{Ps}_{\mathrm{PHC}}$. The initial pressure, $P_{\mathrm{p1,1}}$, should be larger than the charge pressure since the initial pressure is the minimum pressure needed to open the accumulator valve to operate the accumulator. The charge pressure is there so that only a small pressure change is needed to meet the minimum pressure to operate the accumulator. This means the initial pressure $P_{\mathrm{p1,1}}$ is:

$$P_{\mathrm{p1,1}} = 1.11 * \mathrm{Ps}_{\mathrm{PHC}} \tag{7.40}$$

$\mathrm{Ps}_{\mathrm{PHC}}$ is set to 50e5Pa or 50 bar, since the outside water pressure is 250 bar getting 50 bar should be possible.

7.7.2 Upper chamber of cylinder

The upper cylinder is attached to an accumulator. The pressure in the upper cylinder is P_{p2}. The governing equation for P_{p2} is given by (7.41):

$$\dot{P}_{\mathrm{p2}} = \frac{K}{V_{\mathrm{p2,1}}}[-A_{\mathrm{p}}(\dot{z}_{\mathrm{phc}} - \dot{z}_1) - Q_{\mathrm{r,2}}] \tag{7.41}$$

Throttle
(7.41) is adapted to the throttle system using (7.32):

$$\dot{P}_{\mathrm{p2}} = \frac{K}{V_{\mathrm{p2,1}}}[-A_{\mathrm{p}}(\dot{z}_{\mathrm{phc}} - \dot{z}_1) - C_{\mathrm{q,r,2}}(\Delta P_2)] \tag{7.42}$$

Orifice
(7.41) is adapted to the orifice system using (7.35):

$$\dot{P}_{\mathrm{p2}} = \frac{K}{V_{\mathrm{p2,1}}}[-A_{\mathrm{p}}(\dot{z}_{\mathrm{phc}} - \dot{z}_1) - C_{\mathrm{discharge}} A \sqrt{\frac{2}{\rho}|\Delta P_2|}\mathrm{sign}(\Delta P_2)] \tag{7.43}$$

where:

$$\Delta P_2 = P_{\mathrm{p2}} - P_{\mathrm{a3}} \tag{7.44}$$

7.7.3 Lower accumulator

The pressure in the lower accumulator is P_{a1}. Using the isentropic ideal gas law the governing equation for P_{a1} was derived and is given by (7.45):

$$\dot{P}_{\mathrm{a1}} = \frac{P_{\mathrm{a1,1}} n Q_r}{V_{\mathrm{a1,1}}} \tag{7.45}$$

where n is the specific heat ratio.
Throttle
(7.45) is adapted to the throttle system using (7.29):

$$\dot{P}_{\mathrm{a1}} = \frac{P_{\mathrm{a1,1}} n C_{\mathrm{q,r}}(\Delta P)}{V_{\mathrm{a1,1}}} \tag{7.46}$$

Orifice
(7.45) is adapted to the orifice system using (7.34):

$$\dot{P}_{\mathrm{a1}} = \frac{P_{\mathrm{a1},1} n C_{\mathrm{discharge}} A \sqrt{\frac{2}{\rho}|\Delta P|}\mathrm{sign}(\Delta P)}{V_{\mathrm{a1},1}} \tag{7.47}$$

ΔP was defined in (7.39).

7.7.4 Upper accumulator

The pressure in the upper accumulator is P_{a3}. The governing equation for P_{a3} is given by (7.48):

$$\dot{P}_{\mathrm{a3}} = \frac{P_{\mathrm{a3},1} n Q_{\mathrm{r},2}}{V_{\mathrm{a3},1}} \tag{7.48}$$

Throttle
(7.48) is adapted to the throttle system using (7.32):

$$\dot{P}_{\mathrm{a3}} = \frac{P_{\mathrm{a3},1} n C_{\mathrm{q,r},2}(\Delta P_2)}{V_{\mathrm{a3},1}} \tag{7.49}$$

Orifice
(7.48) is adapted to the orifice system using (7.35):

$$\dot{P}_{\mathrm{a3}} = \frac{P_{\mathrm{a3},1} n C_{\mathrm{discharge}} A \sqrt{\frac{2}{\rho}|\Delta P_2|}\mathrm{sign}(\Delta P_2)}{V_{\mathrm{a3},1}} \tag{7.50}$$

ΔP_2 was defined in (7.44).

7.8 Solving the equations

Table 7.2 shows there are 8 variables and 1 input and 8 equations, in principle the system can be solved. The equations were solved using a numerical ODE solver. This was achieved using Simulink. The reason to use Simulink is that the vessel motion model given as a starting point for the thesis was made in Simulink, as mentioned in chapter 4. To ensure that the work of this thesis would be compatible with the vessel model Simulink was used.

The initial conditions are shown in section 7.8.2. Applying these initial conditions the equations can be solved. Initially ode45 was used, this is an explicit solver. The simulation took a long time. It was suspected the system is stiff so ode15s was used, an implicit solver. This was much faster, suggesting the system is stiff. Stiffness generally means the system of equations has two solution variables that vary on significantly different time scales, one has slow and one has fast dynamics [56]. This characterizes the system since there are fast oscillations for Q_{r} whereas z_{c} has slow oscillations for example. Alternatively, a system of equations can be said to be stiff if there is a large separation in the largest and smallest eigenvalues [38].

Table 7.2: Variables

Variables	Equation number
z_1	(7.8)
z_{phc}	(7.12)
z_{c}	(7.15)
z_{d}	(7.18)
P_{p1}	(7.36)
P_{p2}	(7.41)
P_{a1}	(7.45)
P_{a3}	(7.48)
z_{in}	input

7.8.1 The z_{in} variable

The z_{in} variable is a sinusoidal input with a frequency of $\omega = 2\pi/8s = 0.7854$rad/s, a period of 8s is used since this is the peak period of the waves given in the design requirements in section 3.2. The peak period is defined only for irregular waves. Since a lot of the energy in the wave spectrum is at this period it can be taken as the period for a regular wave that approximates the irregular waves. The crane-tip motion will not necessarily have this period but this is a realistic period of what can be expected. The amplitude of the sine wave is 1m.

7.8.2 Initial conditions

For the definitions of the initial condition constants see Figure 7.5. The system is initially at static equilibrium. This means the system initially holds the static weight in water of the hook and payload. This means the initial pressures $P_{\text{p1,1}}$ and $P_{\text{p2,1}}$ need to be defined. From section 6.2.1 the following relation is used from equation (6.11):

$$P_{\Delta\text{p}} = P_{\text{p1,1}} - P_{\text{p2,1}} \tag{7.51}$$

$P_{\text{p1,1}}$ is defined by (7.40). From section 6.2.1, $P_{\Delta\text{p}}$ is obtained from equation (6.12). $P_{\text{p2,1}}$ is found by re-arranging (7.51) and substituting in the knowns $P_{\text{p1,1}}$ and $P_{\Delta\text{p}}$:

$$P_{\text{p2,1}} = P_{\text{p1,1}} - P_{\Delta\text{p}} \tag{7.52}$$

The initial pressure in the accumulator $P_{\text{a1,1}}$ should be equal to the initial pressure at the lower chamber of the cylinder $P_{\text{p1,1}}$ so that the system is in equilibrium. The initial volumes of the lower $V_{\text{p1,1}}$ and upper $V_{\text{p2,1}}$ compartments of the cylinder are equal and such that the piston-head is in the middle of the cylinder. The volume of the accumulator, $V_{\text{a1,1}}$ is chosen as a multiple of $V_{\text{p1,1}}$ with trial and error used to find a suitable value. The initial conditions for the pressure system are summarized in Table 7.3.

For the motion degrees of freedom z_1, z_{phc}, z_{c}, and z_{d} the initial conditions are summarized in Table 7.4.

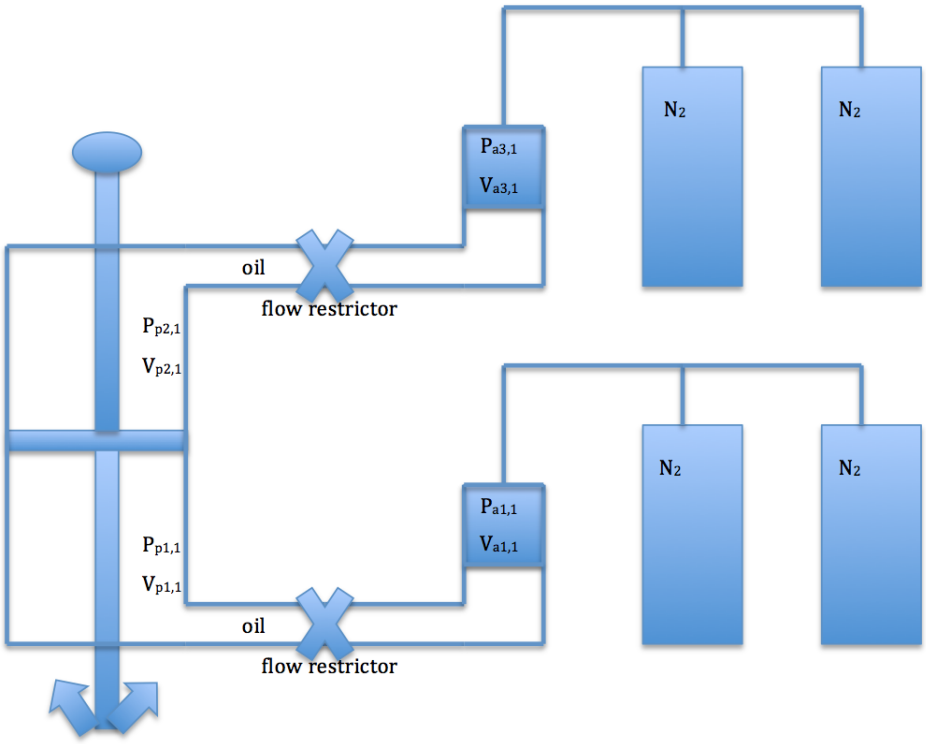

Figure 7.5: Variables for the initial conditions of the pressure system of the PHCS

Table 7.3: Initial conditions for the pressure system

Initial condition constant	Value
$P_{\mathrm{p1,1}}$	$1.11 * \mathrm{Ps_{PHC}}$
$P_{\mathrm{p2,1}}$	$P_{\mathrm{p1,1}} - P_{\Delta \mathrm{p}}$
$P_{\mathrm{a1,1}}$	$P_{\mathrm{p1,1}}$
$P_{\mathrm{a3,1}}$	$P_{\mathrm{p2,1}}$
$V_{\mathrm{p1,1}}$	based on cylinder dimensions
$V_{\mathrm{p2,1}}$	$V_{\mathrm{p1,1}}$
$V_{\mathrm{a1,1}}$	$u * V_{\mathrm{p1,1}}$, u is a positive real number
$V_{\mathrm{a3,1}}$	$V_{\mathrm{a1,1}}$

Table 7.4: Initial conditions for the motions

Variable	Initial condition value
z_1	0[m]
$\dot{z}_1$	0[m/s]
z_{phc}	0[m]
$\dot{z}_{\mathrm{phc}}$	0[m/s]
z_{c}	0[m]
$\dot{z}_{\mathrm{c}}$	0[m/s]
z_{d}	0[m]
$\dot{z}_{\mathrm{d}}$	0[m/s]

7.8.3 State-space equations

The equations above were put into state-space form to determine the eigenvalues. The state variables are shown in Table 7.5.

Table 7.5: State variables and physical variables

state variable	physical variable
q_1	z_1
q_2	$\dot{z}_1 = \dot{q}_1$
q_3	z_{phc}
q_4	$\dot{z}_{\text{phc}} = \dot{q}_3$
q_5	z_c
q_6	$\dot{z}_c = \dot{q}_5$
q_7	z_d
q_8	$\dot{z}_d = \dot{q}_7$
q_9	P_{p2}
q_{10}	P_{a3}
q_{11}	P_{p1}
q_{12}	P_{a1}

The state-space equations are given in the form of (7.53) and (7.54). They were derived in appendix A.3 for the system with the throttle. The throttle was chosen since this is linear. The non-linear water damping terms were linearized. The state-space vectors are shown in (7.55). The state-space matrices are shown in (7.56) and (7.57). The eigenvalues are shown in Table 7.6.

The system of equations represented in the state-space system (7.55), (7.56), and (7.57) represent a stiff system. For the system investigated the eigenvalues are shown in Table 7.6. The magnitude of the largest eigenvalue is 1.3325e+08 and the magnitude of the smallest eigenvalue is 1.5575e-12. This indicates the system is stiff. This supports the earlier assumption for the Simulink model to use a stiff solver.

$$\dot{\mathbf{q}}(t) = \mathbf{A}\mathbf{q}(t) + \mathbf{B}\mathbf{u}(t) \tag{7.53}$$

$$\dot{\mathbf{y}}(t) = \mathbf{C}\mathbf{q}(t) + \mathbf{D}\mathbf{u}(t) \tag{7.54}$$

$$\dot{\mathbf{q}}(t) = \begin{bmatrix} \dot{q}_1 \\ \dot{q}_2 \\ \dot{q}_3 \\ \dot{q}_4 \\ \dot{q}_5 \\ \dot{q}_6 \\ \dot{q}_7 \\ \dot{q}_8 \\ \dot{q}_9 \\ \dot{q}_{10} \\ \dot{q}_{11} \\ \dot{q}_{12} \end{bmatrix}, \mathbf{q}(t) = \begin{bmatrix} q_1 \\ q_2 \\ q_3 \\ q_4 \\ q_5 \\ q_6 \\ q_7 \\ q_8 \\ q_9 \\ q_{10} \\ q_{11} \\ q_{12} \end{bmatrix}, \mathbf{u}(t) = \begin{bmatrix} F_{\text{external}} \\ F_{\text{external,2}} \\ z_{\text{in}} \end{bmatrix}, \dot{\mathbf{y}}(t) = \begin{bmatrix} y_1 \\ y_3 \\ y_5 \\ y_7 \\ y_9 \\ y_{10} \\ y_{11} \\ y_{12} \end{bmatrix} \tag{7.55}$$

$$\mathbf{A} = \begin{bmatrix}
0 & 1 & 0 & 0 & 0 & 0 & 0 & 0 & 0 & 0 & 0 & 0 \\
-\frac{k_{\mathrm{d}}}{\alpha_{\mathrm{hook,payload}}} & -\frac{\beta_{\mathrm{hook,payload}}}{\alpha_{\mathrm{hook,payload}}} & 0 & 0 & 0 & 0 & \frac{k_{\mathrm{d}}}{\alpha_{\mathrm{hook,payload}}} & 0 & \frac{-A_{\mathrm{p}}}{\alpha_{\mathrm{hook,payload}}} & 0 & \frac{A_{\mathrm{p}}}{\alpha_{\mathrm{hook,payload}}} & 0 \\
0 & 0 & 0 & 1 & 0 & 0 & 0 & 0 & 0 & 0 & 0 & 0 \\
0 & 0 & -\frac{k_{\mathrm{c}}}{\alpha_{\mathrm{phc}}} & \frac{-\rho_{\mathrm{water}} C_{\mathrm{d,phc}} D_{\mathrm{phc}} x_{\mathrm{bar,phc}}}{\alpha_{\mathrm{phc}}} & \frac{k_{\mathrm{c}}}{\alpha_{\mathrm{phc}}} & 0 & 0 & 0 & 0 & 0 & 0 & 0 \\
0 & 0 & 0 & 0 & 0 & 1 & 0 & 0 & 0 & 0 & 0 & 0 \\
0 & 0 & \frac{k_{\mathrm{c}}}{M_{\mathrm{c}}} & 0 & \frac{-2k_{\mathrm{c}}}{M_{\mathrm{c}}} & 0 & 0 & 0 & 0 & 0 & 0 & 0 \\
0 & 0 & 0 & 0 & 0 & 0 & 0 & 1 & 0 & 0 & 0 & 0 \\
\frac{k_{\mathrm{d}}}{M_{\mathrm{d}}} & 0 & 0 & 0 & 0 & 0 & \frac{-2k_{\mathrm{d}}}{M_{\mathrm{d}}} & 0 & 0 & 0 & 0 & 0 \\
0 & \frac{KA_p}{V_{\mathrm{p2,1}}} & 0 & -\frac{KA_p}{V_{\mathrm{p2,1}}} & 0 & 0 & 0 & 0 & -\gamma\frac{K}{V_{\mathrm{p2,1}}} & \gamma\frac{K}{V_{\mathrm{p2,1}}} & 0 & 0 \\
0 & 0 & 0 & 0 & 0 & 0 & 0 & 0 & \frac{P_{\mathrm{a3,1}} n\gamma}{V_{\mathrm{a3,1}}} & -\frac{P_{\mathrm{a3,1}} n\gamma}{V_{\mathrm{a3,1}}} & 0 & 0 \\
0 & -\frac{KA_{\mathrm{p}}}{V_{\mathrm{p1,1}}} & 0 & \frac{KA_{\mathrm{p}}}{V_{\mathrm{p1,1}}} & 0 & 0 & 0 & 0 & 0 & 0 & -\frac{K\phi}{V_{\mathrm{p1,1}}} & \frac{K\phi}{V_{\mathrm{p1,1}}} \\
0 & 0 & 0 & 0 & 0 & 0 & 0 & 0 & 0 & 0 & \frac{P_{\mathrm{a1,1}} n\phi}{V_{\mathrm{a1,1}}} & -\frac{P_{\mathrm{a1,1}} n\phi}{V_{\mathrm{a1,1}}}
\end{bmatrix} \tag{7.56}$$

$$\mathbf{B} = \begin{bmatrix}
0 & 0 & 0 \\
\frac{1}{\alpha_{\mathrm{hook,payload}}} & 0 & 0 \\
0 & 0 & 0 \\
0 & \frac{1}{\alpha_{\mathrm{phc}}} & 0 \\
0 & 0 & 0 \\
0 & 0 & \frac{k_{\mathrm{c}}}{M_{\mathrm{c}}} \\
0 & 0 & 0 \\
0 & 0 & \frac{k_{\mathrm{d}}}{M_{\mathrm{d}}} \\
0 & 0 & 0 \\
0 & 0 & 0 \\
0 & 0 & 0 \\
0 & 0 & 0
\end{bmatrix}, \mathbf{C} = \begin{bmatrix}
1 & 0 & 0 & 0 & 0 & 0 & 0 & 0 & 0 & 0 & 0 & 0 \\
0 & 0 & 1 & 0 & 0 & 0 & 0 & 0 & 0 & 0 & 0 & 0 \\
0 & 0 & 0 & 0 & 1 & 0 & 0 & 0 & 0 & 0 & 0 & 0 \\
0 & 0 & 0 & 0 & 0 & 0 & 1 & 0 & 0 & 0 & 0 & 0 \\
0 & 0 & 0 & 0 & 0 & 0 & 0 & 0 & 1 & 0 & 0 & 0 \\
0 & 0 & 0 & 0 & 0 & 0 & 0 & 0 & 0 & 1 & 0 & 0 \\
0 & 0 & 0 & 0 & 0 & 0 & 0 & 0 & 0 & 0 & 1 & 0 \\
0 & 0 & 0 & 0 & 0 & 0 & 0 & 0 & 0 & 0 & 0 & 1
\end{bmatrix}, \mathbf{D} = \begin{bmatrix}
0 & 0 & 0 \\
0 & 0 & 0 \\
0 & 0 & 0 \\
0 & 0 & 0 \\
0 & 0 & 0 \\
0 & 0 & 0 \\
0 & 0 & 0 \\
0 & 0 & 0
\end{bmatrix} \tag{7.57}$$

Table 7.6: Eigenvalues and natural frequencies

Eigenvalue λ	Natural frequency ω_n	Stable?
-1.3325e+8	0	stable
-1.3324e+8	0	stable
-1.0691e-2 + 2.2361e+0i	4.7810e-3	stable
-1.0691e-2 - 2.2361e+0i	4.7810e-3	stable
-8.4639e-7 + 6.6028e-1i	1.2819e-6	stable
-8.4639e-7 - 6.6028e-1i	1.2819e-6	stable
-1.3947e-1 + 7.9705e-2i	8.6823e-1	stable
-1.3947e-1 - 7.9705e-2i	8.6823e-1	stable
-4.5983e-2 + 1.5198e-1i	2.8959e-1	stable
-4.5983e-2 - 1.5198e-1i	2.8959e-1	stable
1.8514e-11	0	marginally unstable
-1.5575e-12	0	stable

7.9 Various design iterations

Various design iterations for the PHCS with two accumulators, shown in Figure 7.3, with different flow restrictors were needed, trying the throttle and orifice iteratively. This is explained by the flow-chart shown in the design approach in chapter 3, the flow-chart is repeated in Figure 7.6. The 'Flawed Model Detected' part on the right of the flow-chart was encountered in this process. The modification was not so extreme to go back to the problem description, instead the red line was followed and a different 'Simulation Model' was used.

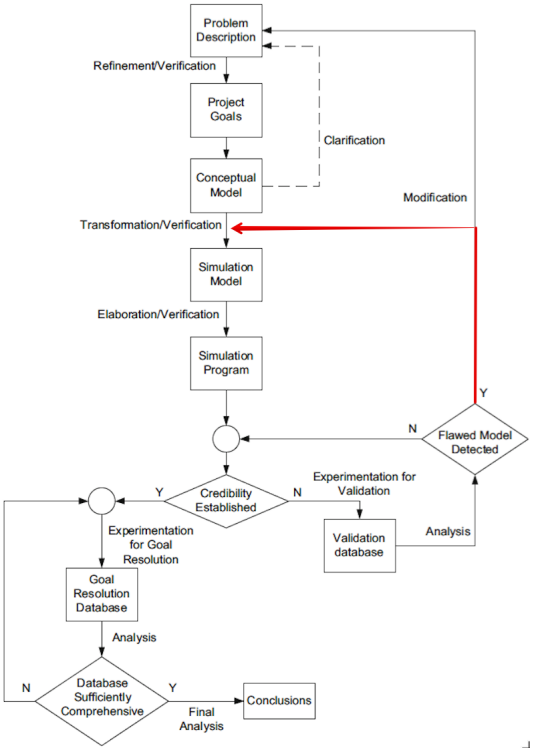

Figure 7.6: Design iteration loop shown [38]

7.9.1 Throttle

The throttle was first used as the flow restrictor. The results are summarized here and the full results are in appendix A.4. The results were poor. V_{p2} and P_{p2} are in phase which is not physical. If the upper cylinder volume shrinks the pressure should increase. This can be attributed to the rod's position (z_1) being unbounded, in the sense that it ignores the confines of the cylinder and is able to go through the cylinder top. Spring stoppers were added to improve the behavior. The spring stoppers did improve the behavior, with a spring stiffness of 6e8N/m used, but this is an undesirable solution. This is because repeated hitting of the spring stoppers would fatigue the system. Thus, the spring stiffeners are a last resort. These should only be used for a rogue wave condition and should not be expected to be used in normal operation. It is better to adjust the stiffness of the system which is governed by accumulator volume. This was done in appendix A.4.3 and it was found there was no accumulator volume found suitable to prevent the piston from hitting the stopper springs. This was considered as reaching the 'Flawed Model Detected' block and meeting the condition such that the next step is to change the 'Simulation Model'. This was implemented by deciding to use the orifice as the flow restrictor, see section 7.9.2.

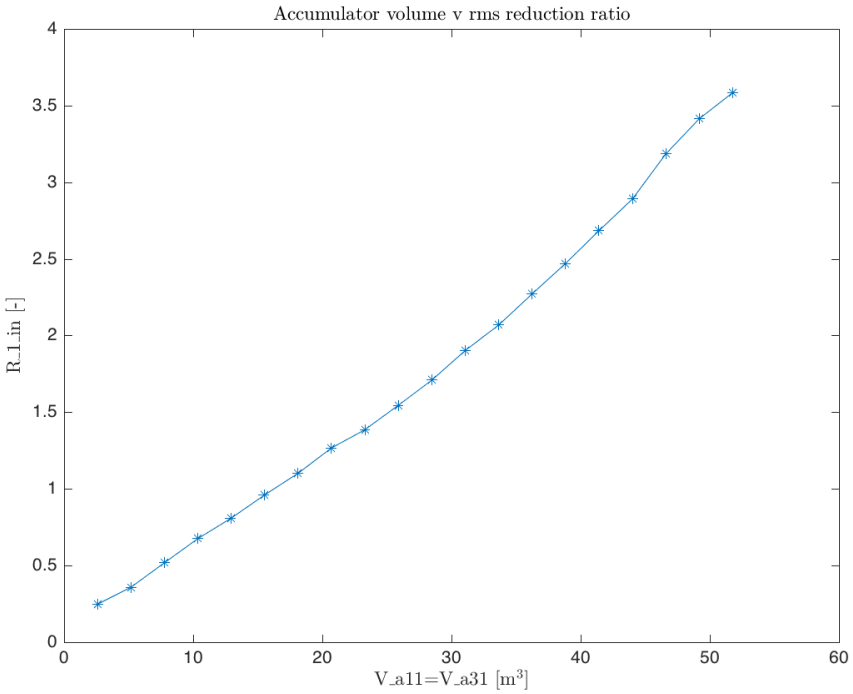

Figure 7.7: Throttle: rms reduction ratio as function of accumulator volume

7.9.2 Orifice

The orifice was used. The results could be improved. It was believed there was poor sizing and dimensions of the system. To solve this, the orifice is removed and the throttle is used again such that the system does not have the non-linear orifice. This should simplify the dynamics of the system and enabled the pressure system to be dimensioned better. This was considered as reaching the 'Flawed Model Detected' block and meeting the condition such that the next step is to change the 'Simulation Model'. This was implemented by deciding to use the throttle as the flow restrictor again, this is done in section 7.9.3.

7.9.3 Throttle again

The throttle was used again since it has weaker characteristics compared to the orifice. This will make it simpler to size the pressure system. The effect of the accumulator volume is investigated. The results are summarized here and the full results are in appendix A.5. A sinusoidal heave input for z_{in} is used. To measure the effectiveness of the PHCS the rms reduction ratio R is used, described in section 11.3.3. R should be smaller than one for an effective PHCS. The closer R is to 0 means better effectiveness. A larger accumulator volume should provide better attenuation of z_1 motion, this means the rms reduction ratio R is lower. See Figure 7.7. The R value increases since there is a large oscillation in z_1 for the first approximately 20s that lowers in amplitude thereafter. This is not the expected behavior of the system. With increasing accumulator volume, the initial amplitude of z_1 increases. The large oscillation is due to the large amplitude pressure signals that occur initially. In contrast, the amplitude of the pressure signals are smaller for the orifice system for the same time period and accumulator volume. The pressures control the movement of the piston which in turn controls the movement of the payload. An explanation for the large pressure amplitude is that the throttle type system is quite sensitive to the pipe diameter and pipe length. Thus it is likely the combination of pipe diameter and pipe length is not suitable and the influence of the correct pipe diameter and pipe length may be critical. The throttle is not investigated further since the orifice system has more promising results.

7.9.4 Orifice again

The orifice is chosen for further investigation since it provides better attenuation of motion. The orifice system also physically provides a better mechanism compared to the throttle. A figure of R against the lower accumulator volume (both accumulators have same volumes) is shown in Figure 7.8. There is no trend like in the case for the system with the throttle (see Figure 7.7). This can be explained by the more complicated dynamics of the orifice. For the throttle, the flow rate is proportional to the pressure drop. In contrast, the orifice system has the flow rate proportional to the square root of the pressure drop. Nevertheless, the orifice shows superior performance with the R value at V_a11≈40 m^3 being the lowest of both systems for the accumulator volume range plotted.

The orifice system produces hydraulic oil flow rates (Q_r and $Q_{r,2}$) that vary extremely high in peak-to-trough values and have very high frequency. This results in the pressure P_{p2} also having highly varying peak-to-trough values and high frequency. The reason for the high peak-to-trough values is that the hydraulic oil does not have any inertia. This means for a pressure change the fluid reacts without restraint resulting in high peak-to-trough values. With fluid inertia added, it takes more effort to accelerate the fluid and make the fluid move so that the flow-rate cannot vary greatly in magnitude with a pressure change. This results in the pressure P_{p2} changing with a lower peak-to-trough value. In section 7.10, fluid inertia is added to the equations governing pressure drop across the orifice and hydraulic oil flow.

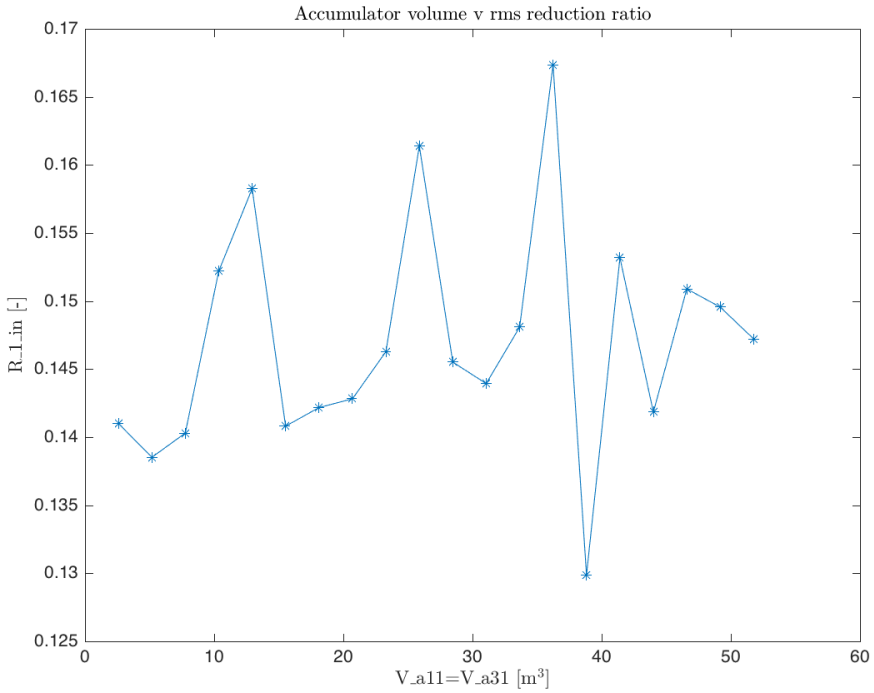

Figure 7.8: Orifice: rms reduction ratio as function of accumulator volume

7.10 Adding fluid inertia

7.10.1 Description of fluid inertia

The equation for pressure as a function of volume flow rate is in equation (7.58):

$$\frac{V}{E}\dot{P} = Q_{in} - Q_{out} \tag{7.58}$$

where V is the volume of the control volume, E is the bulk modulus of the fluid, P is the pressure in the control volume, Q_{in} is volume flow rate into the control volume, and Q_{out} is volume flow rate out of the control volume.

The equation for fluid inertia is in equation (7.59):

$$\rho_{\text{oil}} \frac{L}{A} \dot{Q} = P_{\text{in}} - P_{\text{out}} \tag{7.59}$$

where ρ_{oil} is density of hydraulic oil, L is the orifice length, A is the orifice passage area, Q is the volume flow rate, P_{in} is the pressure upstream of the orifice, and P_{out} is the pressure downstream of the orifice.

From ISO 5167 [57], for a Venturi type orifice the orifice diameters considered are from 0.05m to 0.50m. Assuming these are reasonable diameters for cylinder systems an orifice diameter of 0.15m is chosen so that it falls within the range and not far from the minimum and maximum values. The inertia I is given by:

$$I = \rho_{\text{oil}} \frac{L}{A} \tag{7.60}$$

The orifice length L is used to take into account the added volumes on the two sides of the orifice. To ensure sufficient inertia $L = 3.12\text{m}$ is taken. This gives an inertia of:

$$I = (859\text{kg/m}^3) \frac{3.12\text{m}}{0.25 * \pi * (0.15\text{m})^2} = 1.52\text{e}5\text{kg/m}^4 \tag{7.61}$$

7.10.2 Final non-linear equations: bottom accumulator

See appendix A.6 for the derivation of the non-linear equations for the bottom accumulator. The final equations are 3 differential equations (7.62) (7.63) (7.64) and 1 algebraic equation (7.65) for 4 unknowns P_{p1}, Q_{r}, V_{in}, and P_{a1} so the system is closed. $\dot{z}_1$ and $\dot{z}_{\text{phc}}$ are known as inputs. Constants are K, $V_{\text{p1,1}}$, A_{p}, $P_{\text{a1,1}}$, $V_{\text{a1,1}}$, A, ρ_{oil}, L, and $C_{\text{discharge}}$. These equations are solved numerically for the time-domain simulations:

$$\dot{P}_{\text{p1}} = \frac{K}{V_{\text{p1,1}}} \Big[- A_{\text{p}}(\dot{z}_1 - \dot{z}_{\text{phc}}) - Q_{\text{r}} \Big] \tag{7.62}$$

$$\dot{Q}_{\text{r}} = \frac{A}{\rho_{\text{oil}} L} \Big[P_{\text{p1}} - P_{\text{a1}} - \frac{\text{sign}(Q_{\text{r}}) Q_{\text{r}}^2}{(C_{\text{discharge}} A)^2} \frac{\rho_{\text{oil}}}{2} \Big] \tag{7.63}$$

$$\dot{V}_{\text{in}} = Q_{\text{r}} \tag{7.64}$$

$$P_{\text{a1}} = P_{\text{a1,1}} \Big(\frac{V_{\text{a1,1}}}{V_{\text{a1,1}} - V_{\text{in}}} \Big)^n \tag{7.65}$$

7.10.3 Final non-linear equations: upper accumulator

See appendix A.7 for the derivation of the non-linear equations for the upper accumulator. The final equations are 3 differential equations (7.66) (7.67) (7.68) and 1 algebraic equation (7.69) for 4 unknowns P_{p2}, $Q_{\text{r,2}}$, $V_{\text{in,u}}$, and P_{a3} so the system is closed. $\dot{z}_1$ and $\dot{z}_{\text{phc}}$ are known as inputs. Constants are K, $V_{\text{p2,1}}$, A_{p}, $P_{\text{a3,1}}$, $V_{\text{a3,1}}$, A, ρ_{oil}, L, and $C_{\text{discharge}}$. These equations are solved numerically for time-domain simulations:

$$\dot{P}_{\text{p2}} = \frac{K}{V_{\text{p2,1}}} [-A_{\text{p}}(\dot{z}_{\text{phc}} - \dot{z}_1) - Q_{\text{r,2}}] \tag{7.66}$$

$$\dot{Q}_{\text{r,2}} = \frac{A}{\rho_{\text{oil}} L} \Big[P_{\text{p2}} - P_{\text{a3}} - \frac{\text{sign}(Q_{\text{r,2}}) Q_{\text{r,2}}^2}{(C_{\text{discharge}} A)^2} \frac{\rho_{\text{oil}}}{2} \Big] \tag{7.67}$$

$$\dot{V}_{\text{in,u}} = Q_{\text{r,2}} \tag{7.68}$$

$$P_{a3} = P_{a3,1}\left(\frac{V_{a3,1}}{V_{a3,1} - V_{in,u}}\right)^n \tag{7.69}$$

7.10.4 Non-linear equations

The non-linear equations for the pressure system from section 7.10.2 and 7.10.3, and the equations for the hook/payload mass, PHCS mass, steel rope, and Dyneema rope from section 7.5 are collected and shown in appendix A.8. This set of equations forms the finalized PHCS model. The diagram corresponding to this system is shown in Figure 7.9.

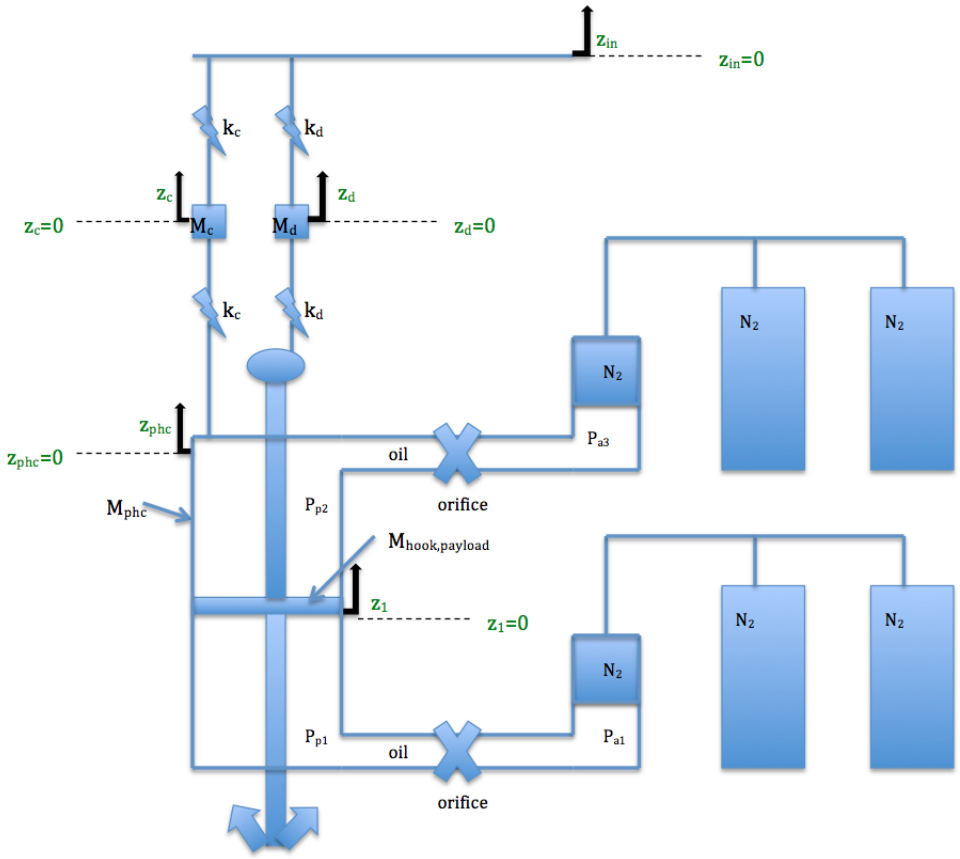

Figure 7.9: Schematic of the PHCS with two accumulators and orifices, fluid inertia is included in the model

7.10.5 Non-linear state-space equations

The non-linear equations in appendix A.8 are put into state-space form in appendix A.9. The variables are simplified for easier readability in appendix A.10.

7.10.6 Linearized state-space equations

The state-space equations with non-linear terms are linearized in appendix A.11 with the resulting linearized state-space equations shown in appendix A.12. The non-linear terms that were linearized were the orifices, the accumulators, and the quadratic damping terms.

7.10.7 A matrix from linearized state-space equations

The state-space equations from appendix A.12 are re-arranged into matrix form in appendix A.12.15. What is important is the **A** matrix which is shown in (7.70). From (7.70) the eigenvalues can be

determined.

$$\mathbf{A} = \begin{bmatrix} 0 & 1 & 0 & 0 & 0 & 0 & 0 & 0 & 0 & 0 & 0 & 0 & 0 & 0 \\ \frac{-k_{\mathrm{d}}}{\alpha_2} & \frac{-\gamma_2}{\alpha_2} & 0 & 0 & 0 & 0 & \frac{k_{\mathrm{d}}}{\alpha_2} & 0 & \frac{A_{\mathrm{p}}}{\alpha_2} & 0 & 0 & \frac{-A_{\mathrm{p}}}{\alpha_2} & 0 & 0 \\ 0 & 0 & 0 & 1 & 0 & 0 & 0 & 0 & 0 & 0 & 0 & 0 & 0 & 0 \\ 0 & 0 & \frac{-k_{\mathrm{c}}}{\alpha_4} & \frac{-\gamma_4}{\alpha_4} & \frac{k_{\mathrm{c}}}{\alpha_4} & 0 & 0 & 0 & 0 & 0 & 0 & 0 & 0 & 0 \\ 0 & 0 & 0 & 0 & 0 & 1 & 0 & 0 & 0 & 0 & 0 & 0 & 0 & 0 \\ 0 & 0 & \frac{k_{\mathrm{c}}}{M_{\mathrm{c}}} & 0 & \frac{-2k_{\mathrm{c}}}{M_{\mathrm{c}}} & 0 & 0 & 0 & 0 & 0 & 0 & 0 & 0 & 0 \\ 0 & 0 & 0 & 0 & 0 & 0 & 0 & 1 & 0 & 0 & 0 & 0 & 0 & 0 \\ \frac{k_{\mathrm{d}}}{M_{\mathrm{d}}} & 0 & 0 & 0 & 0 & 0 & \frac{-2k_{\mathrm{d}}}{M_{\mathrm{d}}} & 0 & 0 & 0 & 0 & 0 & 0 & 0 \\ 0 & \frac{-KA_{\mathrm{p}}}{V_{\mathrm{p1,1}}} & 0 & \frac{KA_{\mathrm{p}}}{V_{\mathrm{p1,1}}} & 0 & 0 & 0 & 0 & 0 & \frac{-K}{V_{\mathrm{p1,1}}} & 0 & 0 & 0 & 0 \\ 0 & 0 & 0 & 0 & 0 & 0 & 0 & 0 & \frac{A}{\rho_{\mathrm{oil}}L} & \frac{-A\epsilon_{10}}{\rho_{\mathrm{oil}}L} & \frac{-A\gamma_{10}}{\rho_{\mathrm{oil}}L} & 0 & 0 & 0 \\ 0 & 0 & 0 & 0 & 0 & 0 & 0 & 0 & 0 & 1 & 0 & 0 & 0 & 0 \\ 0 & \frac{KA_{\mathrm{p}}}{V_{\mathrm{p2,1}}} & 0 & \frac{-KA_{\mathrm{p}}}{V_{\mathrm{p2,1}}} & 0 & 0 & 0 & 0 & 0 & 0 & 0 & 0 & \frac{-K}{V_{\mathrm{p2,1}}} & 0 \\ 0 & 0 & 0 & 0 & 0 & 0 & 0 & 0 & 0 & 0 & 0 & \frac{A}{\rho_{\mathrm{oil}}L} & \frac{-A\epsilon_{13}}{\rho_{\mathrm{oil}}L} & \frac{-A\gamma_{13}}{\rho_{\mathrm{oil}}L} \\ 0 & 0 & 0 & 0 & 0 & 0 & 0 & 0 & 0 & 0 & 0 & 0 & 1 & 0 \end{bmatrix} \tag{7.70}$$

7.11 Conclusion

The system with the orifice as the flow restrictor and two accumulators with fluid inertia is the final model. Fluid inertia was added to smoothen the pressure and hydraulic oil flow-rates. In section 7.3 some hypotheses were made, these are repeated below.

1. The lack of an accumulator at the top of the cylinder is hypothesized to contribute to there being a large difference in amplitude between the pressures P_{p1} and P_{p2}. It is hypothesized that the amplitudes will be more similar with the new design.

2. The lack of the accumulator is hypothesized to contribute to the pressures P_{p1} and P_{a1} not being out of phase significantly. It is hypothesized that they will be more out of phase.

From the developments in this chapter, comments on each statement above can be made

1. There is a larger difference in amplitude between the pressures P_{p1} and P_{p2}. This is opposite to what was hypothesized. It was believed that adding an accumulator would make the pressures more similar in amplitude since each accumulator acts as a soft spring and the symmetry of having an accumulator on each side of the cylinder would make their amplitudes more similar. This turned out to be a wrong hypothesis. This is not a large issue since although there is a large difference in amplitude between the pressures P_{p1} and P_{p2} the system still works.

2. The pressures P_{p1} and P_{a1} are still not more out of phase. The hypothesis that the new design would make the pressures more out of phase is wrong. This is not a significant issue since the pressures are still out of phase slightly and sufficiently.

The motion response is shown in Figure 7.10. The amplitude of z_{d}, the motion of the Dyneema, is larger than for z_{c}. This is expected since the Dyneema rope acts as a softer spring than the steel rope so has a larger response.

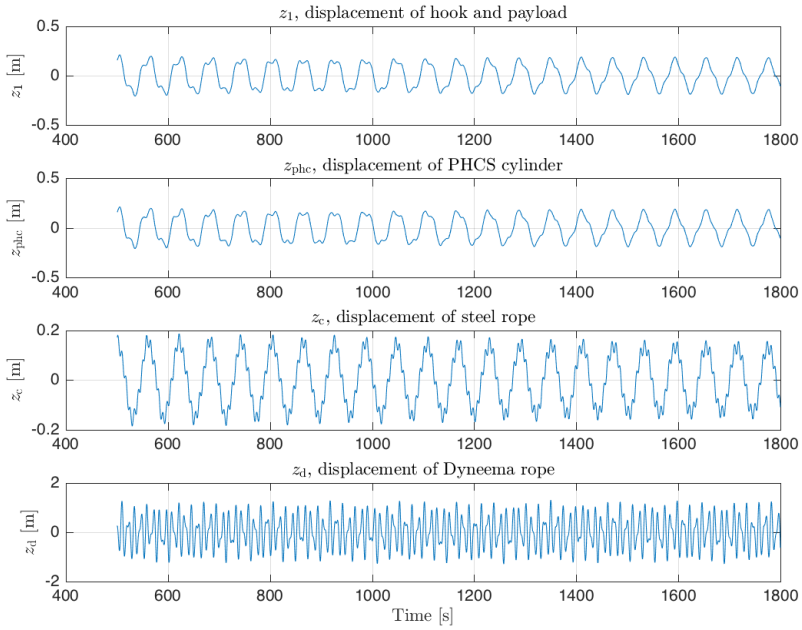

Figure 7.10: Time-series for z_1, z_{phc}, z_{c}, and z_{d} are shown

In this chapter, the design and model of the PHCS were finalized. To do this, first the PHCS with one accumulator was considered with the throttle, the orifice, and the Darcy-Weisbach system used as flow restrictors. The Darcy-Weisbach system was eliminated. Another accumulator was added to the PHCS and the throttle and orifice investigated. Analysis was done to come to the conclusion that the orifice system is most suitable. This led to the final design of two accumulators with the orifice used as the flow restrictor. For the model, fluid inertia was added to smoothen the hydraulic oil volume flow rates and system pressures. This is part of step 3 of the methodology in section 3.3. In chapter 8 the methodology is continued by sizing the pressure system.

Sizing of pressure system 8

8.1 Introduction

The final PHCS model described in section 7.10.4 and shown in Figure 7.9 is used. To size the pressure system, the volumes and pressures, the PHCS is simplified until just the linearized accumulators and hook/payload mass is present, shown in Figure 8.1. This model is called the LAM.

8.2 Sizing of the pressure system

An important part of the PHCS is the sizing of the pressures and volumes of the accumulators. This is done using a more rigorous method in this section, via a hydraulic reference book from Bosch Rexroth [58], compared to the trial and error approach in chapter 7. The pressures and volumes of the accumulators were sized such that their natural frequencies are not encountered in operation. This is important to avoid the counter-productive effect that the PHCS gets excited by the waves via resonance and causes an increase in the motion of the hook/payload. The approach taken was:

1. Choose a natural frequency of the system that is outside the wave frequency range
2. Simplify the system by removing the flow restrictors so that two pressures are removed (P_{p2} and P_{p1}) and the steel rope and Dyneema rope are not included. Assume the hydraulic oil is incompressible so a direct connection exists between the piston-head and the accumulators. These leaves the system with just accumulators. A diagram of the system is shown in Figure 8.1.
3. Size the accumulator pressure and volume to get the natural frequency chosen in step 1. Do this for three hook positions in the cylinder.

The above steps are done in section 8.2. The initial conditions found for the base case, which is the general case, are shown in Table 8.1. A diagram with the variables is shown in Figure 8.2.

For the equations of motion of the system and state-space equations see appendix A.13. The natural frequencies of the system are found from the $\mathbf{A}$ matrix.

Table 8.1: Base case, the variables are shown in Figure 8.2

Variable	Value	Unit	Note
$PS_{PHC,lower}$	1.8e7	[N/m^2]	Charge pressure, lower accumulator
$PS_{PHC,upper}$	8.2722e+05	[N/m^2]	Charge pressure, upper accumulator
$d_{p,tot}$	0.3	[m]	Diameter of piston-head
$P_{\Delta p}$	1.9081e+07	[N/m^2]	Difference in pressure across piston-head required to hold payload and hook in water
$P_{a1,1}$	2e7	[N/m^2]	Initial pressure in the lower accumulator
$P_{a3,1}$	9.1913e+05	[N/m^2]	Initial pressure in the upper accumulator, $P_{a3,1} = P_{a1,1} - P_{\Delta p}$
$V_{a1,1}$	0.1950	[m^3]	Initial volume in lower accumulator
$V_{a3,1}$	0.1769	[m^3]	Initial volume in upper accumulator

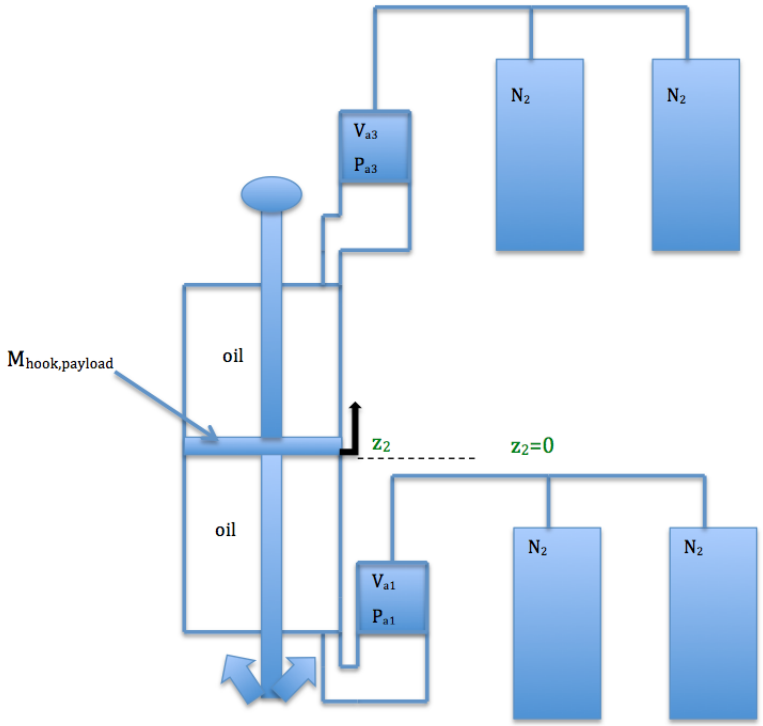

Figure 8.1: A diagram of the PHCS with just accumulators

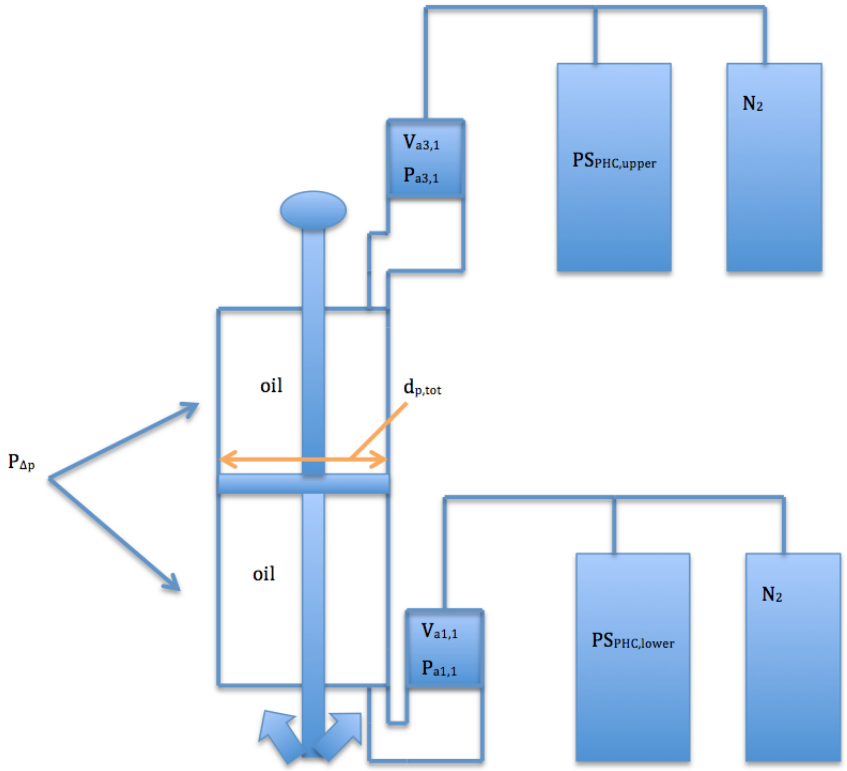

Figure 8.2: A diagram showing the variables defined in Table 8.1

8.2.1 Sizing the system

Assumptions for the accumulators

- Isentropic process (adiabatic and reversible)
- Gas charging is done at the same temperature as operating temperature
- Ideal gas is assumed
- Specific heat ratio for nitrogen is $n = 1.4$

The key pressure and volume parameters are in Table 8.2.

Table 8.2: Key variables

Variable	Unit	Note
P_1	[N/m^2]	minimum pressure to open the fluid valve
P_0	[N/m^2]	charging pressure of the gas space with fluid space depressurized ($P_0 \leq 0.9P_1$)
P_2	[N/m^2]	maximum operating pressure of the hydraulic system
$\frac{P_2}{P_0}$	[-]	maximum operating pressure ratio
V_0	[m^3]	effective gas volume at charging pressure
V_1	[m^3]	gas volume at minimum pressure
V_2	[m^3]	gas volume at maximum operating pressure
ΔV	[m^3]	useful volume

The accumulator is a hydro-pneumatic accumulator that is of the bladder-type. For an isentropic process

the gas volume corresponding to the initial condition is defined by V_0 which is given by (8.1) [58]:

$$V_0 = \frac{\Delta V}{\left(\frac{P_0}{P_1}\right)^{\frac{1}{n}} - \left(\frac{P_0}{P_2}\right)^{\frac{1}{n}}} \tag{8.1}$$

8.2.1.1 Lower accumulator

For the base case, the lower accumulator ΔV, the useful volume, is determined by the volume between the middle position and the bottom spring stoppers. Referenced from the bottom of the cylinder (where the spring stoppers start) the middle position is 50% of the maximum stroke. This means the useful length is L_{useful} in equation (8.2):

$$L_{\text{useful}} = 0.5L_{\text{max,stroke}} - 0L_{\text{max,stroke}} = 0.5L_{\text{max,stroke}} \tag{8.2}$$

With the diameter of the piston-head given by $d_{\text{p,tot}}$ then:

$$\Delta V = L_{\text{useful}}(0.25\pi d_{\text{p,tot}}^2) \tag{8.3}$$

The general process to find the pressures and volumes and other values in Table 8.2 is described for the lower accumulator. First L_{useful} is found. The stroke of the cylinder is $L_{\text{max,stroke}}$= 3m since this is a reasonable length when compared to a comparable Cranemaster PHCS. Then L_{useful} is calculated from (8.2). Second, a value for P_1 and $d_{\text{p,tot}}$ is assumed. P_1 is the initial pressure in the lower accumulator, $P_1 = P_{\text{a1,1}}$. This pressure determines the initial volume of the lower accumulator. According to [58] it is necessary that:

$$P_0 \leq 0.9P_1 \tag{8.4}$$

then it is assumed:

$$P_0 = 0.9P_1 \tag{8.5}$$

The value of P_2 is assumed based on a general value for maximum operating pressure, 6e7N/m^2. This means $\frac{P_2}{P_0}$ can be found. A condition according to [58] is that:

$$\frac{P_2}{P_0} \leq 4 \tag{8.6}$$

this condition is checked for. If this condition is not met, then P_2 is decreased until the condition is met. ΔV is calculated using (8.3) as a function of $d_{\text{p,tot}}$ and L_{useful}. Using (8.1) V_0 is calculated as a function of ΔV, P_0, P_1, and P_2. Using the isentropic relationship:

$$P_0 V_0^n = P_1 V_1^n \tag{8.7}$$

the volume V_1 is calculated as a function of V_0, P_0, and P_1.

V_2 is found using the isentropic relationship:

$$P_1 V_1^n = P_2 V_2^n \tag{8.8}$$

as a function of V_1, P_1, and P_2 or equivalently:

$$V_2 = V_1 - \Delta V \tag{8.9}$$

8.2.1.2 Upper accumulator

For the base case, the upper accumulator ΔV, the useful volume, is determined by the volume between the middle position and upper spring stoppers. Referenced from the upper spring stoppers the middle position is 50% of the maximum stroke. This means the useful length is L_{useful} in equation (8.10):

$$L_{\text{useful}} = L_{\text{max,stroke}} - 0.5L_{\text{max,stroke}} = 0.5L_{\text{max,stroke}} \tag{8.10}$$

$$\Delta V = L_{\text{useful}}(0.25\pi d_{\text{p,tot}}^2) \tag{8.11}$$

For the upper accumulator the initial pressure P_1 ($P_1 = P_{\text{a3,1}}$) is determined $P_1 = P_{\text{a1,1}} - P_{\Delta\text{p}}$, where $P_{\Delta\text{p}}$ is the pressure difference across the piston-head necessary to hold the static weight in water of the hook and payload given by:

$$P_{\Delta\text{p}} = \frac{(M_{\text{hook,payload}} - \rho_{\text{w}} V_{\text{d}})g}{A_{\text{p}}} \tag{8.12}$$

Thus, the upper accumulator initial pressure is dependent on the lower accumulator initial pressure. Then:

$$P_0 = 0.9P_1 \tag{8.13}$$

The value of P_2 is assumed based on a general value for maximum operating pressure, 6e7N/m^2. This means $\frac{P_2}{P_0}$ can be found. A condition according to [58] is that:

$$\frac{P_2}{P_0} \leq 4 \tag{8.14}$$

this condition is checked for. If this condition is not met, then P_2 is decreased until the condition is met. ΔV is calculated using (8.11) as a function of $d_{\text{p,tot}}$ and L_{useful}. Using (8.1) V_0 is calculated as a function of ΔV, P_0, P_1, and P_2. Using the isentropic relationship:

$$P_0 V_0^n = P_1 V_1^n \tag{8.15}$$

the volume V_1 is calculated as a function of V_0, P_0, and P_1. V_2 is found using the isentropic relationship:

$$P_1 V_1^n = P_2 V_2^n \tag{8.16}$$

as a function of V_1, P_1, and P_2 or equivalently:

$$V_2 = V_1 - \Delta V \tag{8.17}$$

8.2.2 Designed for natural frequency

The design wave condition has T_{p}=8s. This is a frequency of 0.125Hz or circular frequency 0.7854rad/s. The wave periods that can be encountered in real-life are assumed to be from 25s to 5s with corresponding frequencies of 0.04Hz to 0.2Hz. The designed for natural frequency should have a period outside this range, T=3s, this is a frequency $f_{\text{design}} = 0.33$Hz or circular frequency $\omega_{\text{design}} = 2.0944$rad/s. It is better to have a natural frequency higher than the range of wave frequencies. This is because the system has damping. If the natural frequency is excited the high frequency means there are many cycles of motion to remove energy helping to limit the excitation.

8.2.3 Base case initial conditions

The base case is where the piston-head is at the middle position of the cylinder. The piston-head is $0.5L_{\text{max,stroke}}$ from the bottom of the cylinder. Using the methods described in sections 8.2.1.1 and 8.2.1.2 the accumulators are dimensioned.

8.2.3.1 Lower accumulator dimensions

Values for the parameters in Table 8.2 are found in Table 8.3 for the lower accumulator using the process described in section 8.2.1.1.

It is a necessary condition that the initial lower accumulator pressure, P_1, is greater than $P_{\Delta\text{p}}$ since the initial upper accumulator pressure is given by the difference $P_1 - P_{\Delta\text{p}}$ and pressure must be non-negative. Since $P_{\Delta\text{p}}$ is a function of piston area and thus piston diameter, $d_{\text{p,tot}}$, then two variables (P_1 and $d_{\text{p,tot}}$)

are changed to change the natural frequency of the hook and payload mass with displacement z_2. The range of values used for P_1 was:

$$0.5\text{e}7\text{N/m}^2 \leq P_1 \leq 7\text{e}7\text{N/m}^2 \tag{8.18}$$

(rising in steps of $0.01\text{e}7\text{N/m}^2$). This maximum is above what would be designed for ($P_{\max}$=$6\text{e}7\text{N/m}^2$) but is used to see any trends. The range of values for $d_{\text{p,tot}}$ was:

$$0.10\text{m} \leq d_{\text{p,tot}} \leq 0.40\text{m} \tag{8.19}$$

(rising in steps of 0.01m). It was found for the range:

$$0.1\text{m} \leq d_{\text{p,tot}} \leq 0.17\text{m} \tag{8.20}$$

that $P_{\Delta\text{p}} > P_{\max}$ which means the required pressure difference to hold the static weight of the hook and payload for the diameter exceeded the maximum pressure possible. Thus the pressure difference cannot be achieved even if one chamber of the cylinder is a vacuum. Thus, the diameters:

$$0.1\text{m} \leq d_{\text{p,tot}} \leq 0.17\text{m} \tag{8.21}$$

are not considered further.

A reasonable diameter value is 0.3m. This will be assumed as the diameter. See Figure 8.3 for natural frequency as a function of P_1 for $d_{\text{p,tot}} = 0.3\text{m}$. Using P_1=$2.0\text{e}7\text{N/m}^2$ the natural frequency is 2.2269rad/s this is close the design natural frequency. Since $P_{\Delta\text{p}} = 1.9\text{e}7\text{N/m}^2$ and P_1=$2.0\text{e}7\text{N/m}^2$ is greater than this then P_1=$2.0\text{e}7\text{N/m}^2$ is used.

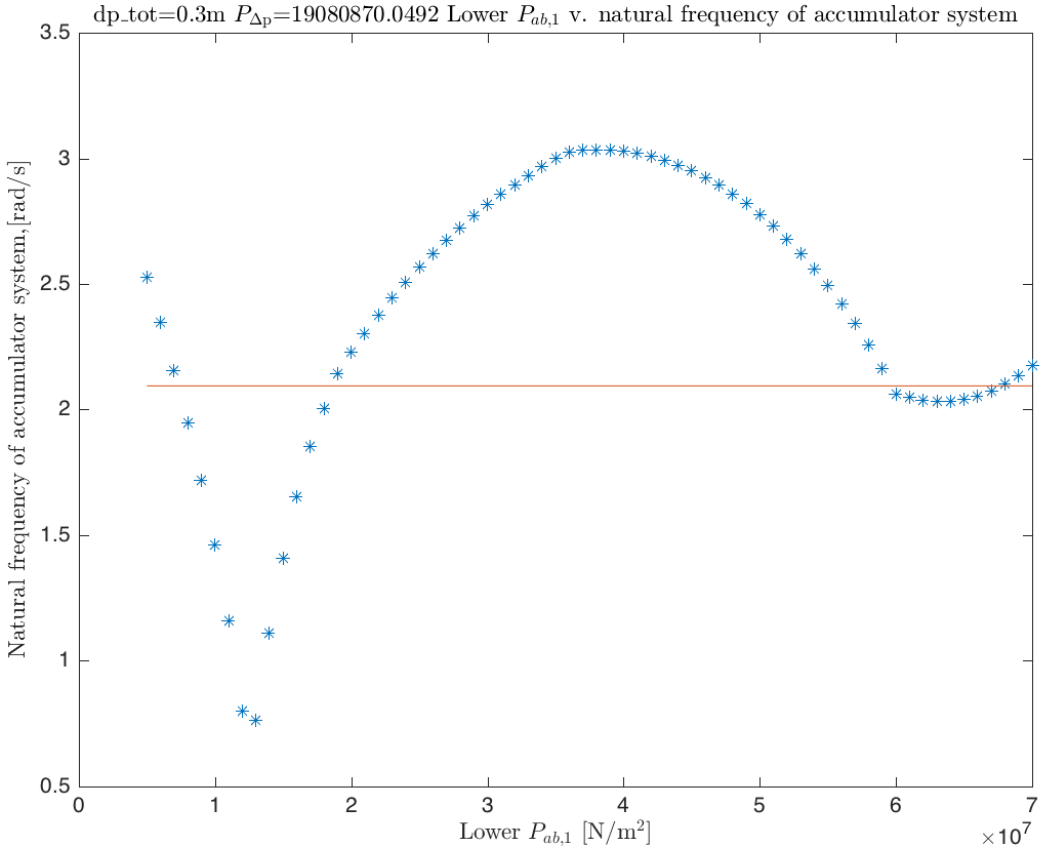

Figure 8.3: For piston-head diameter $d_{\text{p,tot}} = 0.3\text{m}$ the natural frequency of the accumulator system is given as a function of the lower accumulator initial pressure $P_1 = P_{\text{a1,1}}$. The horizontal line corresponds to the design natural frequency.

Now that P_1 and $d_{\text{p,tot}}$ are chosen the other variables in Table 8.2 can be found using the process in section 8.2.1.1. The values are shown in Table 8.3.

Table 8.3: Key variable values, lower accumulator

Variable	Unit	value
P_0	[N/m^2]	1.8e7
P_1	[N/m^2]	2e7
P_2	[N/m^2]	6e7
$\frac{P_2}{P_0}$	[-]	3.3333
V_0	[m^3]	0.2102
V_1	[m^3]	0.1950
V_2	[m^3]	0.0890
ΔV	[m^3]	0.1060

8.2.3.2 Upper accumulator dimensions

Values for the parameters in Table 8.2 are found in Table 8.4 for the upper accumulator using the process described in section 8.2.1.2.

Table 8.4: Key variable values, upper accumulator

Variable	Unit	value
P_0	[N/m^2]	8.2722e+05
P_1	[N/m^2]	9.1913e+05
P_2	[N/m^2]	3.3065e+06
$\frac{P_2}{P_0}$	[-]	3.9972
V_0	[m^3]	0.1908
V_1	[m^3]	0.1769
V_2	[m^3]	0.0709
ΔV	[m^3]	0.1060

8.2.3.3 Summary of base case dimensions

Values from Table 8.3 and Table 8.4 are summarized in Table 8.5 for the base case.

8.2.4 Upper case initial conditions

The upper case is where the piston-head is 10% of $L_{\text{max,stroke}}$ from the top of the cylinder, the top position. See Figure 8.4. The working out of the upper/lower accumulator dimensions for the upper case is shown in appendix A.14.1.

Table 8.5: Base case

Variable	Value	Unit	Note
$PS_{PHC,lower}$	1.8e7	[N/m^2]	Charge pressure, lower accumulator
$PS_{PHC,upper}$	8.2722e+05	[N/m^2]	Charge pressure, upper accumulator
$d_{p,tot}$	0.3	[m]	Diameter of piston-head
$P_{\Delta p}$	1.9081e+07	[N/m^2]	Difference in pressure across piston-head required to hold payload and hook in water
$P_{a1,1}$	2e7	[N/m^2]	Initial pressure in the lower accumulator
$P_{a3,1}$	9.1913e+05	[N/m^2]	Initial pressure in the upper accumulator, $P_{a3,1} = P_{a1,1} - P_{\Delta p}$
$V_{a1,1}$	0.1950	[m^3]	Initial volume in lower accumulator
$V_{a3,1}$	0.1769	[m^3]	Initial volume in upper accumulator
ω_{z_1}	2.2269	[rad/s]	Natural frequency of accumulator system
$\omega_{z_{1,design}}$	2.0944	[rad/s]	Designed natural frequency
ϵ	6.3	[%]	Percent error of natural frequency of accumulator system, relative to design

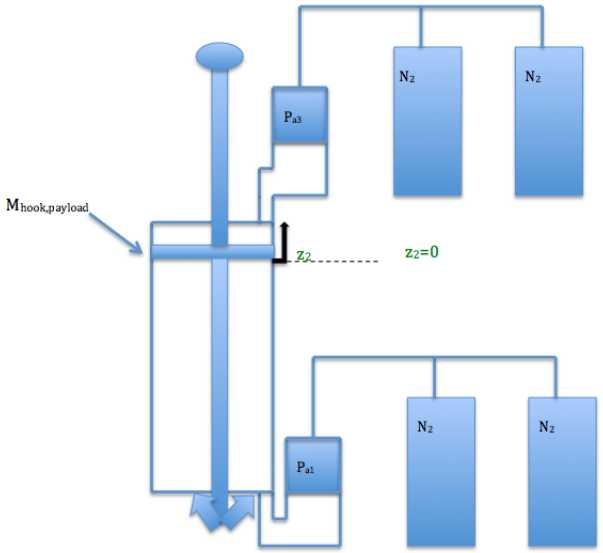

Figure 8.4: A schematic for the upper case

8.2.5 Lower case initial conditions

The lower case is where the piston-head is at 10% of $L_{max,stroke}$ above the bottom of the cylinder. See Figure 8.5. The working out of the upper/lower accumulator dimensions for the lower case is shown in appendix A.14.2.

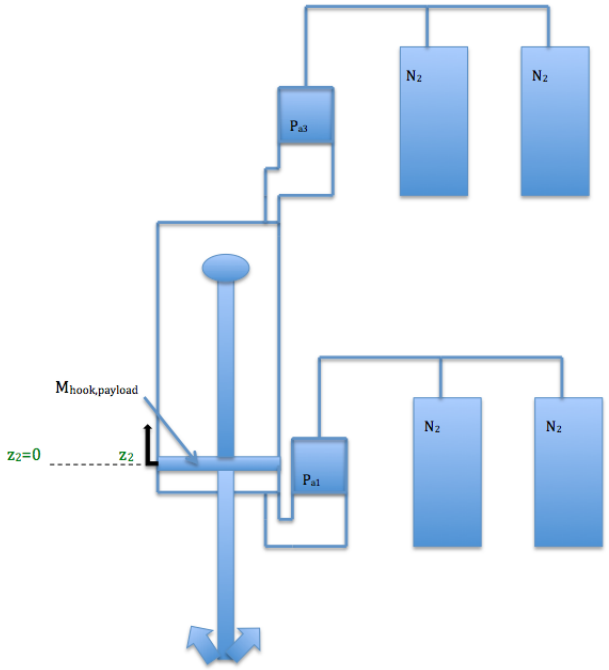

Figure 8.5: A schematic for the lower case

8.2.6 Comparison between cases

8.2.6.1 P-V plot

See Figure 8.6a for the upper case P-V plot. The result is expected. In the upper case, the lower accumulator has more volume available to compress so there is a large amount of work between state 1 and state 2 possible (as measured by the integral). This is because the piston-head can travel across most of the cylinder stroke. In contrast, for the upper accumulator, there is less volume to work with so there is less work possible between states 1 and 2. This is because the piston-head has less room to travel across.

See Figure 8.6b for the lower case P-V plot. The results are opposite to those for the upper case. Using the base case parameters provides more flexibility since the lower and upper accumulators have equal volumes available to compress. Thus, the base case parameters are used in future chapters.

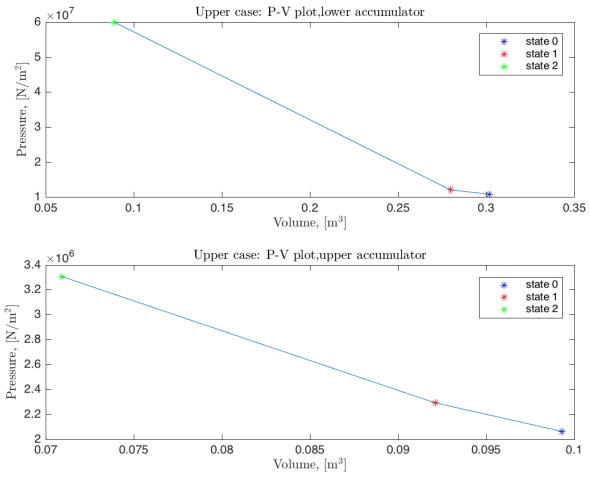

(a) P-V plot, upper case, for both accumulators

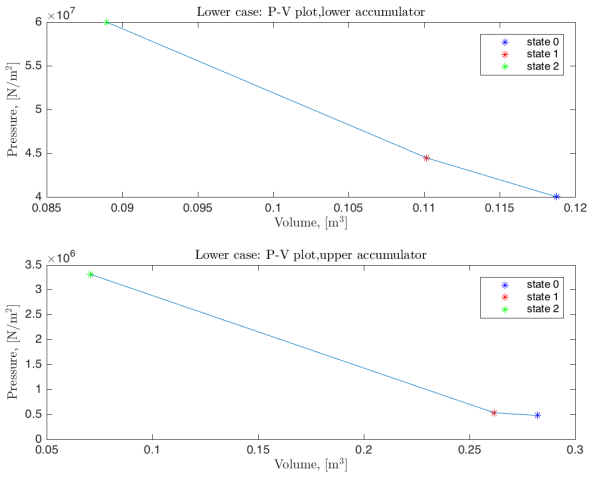

(b) P-V plot, lower case, for both accumulators

Figure 8.6

8.3 Conclusion

The pressure system of the PHCS has been sized. The base case sizing in Table 8.5 is used in future chapters. Step 3 of the methodology in section 3.3 is continued in chapter 9. In chapter 9, the finalized PHCS design made in this chapter is analyzed by determining the natural frequencies of the system.

Natural frequencies of PHCS

9

9.1 Introduction

In this chapter, the natural frequencies of the PHCS are found for three versions of the PHCS model using the base case, upper case, and lower case initial conditions found in chapter 8. These three versions are described below:

1. PHCS with **L**inearized **A**ccumulators, hook/payload mass, and no quadratic damping **M**odel (henceforth called **LAM**), (see Figure 9.1)
2. PHCS with steel **R**ope/Dyneema rope/PHCS cylinder/**L**inearized **A**ccumulators/hook and payload mass and no quadratic damping **M**odel (henceforth called **RLAM**) (see Figure 9.2)
3. PHCS with linearized **O**rifices/steel **R**ope/Dyneema rope/PHCS cylinder/**L**inearized **A**ccumulators/hook and payload mass and linearized quadratic damping **M**odel (henceforth called **ORLAM**) (see Figure 9.3)

Firstly, the natural frequencies of the LAM are found in section 9.2. Secondly, the natural frequencies for the RLAM are found in section 9.3. Thirdly, the natural frequencies for the ORLAM are found in section 9.4.

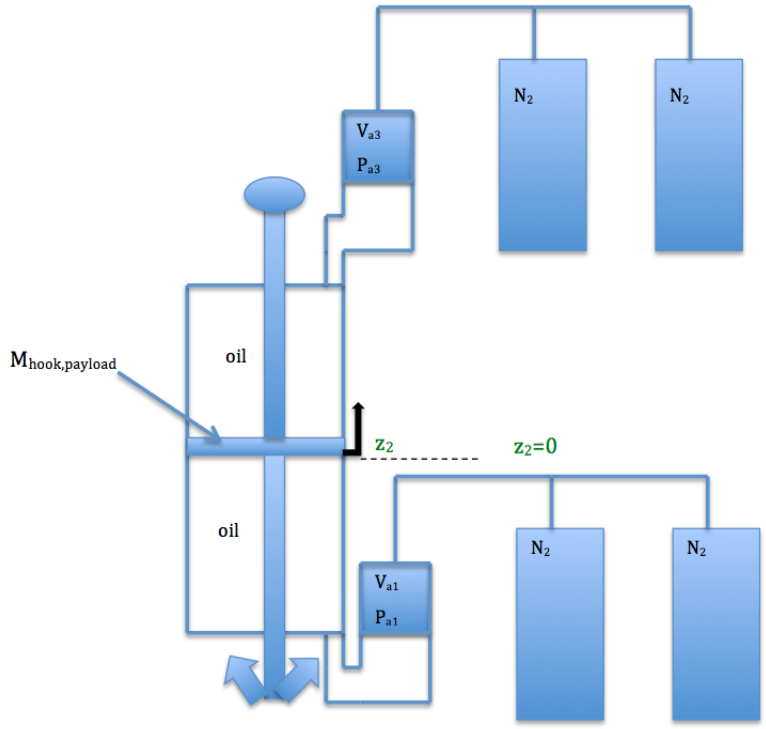

Figure 9.1: A diagram of the LAM

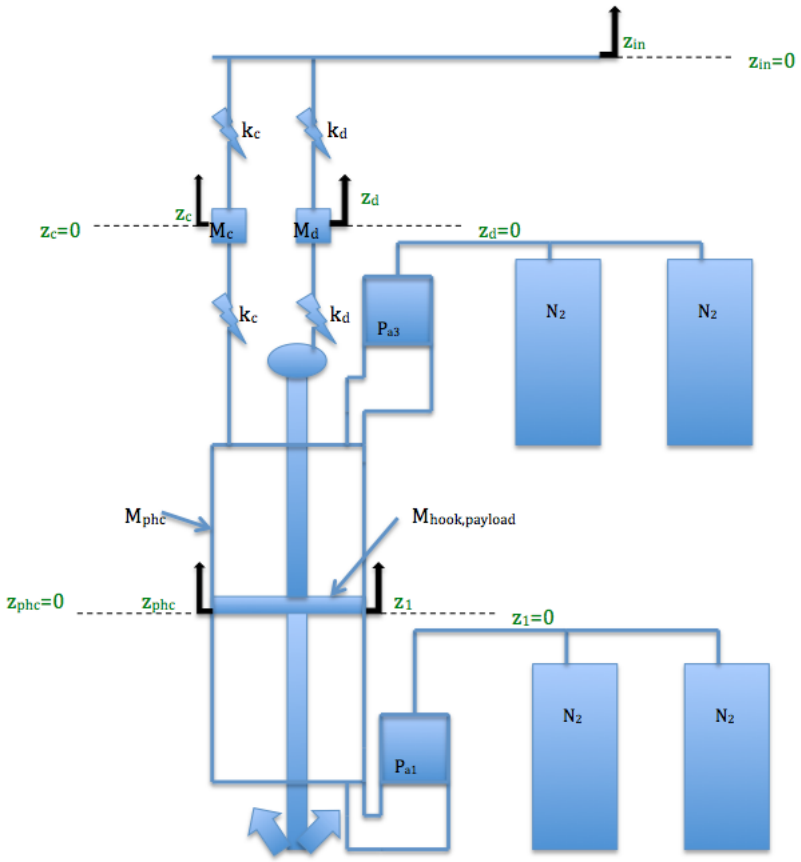

Figure 9.2: A diagram of the RLAM

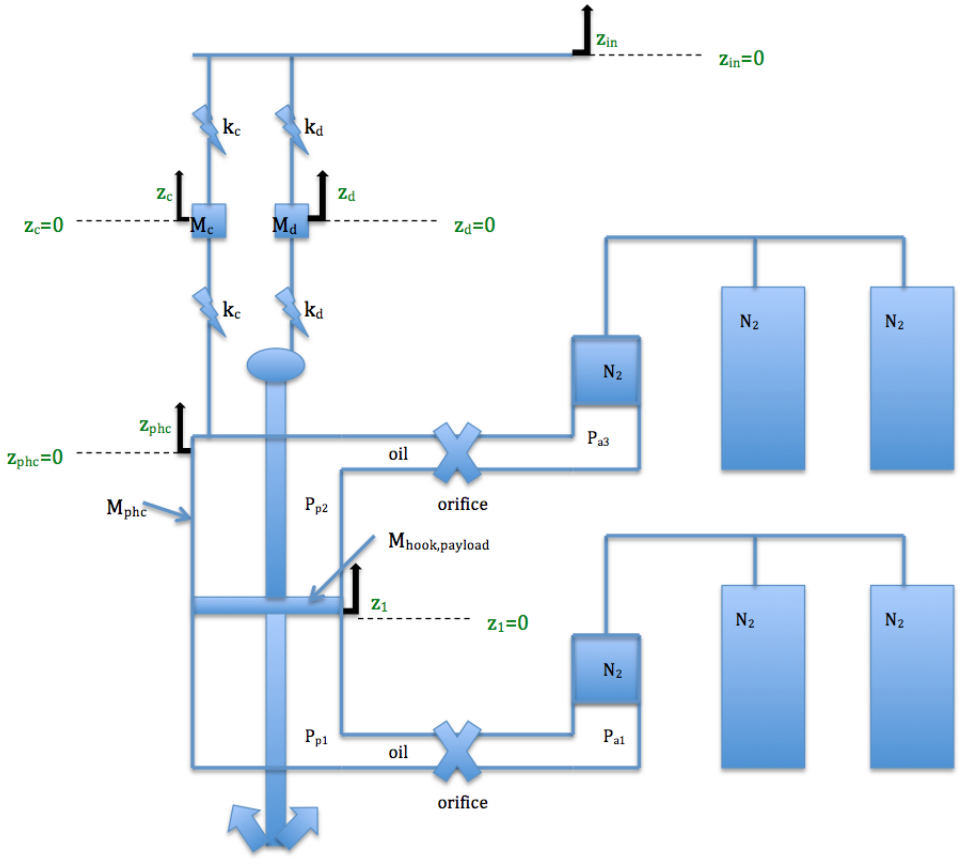

Figure 9.3: A diagram of the ORLAM

9.2 Natural frequencies of the LAM

The LAM is considered, see Figure 9.1 for a diagram of the system.

9.2.1 Base case natural frequencies

The equations of motion and state-space system are shown in appendix A.13. From the **A** matrix in (A.294) the eigenvalues were found. See Table 9.1 for the eigenvalues and natural frequencies obtained using the base case dimensions in Table 8.5. In the LAM there is one mass (hook/payload) and two pressures. The mass corresponds to one degree of freedom. This means there should be one pair of complex conjugate eigenvalues, indeed there is one pair of complex conjugate eigenvalues shown in Table 9.1. This corresponds to a natural frequency of 2.2269rad/s. There is a zero eigenvalue resulting in a zero natural frequency. This is attributed to the pressure since the non-zero natural frequency is attributed to the hook/payload mass.

Table 9.1: LAM: base case eigenvalues, natural frequencies, natural periods

Eigenvalue λ	Natural frequency ω_n [rad/s]	Natural period [s]	Association
0	0	inf	Pressure
0	0	inf	Pressure
2.2269i	2.2269	2.8215	Hook/payload mass
-2.2269i	2.2269	2.8215	Hook/payload mass

9.2.2 Upper case natural frequencies

See Table 9.2 for the eigenvalues and natural frequencies for the upper case.

Table 9.2: Upper case eigenvalues, natural frequencies, natural periods

Eigenvalue λ	Natural frequency ω_n [rad/s]	Natural period [s]
0	0	inf
0	0	inf
1.7689i	1.7689	3.5520
-1.7689i	1.7689	3.5520

9.2.3 Lower case natural frequencies

See Table 9.3 for the eigenvalues and natural frequencies for the lower case.

Table 9.3: Lower case eigenvalues, natural frequencies, natural periods

Eigenvalue λ	Natural frequency ω_n [rad/s]	Natural period [s]
0	0	inf
0	0	inf
4.3213i	4.3213	1.4540
-4.3213i	4.3213	1.4540

9.2.4 Comparison between cases

Table 9.4 shows that the lowest natural frequency occurs when the piston-head is at the upper position.

Table 9.4: Natural frequency for the different cases

Case	Location of piston-head	Natural frequency [rad/s]	Natural frequency [Hz]
Base	middle of cylinder	2.2269	0.3544
Upper	upper end of cylinder	1.7689	0.2815
Lower	bottom of cylinder	4.3213	0.6878
Designed natural frequency	-	2.0944	0.3333

9.3 Natural frequencies of the RLAM

In section 9.2, the LAM was considered. Now the steel rope/Dyneema rope/PHCS cylinder are added to the system to form the RLAM. A diagram of the system is shown in Figure 9.2. The equations of motion and state-space system are shown in appendix A.15. The natural frequencies were found. Note that the dimensions obtained in section 8.2 for the base case, lower case, and upper case are the same. This is because the dimensions are based on the pressures and volumes in the system and the steel rope and Dyneema rope do not influence this. However, there are three additional natural frequencies with the addition of the steel rope, Dyneema rope, and PHCS cylinder.

9.3.1 Base case natural frequencies

The natural frequencies for the base case are shown in Table 9.5. The 2.2295rad/s natural frequency has a 0.1% error with the 2.2269rad/s natural frequency from Table 9.1 for the LAM, so they are the

same natural frequency, from the hook/payload mass. The 0.5090rad/s natural frequency is associated with the Dyneema rope since the Dyneema rope stiffness was changed and only this natural frequency changed. The 0.4095rad/s and 0.1079rad/s natural frequencies are associated with either the steel rope or PHCS cylinder. This is because both changed when the steel rope stiffness changed. It is assumed the higher natural frequency (0.4095rad/s) is directly associated with the steel rope and the lower natural frequency (0.1079rad/s) is associated with the coupled steel rope and PHCS cylinder. This is because the steel rope is directly connected to the PHCS cylinder, perhaps forming a coupled mass. Since natural frequency is inversely proportional to mass then the lower natural frequency should be associated with the higher mass, the coupled mass.

Table 9.5: RLAM: base case eigenvalues, natural frequencies, natural periods

Eigenvalue λ	Natural frequency ω_n [rad/s]	Natural period [s]	Association
0	0	inf	Pressure
0	0	inf	Pressure
0.1079i	0.1079	58.2316	PHCS cylinder
-0.1079i	0.1079	58.2316	PHCS cylinder
0.4095i	0.4095	15.3436	Steel rope
-0.4095i	0.4095	15.3436	Steel rope
0.5090i	0.5090	12.3442	Dyneema rope
-0.5090i	0.5090	12.3442	Dyneema rope
2.2295i	2.2295	2.8182	Hook/payload mass
-2.2295i	2.2295	2.8182	Hook/payload mass

9.3.2 Upper case natural frequencies

See appendix A.15.2 for the natural frequencies for the upper case.

9.3.3 Lower case natural frequencies

See appendix A.15.3 for the natural frequencies for the lower case.

9.4 Natural frequencies of the ORLAM

In section 9.3 the RLAM was considered. Now linearized orifices and linearized quadratic damping are included to form the ORLAM to see how this affects the natural frequencies. A diagram of the system is shown in Figure 9.3. Fluid inertia is included. As mentioned, the dimensions obtained in section 8.2 for the base case, lower case, and upper case are the same. There are additional natural frequencies of the system with the addition of the orifices. The linearized state-space equations were obtained in section 7.10.7. See equation (7.70) for the **A** matrix. The base case natural frequencies are discussed below in section 9.4.1 since the base case is the chosen case of interest.

9.4.1 Base case natural frequencies

See Table 9.6 for the eigenvalues and natural periods. Comparison is made with the LAM in Table 9.1. With the LAM the largest natural frequency is 2.2269rad/s which is nearly equal to the natural frequency for the ORLAM of 2.2020rad/s shown in Table 9.6.

Table 9.6: ORLAM: base case eigenvalues, natural frequencies, natural periods

Eigenvalue λ	Natural frequency ω_n [rad/s]	Natural frequency [Hz]	Natural period [s]	Association
0	0	0	inf	Pressure
0	0	0	inf	Pressure
-9.6626e-5- 0.1035i	0.1035	0.0165	60.7071	PHCS cylinder
-9.6626e-5 + 0.1035i	0.1035	0.0165	60.7071	PHCS cylinder
-4.5410e-4 - 0.3070i	0.3070	0.0489	20.4664	Steel rope
-4.5410e-4 + 0.3070i	0.3070	0.0489	20.4664	Steel rope
-1.9251e-8 - 0.5090i	0.5090	0.0810	12.3442	Dyneema rope
-1.9251e-8 + 0.5090i	0.5090	0.0810	12.3442	Dyneema rope
-2.8066e-4 - 2.2020i	2.2020	0.3505	2.8534	Hook/payload mass
-2.8066e-4 + 2.2020i	2.2020	0.3505	2.8534	Hook/payload mass
-2.4336e-2 - 301.87i	301.87	48.0437	0.0208	Orifice
-2.4336e-2 + 301.87i	301.87	48.0437	0.0208	Orifice
-2.4171e-2 - 303.96i	303.96	48.3763	0.0207	Orifice
-2.4171e-2+ 303.96i	303.96	48.3763	0.0207	Orifice

In the ORLAM there are four masses (hook/payload, PHCS cylinder, steel rope, Dyneema rope). These four masses correspond to four degrees of freedom. This means there should be four sets of complex conjugate eigenvalues at least. There are six sets of complex conjugate eigenvalues shown in Table 9.6. These correspond to six pairs of natural frequency shown in Table 9.6. These are [0.1035, 0.3070, 0.5090, 2.2020, 301.87, 303.96]rad/s. There are two additional high natural frequencies [301.87, 303.96]rad/s relative to the RLAM. These natural frequencies can be attributed to the addition of the orifices. These high natural frequencies did not appear in the system without the orifices, so they are due to the orifices.

With the ORLAM the natural frequency 2.2020rad/s appears. With the RLAM the natural frequency 2.2295rad/s appears. 2.2020rad/s has a 1.2% difference with 2.2295rad/s, so these natural frequencies arise from the same cause, the hook/payload mass.

For the ORLAM, the natural frequencies [0.1035, 0.3070, 0.5090]rad/s in Table 9.6 are attributed to the PHCS cylinder, steel rope, and Dyneema rope respectively. For the RLAM the same natural frequencies are [0.1079, 0.4095, 0.5090]rad/s respectively. The percent errors are [4.1, 33.4,0]%. The PHCS cylinder natural frequency is nearly the same. The steel rope natural frequency is significantly different, 33.4%. This reason for the change is likely due to the addition of the linearized quadratic water damping in the ORLAM relative to the RLAM. This directly affects the PHCS cylinder and since the PHCS cylinder and steel rope are coupled this affects the steel rope. It seems the effect on the steel rope is greater than that on the PHCS cylinder. This may be due to the rope stiffness associated with the steel rope which the PHCS cylinder does not have. The natural frequency associated with the Dyneema rope is the same. This is expected since the Dyneema rope interacts with the hook/payload mass which is present in both models.

Sensitivity study of linearization points

Furthermore, it was necessary to choose linearization points to linearize the orifices. The orifices were linearized about the volume flow rates through the orifices. These volume flow rates were selected based on what are reasonable values for flow rates from the time-domain simulations. The fourth to seventh smallest natural frequencies, [0.5090, 2.2020, 301.87, 303.96]rad/s in Table 9.6, are the most dependent on these linearization points compared to the other natural frequencies. For example,

increasing the linearization volume flow rate from 1e-3m^3/s to 1e-2m^3/s gave percent differences of [1.7e-8, 7.4e-8, 1.2e-6, 1.1e-6]% respectively. For the second and third smallest natural frequencies the percent differences were three orders of magnitude smaller. For the sixth and seventh smallest natural frequencies the percent differences are the largest. This supports that the sixth and seventh smallest natural frequencies, [301.87, 303.96]rad/s are due to the orifices. Various linearization points were tried but the sixth and seventh smallest natural frequencies still have the largest percent difference.

Changing the linearization point, $\dot{z}_{\text{phc}}$, for the cylinder displacement, z_{phc} affected the second and third smallest natural frequencies only, [0.1035, 0.3070]rad/s in Table 9.6. The linearization point was selected based on a reasonable value for $\dot{z}_{\text{phc}}$ from the time-domain simulations. For example, increasing $\dot{z}_{\text{phc}}$ from 0.01m/s to 1m/s resulted in a 1.08% and 1.06% difference in the second and third smallest natural frequencies, whereas the other natural frequencies were unaffected. The difference in small but shows there is some influence. It is logical the second and third smallest natural frequencies are affected since these correspond to the PHCS cylinder and steel rope, respectively. The cylinder is connected to the steel rope so it is reasonable that there is some interaction. Which explains why changing the linearization point for the cylinder velocity affects these natural frequencies.

Changing the linearization point, $\dot{z}_1$, for the hook/payload displacement, z_1 affected the fourth and fifth smallest natural frequencies mainly, [0.5090, 2.2020]rad/s in Table 9.6. The linearization point was selected based on a reasonable value for $\dot{z}_1$ from the time-domain simulations. For example, increasing $\dot{z}_1$ from 0.01m/s to 1m/s resulted in a 6.4e-8% and 6.8e-8% difference in the fourth and fifth smallest natural frequencies respectively, whereas the other natural frequencies had two orders of magnitude smaller percent differences. These are very small changes but shows there is some influence. It is reasonable that the fourth and fifth smallest natural frequencies are affected since these correspond to the Dyneema rope and hook/payload mass. The hook/payload mass has interaction with the Dyneema rope directly. So it reasonable that changing the linearization point for the hook/payload mass velocity affects these natural frequencies.

9.4.2 Upper case natural frequencies

See appendix A.16.1 for the natural frequencies for the upper case.

9.4.3 Lower case natural frequencies

See appendix A.16.2 for the natural frequencies for the lower case.

9.4.4 Comparison between cases

Table 9.7 shows that the base case, where the piston-head is in the middle of the cylinder the natural frequency is second lowest. The natural frequency is highest for when the piston-head is at the lower position. Nevertheless, the base case provides the natural frequency closest to the design natural frequency.

The natural frequency due to the PHCS cylinder, steel rope, and Dyneema rope should not change in the base, upper and lower cases. This is because they are a property of the physical parameters not piston-head position. For the base case in Table 9.6 these natural frequencies are [0.1035, 0.3070, 0.5090]rad/s respectively. In appendix A.16, for the upper case in Table A.13 these natural frequencies are [0.1035, 0.3070, 0.5090]rad/s. For the lower case in Table A.14 these natural frequencies are [0.1035, 0.3070, 0.5093]rad/s. The natural frequencies essentially do not change as would be expected.

Table 9.7: Natural frequency for the different cases

Case	Location of piston-head	Natural frequency [rad/s]	Natural frequency [Hz]
Base	middle of cylinder	2.2020	0.3505
Upper	upper end of cylinder	1.7558	0.2794
Lower	lower end of cylinder	4.2060	0.6694
Designed natural frequency	-	2.0944	0.3333

9.5 Conclusion

The natural frequencies of the PHCS have been identified. This continues step 3 of the methodology in section 3.3. In chapter 10, step 3 is continued with the frequency and time responses of the system to verify the natural frequencies.

Frequency and time responses of PHCS

10

10.1 Introduction

The three versions of the PHCS model in chapter 9 are used to obtain the frequency responses (LAM, RLAM, ORLAM). To obtain the time-domain response the PHCS model with non-linear orifices/steel rope/Dyneema rope/PHCS cylinder/non-linear accumulators/hook and payload mass and non-linear quadratic damping (and fluid inertia) is used (henceforth called **NLORLAM**). The ORLAM used in chapter 9 is a linearized version of the NLORLAM. The NLORLAM system is the same as that described in section 7.10.4 and the diagram of this system is shown in Figure 7.9. The reason to use the fully non-linear system is that the time-domain response is found so there is no need to linearize any elements. Furthermore, the fully non-linear system represents the system closest to reality. This means the results from this system are the most meaningful physically. Thus, it is reasonable to use these time-domain results to verify the frequency domain results.

The frequency response of pressures is shown in section 10.2 and the time response is shown in section 10.3. The frequency response of hook/payload motion z_1 is shown in section 10.4 and the time response is shown in section 10.5.

10.2 Frequency response of pressures

The frequency response is obtained for the LAM and ORLAM. The LAM is chosen since it is the simplest model while still including the pressures and accumulators and the pressures are of interest. The ORLAM includes more elements of the system and is used to verify the LAM results. The frequency response is obtained for the base case initial conditions shown in Table 8.1. The base case is chosen as the case to focus on since this represents the assumed design condition. The frequency responses are obtained using the transfer function obtained from the state-space system.

10.2.1 Base case

10.2.1.1 LAM

In Figures 10.1a and 10.1b the frequency response for the LAM is shown for the base case initial conditions. There is only one peak at 0.354Hz.

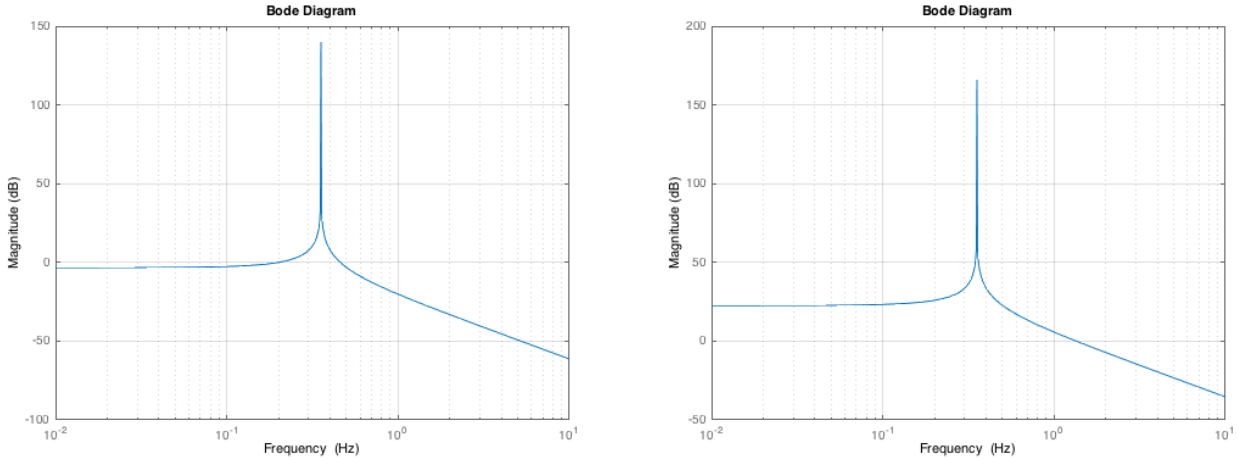

(a) Bode plot for P_{a3}, peak at 0.354Hz

(b) Bode plot for P_{a1}, peak at 0.354Hz

Figure 10.1: Base case, for the LAM

10.2.1.2 The ORLAM

From the ORLAM results in section 9.4.1 in Table 9.6, the closest natural frequency is 0.3505Hz which has a 1% difference with 0.354Hz. These natural frequencies are almost the same.

10.2.2 Upper case

The frequency response of pressures for the upper case initial conditions are in appendix A.17.1.

10.2.3 Lower case

The frequency response of pressures for the lower case initial conditions are in appendix A.17.2.

10.2.4 Three cases

The natural frequencies for the ORLAM are summarized in Tables 10.1/10.2. The natural frequencies are used for the time-domain results in section 10.3.

Table 10.1: Three cases, frequency and magnitude for P_{a3}

Base case	Upper case	Lower case
Frequency [Hz]	Frequency [Hz]	Frequency [Hz]
0.3505	0.2794	0.6694

10.3 Time response of pressures

The time-series response of the pressures is obtained. This is to verify the frequency response results in section 10.2. To do this the NLORLAM described in section 10.1 is used.

Table 10.2: Three cases, frequency and magnitude for P_{a1}

Base case	Upper case	Lower case
Frequency [Hz]	Frequency [Hz]	Frequency [Hz]
0.3505	0.2794	0.6694

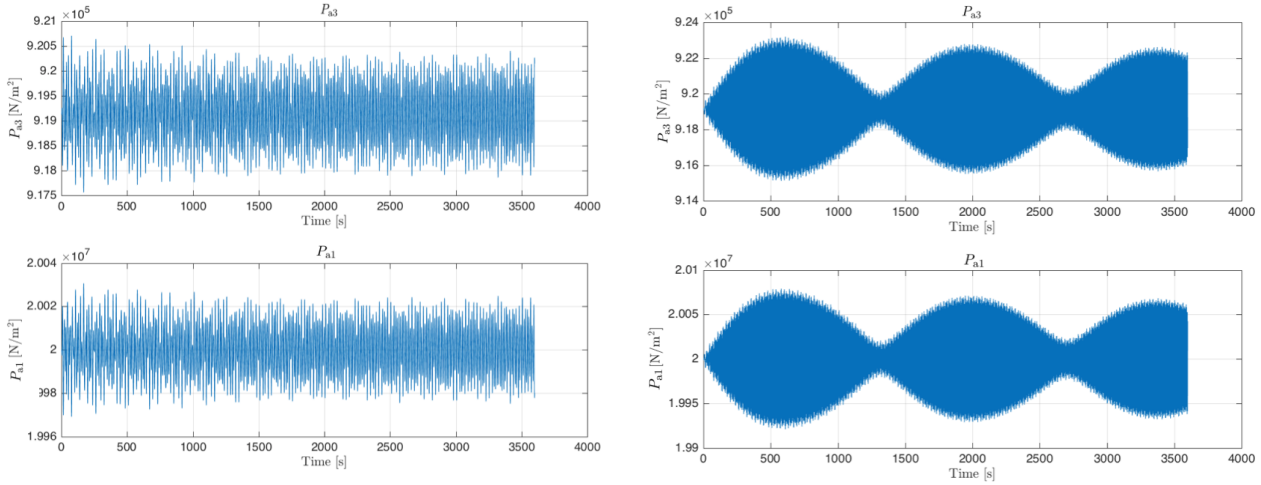

(a) Using the NLORLAM, input frequency is the design wave frequency of 0.125Hz

(b) Using the NLORLAM, input frequency is the natural frequency of 0.3505Hz

Figure 10.2: Base case, time-response of P_{a3} and P_{a1}

For the design wave condition, the harmonic crane tip motion is assumed to have a period the same as the design wave condition, 8s. This corresponds to a frequency of $f = 0.125$Hz or circular frequency $\omega = 2 * \pi/8 = 0.7854$rad/s. The amplitude is 1m for simplicity. A sine wave is used as the harmonic crane tip motion. Other frequencies are used later but the amplitude is 1m always.

10.3.1 Base case

Figure 10.2a shows the pressures P_{a1} and P_{a3} for the design wave condition.

From section 10.2.1.2 the natural frequency corresponding to the peak in the frequency response for pressures P_{a1} and P_{a3} is 0.3505Hz, this is used as the input frequency of the crane tip in Figure 10.2b. There is a beating character in the time-series. This is indicative of the frequency being close to the natural frequency since beating is a phenomenon that occurs when the natural frequency and forcing frequency are close. This is expected because 0.3505Hz is a natural frequency of the system.

10.3.2 Upper case

See appendix A.18.1 for the time response of pressures for the upper case initial conditions.

10.3.3 Lower case

See appendix A.18.2 for the time response of pressures for the lower case initial conditions.

10.3.4 Conclusion, time response of pressures

These time domain results have verified to some extent the frequency response characteristics found in section 10.2.

10.4 Frequency response of hook/payload motion

Firstly, the frequency response is obtained for the RLAM. This system is used instead of the LAM since the RLAM includes the steel/Dyneema rope and PHCS cylinder and these are important for the frequency response of the hook/payload motion. Secondly, the frequency response is obtained for the ORLAM, this is to verify the results from the RLAM.

10.4.1 Base case

See Figure 10.3 for the frequency response of the hook displacement with respect to a harmonic crane tip motion, for the base case. The frequency and magnitude of peaks is shown in Table 10.3. For the ORLAM in section 9.4.1 in Table 9.6 the closest natural frequencies are extracted and put into Table 10.4. The very high natural frequencies of 48.0437Hz and 48.3763Hz in Table 9.6 are not considered since these are not realistic frequencies for real wave conditions thus there would be little value in seeing their effect. The percent differences with the corresponding values in Table 10.3 are shown in Table 10.4. Most of the percent differences are low as would be expected since they are supposed to be the same natural frequencies.

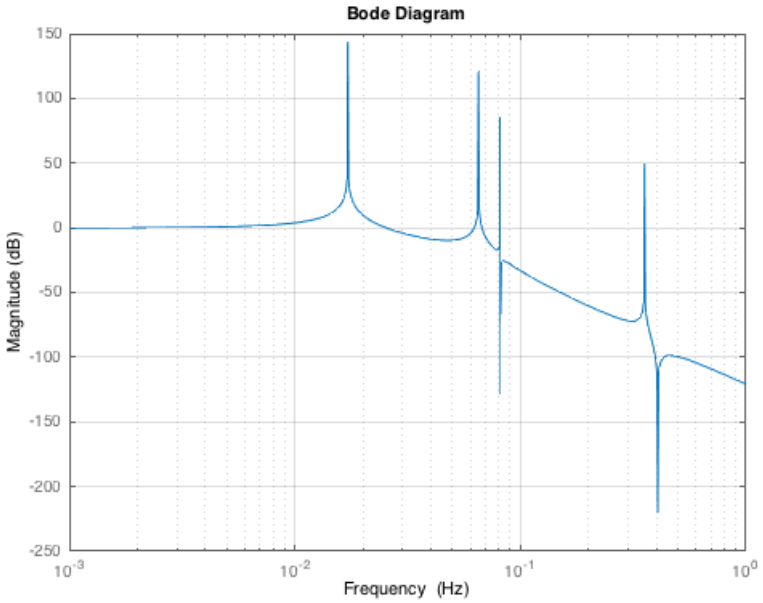

Figure 10.3: Base case, bode plot for z_1, the RLAM.

Table 10.3: Frequency and magnitudes for peaks in Figure 10.3 (RLAM)

Frequency [Hz]	Magnitude [dB]
0.0172	144
0.0652	121
0.081	85
0.355	48.9

Table 10.4: Base case, natural frequencies for the ORLAM with percent differences of values in Table 10.3

Frequency [Hz]	% difference
0.0165	4.2
0.0489	25.1
0.0810	0
0.3505	1.3

10.4.2 Upper case

See appendix A.19.1 for the frequency response of the hook displacement, for the upper case.

10.4.3 Lower case

See appendix A.19.2 for the frequency response of the hook displacement, for the lower case.

10.4.4 Three cases

For the three cases there is a peak at [0.0165, 0.0489, 0.0810]Hz and a peak at another frequency specific to the case. The first three frequencies were discussed in section 9.4.1. They are due to the PHCS cylinder, steel rope, and Dyneema rope respectively.

10.5 Time response of hook/payload motion

The time response of the z_1 motion is obtained. This is to verify the frequency response results in section 10.4. The NLORLAM is used, as mentioned in section 10.3.

The same design wave condition input as in section 10.3 is used.

10.5.1 Base case

Figure 10.4a shows z_1 for the design wave condition. The four frequencies found in the frequency response in Table 10.4 are used as input frequencies to verify the frequency response.

For 0.0165Hz see Figure 10.4b , there is a large amplification of the maximum value of z_1 relative to the design wave condition in Figure 10.4a.

For 0.0489Hz see Figure 10.4c, the maximum value of z_1 is larger relative to the design wave condition case but smaller than the maximum z_1 in the 0.0165Hz case.

For 0.0810Hz see Figure 10.4d , the maximum z_1 is larger relative to the design wave condition but still smaller than the maximum z_1 in the 0.0165Hz case.

For 0.3505Hz see Figure 10.4e, the amplitude of z_1 is the smallest. Since this frequency is an order of magnitude higher than the other frequencies it is likely due to the input frequency being so high that the damping in the system is removing a significant amount of energy. This leads to a limit on the maximum value of z_1.

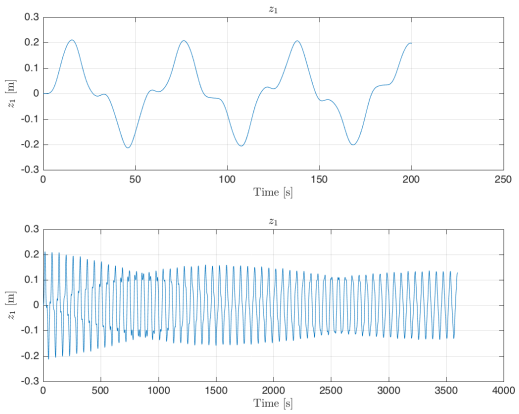

(a) Using the NLORLAM, input frequency is the design wave frequency of 0.125Hz

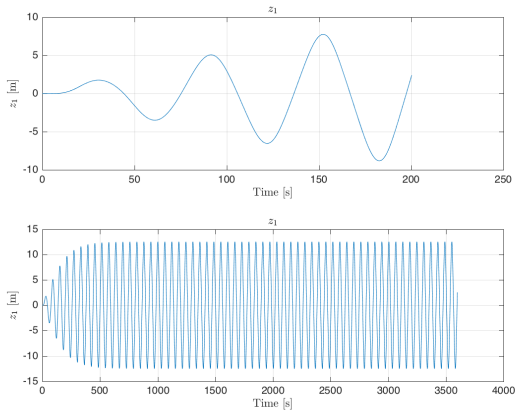

(b) Using the NLORLAM, input frequency is the natural frequency of 0.0165Hz

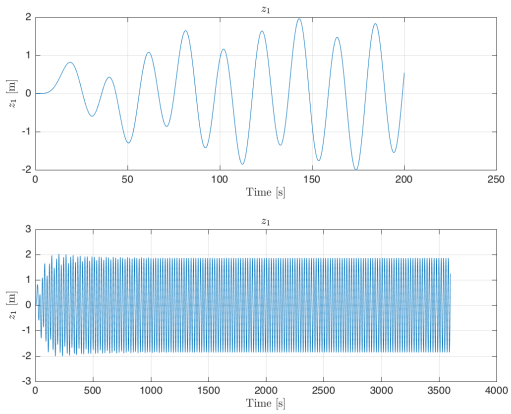

(c) Using the NLORLAM, input frequency is the natural frequency of 0.0489Hz

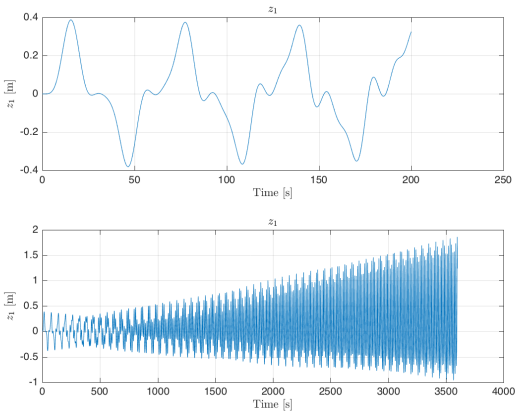

(d) Using the NLORLAM, input frequency is the natural frequency of 0.0810Hz

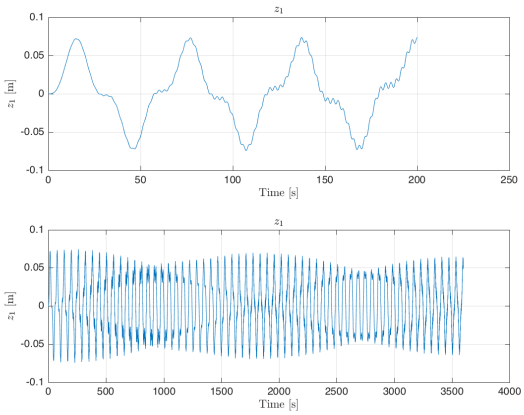

(e) Using the NLORLAM, input frequency is the natural frequency of 0.3505Hz

Figure 10.4: Time-series for z_1 for five input frequencies

10.5.2 Upper case

The time response using upper case initial conditions is shown in appendix A.20.1.

10.5.3 Lower case

The time response using lower case initial conditions is shown in appendix A.20.2.

10.5.4 Conclusion, time response of hook/payload motion

These time domain results have verified to some extent the frequency response characteristics found in section 10.4. The results of the base case are discussed since the initial conditions for the base case are used in further work. As mentioned in section 8.2.2 the design wave period is Tp=8s. This is a frequency of 0.125Hz or circular frequency 0.7854rad/s. The natural frequencies and periods for the base case are shown in Table 10.5. The periods for feasible wave conditions are from 25s to 5s. None of the natural periods are close to the design wave period which is good for avoiding resonance. The real threat is due to the lowest natural frequency 0.0165Hz since this causes a large amplification of z_1 amplitude relative to the input amplitude of 1m, see Figure 10.4b. This frequency has a circular frequency 0.1035rad/s and period 60.7s. This is a large period and outside the wave conditions considered of 25s to 5s hence it is unlikely to be encountered. The next natural frequency 0.0489Hz (20.5s) falls within the wave conditions but does not have a large amplification effect, only slightly when compared to the design wave condition case. Similarly the third natural frequency 0.0810Hz (12.3s) is within the wave conditions but does not have a large amplification effect either. The last natural frequency 0.3505Hz (2.8s) is the designed for natural frequency (0.33Hz or 3s) and though it is a natural frequency because the frequency is so high and there is damping in the system the energy is quickly dissipated so this natural frequency does not get excited much.

Table 10.5: Natural frequencies and periods for the base case

Frequency [Hz]	Frequency [rad/s]	Period [s]
0.0165	0.1035	60.7
0.0489	0.3070	20.5
0.0810	0.5090	12.3
0.3505	2.2020	2.8

10.6 Verifying Simulink results

In appendix A.24, the time-domain results from Simulink are verified by executing the same simulation in MATLAB. The results are essentially the same indicating that Simulink solves the equations correctly. This means either Simulink or MATLAB can be used to contain the numerical model.

10.7 Conclusion

In this chapter, the final design was analyzed by determining the natural frequencies and looking at the frequency and time responses of the system. The main conclusion is that the natural frequencies of the system have been identified. This provides a criterion to check the system's performance in relation to the operating environment. If the operating environment has a frequency close to a natural frequency of the system, then it should be checked if this will be an issue in operation. Since the main objective is to design a hybrid heave compensation system the passive part of the hybrid compensation system has been designed. It has been verified that this passive heave compensation system will not experience resonance in the design wave condition (Tp=8s and Hs=2.5m). In chapter 11, step 3 of the methodology

in section 3.3 is finalized by assessing how well the PHCS can reduce the heave motion, quantified with some criteria of performance.

11 Performance of the PHCS

11.1 Introduction

This chapter will investigate the time-domain results of the PHCS by itself. To obtain the time-domain results the NLORLAM described in section 10.1 is used. The irregular and regular crane-tip motion signals are described. Then, three measures of performance are described and applied to the results for various wave periods and wave heights. Additionally, the natural periods of the PHCS (obtained from the ORLAM) are used as the wave periods. Finally, the time-domain results of key variables in the PHCS, such as pressure, are discussed.

11.2 Number of wave frequency components

To generate an irregular sea the Pierson-Moskowitz wave spectrum is used. Other spectrums can be used, such as the JONSWAP spectrum. The Pierson-Moskowitz spectrum assumes deep-water and a fully-developed sea. In contrast, the JONSWAP spectrum assumes a not fully-developed sea state and also deep-water. The JONSWAP spectrum represents a sea with short fetch (fetch is the distance to the upwind coastline). This means the waves grow rapidly. Whereas with the Pierson-Moskowitz spectrum the waves do not grow since the wave breaking balances the transfer of energy from wind to waves. For the Pierson-Moskowitz spectrum, the significant wave height and peak frequency depend only on the wind speed [59]. This means the Pierson-Moskowitz spectrum relies on the wind-speed and is independent of the fetch. Since the vessel will in reality by at varying distance to the coast, meaning fetch is changing, it is simpler to assume a fully-developed sea instead of taking into account a sea state varying with fetch. Thus, the Pierson-Moskowitz spectrum is chosen.

It is assumed the free surface elevation is statistically stationary and normally distributed for the duration of the time simulation. To define the number of wave frequencies in the simulation, the minimum interval for discrete frequencies of ω was calculated using the simulation time (11.1) [60] [44]:

$$\Delta\omega < \frac{2\pi}{t_{\text{sim}}} \tag{11.1}$$

It is assumed the energy in the wave spectrum is negligible outside the frequency range from ω_{min} to ω_{max}. This means the number of wave frequencies present, N, can be calculated using $\Delta\omega$, ω_{min}, and

$\omega_{\max}$ (11.2) [60]:

$$N > \frac{(\omega_{\max} - \omega_{\min})}{\Delta\omega} \tag{11.2}$$

Using a simulation time $t_{\text{sim}} = 1800$s in (11.1) gives $\Delta\omega$ =0.0035rad/s. A trial and error approach was used by varying N and sorting the wave spectrum frequencies to obtain $\omega_{\max}$ and $\omega_{\min}$. It was found that using $N = 582$ produced $\omega_{\max} = 2.5312$rad/s and $\omega_{\min} = 0.5$ rad/s. Using these values of $\omega_{\max}$, $\omega_{\min}$, and $\Delta\omega$ in (11.2) gives $N = 582$. Since this agrees with the inequalities in (11.1) and (11.2), then $N = 582$ is used as the number of wave frequencies.

The number of wave frequency components for a simulation time of $t_{\text{sim}} = 1800$s is 582. This means the Pierson-Moskowitz spectrum is discretized with 582 bins, show in Figure 11.1. Having a sufficient number of wave frequency components is important so that the Pierson-Moskowitz spectrum is well-discretized. Discretizing the Pierson-Moskowitz spectrum with 10 bins, shown in Figure 11.2, illustrates this point. Since not enough bins are used the energy in the time-series representation will not reflect the energy in the spectrum accurately. Furthermore, since an irregular sea is desired it is important to have sufficient wave frequency components so that in the time-domain the waves do not repeat too much, leading to a less random sea. This can occur for a long simulation time with an insufficient number of wave frequencies.

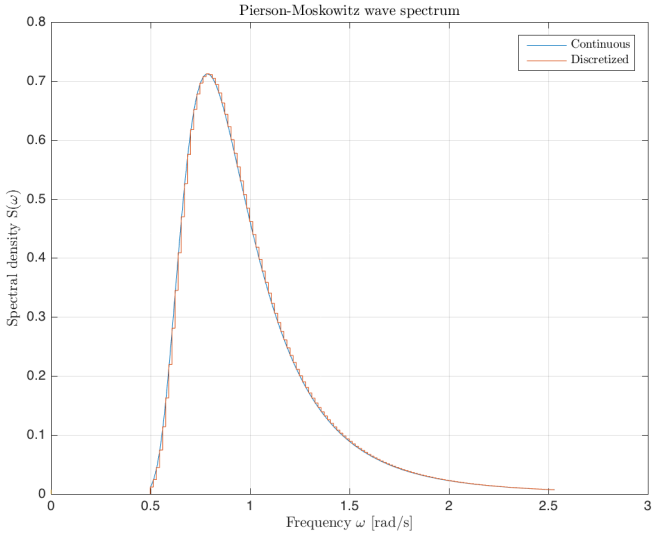

Figure 11.1: Pierson-Moskowitz spectrum discretized with 582 frequency bins

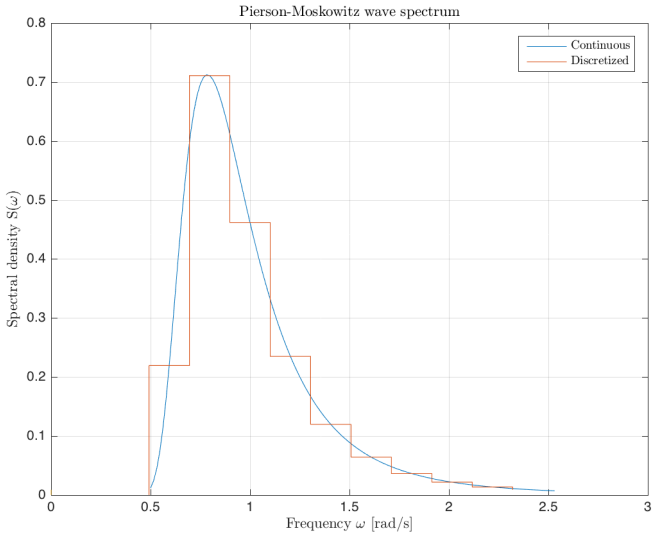

Figure 11.2: Pierson-Moskowitz spectrum discretized with 10 frequency bins

11.3 Parameters of performance

The three parameters used to quantify the performance of the PHCS are defined below.

11.3.1 Significant double amplitude

The significant double amplitude (SDA) of the z_1 (hook/payload motion) time-series is given by the symbol γ. The SDA is defined as the mean of the one-third highest crest-to-trough values of the z_1 time-series [61].

11.3.2 Compensation rate

The compensation rate is given by the symbol β. The compensation rate is defined by (11.3) [48]:

$$\beta = \frac{(A_{\text{in}} - A_1)}{A_{\text{in}}} * 100\% \tag{11.3}$$

where:

$$A_{\text{in}} = \max[z_{\text{in}} - \text{mean}(z_{\text{in}})] \tag{11.4}$$

$$A_1 = \max[z_1 - \text{mean}(z_1)] \tag{11.5}$$

A compensation rate of 0% indicates neither attenuation nor amplification of hook and payload motion whereas a value closer to 100% indicates the PHCS is more effective and a negative value indicates the PHCS is amplifying the motion.

11.3.3 Rms reduction ratio

The rms reduction ratio is given by the symbol R. The rms reduction ratio is defined by (11.6) [62]:

$$R = \frac{\sigma_{z_1}}{\sigma_{z_{\text{in}}}} \tag{11.6}$$

where σ_{z_1} is the standard deviation of the z_1 signal and $\sigma_{z_{\text{in}}}$ is the standard deviation of the z_{in} signal (crane-tip motion).

R should be less than one for an effective PHCS. The closer R is to 0 means the system is more effective. If σ_{z_1} is small this means the z_1 signal is close to the mean of the signal most of the time. Ideally the mean of z_1 is 0 so there is no static offset. The standard deviation of z_{in} for the regular input is $\frac{\text{H}}{2\sqrt{2}}$, where H is the wave height, since the input is a sine wave.

11.4 Obtaining results

11.4.1 Obtaining SDA

To obtain the SDA of z_1 the vertical distances between consecutive crests and troughs in the time series were obtained using a peak-finding algorithm. The distances were sorted and the mean of the highest one-third values taken to obtain the SDA.

To see if the simulation time is sufficient it is estimated what maximum wave height can be expected for a 3 hour simulation time. Assuming the irregular wave elevations generated by the Pierson-Moskowitz spectrum can be described using a normal distribution then the wave amplitude statistics will follow a Rayleigh distribution [41]. The probability density function of the Rayleigh distribution is given by:

$$f(x) = \frac{x}{\sigma^2}\exp\left(-\left(\frac{x}{\sigma\sqrt{2}}\right)^2\right) \tag{11.7}$$

where σ is the standard deviation. The probability that a wave amplitude ζ_{a} exceeds a value a is given by integrating (11.7) from a to ∞:

$$P\{\zeta_{\text{a}} > a\} = \int_{\text{a}}^{\infty} f(x)\text{d}x \tag{11.8}$$

$$P\{\zeta_{\text{a}} > a\} = \frac{1}{\sigma^2}\int_{\text{a}}^{\infty} x\exp\left(-\left(\frac{x}{\sigma\sqrt{2}}\right)^2\right)\text{d}x \tag{11.9}$$

$$P\{\zeta_{\text{a}} > a\} = \exp\left(-\frac{a^2}{\sigma^2 2}\right) \tag{11.10}$$

The crest-to-trough wave height is H_{w}, an arbitrary wave height is $H = 2a$, and the significant wave height is $H_{1/3} = 4\sigma$, putting these into (11.10):

$$P\{H_{\text{w}} > H\} = \exp\left(-\frac{(\frac{H}{2})^2}{(\frac{H_{1/3}}{4})^2 2}\right) \tag{11.11}$$

$$P\{H_{\text{w}} > H\} = \exp\left(-2\left(\frac{H}{H_{1/3}}\right)^2\right) \tag{11.12}$$

(11.12) gives the probability that a wave height H is exceeded in a wave field with significant wave height $H_{1/3}$. As a rule of thumb, the maximum wave height that can be expected in a 3 hour storm is the wave height exceeded once in every 1000 waves. The reasoning is that it will take at least 3 hours for 1000 waves to appear and in 3 hours the worst part of a storm will likely be over [41]. To find this maximum wave height (11.12) is used with $H = H_{\max}$ and $P\{H_{\text{w}} > H_{\max}\} = \frac{1}{1000} = 0.001$:

$$0.001 = \exp\left(-2\left(\frac{H_{\max}}{H_{1/3}}\right)^2\right) \tag{11.13}$$

Solving for $H_{\max}$:

$$\ln(0.001) = -2\left(\frac{H_{\max}}{H_{1/3}}\right)^2 \tag{11.14}$$

$$H_{\max} = \sqrt{\frac{\ln(0.001)}{-2}} H_{1/3} \tag{11.15}$$

$$H_{\max} \approx 1.86 H_{1/3} \tag{11.16}$$

In the time-domain simulation it is seen if the maximum wave height observed exceeds the theoretical maximum wave height in (11.16). The results are shown in Table 11.1. As expected the trend for increasing $H_{1/3}$ is an increasing maximum wave height observed. Using a 6 hour simulation resulted in a maximum wave height slightly below that given by (11.16) with a 0.9% percent error. It is not necessary that the maximum wave height is exceeded since the waves are random. However, there is a high chance that it is exceeded and an explanation could be that the waves are not truly random. This is because the toolbox WAFO [63] was used and since it is uses algorithms it can only generate pseudo-random waves. Nonetheless, it is computationally expensive to run a 6 hour simulation. Furthermore, the equation (11.16) is based on an assumption and there is no law from nature that the assumption is necessarily correct. Thus, it is acceptable that the maximum wave height from (11.16) is not exceeded. The simulation time is kept at 1800s (half an hour) since this is judged as sufficiently long from a statistical point of view and from a computationally cost-effective point of view.

Table 11.1: For $H_{1/3}$ =0.5m, the maximum wave height observed and the theoretical maximum wave height for various simulation times

Simulation time [hr]	Maximum wave height observed [m]	Theoretical maximum wave height [m]
0.5	0.6221	0.92
2	0.6226	0.92
3	0.73	0.92
6	0.91	0.92

11.5 Results irregular and regular input: various periods and wave heights

The PHCS was used with irregular and regular input.

- To specify the irregular input an irregular wave spectrum was used. To specify the irregular wave spectrum a peak period, Tp, and significant wave height, Hs, were used. These parameters were used to generate the wave spectrum, from the wave spectrum the vessel motions were obtained, and the crane-tip motion was then obtained from these vessel motions. This irregular crane-tip motion was the input to the PHCS. Beam waves were assumed. The reason to use beam waves was explained in section 5.5.1 but is essentially that roll and heave response to beam waves is generally larger than roll and heave response to other wave headings. Since a wave spectrum and uniformly distributed random phases for the wave components are used then crane-tip motions are random for each simulation. This means a stochastic approach is used since the crane-tip motion is unpredictable due to the random variables present.

- To specify the regular input a sinusoidal motion for the crane-tip motion was assumed. To specify the sine wave a period, T, and wave height, H, were used.

The reason to use regular wave input is two-fold, one is to verify the irregular wave results and another is to see more clearly the effect of a certain wave period. This is because the irregular wave results depend on the peak period and significant wave height, which are statistical quantities. This means the actual waves will have energy distributed among many wave periods. So if a certain period is used as the peak period there may not be an obvious response to this since wave energy is present at many

other wave periods. With the regular wave input a specific period is used so that the response to this period can be clearly seen.

The design conditions are irregular waves with Tp=8s and Hs=2.5m. Thus, this Tp and Hs are used as a basis for the analysis below. Three measures of motion of the hook and payload mass, z_1, are used. These are the SDA, compensation rate, and rms reduction ratio R, defined in section 11.3.

The results for SDA are shown in section 11.5.1, for compensation rate β in section 11.5.2, and for R ratio in 11.5.3. For each measure of motion four sets of parameters were used. Two sets for irregular input:

- Fixed Tp=8s, various Hs values [0.50, 0.75, 1.00, 1.25, 1.50, 1.75, 2.00, 2.25, 2.50, 2.75, 3.00, 3.25, 3.50]m and various water depths [1000, 1500, 2000, 2500]m
- Fixed Hs=2.5m, various Tp values [2, 3, 4, 5, 6, 7, 8, 9, 10, 11, 12, 13]s and various water depths [1000, 1500, 2000, 2500]m

And two sets for regular input:

- Fixed T=8s, various H values [0.50, 0.75, 1.00, 1.25, 1.50, 1.75, 2.00, 2.25, 2.50, 2.75, 3.00, 3.25, 3.50]m and various water depths [1000, 1500, 2000, 2500]m
- Fixed H=2.5m, various T values [2, 3, 4, 5, 6, 7, 8, 9, 10, 11, 12, 13]s and various water depths [1000, 1500, 2000, 2500]m

11.5.1 SDA

The SDA was defined in section 11.3.1. A larger SDA value indicates the hook and payload moves more which is undesirable. The input signal has a peak-to-trough value of 2.5m for the regular input and Hs=2.5m for the irregular input. This means the double amplitude for the input signal is 2.5m for the regular input. This provides a measure to judge the performance of the PHCS when looking at the SDA values. An SDA value below 2.5m means the PHCS reduces heave motion. The regular input results show a clearer trend since all the wave energy is concentrated at one period, so these results are focused on.

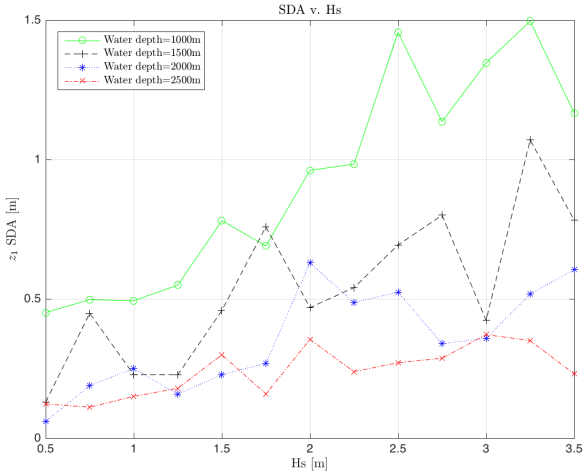

(a) SDA(Hs,wd) (irregular), for Tp=8s

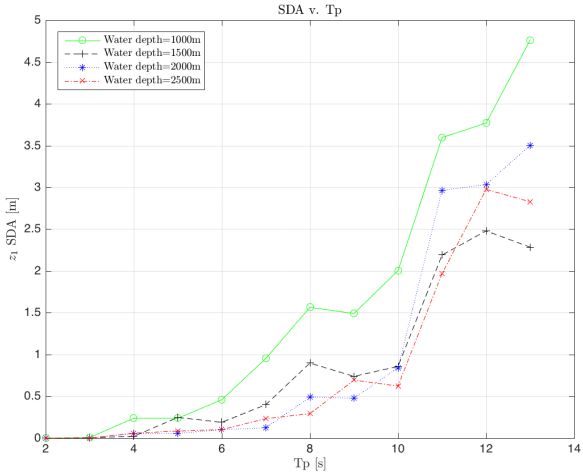

(b) SDA(Tp,wd) (irregular), for Hs=2.5m

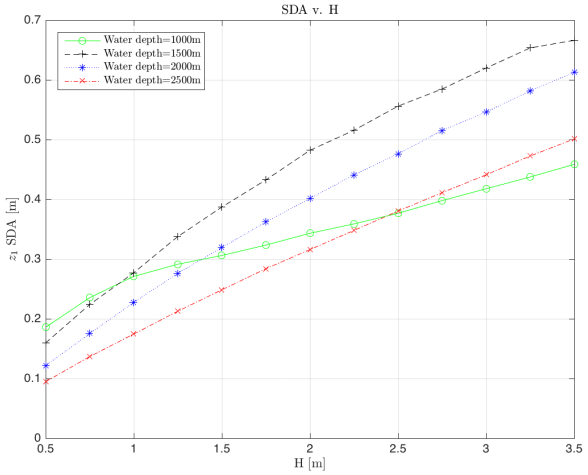

(c) SDA(H,wd) (regular), for T=8s

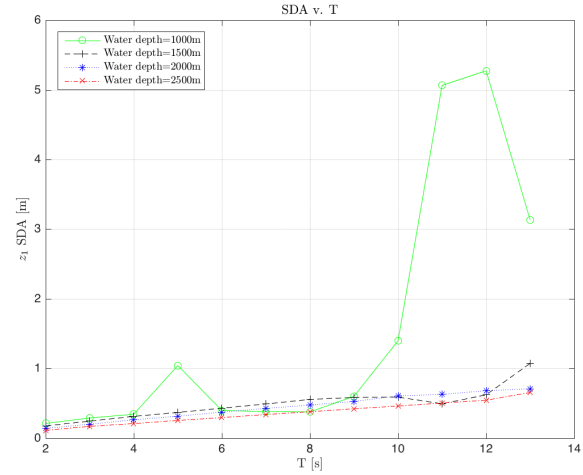

(d) SDA(T,wd) (regular), for H=2.5m

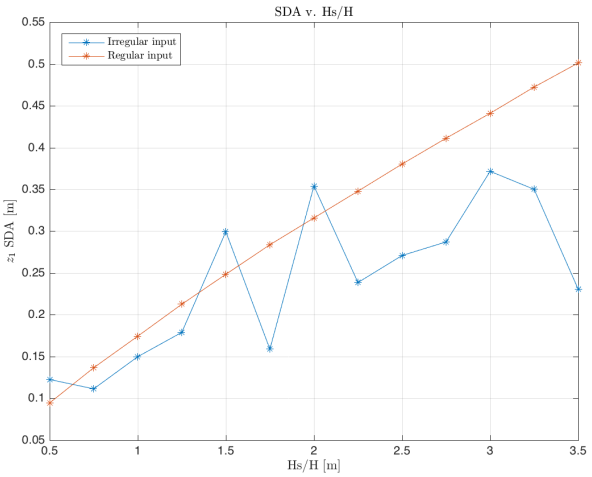

(e) Water depth: 2500m

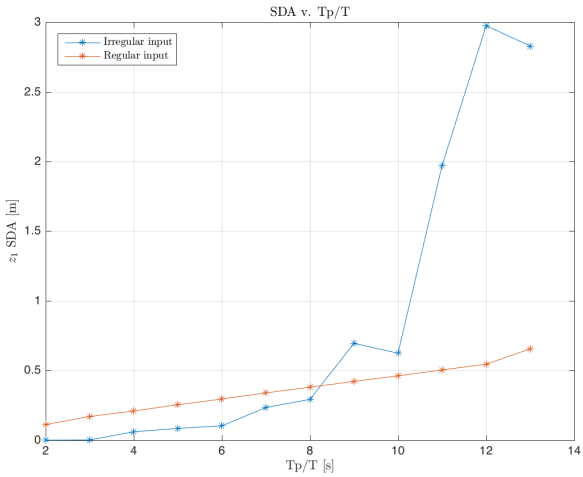

(f) Water depth: 2500m

Figure 11.3: SDA: Irregular and regular input results

11.5.1.1 Varying Tp/T

For the irregular input, the SDA values were found for fixed Hs=2.5s as a function of Tp and water depth, see Figure 11.3b for results. For the regular input, the SDA values were found for fixed H=2.5m

as a function of T and water depth, see Figure 11.3d for results.

Since the 2500m water depth is the operating condition of interest this water depth is used in Figure 11.3f to more clearly show the effect of wave period. The regular input result shows the trend clearly, with increasing wave period the SDA increases. This indicates that lower frequency waves (larger periods) are able to excite the hook and payload mass more than higher frequency waves (lower periods waves). This is logical since lower frequency waves provide less opportunity for the damping present in the system to remove energy which allows a higher SDA value.

For SDA as a function of T, for water depth of 1000m, there is a peak in SDA at 12s period in Figure 11.3d .

Natural frequency is dependent on a system's mass and stiffness. It was chosen to vary the stiffness of the Dyneema and steel rope. This was done instead of changing the mass (by density) since for the long ropes considered changing the stiffness seems more interesting. For example, the effect of an object's change in stiffness when holding the object is more interesting than a change in its mass. Furthermore, from a manufacturing point of view changing the stiffness of the Dyneema rope is likely easier since a different fiber can be used whereas changing the mass is more difficult since all fibers are relatively light. The stiffness is changed by changing the length of the Dyneema and steel rope since the stiffness is inversely proportional to length. The length used to calculate the mass is kept at the default value, so the mass does not change.

The natural periods for the water depths of [2500, 2000, 1500, 1000]m were found in Table 11.4. A natural period exists at close to 12s for the 1000m water depth in Figure 11.3d. As shown in Table 11.4, this natural period is 11.36s. The peak in SDA at 12s period shifts to a lower period with increasing steel rope stiffness. For example, with a 50% higher steel rope stiffness the peak at 12s shifts to 9s, see Figure 11.4b. A natural period exists at 9.28s for the 50% higher steep rope stiffness as shown in Table 11.2. Thus, the shifted peak is due to the shifted natural period from 11.36s to 9.28s. This natural period is associated with the steel rope. The effect on natural period of other increased steel rope stiffnesses is shown in Table 11.2. Since the natural period is inversely proportional to rope stiffness, a larger stiffness results in a smaller natural period. To clearly show the effect of steel rope stiffness, only the 1000m water depth is considered in Figure 11.4c. The black line is the case for normal steel rope stiffness, with a peak in SDA at 12s. An increasing steel rope stiffness results in a decrease of the period associated with the peak in SDA.

Furthermore, note that a peak in SDA for the water depth of 1500m appears at 12s when increasing the steel rope stiffness by 50% in Figure 11.4b. This is explained with the same reasoning of a natural period being shifted to a lower period. For 1500m with normal steel rope stiffness there is a natural period at 14.95s (out of the range of the graph) and for 1000m the natural period shifts to 12.21s. Thus, the peak at 12s is due to the natural period of 12.21s.

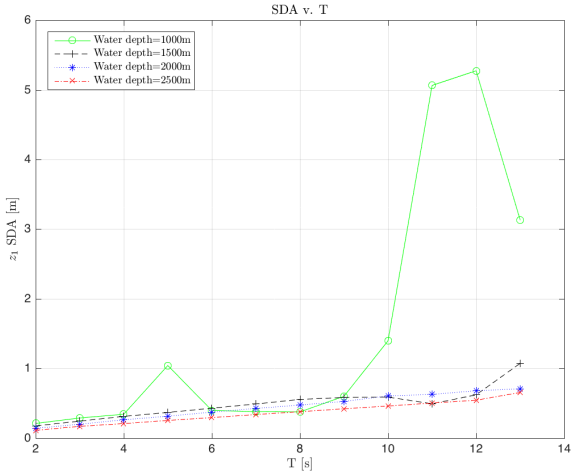

(a) Figure 11.3d is repeated for comparison

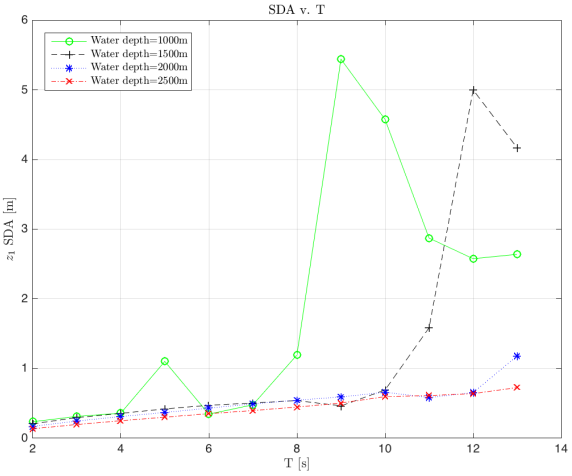

(b) SDA(T,wd), steel rope stiffness increased by 50% relative to the case in Figure 11.4a

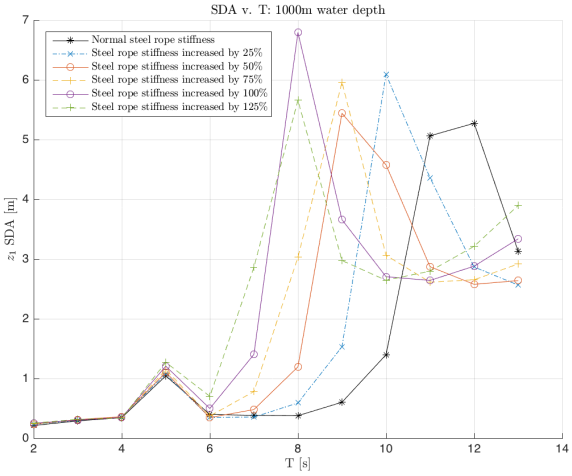

(c) SDA(T), water depth of 1000m, steel rope stiffness increased by various factors. For the natural periods associated with the increases in stiffness see Table 11.2

Figure 11.4

Table 11.2: Natural periods for 1000m water depth as function of increased steel rope stiffness

Steel rope stiffness increase [%]	0 (default case)	25	50	75	100	125
Natural period	11.36	10.16	9.28	8.59	8.03	7.57

In contrast, in Figure 11.3d the peak at 5s for a water depth of 1000m does not shift with a 50% higher steel rope stiffness. A natural period exists at 4.95s and the peak at 5s is due to the influence of this natural period. This natural period is associated with the Dyneema rope. This is demonstrated by increasing the Dyneema rope stiffness by 50%, shown in Figure 11.5b. Considering the water depth of 1000m, the peak at 12s is unaffected but the peak at 5s shifts to a lower period, 4s (since the natural period of 4.95s shifts to 4.05s, due to the increase in Dyneema stiffness). This is expected since a larger stiffness results in a smaller natural period. The effect on the associated natural period of increasing the Dyneema rope stiffness by other amounts is shown in Table 11.3.

To verify that the peak in SDA at 5s in Figure 11.3d is due to exciting a natural period the time-series

is shown. Using T=5s for the 1000m water depth the z_1 (hook and payload mass displacement) and z_d (Dyneema rope displacement) time-series have a beating character verifying that 5s is close to a natural period, see Figure 11.6a. For water depths of [1500, 2000, 2500]m there is no beating character to z_1, see Figures 11.6b, 11.6c, and 11.6d respectively.

Furthermore, when increasing the Dyneema rope stiffness by 50%, in Figure 11.5b, for the 1500m water depth there is a peak in SDA appearing now at 6s. This is close to the natural period of 6.05s which was at 7.41s when the normal Dyneema rope stiffness was used in Figure 11.5a. This natural period at 7.41s is not close enough to the input period of 8s for the natural period to have a significant effect on the SDA in Figure 11.5a although it has some influence on the motion of z_d as shown in Figure 11.8b.

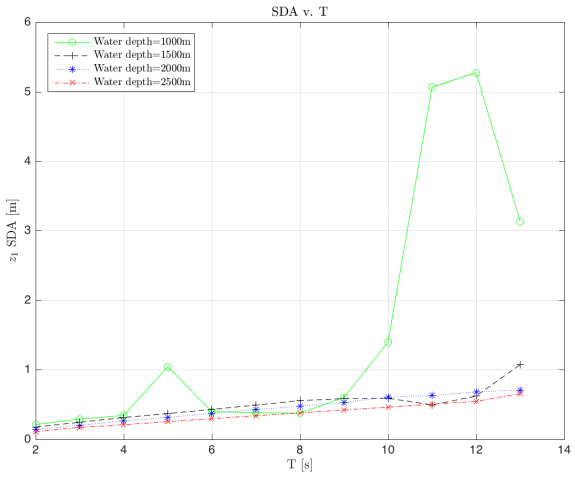

(a) Figure 11.3d is repeated for comparison

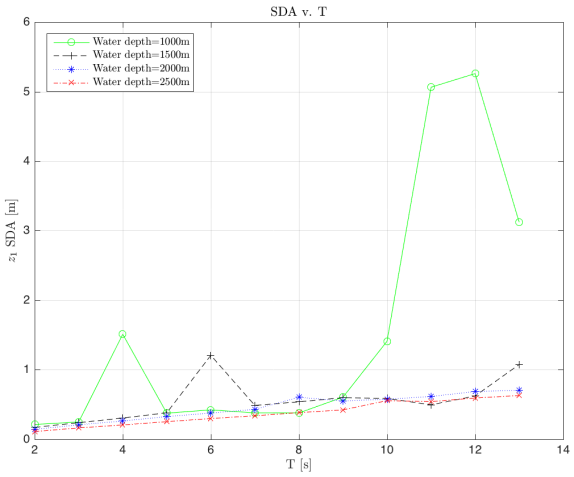

(b) SDA(T,wd), Dyneema rope stiffness increased by 50% relative to the case in Figure 11.5a

Figure 11.5

Table 11.3: Natural periods for 1000m water depth as function of increased Dyneema rope stiffness

Dyneema rope stiffness increase [%]	0	25	50	75	100	125
Natural period	4.95	4.43	4.05	3.75	3.52	3.33

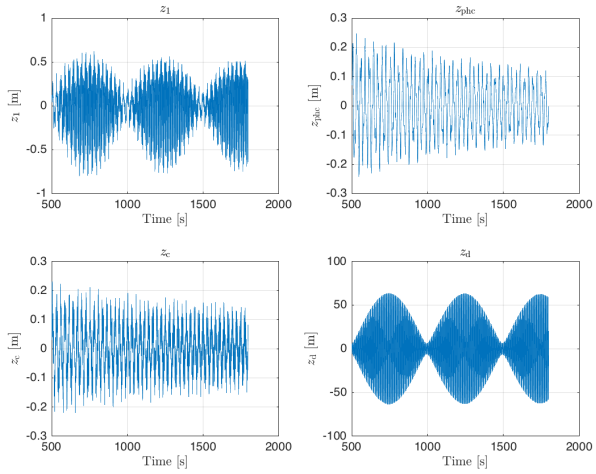

(a) water depth: 1000m, T=5s, H=2.5m

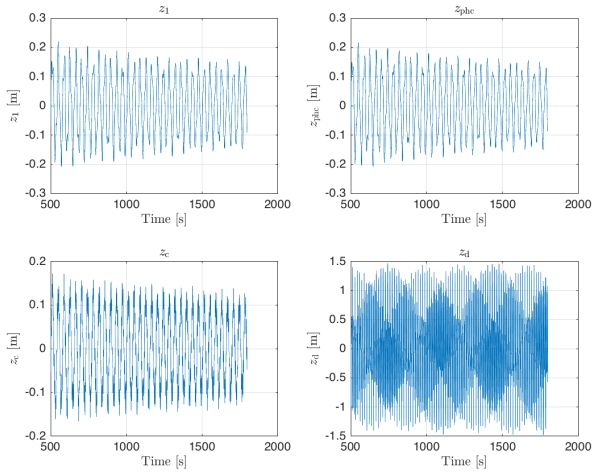

(b) water depth: 1500m, T=5s, H=2.5m

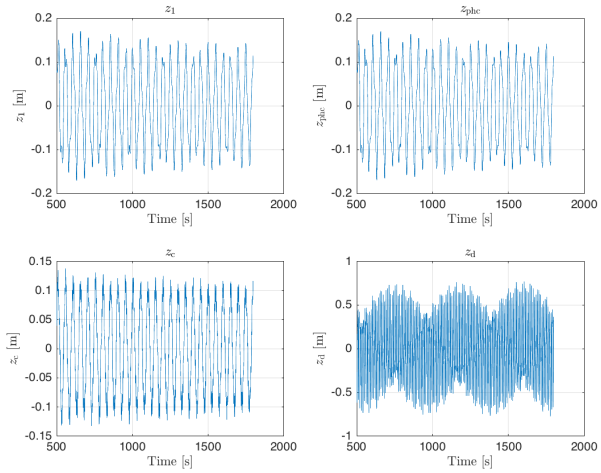

(c) water depth: 2000m, T=5s, H=2.5m

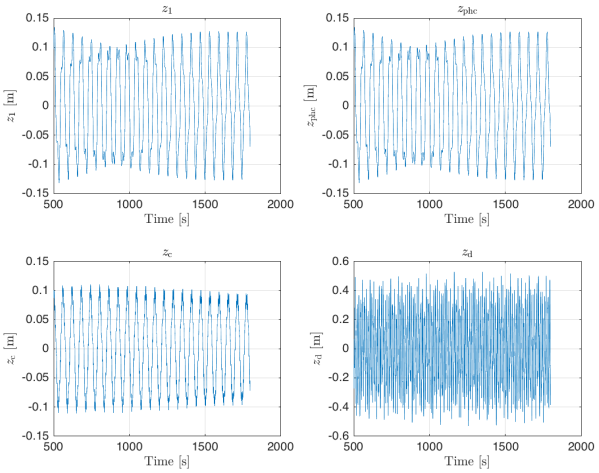

(d) water depth: 2500m, T=5s, H=2.5m

Figure 11.6

For the larger water depths of 2000/2500m, the steel/Dyneema ropes are less stiff (since stiffness is inversely proportional to rope length and rope length is proportional to water depth) which means the natural periods are higher. In other words, natural period is proportional to rope length. In Figure 11.3d, the natural period associated with the Dyneema rope is within the range of the graph. However, the natural period does not coincide with the periods used in the graph. Although some of the natural periods are close. For example, for 2000m there is a natural period at 9.88s, as shown in Table 11.4. There is no clear peak as was the case for the shallower water depths such as 1000m. In Figure 11.3d, for 1000m a natural period at 11.36s manifested itself as a clear peak at a 12s period on the graph. The response is more sensitive at the shallower water depths. It is not clear why this occurs. Taking into account lateral motion of the steel/Dyneema rope, which contributes drag thus dissipating energy and reducing SDA for large water depths would be an explanation. However, lateral motion of the steel/Dyneema rope was not included so this explanation is not correct.

It should be noted that the natural period associated with the Dyneema rope is smaller than the natural period associated with the steel rope. The mass of the steel is significantly larger than that of the Dyneema. The natural period is proportional to the mass. This contributes to the natural period of the Dyneema rope being smaller than the natural period associated with the steel rope.

Table 11.4: Natural periods for [2500, 2000, 1500, 1000]m water depths

	Natural period [s]			
Water depth [m]	**2500**	**2000**	**1500**	**1000**
Natural period 1	2.85	2.85	2.85	2.85
Natural period 2	12.34	9.88	7.41	4.95
Natural period 3	20.47	17.91	14.95	11.36
Natural period 4	60.72	49.66	38.64	27.68

Time-series for T=12s, H=2.5m, and 1000m water depth

The time-series data associated with the T=12s, H=2.5m, and 1000m water depth situation is shown in Figure 11.7. The enlarged motion of z_1 relative to the input z_{in} is clear in Figure 11.7.

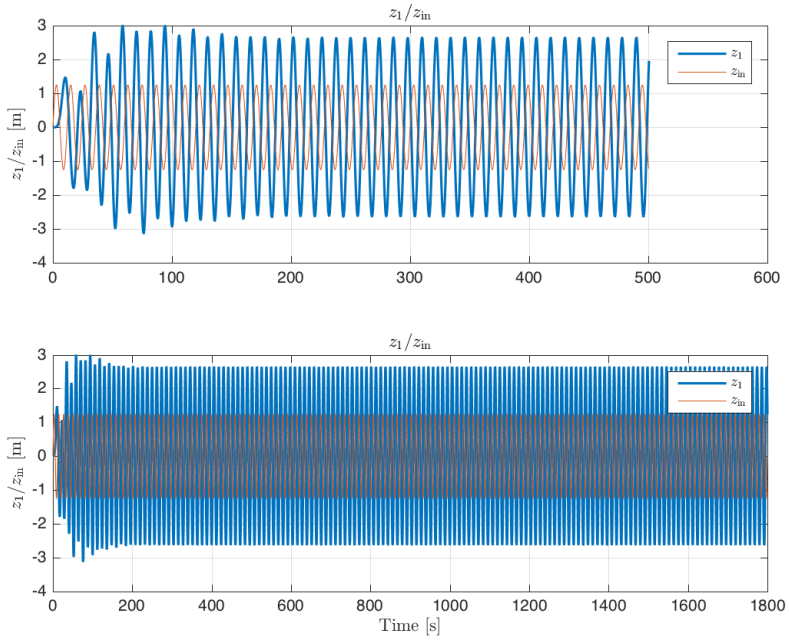

Figure 11.7: z_1 (hook and payload motion) and z_{in} (crane-tip motion), top sub-plot shows data for time from 0s to 500s. There is some transient behavior initially, as would be expected. The bottom sub-plot shows the full simulation time from 0s to 1800s.

11.5.1.2 Varying Hs/H

For the irregular input, the SDA values were found for fixed Tp=8s as a function of Hs and water depth, see Figure 11.3a for results. For the regular input, the SDA values were found for fixed T=8s as a function of H and water depth, see Figure 11.3c for results.

Since the 2500m water depth is the operating condition of interest this water depth is used in Figure 11.3e to more clearly show the effect of wave height. The regular input result shows the trend clearly, with increasing wave height the SDA increases as would be expected. This shows that for more violent wave conditions the PHCS passes through more energy to the hook and payload mass. This is an expected result.

For SDA as a function of H (for fixed T=8s) there is a difference in magnitude and trend for water depth of 1000m compared to other water depths in Figure 11.3c.

In Figure 11.3c, for water depths of [1500, 2000, 2500]m the trend is that SDA is larger for a given H value for smaller water depths. A possible explanation is that the ropes have smaller mass for smaller water depths meaning they have less inertia so have more motion for a given acceleration. This competes with the larger rope stiffness for smaller water depths which would decrease the motion for a given force. For the 1000m water depth this trend does not hold. It is seen that for water depths of [1500, 2000, 2500]m the SDA value increases more steeply as a function of H than for the 1000m water depth. This gives the line for the 1000m water depth a different trend and magnitude.

In Table 11.4 it is shown that none but one of the natural periods for any water depth is close to 8s (the closest being 7.41s for water depth of 1500m). For H=2m and T=8s the time-series results for various water depths are shown in Figure 11.8. Figure 11.8b shows that for water depth of 1500m there is a beating character to z_{d} indicating the input period is close enough to the natural period of 7.41s to have an effect, although the effect is not that large, as mentioned earlier. For water depths of [1000, 2000, 2500]m for z_{d} there is no beating trend, indicating a natural period does not have influence. Thus, it seems the different trend for the 1000m water depth line is not related to a natural period issue.

A possible explanation for the break away from the trend for 1000m water depth is that the non-linearities in the system (orifice, accumulators, quadratic water drag) have some contribution. Although it is unclear what the contribution is.

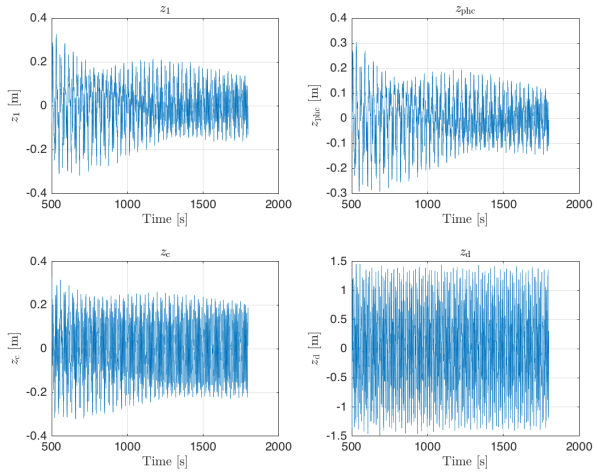

(a) water depth: 1000m, H=2m, T=8s

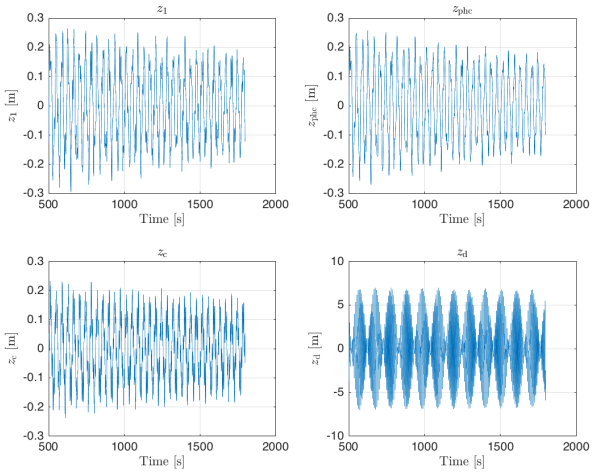

(b) water depth: 1500m, H=2m, T=8s

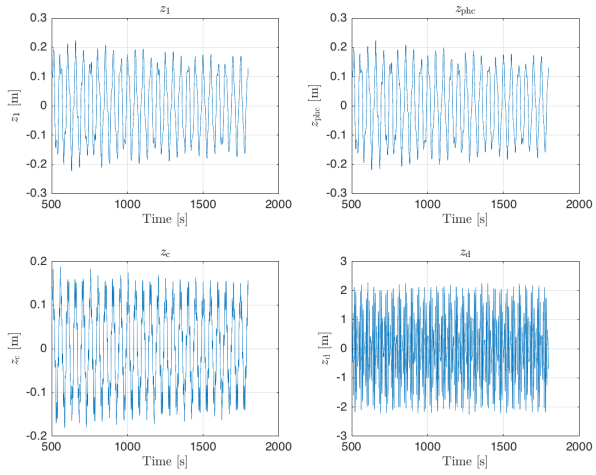

(c) water depth: 2000m, H=2m, T=8s

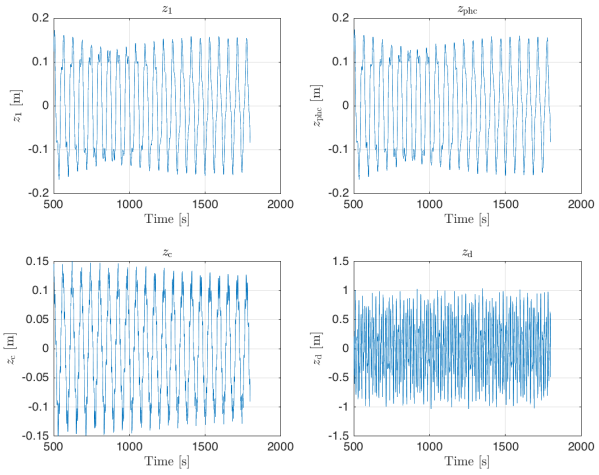

(d) water depth: 2500m, H=2m, T=8s

Figure 11.8

11.5.2 Compensation rate β

The SDA results in section 11.5.1 give measures of the motion of the hook and payload mass. However, they do not provide a clear measure of how effective the PHCS is at reducing the motion. To quantify this a relative measure is needed, the compensation rate β defined in section 11.3.2 is such a relative measure.

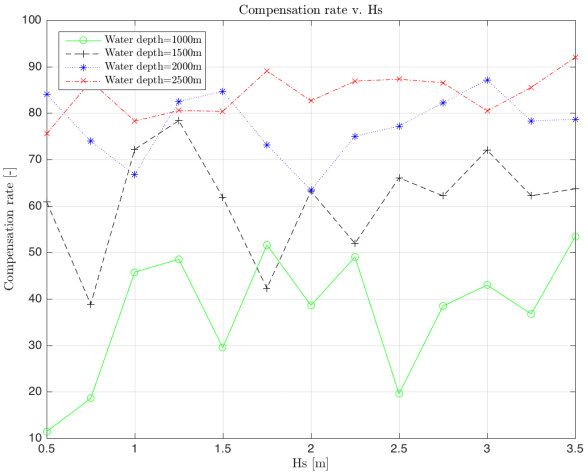

(a) β(Hs,wd) (irregular), for Tp=8s

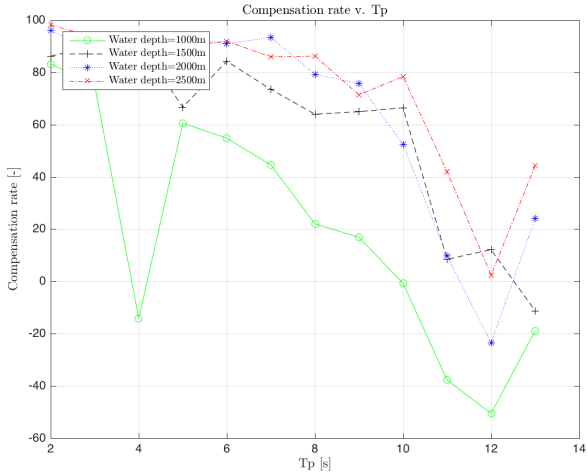

(b) β(Tp,wd) (irregular), for Hs=2.5m

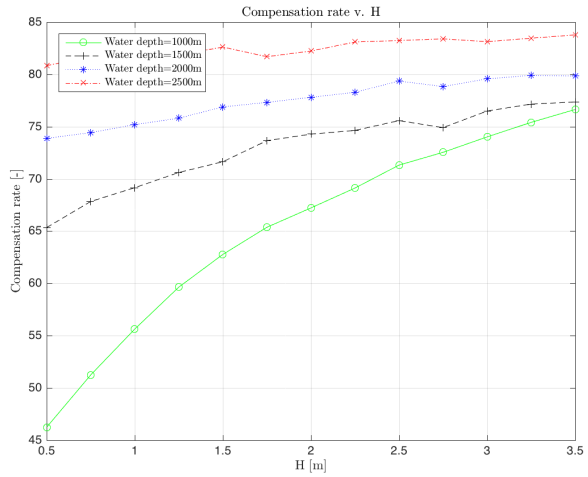

(c) β(H,wd) (regular), for T=8s

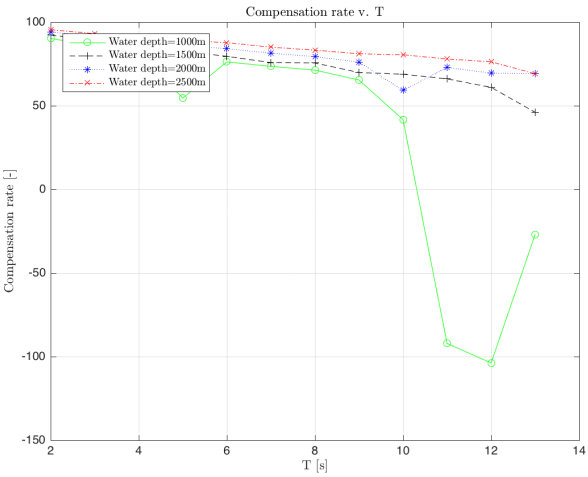

(d) β(T,wd) (regular), for H=2.5m

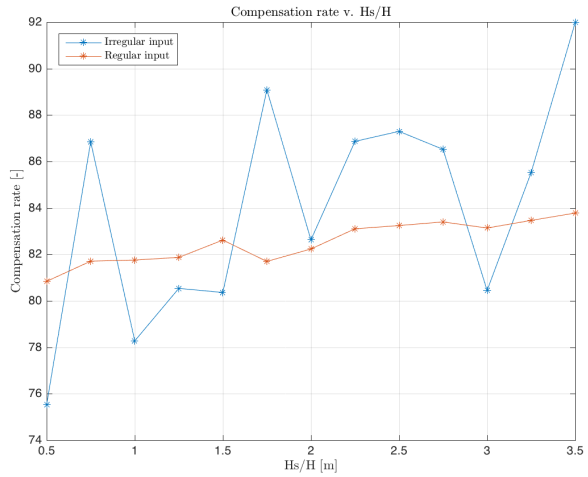

(e) Water depth: 2500m

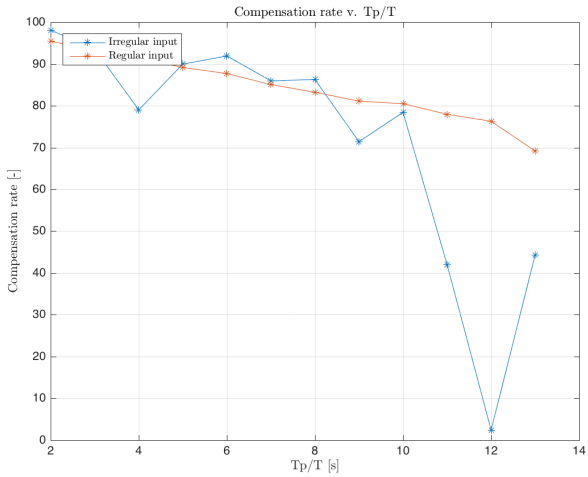

(f) Water depth: 2500m

Figure 11.9: Compensation rate: Irregular and regular input results

11.5.2.1 Varying Tp/T

For the irregular input, the compensation rate was found for fixed Hs=2.5s as a function of Tp and water depth, see Figure 11.9b for results. For the regular input, the compensation rate was found for

fixed H=2.5m as a function of T and water depth, see Figure 11.9d for results. The regular results are focused on, as explained earlier. For the 1000m water depth there are sharp decreases in β at 5s and 12s periods. This corresponds to the peaks in SDA at 5s and 12s periods in Figure 11.3d for the SDA. The meaning is logical, a peak in SDA means there is poor compensation rate.

Since the 2500m is the operating condition of interest this water depth is used in Figure 11.9f to more clearly show the effect of wave period. The regular input result shows the trend clearly, with increasing wave period the compensation rate decreases. This indicates the PHCS is less effective with increasing wave period. This can be explained by the fact that lower frequency (higher period) waves will cause motion in the system to experience less damping compared to a higher frequency wave.

11.5.2.2 Varying Hs/H

For the irregular input, the compensation rate was found for fixed Tp=8s as a function of Hs and water depth, see Figure 11.9a for results. For the regular input, the compensation rate was found for fixed T=8s as a function of H and water depth, see Figure 11.9c for results. The regular results are focused on, as explained earlier. There is a consistent trend in Figure 11.9c, with increasing water depth the compensation rate increases (better performance).

Since the 2500m is the operating condition of interest this water depth is used in Figure 11.9e to more clearly show the effect of wave height. The regular input result shows the trend clearly, with increasing wave height the compensation rate increases. This means the PHCS is more effective for larger wave height. This can be explained by the fact that a larger wave height can provide more energy which enables the system to work more effectively.

11.5.3 R ratio

The rms reduction ratio (R) was defined in section 11.3.3. It gives a measure of the standard deviation of the z_1 signal. The results for R are shown below.

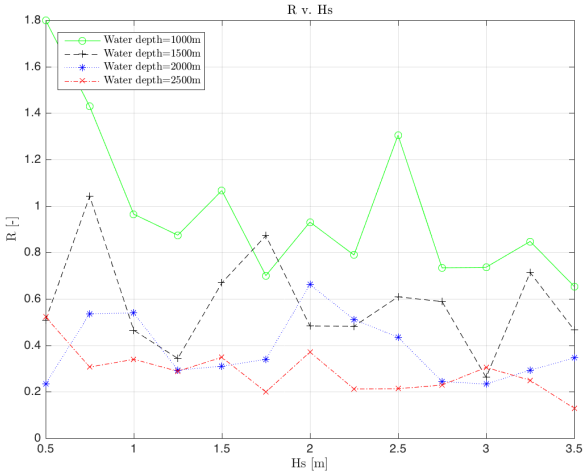

(a) R(Hs,wd) (irregular), for Tp=8s

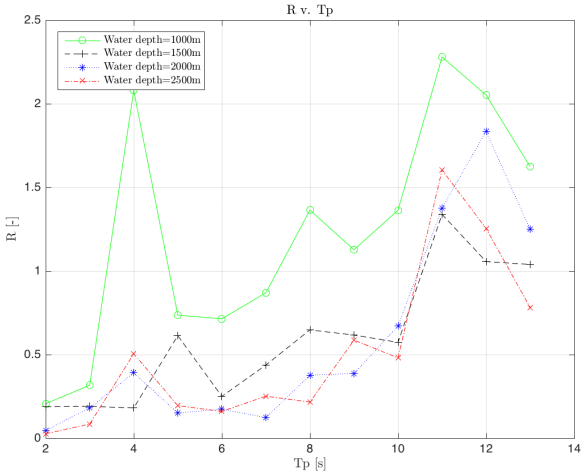

(b) R(Tp,wd) (irregular), for Hs=2.5m

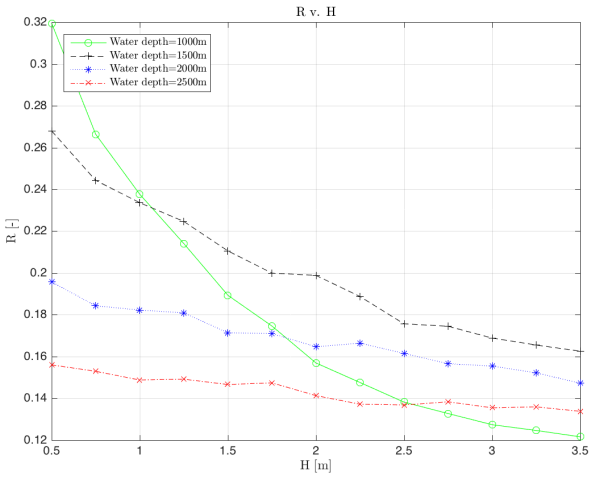

(c) R(H,wd) (regular), for T=8s

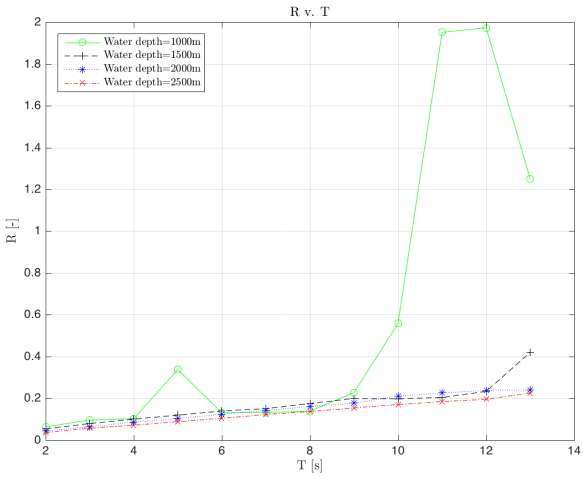

(d) R(T,wd) (regular), for H=2.5m

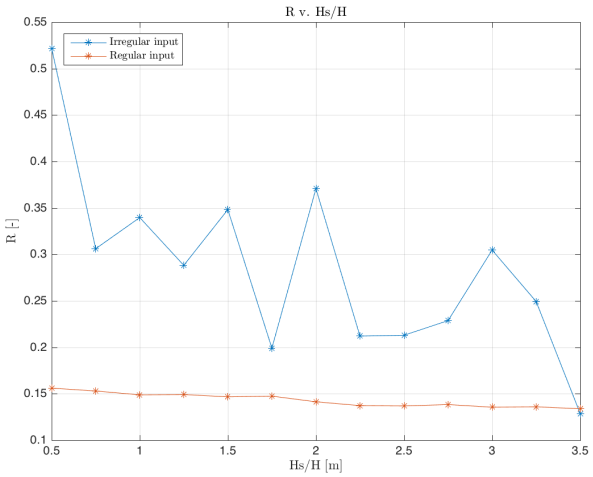

(e) Water depth: 2500m

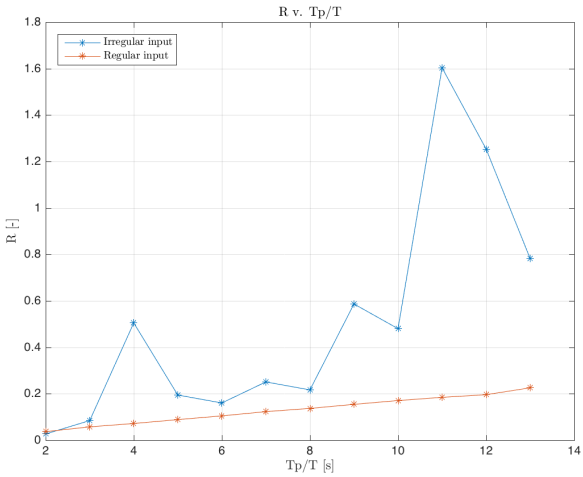

(f) Water depth:2500m

Figure 11.10: R ratio: Irregular and regular input results

11.5.3.1 Varying Tp/T

For the irregular input, R was found for fixed Hs=2.5s as a function of Tp and water depth, see Figure 11.10b for results. For the regular input, R was found for fixed H=2.5m as a function of T and water

depth, see Figure 11.10d for results. The regular results are focused on, as explained earlier. There is a peak in R at 5s and 12s. This is consistent with the SDA results in Figure 11.3d. This is because a peak in R means there is poor compensation which corresponds to a high SDA value. The reasons for the peaks were given earlier and are not repeated

Since the 2500m is the operating condition of interest this water depth is used in Figure 11.10f to more clearly show the effect of wave period. The regular input result shows the trend clearly, with increasing wave period R increases. This indicates the PHCS has lower performance with increasing wave period. This was explained when discussing the results of the compensation rate in section 11.5.2.

11.5.3.2 Varying Hs/H

For the irregular input, R was found for fixed Tp=8s as a function of Hs and water depth, see Figure 11.10a for results. For the regular input, R was found for fixed T=8s as a function of H and water depth, see Figure 11.10c for results. The regular results are focused on, as explained earlier. Considering water depths [1500, 2000, 2500]m with increasing water depth the R value decreases for a given H. This is consistent with the decrease in SDA, for fixed H, for increasing water depth when considering [1500, 2000, 2500]m in Figure 11.3c. This is because a lower R means better compensation performance which means a lower SDA. The trend for 1000m water depth deviates from the rest of the water depths. This was discussed earlier.

Since the 2500m is the operating condition of interest this water depth is used in Figure 11.10e to more clearly show the effect of wave height. The regular input result shows the trend clearly, with increasing wave height the R decreases. This means the PHCS is better when working with larger wave height. This was explained when discussing the results of the compensation rate in section 11.5.2.

11.5.4 Summary

The numerical data is shown in the tables below for the water depth of 2500m. For irregular input, see Table 11.5 for key parameters as a function of Hs and see Table 11.6 for key parameters as a function of Tp. For regular input, see Table 11.7 for key parameters as a function of H and see Table 11.8 for key parameters as a function of T.

A summary of results for irregular and regular input for the design condition of Tp/T=8s and Hs/H=2.5m for water depth of 2500m is shown in Table 11.9. Focusing on regular input, the results show that at design conditions the PHCS provides attenuation of motion with $R = 0.137$ and a compensation rate of 83.2%.

Table 11.5: SDA, R, and β as a function of Hs, for Tp=8s, for water depth of 2500m

Hs [m]	SDA [m]	R [-]	β [%]
0.50	0.123	0.522	75.54
0.75	0.111	0.306	86.85
1.00	0.150	0.340	78.28
1.25	0.179	0.288	80.54
1.50	0.299	0.348	80.36
1.75	0.159	0.199	89.08
2.00	0.354	0.371	82.62
2.25	0.239	0.212	86.87
2.50	0.271	0.213	87.30
2.75	0.287	0.229	86.52
3.00	0.372	0.305	80.45
3.25	0.350	0.249	85.53
3.50	0.231	0.129	91.98

Table 11.6: SDA, R, and β as a function of Tp, for Hs=2.5m, for water depth of 2500m

Tp [s]	SDA [m]	R [-]	β [%]
2	3.1e-5	0.027	98.09
3	0.002	0.084	93.53
4	0.060	0.505	79.02
5	0.085	0.194	89.96
6	0.103	0.160	91.91
7	0.234	0.251	85.97
8	0.293	0.216	86.27
9	0.695	0.587	71.42
10	0.624	0.480	78.43
11	1.970	1.604	42.01
12	2.975	1.254	2.43
13	2.828	0.782	44.34

Table 11.7: SDA, R, and β as a function of H, for T=8s, for water depth of 2500m

H [m]	SDA [m]	R [-]	β [%]
0.50	0.095	0.156	80.84
0.75	0.137	0.153	81.71
1.00	0.174	0.149	81.76
1.25	0.213	0.149	81.87
1.50	0.248	0.147	82.62
1.75	0.284	0.147	81.70
2.00	0.316	0.141	82.23
2.25	0.348	0.137	83.10
2.50	0.380	0.137	83.24
2.75	0.411	0.138	83.40
3.00	0.441	0.135	83.14
3.25	0.472	0.136	83.46
3.50	0.501	0.134	83.78

Table 11.8: SDA, R, and β as a function of T, for H=2.5m, for water depth of 2500m

T [s]	SDA [m]	R [-]	β [%]
2	0.112	0.037	95.47
3	0.170	0.057	93.13
4	0.210	0.072	91.51
5	0.254	0.089	89.15
6	0.295	0.105	87.71
7	0.340	0.123	85.06
8	0.380	0.137	83.24
9	0.422	0.154	81.10
10	0.461	0.171	80.49
11	0.504	0.184	77.96
12	0.545	0.196	76.29
13	0.656	0.225	69.15

Table 11.9: SDA, R, and β for regular and irregular input, for water depth of 2500m

Hs [m] (Tp=8s)	SDA [m]	R [-]	β [%]
2.50	0.271	0.213	87.30
H [m] (T=8s)	SDA [m]	R [-]	β [%]
2.50	0.380	0.137	83.24

11.6 Results irregular and regular input: natural periods and Hs/H=2.5m

Using Table 10.4, the natural frequencies of the ORLAM are converted to natural periods in Table 11.10. These natural periods are used to obtain SDA, β, and R below as was done in section 11.5. The reason to use the natural frequencies of the ORLAM is that this is the linearized version of the NLORLAM and the time-domain results are obtained using the NLORLAM. These natural frequencies

are the closest approximation to the natural frequencies of the NLORLAM.

Table 11.10: Base case, natural periods for the ORLAM

Frequency [Hz]	Natural period [s]
0.0165	60.7
0.0489	20.5
0.0810	12.3
0.3505	2.9

The results are shown in sections 11.6.1, 11.6.2, and 11.6.3. For each measure of motion two sets of parameters were used. One set for irregular input:

- Fixed Hs=2.5m, various Tp values [2.9, 12.3, 20.5, 60.7]s and various water depths [1000, 1500, 2000, 2500]m

And one set for regular input:

- Fixed H=2.5m, various T values [2.9, 12.3, 20.5, 60.7]s and various water depths [1000, 1500, 2000, 2500]m

11.6.1 SDA, natural periods

For the irregular input, the SDA values were found for fixed Hs=2.5s as a function of Tp and water depth, see Figure 11.11a for results. For the regular input, the SDA values were found for fixed H=2.5m as a function of T and water depth, see Figure 11.11b for results. It is important to note that the natural periods were determined assuming a water depth of 2500m. For the regular input case this explains why the SDA value as a function of T for a water depth of 1500m does not reach the same magnitude as for a water depth of 2500m, for example.

In Figure 11.11c the regular and irregular input results are shown for the operating water depth of 2500m. As the natural period is increased the SDA is increased. The SDA values are relatively small for the first two natural periods 2.9s and 12.3s. This indicates they are not as important as the last two natural periods 20.5s and 60.7s where SDA is very large. Nevertheless, these two periods are large for real seas, it is unlikely these periods would be encountered in real-life so they are not a real threat. The natural period of 12.3s seems to pose the largest threat since this is a realistic wave period and the SDA value is quite large, although smaller than the input signal height of 2.5m.

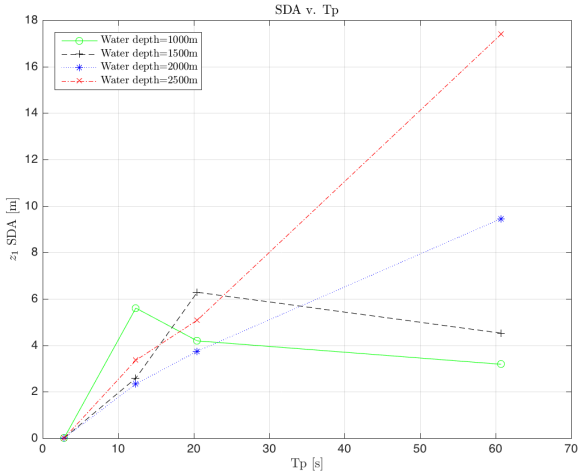

(a) SDA(Tp,wd) (irregular), for Hs=2.5m

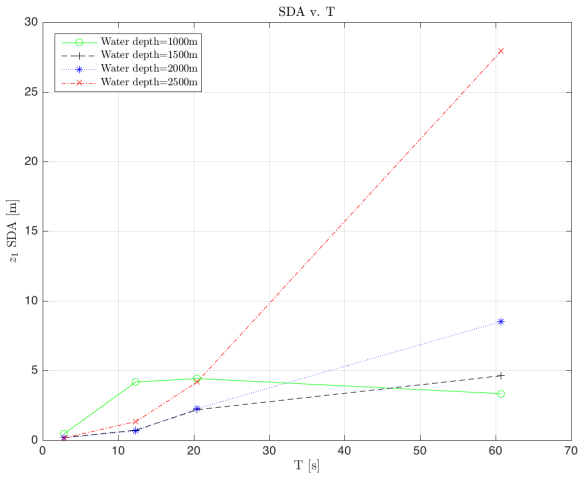

(b) SDA(T,wd) (regular), for H=2.5m

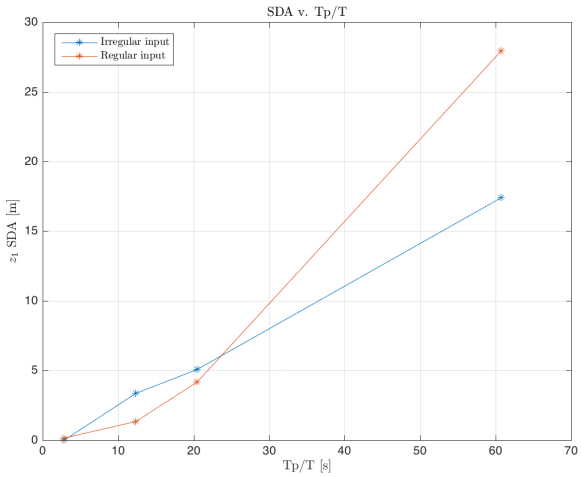

(c) SDA, water depth: 2500m

Figure 11.11: Irregular and regular input results

11.6.2 Compensation rate β, natural periods

For the irregular input, the compensation rate was found for fixed Hs=2.5s as a function of Tp and water depth, wd, see Figure 11.12a for results. For the regular input, the compensation rate was found

for fixed H=2.5m as a function of T and wd, see Figure 11.12c for results.

In Figure 11.12e the results are shown for the operating water depth of 2500m. The regular results are focused on, as explained earlier. As the natural period is increased the compensation rate becomes negative indicating an amplification of the motion. It is expected there is an amplification motion since these periods correspond to the natural periods of the system. At the last two natural periods 20.5s and 60.7s, the compensation rate is negative by a large degree.

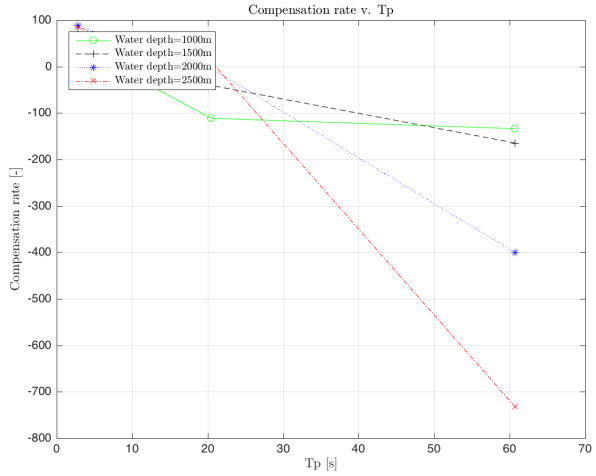

(a) β(Tp,wd) (irregular), for Hs=2.5m

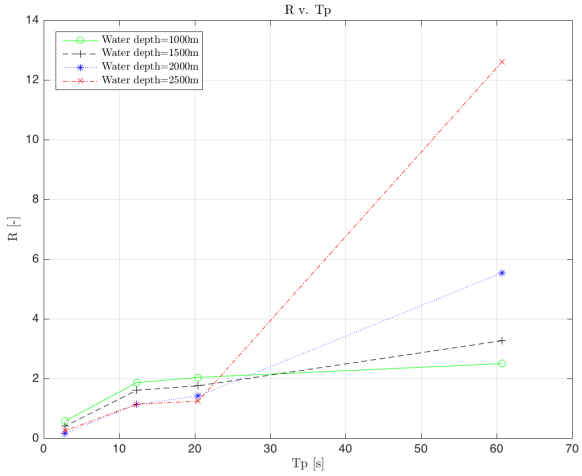

(b) R(Tp,wd) (irregular), for Hs=2.5m

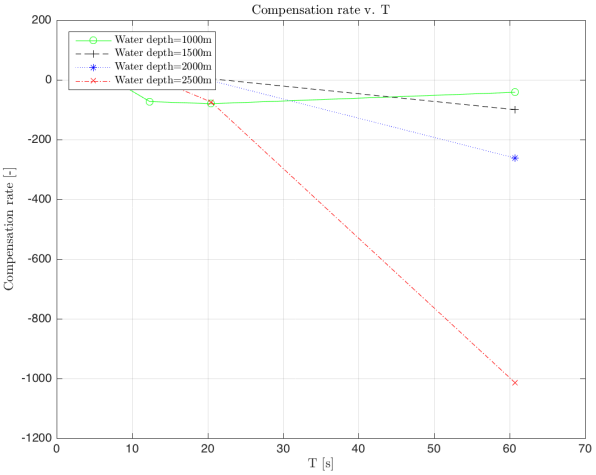

(c) β(T,wd) (regular), for H=2.5m

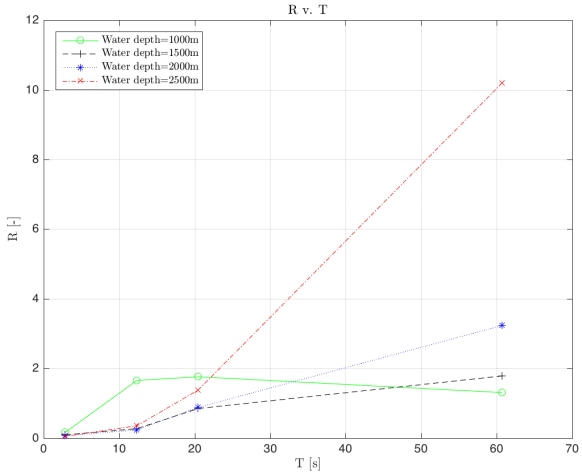

(d) R(T,wd) (regular), for H=2.5m

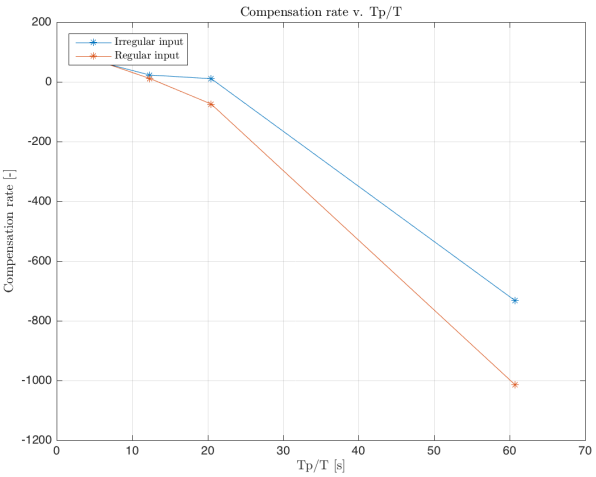

(e) β, water depth: 2500m

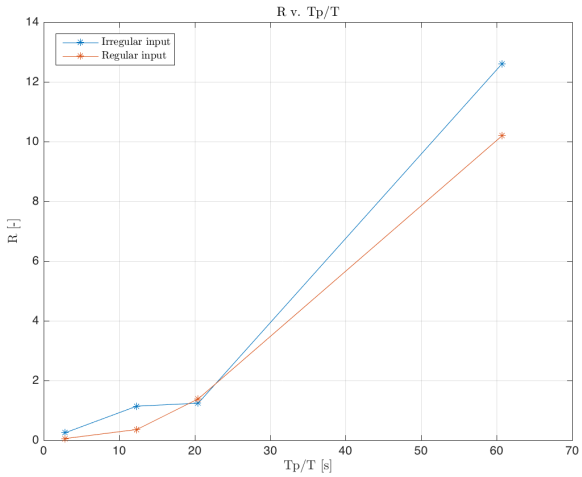

(f) R, water depth: 2500m

Figure 11.12: Irregular and regular input results

11.6.3 R ratio, natural periods

For the irregular input, R was found for fixed Hs=2.5s as a function of Tp and water depth, wd, see Figure 11.12b for results. For the regular input, R was found for fixed H=2.5m as a function of T and

wd, see Figure 11.12d for results.

In Figure 11.12f the results are shown for the operating water depth of 2500m. The regular results are focused on, as explained earlier. As the natural period is increased the R becomes larger indicating an amplification of the motion. The response at the last two natural periods 20.5s and 60.7s, has R greater than one and much greater than one for 60.7s.

11.6.4 Summary

For irregular and regular input, see Table 11.11 and Table 11.12 respectively, for the parameters of performance as a function of the natural periods for water depth of 2500m.

Considering Table 11.12, there is a large amplification of the hook/payload motion at the natural periods of 20.5s and 60.7s. For the natural period of 2.9s there is small amplification of motion. This is likely due to this period being relatively low which corresponds to a high frequency. This high frequency of input motion in combination with the damping within the system will cause the motion to be attenuated. This is because there are many cycles of motion due to the high frequency allowing damping to have a strong effect. For the natural period of 12.3s there is a no amplification of motion as measured by β.

Table 11.11: Irregular input: SDA, R, and β as a function of Tp, for Hs=2.5m, for water depth of 2500m

Tp [s]	SDA [m]	R [-]	Compensation rate, β [%]
60.7	17.39	12.61	-732.76
20.5	5.08	1.24	10.70
12.3	3.36	1.14	22.88
2.9	0.01	0.25	85.22

Table 11.12: Regular input: SDA, R, and β as a function of T, for H=2.5m, for water depth of 2500m

T [s]	SDA [m]	R [-]	Compensation rate, β [%]
60.7	27.93	10.19	-1014.56
20.5	4.18	1.38	-74.27
12.3	1.34	0.36	11.28
2.9	0.16	0.06	93.09

11.7 Time domain results

The time domain results are shown for the design condition of Tp=8s and Hs=2.5m in water depth of 2500m in sections 11.7.1 and 11.7.2.

11.7.1 Irregular input results

For the irregular input the design conditions mean Tp=8s, Hs=2.5m, and a water depth of 2500m is used. See Figures 11.13a, 11.14a, 11.15a, 11.16a, and 11.17a. The first 500s of the simulation is not focused on since during this time a ramp function is used to increase the wave input to the vessel model to avoid transient behavior in the system. This works by multiplying a linear function $y(t) = \frac{1}{500}t$ with the wave amplitude to gradually increase the forces on the vessel.

11.7.2 Regular input results

The design conditions for the regular input are T=8s, H=2.5m, and a water depth of 2500m. See Figures 11.13b, 11.14b, 11.15b, 11.16b, and 11.17b.

11.7.3 Discussion of results

In the discussion below, the regular input results are focused on.
In Figure 11.13, the time-series for z_1 (hook and payload motion) and z_{in} (crane-tip motion) are shown for irregular and regular input. The regular input results show the attenuation of motion clearly.

In Figure 11.14, the time-series for z_1, z_{phc}, z_{c}, and z_{d} are shown for irregular and regular input. The regular input results are focused on and are as expected. The regular input results show the displacement of Dyneema rope, z_{d}, is much larger than the displacement of the other degrees of freedom. This is reasonable since the Dyneema acts as a much softer spring than the steel rope. z_1 is small in maximum value since this is the movement of the hook/payload mass which is the mass to be controlled. Furthermore, z_{phc} has a small maximum value since this degree of freedom corresponds to the PHCS cylinder. The piston connected to the hook/payload mass oscillates within the PHCS cylinder so it is important the PHCS cylinder does not move significantly so that the hook/payload mass motion can be controlled effectively. Thus, z_{phc} should have a small maximum value.

In Figure 11.15, the time-series for Q_{r} and Q_{r2} are shown for irregular and regular input. The regular input results show that the flow-rate has lower frequency and magnitude now that fluid inertia is included, compared to when there was no fluid inertia in section 7.9.4. With the fluid inertia the flow-rate through the orifice cannot change instantaneously with a pressure change. The fluid inertia also limits the magnitude of the flow-rate. These were issues when the fluid inertia was not included, where flow-rate would change at an unrealistically high frequency and would have highly-varying magnitude.

In Figure 11.16, the pressures P_{a1}, P_{p1}, P_{a3}, and P_{p2} are shown for irregular and regular input. The regular input results show pressure magnitudes that vary across a reasonable range and do not have unrealistically high frequency, as was the case without fluid inertia. The fluid inertia means it takes more time for the fluid to move resulting in a slower pressure change. Without the inertia the pressure would respond instantaneously to a volume change in the accumulator or PHC cylinder chamber. The fluid inertia also limits the magnitude of the pressures. Having smoother changes in the pressures is important so that the PHCS works as intended.

In Figure 11.17, the volume V_{p1} (volume in lower chamber of cylinder) and V_{p2} (volume in upper chamber of cylinder) are shown for irregular and regular input. For both types of input the volumes vary inversely proportional, when one volume increases the other decreases. This is physically correct. This is because the PHCS cylinder is a fixed control volume and the piston-head can only move within this volume.

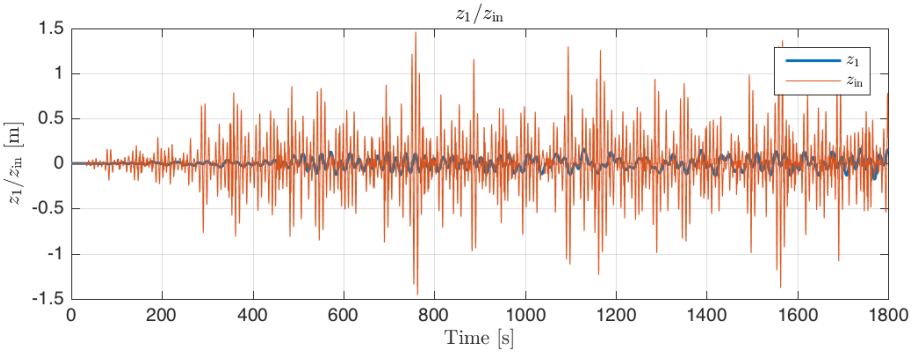

(a) Irregular input. z_1 (hook and payload motion) and z_{in} (crane-tip motion)

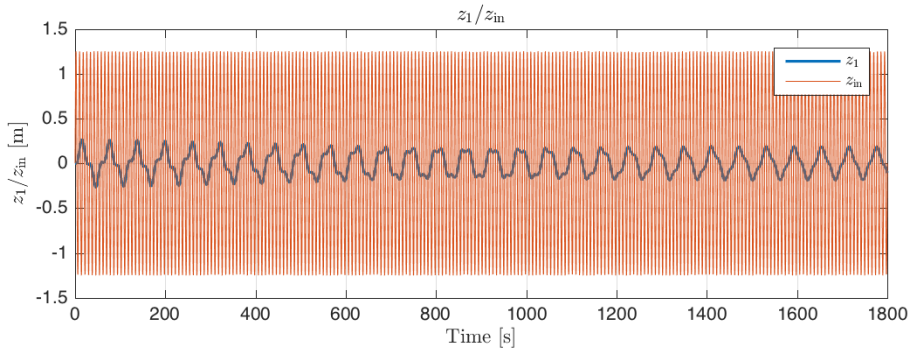

(b) Regular input. z_1 and z_{in}

Figure 11.13: Irregular and regular input results

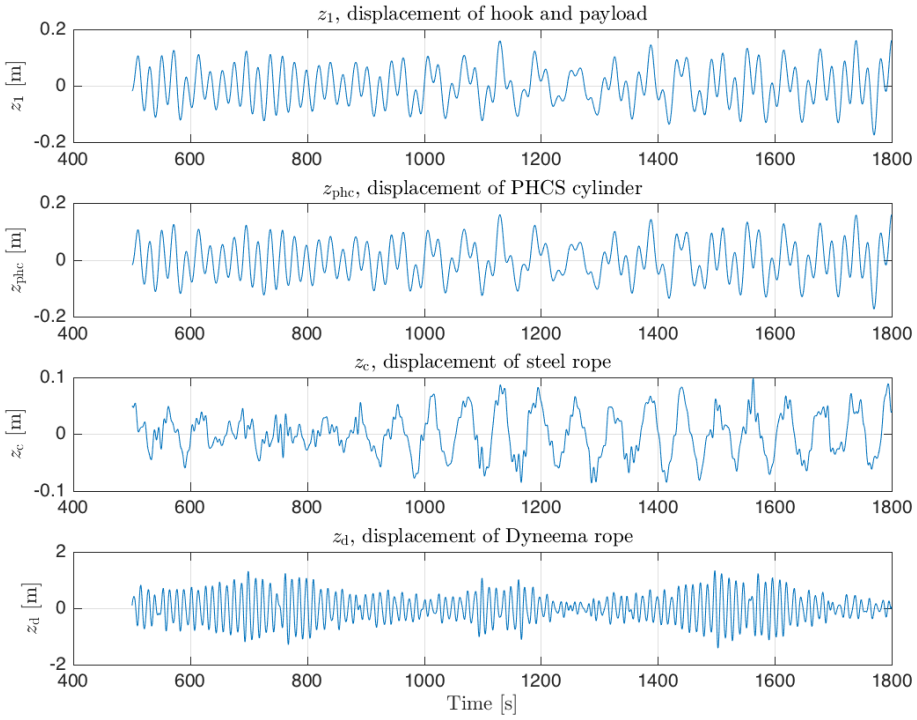

(a) Irregular input. z_1, z_{phc}, z_{c}, and z_{d} are shown in the sub-plots. The simulation is shown from 500s to 1800s since the first 500s is the ramp-up transient period of the vessel model so is not meaningful to discuss.

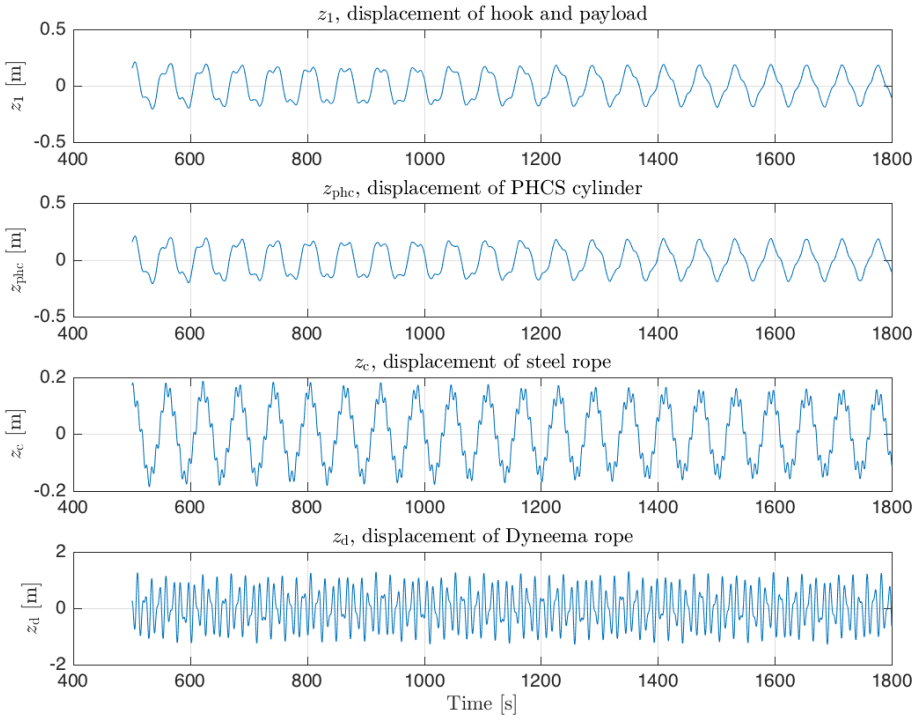

(b) Regular input. z_1, z_{phc}, z_{c}, and z_{d} are shown in the sub-plots. The simulation is shown from 500s to 1800s to be consistent with the time-range for irregular input in Figure 11.14a

Figure 11.14: Irregular and regular input results

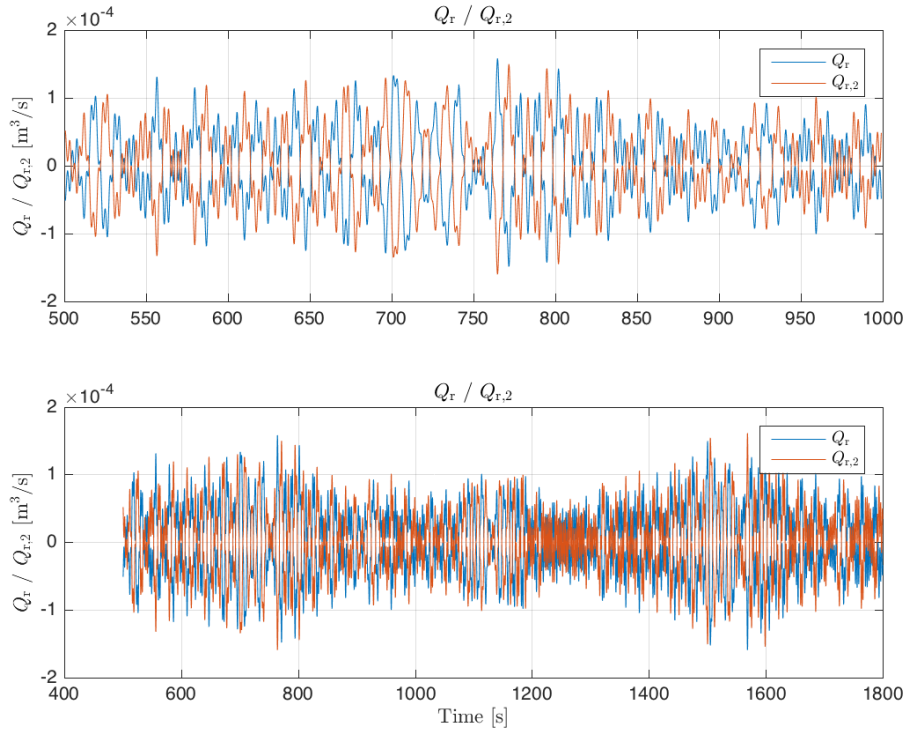

(a) Irregular input. Q_r is the volume flow-rate through the lower orifice and $Q_{r,2}$ is the volume flow-rate through the upper orifice, top sub-plot shows time from 500s to 1000s, this is to show the frequency of the signal. The bottom sub-plot shows the simulation from 500s to 1800s to show the overall time-series.

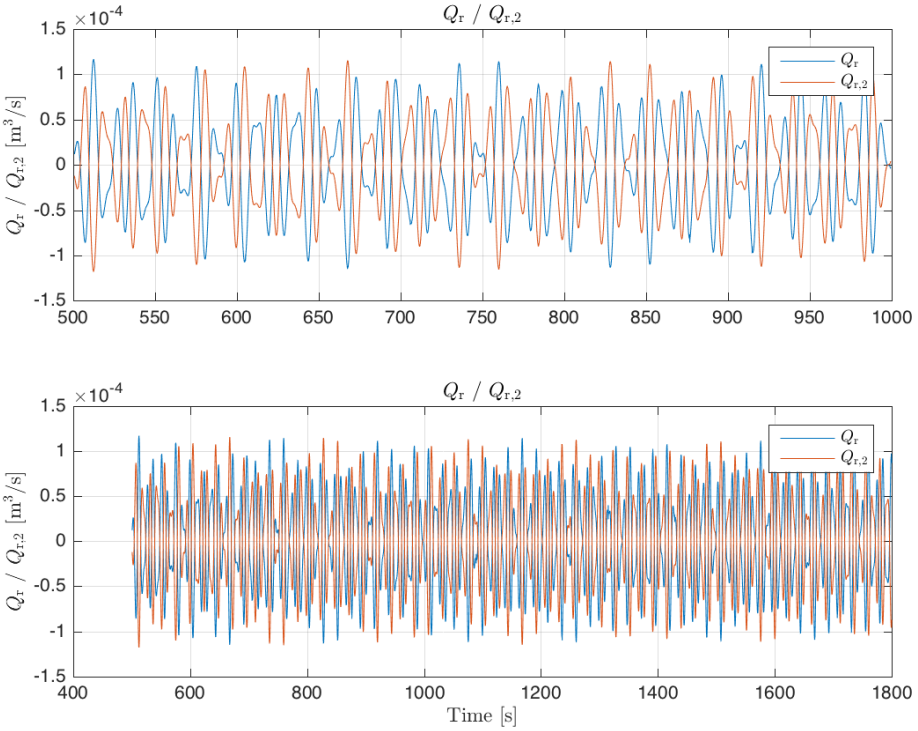

(b) Regular input. Q_r is the volume flow-rate through the lower orifice and $Q_{r,2}$ is the volume flow-rate through the upper orifice. Comparison can be made with the irregular input in Figure 11.15a.

Figure 11.15: Irregular and regular input results

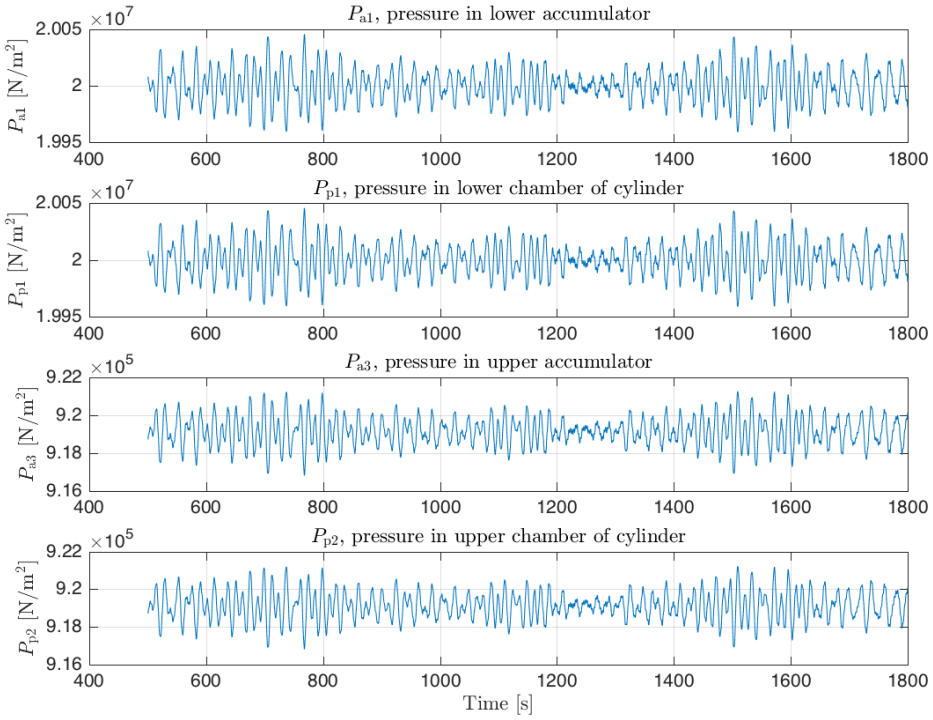

(a) Irregular input. P_{a1}, P_{p1}, P_{a3}, and P_{p2} are the pressures in the system.

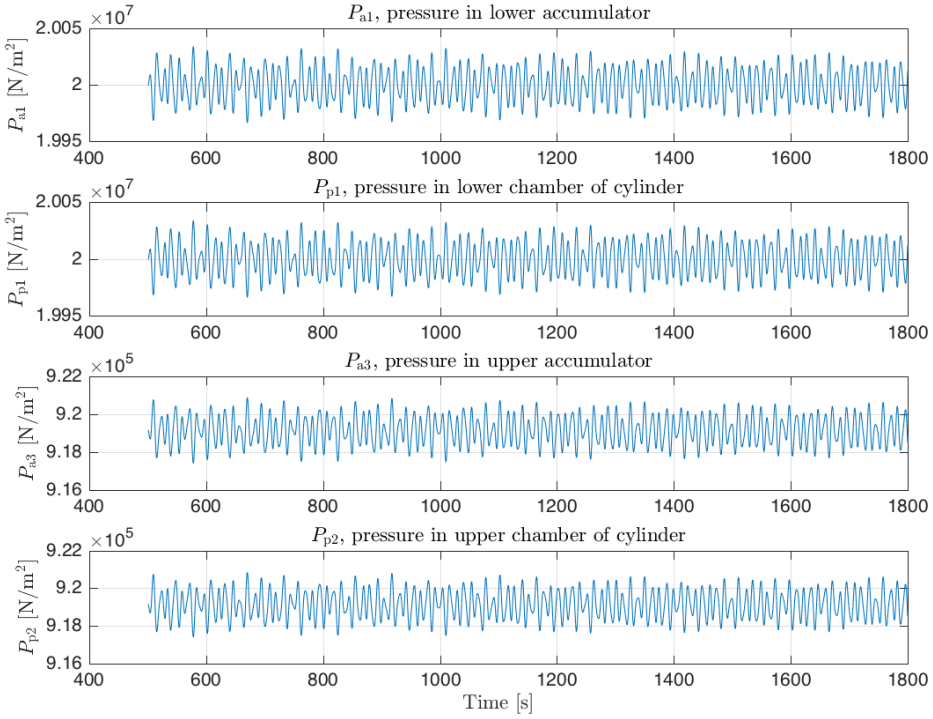

(b) Regular input. P_{a1}, P_{p1}, P_{a3}, and P_{p2} are the pressures in the system. Comparison can be made with the irregular input in Figure 11.16a.

Figure 11.16: Irregular and regular input results

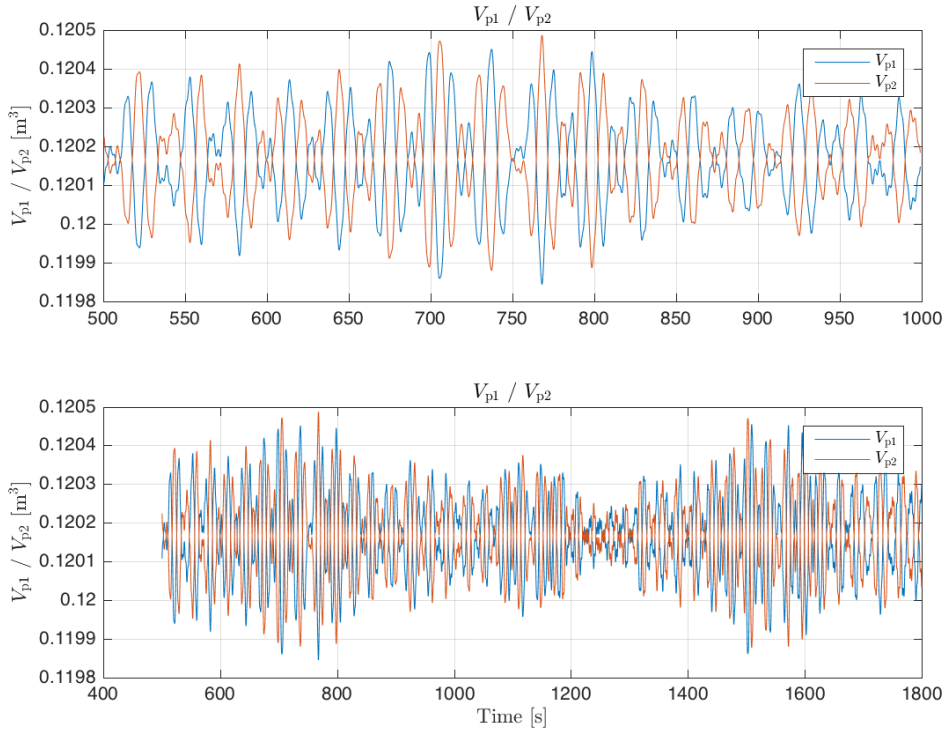

(a) Irregular input. V_{p1} is the volume in the lower chamber of the cylinder and V_{p2} is the volume in the upper chamber of the cylinder.

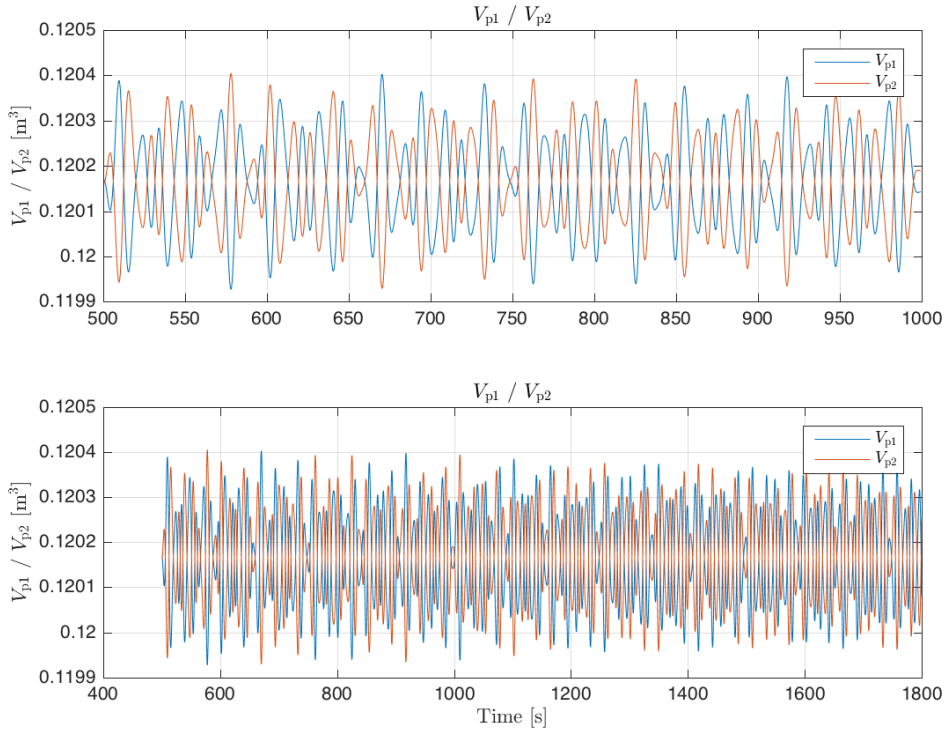

(b) Regular input. V_{p1} is the volume in the lower chamber of the cylinder and V_{p2} is the volume in the upper chamber of the cylinder. Comparison can be made with the irregular input in Figure 11.17a.

Figure 11.17: Irregular and regular input results

11.8 Conclusion

In this chapter, step 3 of the methodology in section 3.3 was completed by assessing the PHCS by itself to see how well it can reduce heave motion by quantifying the performance with criteria of performance. In chapter 12, step 4 of the methodology is started by coupling the PHCS with the vessel.

C-PHCS 12

12.1 Introduction

The PHCS is coupled with the vessel and crane models so that the PHCS gives feed-back to the vessel model, this gives the coupled PHCS model defined as C-PHCS. A regular wave is used as input to the vessel model and from the vessel model the crane-tip model produces the input signal to the PHCS. This is step 4 of the methodology outlined in section 3.3

12.2 Time-domain results

The design conditions of T=8s, H=2.5m and water depth of 2500m are used. It was found that the feed-back to the vessel provided by the PHCS has a negligible effect on the vessel. Thus, there is hardly a difference with the results of the PHCS when using regular input, as was done in chapter 11. The results for T=8s are shown in Figure 12.1 with R= 0.140, β=84.65%, and SDA=0.344m. This is similar to the results without coupling with the vessel of R=0.137, β=83.24%, and SDA=0.380m. The results are compared in Table 12.1, the percent differences are [2.2%, 1.7%, 9.5%] respectively for R, β, and SDA.

Table 12.1: Difference between PHCS and C-PHCS

	PHCS			**C-PHCS**			**Percent difference**		
Wave period [s]	R[-]	β [%]	SDA [m]	R[-]	β [%]	SDA [m]	R [%]	β [%]	SDA [%]
8	0.14	83.24	0.38	0.14	84.65	0.34	2.2	1.7	9.5
12.34	0.36	11.28	1.34	0.19	63.04	0.51	46.4	458.9	61.9
20.46	1.38	-74.27	4.18	1.57	-76.46	3.69	13.8	2.9	11.7
60.70	10.19	-1014.56	27.93	11.48	-959.70	24.53	12.7	5.4	12.2

Selected natural periods of the PHCS from Table 9.6 are used as periods for the wave. The chosen natural periods are [12.34, 20.46, 60.70]s. The natural periods of [0.0207, 0.0208, 2.85]s are too small. The natural periods are used to see if there is any special behavior occurring since the natural periods are used. For natural periods [12.34, 20.46, 60.70]s the results are shown in Figures 12.3a, 12.3b, and

12.3c respectively. The results are compared in Table 12.1. The results are similar except for the 12.34s period here the percent differences are [46.4%, 458.9%, 61.9%] respectively for R, β, and SDA. This can be explained by Figure 12.2 which shows the result when only the PHCS is used. The z_{in} amplitude is close to 1.25m whereas for the C-PHCS it is approximately 1m in Figure 12.3a. The reduction in amplitude is because the vessel model and crane-tip model attenuate the motion. The z_1 signal grows in time for both cases although it grows quicker in the case of the PHCS since the z_{in} amplitude is larger, this explains the large difference in R, β, and SDA values.

The main effect of the coupling with the vessel is that the input signal z_{in} to the PHCS is attenuated due to the vessel model and crane-tip model. This results in lower SDA values relative to the PHCS only (better performance). The β values are improved as well whereas the R values are slightly worse (higher). This is likely because the standard deviation of z_{in} ($\sigma_{z_{\text{in}}}$) for the C-PHCS is lower relative to the PHCS since the wave amplitude is lower and standard deviation is proportional to the amplitude. Since $\sigma_{z_{\text{in}}}$ is in the denominator of the equation for R it will increase R for smaller $\sigma_{z_{\text{in}}}$.

To see the importance of the vessel's natural roll period on the PHCS the natural roll period of the vessel 16.3s is used, see Figure 12.3d. The results is an enlarged crane-tip motion with no special behavior due to using the vessel's natural roll period.

The feed-back of the PHCS on the vessel is negligible as shown in Figure 12.4. There is no visible difference by eye between the coupled and uncoupled system.

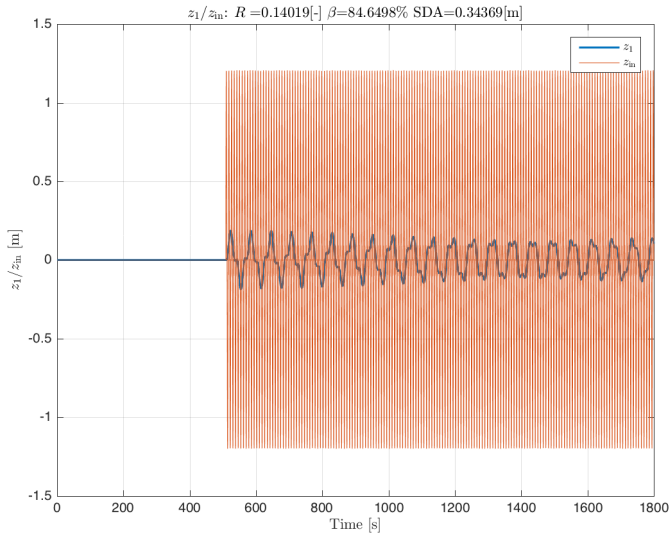

Figure 12.1: C-PHCS: T=8s, the first 500s are a ramp-up period for the vessel model and are removed from the analysis

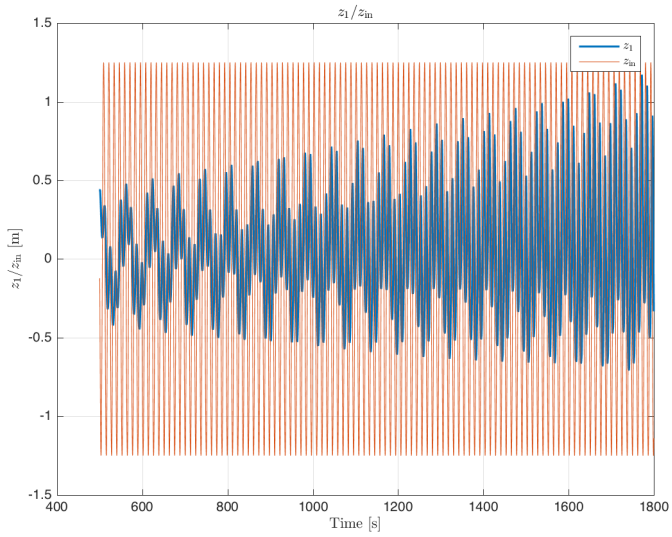

Figure 12.2: PHCS: T=12.34s, the first 500s are removed to be consistent with the figures above

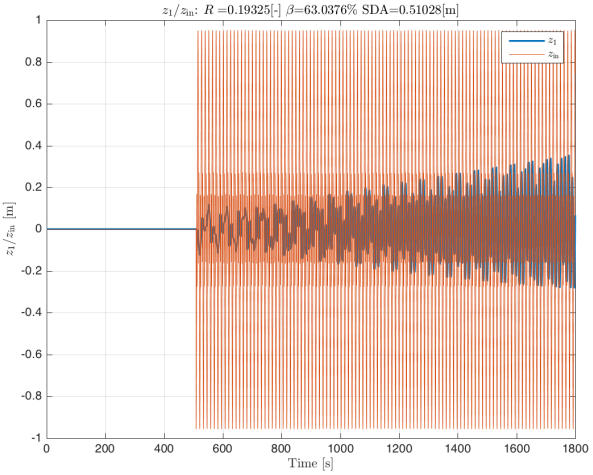

(a) T=12.34s

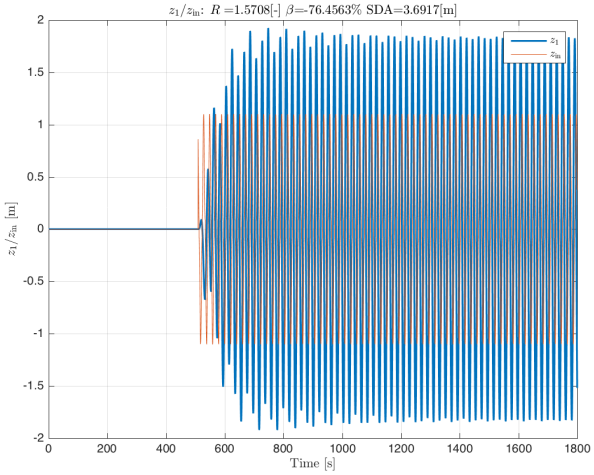

(b) T=20.46s

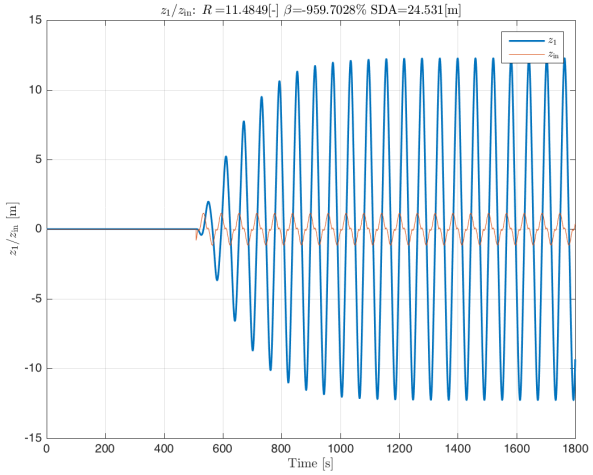

(c) T=60.70s

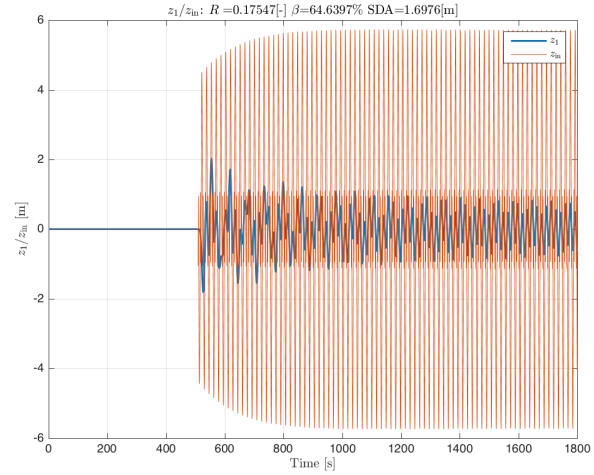

(d) T=16.3s

Figure 12.3: C-PHCS: The first 500s are a ramp-up period for the vessel model and are not included in the analysis

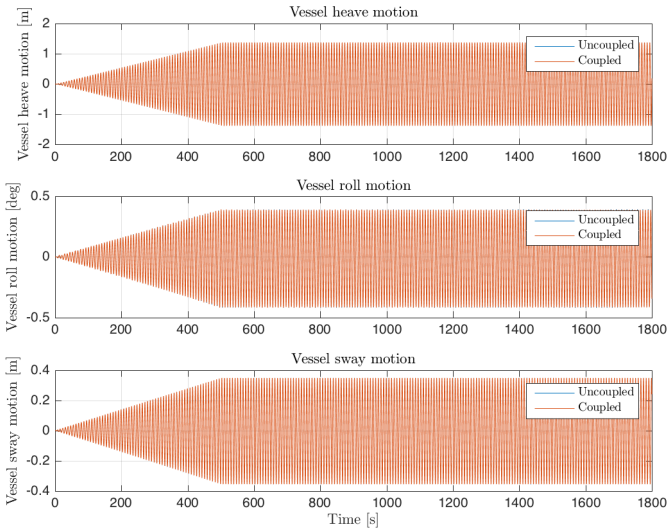

Figure 12.4: Coupled refers to the C-PHCS and uncoupled refers to the PHCS only

12.3 Conclusion

The effect of coupling the PHCS with the vessel model is not significant since the PHCS does not have a significant feed-back effect on the vessel. The primary effect is that the input signal z_{in} to the PHCS is lowered in magnitude due to the vessel and crane-tip. This results in improved PHCS performance as shown by the SDA value. Furthermore, for the design condition of T=8s there is no amplification of the z_1 motion indicating the C-PHCS does not have a natural frequency coinciding with the design wave frequency. Overall, the C-PHCS model has good performance in reducing heave motion with R, β, and SDA values generally close to those for the PHCS only. In chapter 13, the active heave compensation system is coupled to the C-PHCS model. This is step 5 of the methodology in section 3.3.

C-HHCS 13

13.1 Introduction

The AHCS design is chosen and coupled with the PHCS, crane-tip and vessel models, to form the C-HHCS model. The effect of enabling the AHCS on the performance of the C-HHCS is discussed.

13.2 Research question

In section 1.3, the main research question is:

How important is the change in natural period from when the active heave compensation system is disabled to when the active heave compensation is enabled on resonance?

The research question was obtained by considering the scenario described by Mannigel [3] shown in Figure 13.1. The natural period of the pile is 11s, the natural roll period of the vessel is 12.3s, and the swell period is 12s. The natural period of the coupled pile and vessel system is 18.5s. From the research question it is assumed when the AHCS is disabled the coupled pile and vessel system has a natural period. It is assumed when the AHCS is enabled the effect is for there to be some de-coupling between the vessel and the pile. This means the natural period of the coupled pile and vessel system does not exist anymore. Instead, the vessel assumes its natural roll period and the pile assumes its natural period. This is what is meant by the change in natural period from when the AHCS is disabled to when it is enabled. For the case of Mannigel [3] since the vessel roll natural period, pile natural period, and wave period are quite close (11s, 12.3s, and 12s respectively) then resonance does occur. The influence of resonance is shown by the crane tip acceleration in Figure 13.2a and by the vessel roll amplitude increase in Figure 13.2b.

The research question is addressed in section 13.9.6.

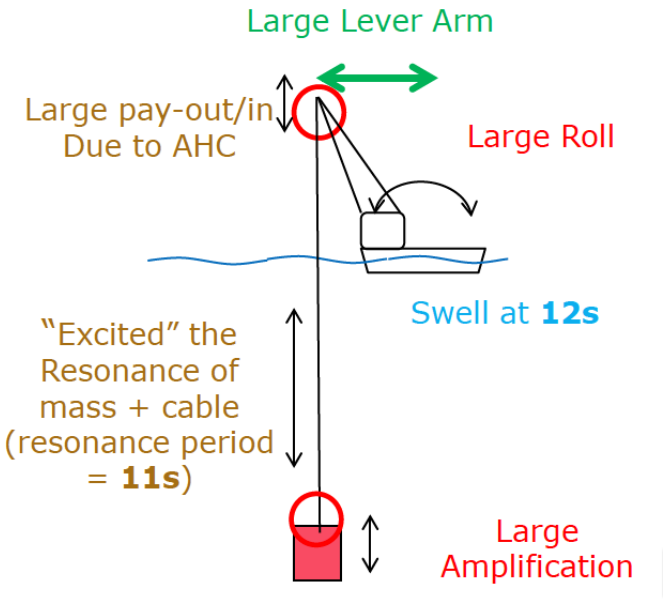

Figure 13.1: Scenario [3]

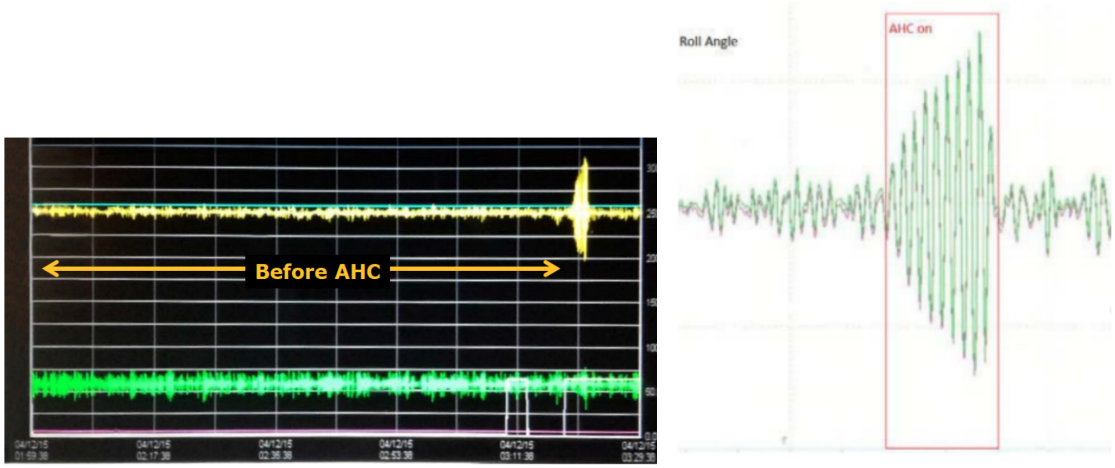

(a) Resonance shown by crane tip acceleration [3]

(b) Resonance shown by roll of vessel [3]

Figure 13.2

13.3 AHC design

The PHCS balances the load of the payload with the pressure difference in the cylinder. This means the passive part takes a larger proportion of the force and the active part takes a smaller proportion of the force. The AHCS is an electric rotary design. The main reasons to use an electric system are the lower power consumption, higher efficiency, and smaller size relative to a hydraulic system, as discussed in the literature review in section 2.2.5.

13.3.1 Variable frequency drive (VFD)

Since this thesis aims to use an electric winch for the AHCS part it is useful to consider ways to operate an electric winch. To power the electric winch a motor is used. There are various motors available. The main types of motors, in order of increasing efficiency, are: salient-pole permanent magnet (PM), non-salient PM, synchronous-reluctance, switched-reluctance, and induction [64]. Although the induction

motor is the least efficient in this comparison it is a relatively simple design, widely manufactured and thus is relatively inexpensive. Therefore, the induction motor is selected. Various drives can be used to control the electric motor. For induction motors the variable frequency drive (VFD) has been used extensively and shown to be effective. Thus, the VFD is used to control the electric induction motor. There are various motor-control methods. These methods are how the VFD controls the motor. There are four main types of motor-control methods for an induction motor coupled to a VFD [65]:

1. V/f (volts-per-hertz)
2. V/f with encoder
3. open-loop vector
4. closed-loop vector

The main difference between these control methods is how they calculate the motor's voltage requirements in time. These methods use pulse-width modulation (PWM), which is a method that varies the width of a fixed signal by modulating pulse durations to generate a variable analog signal [65].

Since torque is more important than speed for an electric crane winch it seems the best way is to use closed-loop vector control. This is because closed-loop vector control uses encoder feed-back with vector control which enables 200% of the motor's rated torque at 0 rpm. This is attractive for cranes which need to hold a load without moving. Also, closed-loop control can operate a motor in torque-control mode which lets the VFD control motor torque rather than motor speed. This is vital whenever torque is more important than speed, which is the case for the crane winch [65].

To control the electric motor a variable frequency drive (VFD) is used. A specific motor-control method is not used since modelling in this detail would result in the simulations taking a long time and would not be practical for this thesis. With a VFD it is possible to assume that the motor torque generated is independent of the motor rotation speed [36]. This allows the electric motor to be controlled using a throttle so that that torque T_e of the motor is controlled with the throttle d via equation (13.1). This is better than modelling the entire electric motor such as current and voltage since these simulations would take very long and would be impractical for this thesis.

$$T_e = \begin{cases} T_{e,max} d & : -1 \leq d \leq 1 \end{cases} \tag{13.1}$$

13.3.2 Methods for controlling heave

One method to control heave is to prevent any changes in rope tension [53]. Another method is to use trajectory tracking of the payload in an earth-fixed coordinate frame [34]. Johansen et al. achieved this using feedforward with an estimate of the vessel's vertical velocity [27]. Since the sea-bed landing is of most interest, the trajectory tracking can be modified to hold the payload at a fixed position, right above the sea-bed.

The trajectory tracking was used by controlling the motion of the payload and hook mass with the winch. Since the Dyneema rope is connected to the winch to connect to the payload/hook mass this affects the Dyneema rope extension as well. The result is shown in Figure 13.3a. The Dyneema displacement z_d is too large. Thus, trajectory tracking was combined with controlling rope tension. The result is shown in Figure 13.3b. The Dyneema displacement is smaller and more reasonable. This means two control loops should be used, one for the displacement of the hook/payload and the other for the tension in the Dyneema. The disadvantage of having two loops is that there is the chance they interfere with each other. Nicoll et al. tried this approach [36] and stated that the controllers should not interfere significantly with each other since the tension controller responds to high frequency disturbances from the heaving motion of the crane-tip whereas the displacement controller limits the low frequency drift from the desired position. Thus, this approach with two loops is used. This concept is similar to that of

Skaare and Egeland [29] discussed in the literature review section 2.3.1.2 where a parallel force/position controller was used. The time-delay between the actuator and the payload at the end of the rope is neglected. In reality there is a time-delay due to the finite speed of longitudinal pressure waves in ropes [34].

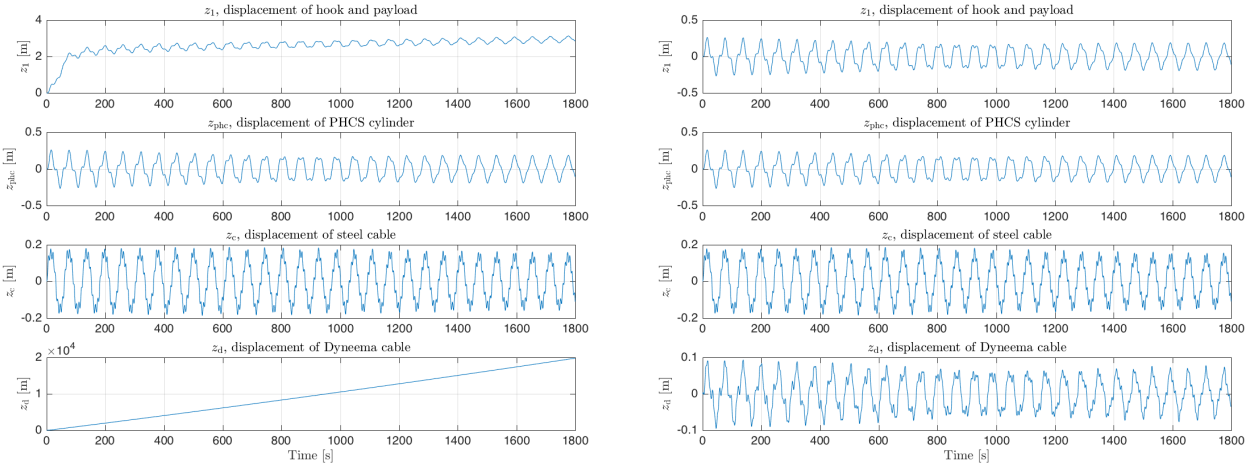

(a) One control loop is used, using P control, controlling z_1

(b) Two control loops used, using P control for both loops, controlling z_1 and F_d

Figure 13.3

13.3.3 PID control

The use of PID control is investigated. The main components of a PID control system are the PID controller, the reference signal, and the plant, see Figure 13.4. The equation for a PID controller is given by (13.2) [66]:

$$u(t) = k_p e(t) + k_i \int_0^t e(\tau)\mathrm{d}\tau + k_d \frac{\mathrm{d}}{\mathrm{d}t} e(t) \tag{13.2}$$

where $u(t)$ is the plant input and $e(t)$ is the tracking error which is the difference between the desired input value $r(t)$ and the plant output $y(t)$. k_p is the proportional gain which is multiplied with the error. This is useful to decrease the steady-state error in the output. k_i is the integral gain which is multiplied with the integral of the error. This is used to remove the steady-state error left over. k_d is the derivative gain which is multiplied with the derivative of the error. This is used to decrease the time it takes to have a steady output.

Taking the Laplace transform of (13.2) gives:

$$U(s) = k_p E(s) + k_i \frac{E(s)}{s} + k_d \Big(sE(s) - e(0) \Big) \tag{13.3}$$

where $e(0)$ is the initial error signal.

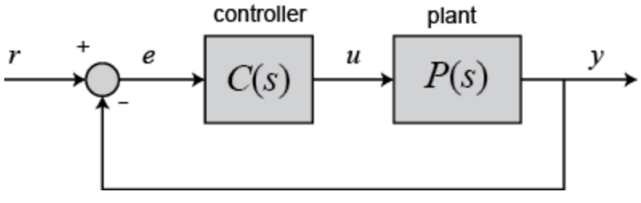

Figure 13.4: PID controller with plant [67]

If it is possible to derive a mathematical model of the plant then various design techniques can be used to determine parameters of the controller [68]. If the plant is too complex for a mathematical model to be derived then an analytical approach cannot be used to determine the parameters of the controller. The plant in this project is complex but an analytical expression for the mathematical model can be obtained. This was done by obtaining the state-space equations and using the MATLAB function 'ss2tf' to obtain the transfer function matrix. Despite having obtained this model, the transfer functions of interest are high order, for the transfer function $\frac{z_1(s)}{r_1(s)}$ the numerator is order 10 and denominator order 16. This makes it complicated to use analytical methods such as the frequency-response approach. This means that an experimental approach is used. A common experimental approach is to use the Ziegler-Nichols rules. The Ziegler-Nichols rules approach gives a reasoned guess for the parameters and gives a starting point for fine tuning [68]. To do this, values for k_p, k_i and k_d are determined based on the transient response characteristics of the plant. This was tried using the method of first having only proportional control and increasing the gain until a critical value where the output has sustained oscillations. It was not possible to find this critical gain. Since the system is quite complex it was decided to use the numerical optimization algorithm within Simulink to find the gain constants.

13.3.4 Designing for stability

- First, the controller should be stable. Stability is defined as: all the poles of closed-loop transfer function of the system must have negative real parts. This can be expressed as the real parts of the eigenvalues of the system being negative [68]. For a multiple-input multiple-output system like that used here, the system is stable if and only if every pole of every transfer function in the transfer function matrix has a negative real part and every transfer function is proper (meaning the number of poles is greater than or equal to the number of zeros)
- Second, it is important that the controller has enough relative stability [68]. To quantify this, the gain and phase margins are used as design criteria.

13.3.4.1 Gain and phase margin

The phase margin γ is 180° plus the phase angle ϕ of the open-loop transfer function at the gain crossover frequency [68]:

$$\gamma = 180^\circ + \phi \tag{13.4}$$

The phase margin is the amount of additional phase lag at the gain cross-over frequency required to bring the system to the beginning of instability. The gain cross-over frequency is the frequency where the magnitude of the open-loop transfer function ($|G(j\omega)|$ is 1. For a system to be stable, the phase margin must be positive, ideally the phase margin is between 45° and 60°.

The gain margin is the reciprocal of the magnitude $|G(j\omega)|$ at the frequency where the phase angle is -180° [68] (phase cross-over frequency). If ω_1 is the frequency at which the phase angle of the open-loop transfer function is -180° the gain margin is K_g:

$$K_\mathrm{g} = \frac{1}{|G(j\omega_1)|} \tag{13.5}$$

In dB the gain margin is:

$$K_\mathrm{g} = 20\log(K_\mathrm{g}) = -20\log(|G(j\omega_1)|) \tag{13.6}$$

K_g in dB is positive if $K_\mathrm{g} > 1$ and K_g in dB is negative if $K_\mathrm{g} < 1$. For a stable system, the gain margin tells how much the gain can be increased before the system is unstable. For an unstable system, the gain margin indicates the magnitude by which the gain must be decreased to make the system stable [68]. The gain margin ideally is between 5 and 10 dB.

13.3.5 LTI v time-varying

The state-space system has time-varying coefficients. This means the A, B, C, D matrices are not all time-invariant. To obtain the transfer function matrix using 'ss2tf(A, B, C, D)' the assumption is that the matrices are linear and time-invariant (LTI). Since they are not actually time-invariant, then the transfer function matrix is not entirely correct, a limitation of this analysis.

13.4 Equations of motion

The contribution of the AHCS to the Dyneema extension is $z_{\mathrm{d,a}}$ shown in (13.7):

$$z_{\mathrm{d,a}} = \phi_{\mathrm{w}} r_{\mathrm{w}} \tag{13.7}$$

Where ϕ_{w} is the angle of the winch and r_{w} is the winch radius.

From appendix A.8 the equation for z_{d} for the PHCS is given by (A.140). This is repeated in (13.8). To indicate this is the contribution of the PHCS to the movement of the Dyneema rope the variable z_{d} is re-written as $z_{\mathrm{d,p}}$, this is shown in (13.9):

$$\ddot{z}_{\mathrm{d}} = \frac{1}{(M_{\mathrm{d}})}\left[- k_{\mathrm{d}}(z_{\mathrm{d}} - z_{\mathrm{in}}) - k_{\mathrm{d}}(z_{\mathrm{d}} - z_1)\right] \tag{13.8}$$

$$\ddot{z}_{\mathrm{d,p}} = \frac{1}{(M_{\mathrm{d}})}\left[k_{\mathrm{d}}(-z_{\mathrm{d,p}} + z_{\mathrm{in}} - z_{\mathrm{d,a}}) - k_{\mathrm{d}}(z_{\mathrm{d,p}} - z_1)\right] \tag{13.9}$$

The first term in (13.9) introduces coupling between the PHCS and AHCS. This is why it depends on $z_{\mathrm{d,a}}$ and $z_{\mathrm{d,p}}$. This term is written as F_{d} in (13.10). The Dyneema spring force F_{d} depends on the winch payout $z_{\mathrm{d,a}}$, the Dyneema rope displacement $z_{\mathrm{d,p}}$ interacting with the PHCS, and the crane-tip motion z_{in}. The reason to use $z_{\mathrm{d,a}}$ is that a positive value means the Dyneema is fed out, if the Dyneema mass is pulled downwards (causing an upwards force on the Dyneema mass) then the Dyneema being fed out acts to reduce the extension of the Dyneema and the tension. The Dyneema spring force F_{d} acts on the crane-tip to cause a roll moment on the vessel, shown in (13.12). It is assumed the worst case scenario, where the crane jib is extended as far horizontally as possible by a distance y_{b} to produce moments P_{d} and P_{c}. It is also assumed the roll moment acts in the positive roll direction, acting as a positive moment. The steel rope spring force from the PHCS cylinder and steel rope is included as a force acting at the same location as the crane-tip shown in (13.11), this also produces a roll moment on the vessel, shown in (13.13):

$$F_{\mathrm{d}} = k_{\mathrm{d}}(z_{\mathrm{in}} - z_{\mathrm{d,p}} - z_{\mathrm{d,a}}) \tag{13.10}$$

$$F_{\mathrm{c}} = k_{\mathrm{c}}(z_{\mathrm{in}} - z_{\mathrm{c}}) \tag{13.11}$$

$$P_{\mathrm{d}} = y_{\mathrm{b}} F_{\mathrm{d}} \tag{13.12}$$

$$P_{\mathrm{c}} = y_{\mathrm{b}} F_{\mathrm{c}} \tag{13.13}$$

Applying Newton's second law to the winch in Figure 13.5 gives:

$$J_{\mathrm{w}}\ddot{\phi}_{\mathrm{w}} = T_{\mathrm{e}} + F_{\mathrm{d}} r_{\mathrm{w}} - \mathrm{sign}(\dot{\phi}_{\mathrm{w}}) T_{\mathrm{b}} - B_{\mathrm{w}}\dot{\phi}_{\mathrm{w}} \tag{13.14}$$

Where J_{w} is the moment of inertia of the winch, ϕ_{w} is the rotation angle of the winch, T_{e} is the torque of the motor, F_{d} is the tension in Dyneema, T_{b} is the brake torque, and B_{w} is a rotational damping coefficient. A paper on an AHCS using a winch by Nicoll et al. [36] was used.
Re-arranging for $\ddot{\phi}_{\mathrm{w}}$ gives (13.15).

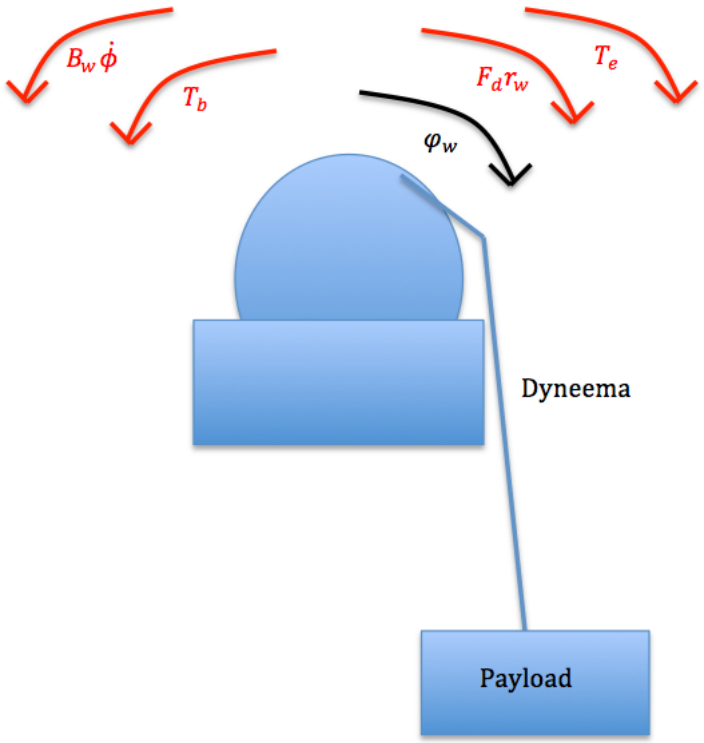

Figure 13.5: Winch

$$\ddot{\phi}_{\mathrm{w}} = \frac{T_{\mathrm{e}} + F_{\mathrm{d}} r_{\mathrm{w}} - \mathrm{sign}(\dot{\phi}_{\mathrm{w}}) T_{\mathrm{b}} - B_{\mathrm{w}} \dot{\phi}_{\mathrm{w}}}{J_{\mathrm{w}}} \tag{13.15}$$

To control the winch a throttle is used d. This governs the torque produced by the winch motor. There is a linear relationship between torque and throttle:

$$T_{\mathrm{e}} = \begin{cases} T_{\mathrm{e,max}} d & : -1 \leq d \leq 1 \end{cases} \tag{13.16}$$

Where $T_{\mathrm{e,max}}$ is the maximum torque produced by the motor, which is a constant. This is because it is assumed the motor torque generated is independent of the motor rotation speed. This is possible through using a VFD [36]. To limit the payout speed of Dyneema a brake controller is needed [36].

A payout penalty is defined:

$$p = |\dot{z}_{\mathrm{d,a}}| - \dot{z}_{\mathrm{d,a,max}} \tag{13.17}$$

where p is the payout penalty. This payout penalty governs the brake torque, T_{b}:

$$T_{\mathrm{b}} = \begin{cases} \frac{2T_{\mathrm{e,max}}}{0.05\dot{z}_{\mathrm{d,a,max}}} p & : p \geq 0 \\ 0 & : p < 0 \end{cases} \tag{13.18}$$

$\dot{z}_{\mathrm{d,a,max}}$ is the constant maximum allowable payout rate, and $\dot{z}_{\mathrm{d,a}}$ is the payout rate:

$$\dot{z}_{\mathrm{d,a}} = \dot{\phi}_{\mathrm{w}} r_{\mathrm{w}} \tag{13.19}$$

It is assumed that the pressures from the accumulators in the PHCS cancel out the static wet weight of the hook/payload. This is because the static wet weight of the hook/payload is held by the piston and the piston is floating inside the cylinder, held in place by the pressures from the accumulators. Thus, the static weight of the hook/payload is transferred to the accumulator system. This means

that the Dyneema, which is attached to the piston, does not experience tension due to the static wet weight of the hook/payload. This is an idealization and in reality there will likely be some tension in the Dyneema. This tension is included since the Dyneema should be in tension so that the winch can work. Furthermore, the PHCS cylinder is held by the steel ropes which are attached to the crane. The connection is made to the crane and not to the AHCS winch. Thus, in this sense the steel ropes are independent of the AHCS winch. This means the AHCS winch only interacts with the forces acting on the Dyneema.

The $z_{\mathrm{d,p}}$ is used with other elements of the system. It is used with the equation of motion for the hook/payload mass (A.137) from appendix A.8 repeated below in (13.20). By using $z_{\mathrm{d,p}}$ in (13.20) the hook and payload mass is controlled by the winch to some extent. The is because $z_{\mathrm{d,p}}$ is coupled with $z_{\mathrm{d,a}}$:

$$\begin{aligned}\ddot{z}_1 = \frac{1}{(M_{\mathrm{hook,payload}} + A_{\mathrm{hook,payload}})} \\ \Big[P_{\mathrm{p1}}A_{\mathrm{p}} - P_{\mathrm{p2}}A_{\mathrm{p}} + F_{\mathrm{water}} - F_{\mathrm{water}} + \rho_{\mathrm{water}}V_{\mathrm{d}}g \\ -M_{\mathrm{hook,payload}}g - \frac{1}{2}\rho_{\mathrm{water}}C_{\mathrm{d,hook,payload}}D_{\mathrm{hook,payload}}|\dot{z}_1|\dot{z}_1 - k_{\mathrm{d}}(z_1 - z_{\mathrm{d,p}})\Big]\end{aligned} \tag{13.20}$$

13.4.1 Equation of motion for winch

Substituting (13.19) into (13.17) gives:

$$p = |\dot{\phi}_{\mathrm{w}}r_{\mathrm{w}}| - \dot{z}_{\mathrm{d,a,max}} \tag{13.21}$$

Substituting (13.21) into (13.18) gives (13.22):

$$T_{\mathrm{b}} = \begin{cases} \frac{2T_{\mathrm{e,max}}}{0.05\dot{z}_{\mathrm{d,a,max}}}(|\dot{\phi}_{\mathrm{w}}r_{\mathrm{w}}| - \dot{z}_{\mathrm{d,a,max}}) & : p \geq 0 \\ 0 & : p < 0 \end{cases} \tag{13.22}$$

Substituting (13.10) for F_{d}, (13.22) for T_{b}, into (13.15) gives (13.23):

$$\ddot{\phi}_{\mathrm{w}} = \frac{T_{\mathrm{e}} + \Big(k_{\mathrm{d}}(z_{\mathrm{in}} - z_{\mathrm{d,p}} - z_{\mathrm{d,a}})\Big)r_{\mathrm{w}} - \mathrm{sign}(\dot{\phi}_{\mathrm{w}})\Big(\frac{2T_{\mathrm{e,max}}}{0.05\dot{z}_{\mathrm{d,a,max}}}(|\dot{\phi}_{\mathrm{w}}r_{\mathrm{w}}| - \dot{z}_{\mathrm{d,a,max}})\Big) - B_{\mathrm{w}}\dot{\phi}_{\mathrm{w}}}{J_{\mathrm{w}}} \tag{13.23}$$

Substituting (13.16) for T_{e} into (13.23) gives (13.24), the equation of motion for the winch:

$$\ddot{\phi}_{\mathrm{w}} = \frac{T_{\mathrm{e,max}}d + \Big(k_{\mathrm{d}}(z_{\mathrm{in}} - z_{\mathrm{d,p}} - z_{\mathrm{d,a}})\Big)r_{\mathrm{w}} - \mathrm{sign}(\dot{\phi}_{\mathrm{w}})\Big(\frac{2T_{\mathrm{e,max}}}{0.05\dot{z}_{\mathrm{d,a,max}}}(|\dot{\phi}_{\mathrm{w}}r_{\mathrm{w}}| - \dot{z}_{\mathrm{d,a,max}})\Big) - B_{\mathrm{w}}\dot{\phi}_{\mathrm{w}}}{J_{\mathrm{w}}} \tag{13.24}$$

13.4.2 System parameters

See Table 13.1 for the system parameters. The radius is based on the radius of a winch Jumbo has used in the design from Parkburn, a radius $r_{\mathrm{w}} = 1.5$m. The mass of the same winch is $M_{\mathrm{w}} = 32$t. To calculate the moment of inertia of the winch, J_{w}, it is assumed the winch is a solid cylinder with the moment of inertia taken around the central axis of the cylinder, this means:

$$J_{\mathrm{w}} = \frac{1}{2}M_{\mathrm{w}}r_{\mathrm{w}}^2 \tag{13.25}$$

A solid cylinder is assumed instead of a hollow cylinder since this is a closer approximation to the winch than a hollow cylinder. The mass of the winch is assumed to not include the rope. This is because the winch is a traction winch so only four loops of Dyneema are around the winch at any time and the mass

of four loops is small. The rest of the Dyneema is stored on the storage winch, this part is not modelled to simplify the dynamics. Furthermore, the maximum torque the motor can provide is determined by considering the power of the motor. The total power is 440kW. The relationship between power and torque is:

$$P = \tau\omega \tag{13.26}$$

where P is power, τ is torque, and ω is angular velocity. Re-arranging for torque:

$$\tau = \frac{P}{\omega} \tag{13.27}$$

It was assumed that the motor torque is independent of the rotation speed since a VFD is used. This means an arbitrary ω is used to obtain maximum torque. The angular velocity is limited by the maximum payout rate. The maximum payout rate is the maximum value of:

$$\dot{z}_{\mathrm{d,a}} = \dot{\phi}_{\mathrm{w}} r_{\mathrm{w}} \tag{13.28}$$

or:

$$\dot{z}_{\mathrm{d,a,max}} = \dot{\phi}_{\mathrm{w,max}} r_{\mathrm{w}} = \omega_{\mathrm{max}} r_{\mathrm{w}} \tag{13.29}$$

$$\omega_{\mathrm{max}} = \frac{\dot{z}_{\mathrm{d,a,max}}}{r_{\mathrm{w}}} \tag{13.30}$$

Assuming the maximum payout rate is 10m/s then the maximum angular velocity is:

$$\omega_{\mathrm{max}} = \frac{10\mathrm{m/s}}{1.5\mathrm{m}} = 6.67\mathrm{rad/s} \tag{13.31}$$

Assuming the maximum power is 95% of the total power, to take into account friction and resistance losses, then the maximum power is $P_{\mathrm{max}} = 418\mathrm{kW}$. Using (13.27) gives an expression for maximum torque:

$$\tau_{\mathrm{max}} = \frac{P_{\mathrm{max}}}{\omega_{\mathrm{min}}} \tag{13.32}$$

The minimum pay-out rate, ω_{min}, is arbitrarily chosen as 1% of ω_{max}, thus $\omega_{\mathrm{min}} = 0.0667\mathrm{rad/s}$. Substituting $P_{\mathrm{max}} = 418\mathrm{kW}$ and $\omega_{\mathrm{min}} = 0.0667\mathrm{rad/s}$ into (13.32):

$$\tau_{\mathrm{max}} = \frac{418\mathrm{kW}}{0.0667\mathrm{rad/s}} \tag{13.33}$$

$$\tau_{\mathrm{max}} = 6.27\mathrm{e}6\mathrm{Nm} \tag{13.34}$$

To determine the rotational damping coefficient, the work by Nicoll et al. [36] was used. Nicoll et al. used a rotational damping value of $B_{\mathrm{w}} = 0.025\mathrm{Nms}$ and a maximum torque $T_{\mathrm{e,max}} = 1\mathrm{e}5\mathrm{Nm}$. This gives a ratio of rotational damping value to maximum torque of 2.5e-7s. Assuming the same ratio, the rotational damping value for this motor is given by:

$$B_{\mathrm{w}} = 6.27\mathrm{e}6\mathrm{Nm} * 2.5\mathrm{e} - 7\mathrm{s} = 1.57\mathrm{Nms} \tag{13.35}$$

Table 13.1: System parameters

Parameter	Value
r_{w}	1.5 [m]
M_{w}	32e3 [kg]
J_{w}	36e3 [kgm^2]
$T_{\mathrm{e,max}}$	6.27e6 [Nm]
B_{w}	1.57 [Nms]
$\dot{z}_{\mathrm{d,a,max}}$	10[m/s]

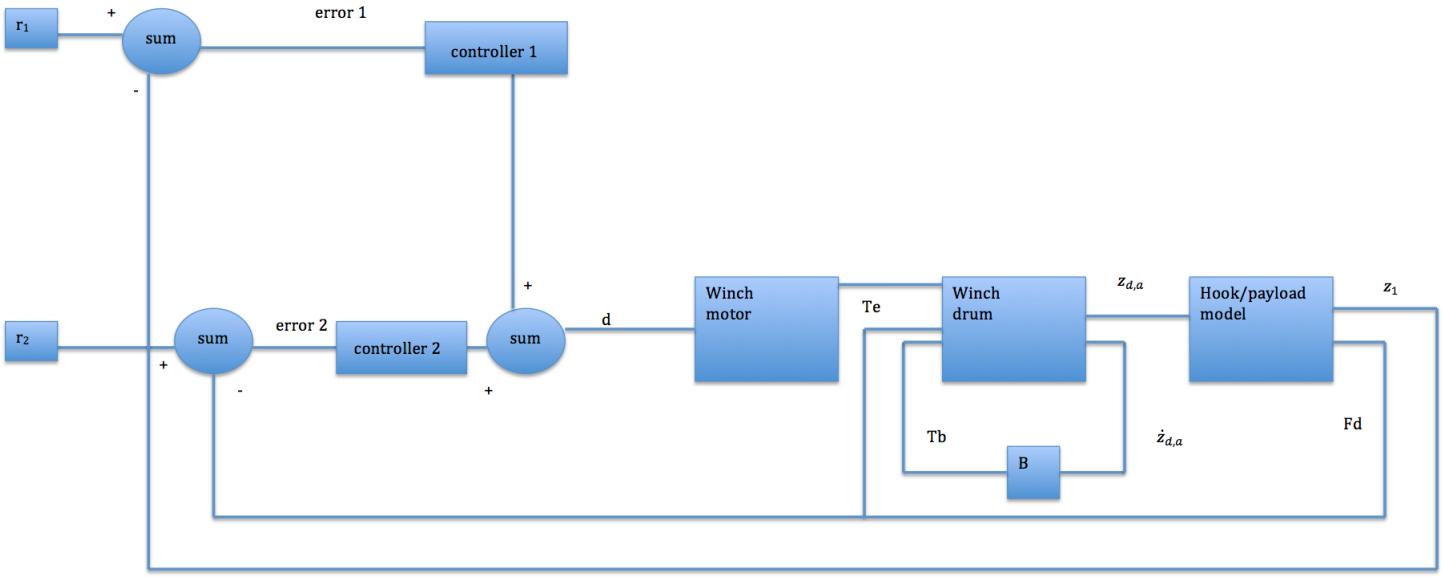

Figure 13.6: Closed loop control block diagram

13.4.3 PID controller interaction

The control block diagram used is shown in Figure 13.6. As mentioned in section 13.3.2, two control loops are used. One controls the tension in the Dyneema, F_{d}, and the other controls the displacement of the hook/payload, z_1.
The controller blocks are described:

- The controller for the displacement (controller 1) has input as the error between the displacement set point and the current displacement of hook/payload, the output is a throttle.
- The controller for the tension (controller 2) has input as the error between the tension set point and the current Dyneema tension, the output is a throttle.

The two throttle outputs are summed to produced the summed throttle which is used in (13.16) to produce the motor torque, T_{e}. This motor torque is put into the winch equation (13.15) to determine ϕ_{w} which is used in (13.7) to calculate $z_{\mathrm{d,a}}$. $z_{\mathrm{d,a}}$ is then used in (13.9) to find $z_{\mathrm{d,p}}$, this $z_{\mathrm{d,p}}$ is used in (13.20) to find z_1.

13.5 PI controller, open-loop model

The open-loop model of Figure 13.6 is in Figure 13.7. The transfer function for this is obtained below.

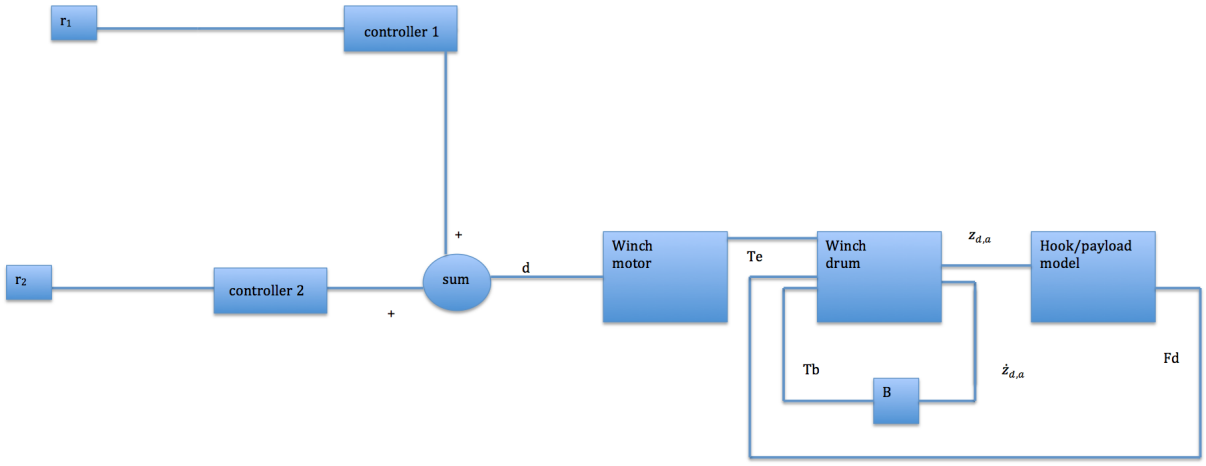

Figure 13.7: Open loop model

13.5.1 Loop controlling z_1, displacement

$$u_1(t) = k_{\mathrm{p},1} r_1(t) + k_{\mathrm{i},1} \int_0^t r_1(\tau_1)\mathrm{d}\tau_1 \tag{13.36}$$

Removing the integral for convenience so that there is only one dependent variable t:

$$u_1(t) = k_{\mathrm{p},1} r_1(t) + k_{\mathrm{i},1}(r_1(t) - r_1(0)) \tag{13.37}$$

13.5.2 Loop controlling F_{d}, tension

$$u_2(t) = k_{\mathrm{p},2} r_2(t) + k_{\mathrm{i},2} \int_0^t r_2(\tau_2)\mathrm{d}\tau_2 \tag{13.38}$$

Removing the integral for convenience so that there is only one dependent variable t:

$$u_2(t) = k_{\mathrm{p},2} r_2(t) + k_{\mathrm{i},2}(r_2(t) - r_2(0)) \tag{13.39}$$

Combining (13.37) and (13.39) to give the throttle d:

$$d(t) = u_1(t) + u_2(t) \tag{13.40}$$

$$d(t) = k_{\mathrm{p},1} r_1(t) + k_{\mathrm{i},1}(r_1(t) - r_1(0)) + k_{\mathrm{p},2} r_2(t) + k_{\mathrm{i},2}(r_2(t) - r_2(0)) \tag{13.41}$$

Collecting like terms:

$$d(t) = [k_{\mathrm{p},1} + k_{\mathrm{i},1}] r_1(t) - k_{\mathrm{i},1} r_1(0) + [k_{\mathrm{p},2} + k_{\mathrm{i},2}] r_2(t) - k_{\mathrm{i},2} r_2(0) \tag{13.42}$$

13.5.3 Final equation of motion for winch

The equation of motion for the winch in (13.24) changes since the throttle d has open-loop control. This changes the motor torque T_{e}. Substituting (13.42) for d into the equation for T_{e} (13.16) gives (13.43):

$$T_{\mathrm{e}} = T_{\mathrm{e,max}} \Bigg([k_{\mathrm{p},1} + k_{\mathrm{i},1}] r_1(t) - k_{\mathrm{i},1} r_1(0) + [k_{\mathrm{p},2} + k_{\mathrm{i},2}] r_2(t) - k_{\mathrm{i},2} r_2(0) \Bigg) \tag{13.43}$$

Substituting (13.43) for T_{e}, (13.10) for F_{d}, and (13.22) for T_{b} into (13.15) gives (13.44):

$$\ddot{\phi}_{\mathrm{w}} = \frac{T_{\mathrm{e,max}} \Bigg([k_{\mathrm{p},1} + k_{\mathrm{i},1}] r_1(t) - k_{\mathrm{i},1} r_1(0) + [k_{\mathrm{p},2} + k_{\mathrm{i},2}] r_2(t) - k_{\mathrm{i},2} r_2(0) \Bigg) + \Big(k_{\mathrm{d}} (z_{\mathrm{in}} - z_{\mathrm{d,p}} - z_{\mathrm{d,a}}) \Big) r_{\mathrm{w}}}{J_{\mathrm{w}}} + \frac{-\mathrm{sign}(\dot{\phi}_{\mathrm{w}}) \Big(\frac{2 T_{\mathrm{e,max}}}{0.05 \dot{z}_{\mathrm{d,a,max}}} (|\dot{\phi}_{\mathrm{w}} r_{\mathrm{w}}| - \dot{z}_{\mathrm{d,a,max}}) \Big) - B_{\mathrm{w}} \dot{\phi}_{\mathrm{w}}}{J_{\mathrm{w}}} \tag{13.44}$$

13.6 HHCS equations

The equations for the PHCS and AHCS combined to form the HHCS are in appendix A.21.

13.7 Non-linear HHCS state-space equations

The non-linear state-space equations for the HHCS are in appendix A.22.

13.8 Linear HHCS state-space equations

The linearized state-space equations for the HHCS are in appendix A.23.

13.9 Response

13.9.1 Simulink tuning

The reference signal for displacement z_1 is 0 since it is aimed to minimize motion of the hook/payload. The Dyneema rope needs to be in tension this means there should be initial tension and the reference signal for tension should be non-zero. The reference signal for tension F_{d} is 10% of the static wet weight of the hook and payload mass. The numerical optimization algorithm within Simulink was used to find the gain constants.

Initially, proportional (P) control was used for both controllers in Figure 13.6. To improve the results, proportional integral control was used (PI) this was more effective. Proportional derivative (PD) control and PID control were tested but did not provide better results than PI control. Using D control is undesirable since the non-linear nature of the system means the signals are not always smooth. This presents a problem when differentiating the signal to use the derivative control. In theory PID control provides the best control since it takes into account the past, present, and future of the signal. It was decided to not investigate PID or PD control further.

Still the HHCS does not out-perform the PHCS in every measure of performance. A possible explanation is that that numerical optimization algorithm in Simulink has found a local optimization point instead of a global optimization point. More detailed control design can be done but this is outside the scope of this thesis. For industrial active heave compensation systems the control schemes are much more complex thus it cannot be expected that a PID-type controller implemented in this thesis would be highly effective. Further discussion on why the HHCS does not out-perform the PHCS is in section 13.9.5.

13.9.2 Stability by eigenvalues

From section 13.9.1, the parameters for controller 1 in Figure 13.6 are $k_{\mathrm{p},1} = 0$ (P gain) and $k_{\mathrm{i},1}$ =-2.38e-6 (I gain) and for controller 2 $k_{\mathrm{p},2}$ =-5.24e-7 (P gain) and $k_{\mathrm{i},2}$=-1.14e-10 (I gain) . The state-space matrices for the open-loop system are shown in appendix (A.23.4). From the A matrix the eigenvalues are found using these parameters for the controller in Table 13.2. All the real parts are negative, meaning the system is stable.

Table 13.2: Eigenvalues, natural frequencies, natural periods

Eigenvalue λ	Natural frequency ω_{n} [rad/s]	Natural period [s]
-4.6266e-18	0	inf
-3.1367e-16	0	inf
-5.1338e-05	0	inf
-1044.9	0	inf
-0.00046 - 0.1835i	0.1835	34.2323
-0.00046 + 0.1835i	0.1835	34.2323
-2.5747e-05 - 0.5090i	0.5090	12.3434
-2.5747e-05 + 0.5090i	0.5090	12.3434
-9.5059e-05 - 0.5472i	0.5472	11.4814
-9.5059e-05 + 0.5472i	0.5472	11.4814
-0.00028 - 2.2020i	2.2020	2.8534
-0.00028 + 2.2020i	2.2020	2.8534
-0.0243 - 301.8674i	301.8674	0.0208
-0.0243 + 301.8674i	301.8674	0.0208
-0.0242 - 303.9571i	303.9571	0.0207
-0.0242+ 303.9571i	303.9571	0.0207

13.9.3 Gain and phase margin

The phase and gain margins are found for the PI gains used in section 13.9.2. Four transfer functions are available; $\frac{z_1(s)}{r_1(s)}$, $\frac{F_{\mathrm{d}}(s)}{r_1(s)}$, $\frac{z_1(s)}{r_2(s)}$, and $\frac{F_{\mathrm{d}}(s)}{r_2(s)}$. Where r_1 is the reference signal for z_1 and r_2 is the reference signal for F_{d}. The transfer function of interest is $\frac{z_1(s)}{r_1(s)}$ since this gives the motion of the hook/payload.

Table 13.3 shows the gain/phase margins. The gain margin is 97.1dB and the phase margin is infinite. The phase margin is infinite since the gain cross-over frequency is never encountered. These gain and

phase margins are unrealistic. This is because generally a real physical system should not have any parameter that is tending to infinity. As mentioned in section 13.3.5 to obtain the state-space matrices the equations for the AHCS had to be simplified and the terms in the **A** matrix are not all constant. This could lead to the gain and phase margins being unrealistic. Nevertheless, the gain and phase margins indicate the system is relatively robust. If the gain and phase margins have a large error it is still possible the correct gain and phase margins provided good relative stability. The time response is shown in section 13.9.4.

Table 13.3: Gain and phase margins

Transfer function	Gain margin [dB]	Phase cross-over frequency [rad/s]	Phase margin [°]	Gain cross-over frequency [rad/s]
$\frac{z_1(s)}{r_1(s)}$	97.1	0.5090	Inf	not defined
$\frac{F_d(s)}{r_1(s)}$	-4.161	0	-88.1	0.0015
$\frac{z_1(s)}{r_2(s)}$	110.2	0.5090	Inf	not defined
$\frac{F_d(s)}{r_2(s)}$	8.9	0	-81.3	3.3e-4

13.9.4 Time response

For the design conditions of H=2.5m, T=8s, water depth of 2500m the C-HHCS performance parameters are SDA=0.402m, R=0.203, and β=63.06%. Performance is worse than the C-PHCS which achieved SDA=0.344m, $R = 0.140$ and $\beta = 84.65\%$ from Table 12.1. For the C-HHCS the SDA is 16.9% higher than for the C-PHCS, the R is 45.0% higher, and the β is 25.5% lower.

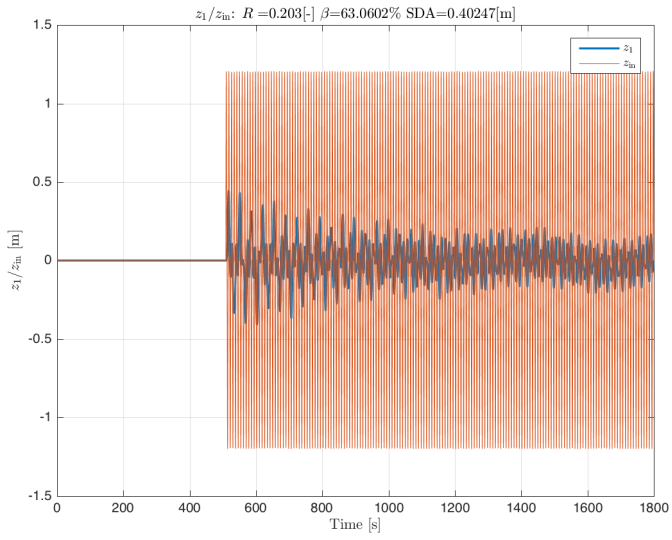

Figure 13.8: C-HHCS: Motion results (8s period)

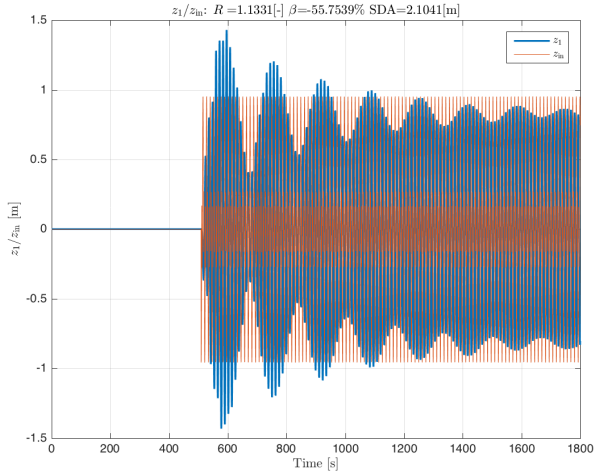

(a) T=12.34s

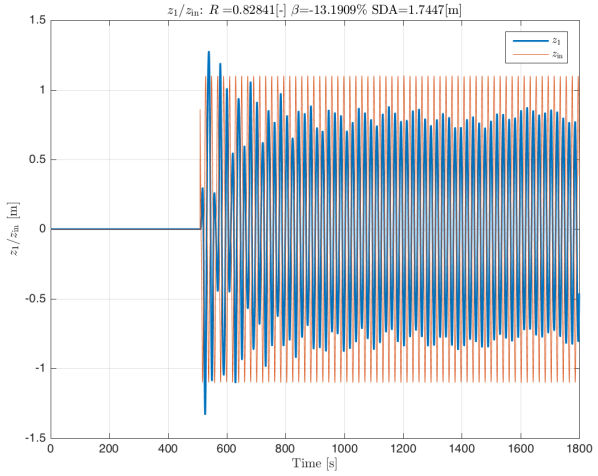

(b) T=20.46s

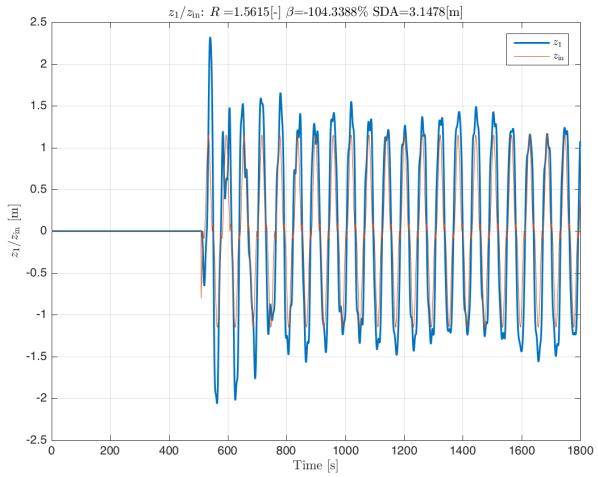

(c) T=60.70s

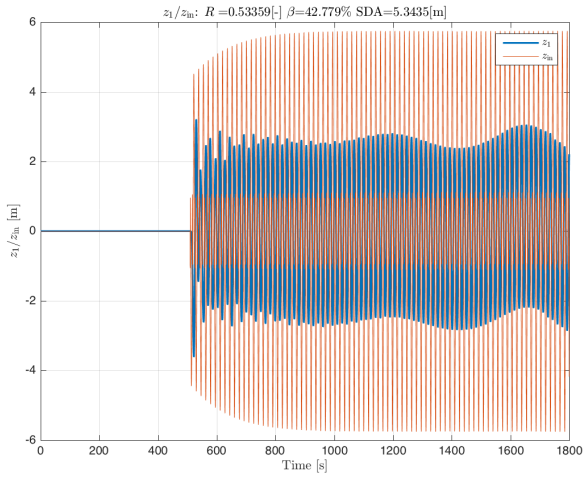

(d) T=16.3s

Figure 13.9: C-HHCS: The first 500s are a ramp-up period for the vessel model and are not included in the analysis

13.9.5 Comparison with C-PHCS

Table 13.4: Summary of data from C-PHCS, C-HHCS

	C-PHCS			**C-HHCS**			**Percent difference**		
Wave period [s]	R[-]	β [%]	SDA [m]	R [-]	β [%]	SDA [m]	R [%]	β [%]	SDA [%]
8	0.14	84.65	0.34	0.20	63.06	0.40	42.9	25.5	17.6
12.34	0.19	63.04	0.51	1.13	-55.75	2.10	494.7	188.4	311.8
16.30	0.18	64.64	1.69	0.53	42.78	5.34	194.4	33.8	215.9
20.46	1.57	-76.46	3.69	0.83	-13.19	1.74	47.1	82.7	52.8
60.70	11.48	-959.70	24.53	1.56	-104.34	3.15	86.4	89.1	87.2

The design conditions of H=2.5m and water depth of 2500m are considered with various periods. The time response for 8s period shows attenuation of motion, see Figure 13.8. As was done in chapter 12, in Figure 13.9 the time response for the natural periods of the PHCS [12.34, 20.46, 60.70]s and the roll natural period of the vessel, 16.3s, are shown.

See Table 13.4 for the numerical values of the results from the C-PHCS and C-HHCS. To compare performance the SDA is used since this provides a measure of how much the hook/payload moves. This provides a clear way to observe the effect of the active system.

Figure 13.10a shows SDA as a function of input period for the C-PHCS and C-HHCS. The C-HHCS has higher values than the C-PHCS. This means the AHCS amplifies the motion relative to when only the PHCS is used. At 12s the C-HHCS has a peak in SDA. For the C-PHCS, there is a peak at 13s but the magnitude of the peak is smaller than for the C-HHCS. These peaks arise from resonance due to the natural period at 12.34s. The AHCS amplifies the motion from the resonance. A time-series comparison between the C-PHCS and C-HHCS at the 12.34s period is shown in Figure 13.11a, showing the influence of resonance by beating in the C-HHCS results. The influence on the vessel of the C-PHCS and C-HHCS is negligible, see Figure 13.11b. This means the peak in SDA for the C-HHCS is due to the effect of the AHCS rather than the coupling with the vessel. Furthermore, at the 16.3s natural roll period of the vessel, the C-HHCS has worse performance than the C-PHCS from comparing Figure 13.9d with Figure 12.3d. For the design period, T=8s, in Figure 13.12, the time-series of z_1 from the C-HHCS and C-PHCS results are shown. The C-HHCS again has worse performance than the C-PHCS.

At the 20.46s natural period the C-HHCS has better performance than the C-PHCS, comparing Figure 13.9b with Figure 12.3b. This is also the case for the 60.70s natural period. This is opposite to the case of the 8s, 12.34s, and 16.3s periods, where the C-HHCS has worse performance. It appears at the higher periods the C-HHCS has better performance than the C-PHCS. This could be related to the two loop control strategy where one loop controls the displacement z_1 and another the tension in the Dyneema rope. The I gain for the controller for z_1 has a larger magnitude than the P and I gains for the controller for the tension, suggesting the controller for z_1 has a larger influence. The larger input periods mean there are lower frequency z_1 and tension disturbances. Since the controller for z_1 sees lower frequency disturbances and likely has a larger influence than the other controller this enables the controller to be more effective than the other one. The lower frequency disturbances mean there is more time for a control action to correct a particular disturbance before the disturbance changes. This could explain why at larger input periods the AHCS is more effective than at smaller periods, so the C-HHCS is more effective.

It is attempted to explain why when the AHCS is enabled the heave compensation performance is worse relative to when the AHCS is disabled, independent of the period used. The simplest explanation is that the controller parameters are not optimal. However, this is not the only explanation. Another explanation is that the control strategy of two control loops, one for tension in the Dyneema and one for displacement z_1 is not ideal for the way the PHCS is coupled with the AHCS. The controller is directly controlling the Dyneema rope attached to the hook/payload. The steel rope connecting the PHCS cylinder to the crane-tip is not controlled directly. The steel rope has a role in the movement of the hook/payload, though less of a role than the Dyneema rope. Nevertheless, the steel rope displacement, z_c, should perhaps be considered more directly in the control strategy. This is because the steel rope acts as a stiffer spring than the Dyneema rope so it has a strong influence in the entire HHCS. The displacement of the steel rope, z_c, could be considered in a third control loop leading to a different control strategy. As mentioned in section 13.3.2, it is possible that the two loops interfere with one another. Nicoll et al. [36] said this was unlikely since the loop for tension responds to high frequency disturbances and the loop for displacement responds to lower frequency disturbances. However, for the HHCS this may not be the case, there could be interference between the two controllers. Furthermore, the kind of controller used is a PI controller. Other kinds of controllers within the PID scope were used such as PI, PD, and PID. PI provided the most effective control out of these. Another kind of controller could be attempted while using the same control strategy of the two control loops mentioned earlier. Alternatively, a different control strategy with a different kind of controller could provide a better control effect. This can be done for further work.

To show the performance using the other parameters, see Figure 13.10b for R v. T, see Figure 13.10c for β v. T, these results agree with those in Figure 13.10a for SDA v. T.

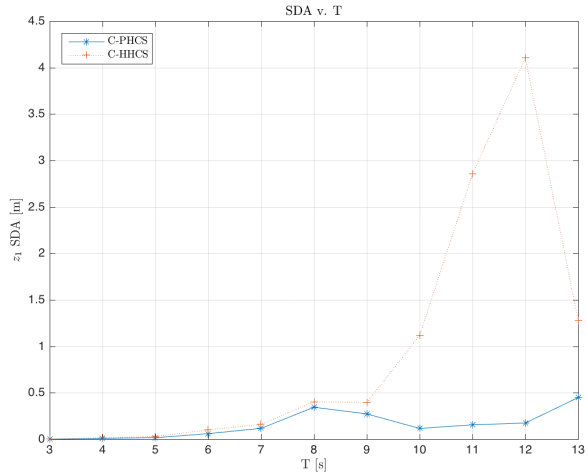

(a) SDA v. T

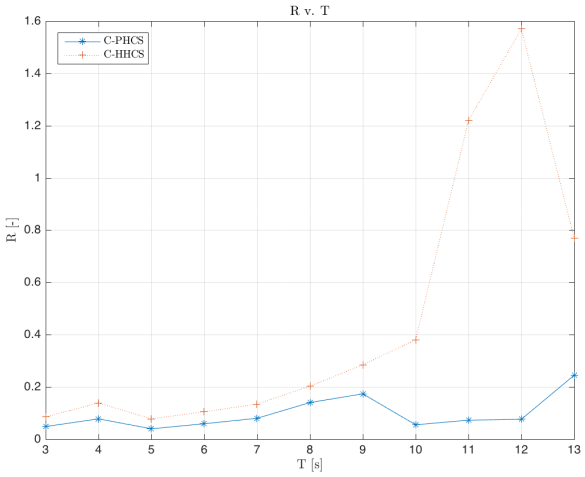

(b) R v. T

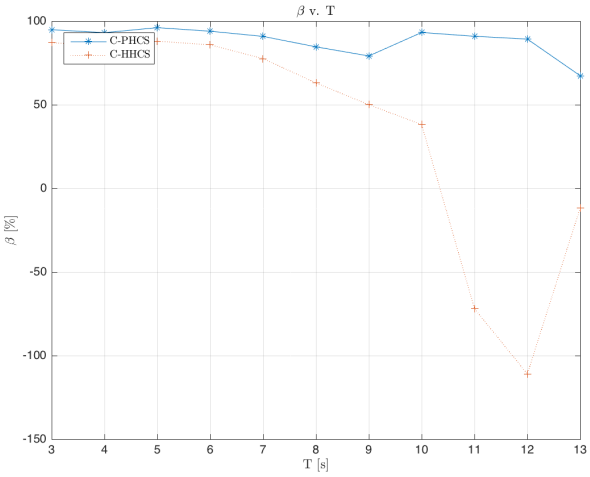

(c) β v. T

Figure 13.10

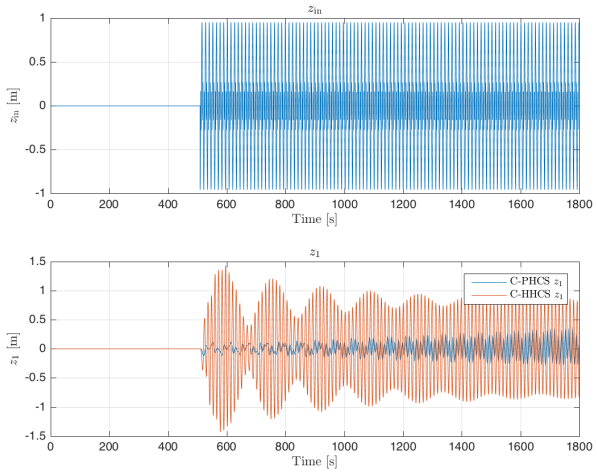

(a) Motion results (12.34s period), for C-HHCS and C-PHCS

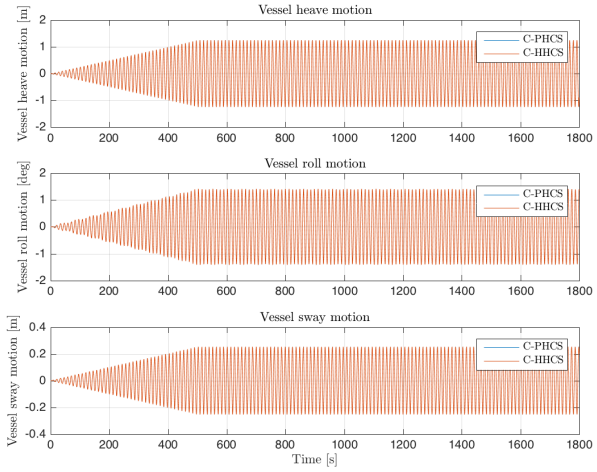

(b) Vessel heave, roll, and sway motions for 12.34s wave period. There is a negligible difference between the C-PHCS and C-HHCS.

Figure 13.11

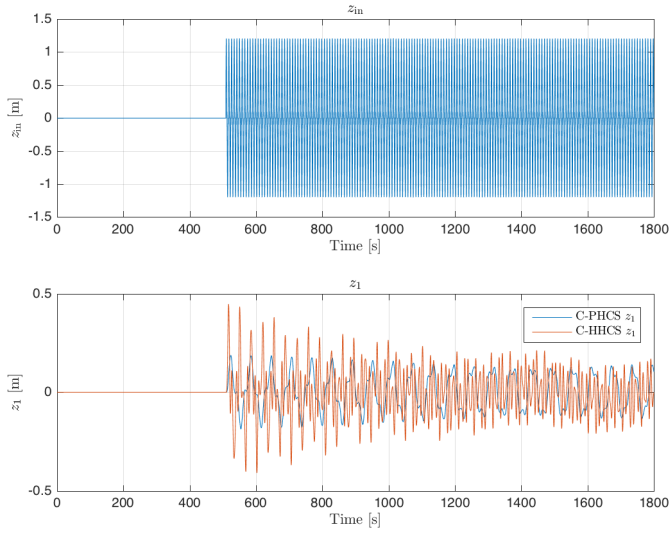

Figure 13.12: Motion results (8s period)

13.9.6 Addressing research question

The research question in section 1.3 is addressed:

How important is the change in natural period from when the active heave compensation system is disabled to when the active heave compensation is enabled on resonance?

From the research question it is assumed when the AHCS is disabled the C-HHCS has a natural period. It is assumed when the AHCS is enabled the effect is for there to be some de-coupling between the vessel and the PHCS. This means the natural period of the C-HHCS does not exist anymore. Instead, the vessel assumes its natural roll period (16.3s) and the PHCS assumes its natural periods (12.34s, 20.46s, 60.70s). If the wave period is close to any of these natural periods, then resonance occurs.

It was found the issues of vessel roll amplitude increase and crane-tip acceleration, in section 13.2, when activating the AHCS did not appear. The answer to the research question is: the change in natural period when activating the AHCS is not important on resonance. In fact, enabling the AHCS does not lead to a change in natural period that influences the resonance behavior. Instead it was found, assuming the wave period is at a natural period of the PHCS, the controller is responsible for the resonance motion being amplified. It should be noted that the resonance occurs whether or not the AHCS is enabled, but enabling the AHCS amplifies the resonance.

The natural period of the C-HHCS was not determined since this was not important to know, what is important is the behavior of the vessel and PHCS when the AHCS is enabled. The natural roll period of the vessel (16.3s) as well as the natural periods of the PHCS (12.34s, 20.46s, 60.70s) were used as wave periods and the compensation performance found in Table 13.4. To measure resonance, the SDA value is used. At 12.34s and 16.3s, the resonance of the C-HHCS was larger than that for the C-PHCS. Enabling the AHCS enlarges the resonance. This was explained in section 13.9.5 as due to the controller. At 16.3s, there is resonance in the roll motion of the vessel since this is the natural roll period, this contributes to the enlarged SDA. However, at the other natural periods the vessel motions are not noticeably influenced by the HHCS, whether the AHCS is enabled or not. At 20.46s and 60.70s, the resonance of the C-HHCS was smaller than that of the C-PHCS. This was explained in section 13.9.5 as being because the AHCS had more time to have an effect due to the lower wave period so it could reduce the resonance.

A replication of the scenario investigated by Mannigel [3] described in section 13.2 is considered. This means the vessel roll period is the same as one of the natural periods of the PHCS, for example 12.34s and the wave period is also 12.34s. Then it is expected the SDA for the C-HHCS will be larger than that for the C-PHCS. The factor by which the SDA for the C-HHCS is larger than for the C-PHCS is expected to be even larger than that found for 12.34s in Table 13.4, where the vessel natural period is 16.3s so the vessel was not excited at resonance. If the vessel is excited at resonance it will contribute to larger crane-tip motion and hook/payload motion and thus SDA.

Mannigel [3] claimed for the scenario described in section 13.2 that when disabling the AHCS the resonance motion stopped abruptly. This is supported by Figure 13.2a where the crane-tip acceleration has a steep reduction. Mannigel's explanation is that this was because the natural period of the system changed when the AHCS was disabled so the resonance stopped. It can be argued that if this was the reason the resonance motion would not stop so abruptly. If the reason is that the controller was amplifying the motion due to an issue with the controller design this seems more likely. This is because the pile was at a 1200m water depth. There is a reasonable amount of damping and added mass from water at this water depth. For the change in natural period to have an effect it is expected it would take some time due to the system being distributed over such a large water depth. Furthermore, there is a time-delay for motion at one of the rope to propagate to the other end. The longitudinal propagation of motion for the rope can be described with the rod model, using the wave speed the time-delay for motion to propagate from one end to the other is:

$$T_{\mathrm{d}} = L_{\mathrm{c}}\sqrt{\frac{\rho}{E}} \tag{13.45}$$

where ρ is the density, E is the modulus, and L_{c} is the length. Assuming high tensile steel, for a 1200m rope the time-delay is approximately 2.4s. If the controller was amplifying the motion this time-delay is sufficiently small to allow for the abrupt end of the resonance motion. It is smaller than the expected time for a change in natural period of the system to have an effect. Thus, Mannigel's explanation is not favored, instead it is believed the phenomenon was due to an issue with the controller design. However, a limitation of this argument is that the controller used by Mannigel is different from the one used in this investigation, so it is difficult to provide a clear answer.

13.10 Conclusion

In this chapter, modelling of the AHCS was done. The PHCS and AHCS were combined with the vessel model and crane-tip model and results shown. The effect of the AHCS is to amplify the motion, especially at certain natural periods of the PHCS. When enabling the active part the vessel motions are not affected noticeably for any of the periods considered. This means the amplification of motion when enabling the active part is due to the HHCS solely and not from an interaction with the vessel. This is part of step 5 of the methodology in section 3.3. In chapter 14 a sensitivity study is done to see the effect of taking into account water damping and added mass on the Dyneema rope by considering coupled axial and transverse motion.

Sensitivity study: continuous rope model

14

14.1 Introduction

The large design water depth of 2500m means the damping due to water will reduce the heave motion of the rope attached to the hook/payload. In this chapter, this reduction in heave motion of the rope will be considered to do a sensitivity study.

14.2 Steel rope versus Dyneema rope

The Dyneema rope is more susceptible to the damping from water in deep water. This is because the Dyneema rope has a much smaller weight in water than the steel rope. This means, in the absence of current, the Dyneema rope forms a shallow catenary whereas the steel rope forms a large catenary. The larger catenary can absorb more energy by reducing the catenary [69]. In contrast, the Dyneema rope benefits less from this mechanism meaning it has larger motions when the rope is being moved at its ends by the crane-tip for example.

Furthermore, as mentioned in section 7.5.5 the ratio $\rho_{\text{water}}/\rho_{\text{rope}}$ is higher for the Dyneema rope than the steel rope. This means the added mass has a stronger effect for the Dyneema rope than the steel rope.

For the two reasons above it is decided to model the Dyneema rope as a continuous structural element and not the steel rope. The rope is modelled as a string and rod that are coupled. The equations of motion and coupling are described below.

14.3 String

The coordinate system is shown in Figure 14.1.

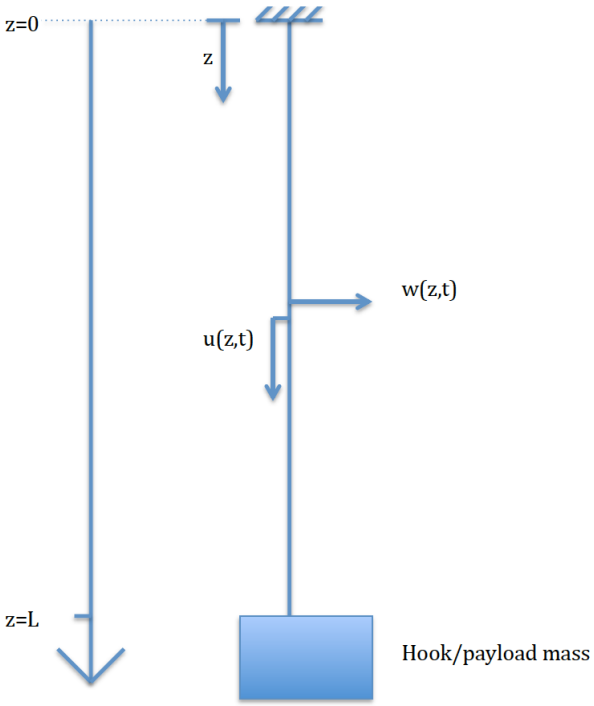

Figure 14.1: Coordinate system

14.3.1 Equation of motion

The equation of motion for a string in a general form is:

$$\rho A \frac{\partial^2 w(z,t)}{\partial t^2} = \frac{\partial}{\partial z}\left(T \frac{\partial w(z,t)}{\partial z}\right) + q_1(z,t) \tag{14.1}$$

where ρ is the density of the Dyneema rope, A is the cross-sectional area of the Dyneema rope, w is the transverse displacement, z is the coordinate along the axis, T is the tensile axial force in the rope, and q_1 is external force.

14.3.2 Assumptions

- Continuous
- One-dimensional model
- Cross-sectional area A is constant along the length

The mechanical behavior of the rope, which is much longer in one direction than in the two others, depends on the time and position along the rope.

14.4 Rod

14.4.1 Equation of motion

A general form of the equation of motion is:

$$\rho A \frac{\partial^2 u}{\partial t^2} = EA \frac{\partial}{\partial z}\left(\frac{\partial u}{\partial z}\right) + q(z,t)A \tag{14.2}$$

where E is the modulus of the material and q is the body force.

14.4.2 Assumptions

- Thin rod
- Particles move along the longitudinal axis only
- Straight, prismatic rod, cross-sectional area A is constant along the length
- Elastic, homogeneous rod, E is constant along the length

14.4.3 Wave equation

Both (14.2) and (14.1) are analogies of the wave equation. This means for motion at one end to have an effect at the other end a finite amount of time is needed.

14.5 Coupling terms

The string (14.1) and rod (14.2) equations of motion are coupled with the coupling terms described below.

14.5.1 String

In (14.1) the T term is given by:

$$T = EA\frac{\partial u}{\partial z} \tag{14.3}$$

This is derived by considering the stress in the rod σ:

$$T = \sigma A \tag{14.4}$$

Where σ is from:

$$\sigma = E\epsilon \tag{14.5}$$

Where the strain ϵ is:

$$\epsilon = \frac{\partial u}{\partial z} \tag{14.6}$$

Substituting T into (14.1) gives:

$$\rho A\frac{\partial^2 w}{\partial t^2} - EA\frac{\partial}{\partial z}\left(\frac{\partial u}{\partial z}\frac{\partial w}{\partial z}\right) = q_1(z,t) \tag{14.7}$$

Where q_1 is the external force due to the water:

$$q_1(z,t) = -A_{\text{mass}}\frac{\partial^2 w}{\partial t^2} - \frac{1}{2}\rho_{\text{water}}C_{\text{d}}D_{\text{rope}}\left|\frac{\partial w}{\partial t}\right|\frac{\partial w}{\partial t} \tag{14.8}$$

where A_{mass} is the added mass per meter, ρ_{water} is the density of water, C_{d} is the drag coefficient, D_{rope} is the diameter of the rope.
Substituting q_1 into (14.7) and then simplifying and applying the product rule gives:

$$\frac{\partial^2 w}{\partial t^2} = \frac{EA}{\rho A + A_{\text{mass}}}\left(\frac{\partial u}{\partial z}\frac{\partial^2 w}{\partial z^2} + \frac{\partial^2 u}{\partial z^2}\frac{\partial w}{\partial z}\right) - \frac{\frac{1}{2}\rho_{\text{water}}C_{\text{d}}D_{\text{rope}}}{\rho A + A_{\text{mass}}}\left|\frac{\partial w}{\partial t}\right|\frac{\partial w}{\partial t} \tag{14.9}$$

14.5.2 Rod, q

In (14.2) the q term is given by:

$$q = E\frac{\partial w}{\partial z}\frac{\partial^2 w}{\partial z^2} \tag{14.10}$$

Substituting q into (14.2) and simplifying:

$$\frac{\partial^2 u}{\partial t^2} = \frac{E}{\rho}\frac{\partial^2 u}{\partial z^2} + \frac{E}{\rho}\frac{\partial w}{\partial z}\frac{\partial^2 w}{\partial z^2} \tag{14.11}$$

14.5.3 Equations

The equations to solve are (14.9) and (14.11), they are repeated below:

$$\frac{\partial^2 w}{\partial t^2} = \frac{EA}{\rho A + A_{\text{mass}}}\left(\frac{\partial u}{\partial z}\frac{\partial^2 w}{\partial z^2} + \frac{\partial^2 u}{\partial z^2}\frac{\partial w}{\partial z}\right) - \frac{\frac{1}{2}\rho_{\text{water}} C_{\text{d}} D_{\text{rope}}}{\rho A + A_{\text{mass}}}\left|\frac{\partial w}{\partial t}\right|\frac{\partial w}{\partial t} \tag{14.12}$$

$$\frac{\partial^2 u}{\partial t^2} = \frac{E}{\rho}\frac{\partial^2 u}{\partial z^2} + \frac{E}{\rho}\frac{\partial w}{\partial z}\frac{\partial^2 w}{\partial z^2} \tag{14.13}$$

14.6 Boundary conditions

14.6.1 String

The equation is second order in space so at each end there is one boundary condition (BC).

14.6.1.1 Crane-tip side

At the end of the string attached to the crane-tip there is a kinematic BC, sway motion of the crane-tip:

$$w(z = 0, t) = y_{\text{crane-tip}}(t) \tag{14.14}$$

14.6.1.2 Hook side

At the end of the string attached to the payload there is a dynamic BC, given by the product of the mass of the hook/payload and second time derivative of w:

$$T\frac{\partial w}{\partial z} = -M_{\text{hook,payload}}\frac{\partial^2 w}{\partial t^2} \tag{14.15}$$

T was given earlier in (14.3), substituting this in and re-arranging for $\frac{\partial w}{\partial z}$:

$$\frac{\partial w}{\partial z}(z = L, t) = \frac{-M_{\text{hook,payload}}\frac{\partial^2 w(L,t)}{\partial t^2}}{(EA\frac{\partial u(L,t)}{\partial z})} \tag{14.16}$$

14.6.2 Rod

14.6.2.1 Crane-tip side

At the end of the rod attached to the crane-tip there is a kinematic BC, heave motion of the crane-tip:

$$u(z = 0, t) = z_{\text{crane-tip}}(t) \tag{14.17}$$

14.6.2.2 Hook side

At the end of the rod attached to the payload there is a dynamic BC, given by the product of the mass of the hook/payload and second time derivative of u:

$$EA\frac{\partial u}{\partial z} = -M_{\text{hook,payload}}\frac{\partial^2 u}{\partial t^2} \tag{14.18}$$

Re-arranging for $\frac{\partial u}{\partial z}$:

$$\frac{\partial u}{\partial z}(z = L, t) = -\frac{M_{\text{hook,payload}}\frac{\partial^2 u(L,t)}{\partial t^2}}{EA} \tag{14.19}$$

14.7 Initial conditions

The equations are second order in time so two initial conditions (IC) are needed for each equation. Both string and rod are initially not displaced nor having a velocity.

14.7.1 String

$$w(z, t = 0) = 0 \tag{14.20}$$

$$\frac{\partial w}{\partial t}(z, t = 0) = 0 \tag{14.21}$$

14.7.2 Rod

$$u(z, t = 0) = 0 \tag{14.22}$$

$$\frac{\partial u}{\partial t}(z, t = 0) = 0 \tag{14.23}$$

14.8 Solution

The equations of motion are given by (14.13) and (14.12). The boundary conditions are given in section 14.6 and the initial conditions in section 14.7. With these governing equations the system can be solved. The partial differential equation (PDE) represented by (14.13) and by (14.12) are both non-linear. In general, a non-linear PDE can be solved analytically for only certain types of equations [70]. It is not known if there is an analytical solution to the PDEs considered. In contrast, a numerical solver can in most cases obtain the numerical solution. For this reason, the PDEs are solved with a numerical solver.

As mentioned in chapter 12 the effect of the coupling between the vessel and the PHCS is negligible. So it is not necessary to considered the PHCS coupled with the vessel, the PHCS can be considered by itself. As mentioned in chapter 13 the HHCS has performance that is highly dependent on the control parameters used. Since the control parameters were selected in a relatively simple manner they do not provide very effective performance. To more clearly see the effect of using the continuous rope model it is better to use it with the simplest model possible, thus the PHCS by itself is used. The PHCS is implemented in a numerical solver in MATLAB thus MATLAB is used to solve the PDEs so that the PDEs can be coupled with the PHCS.

14.8.1 Numerical method of lines

The method of lines is used to solve the PDEs numerically. This is done by discretizing the PDEs in space and then solving the equations in time using an available solver, ‘ode45’ was used since this was the fastest. When coupling the PDEs with the PHCS a stiff solver, ‘ode23s’, was used since the PHCS has a stiff system of equations. The PDEs alone were solved using ‘ode23s’ to compare with the results of ‘ode45’, the results were essentially the same. The difference is the ‘ode23s’ solver took longer than the ‘ode45’ solver. Nevertheless, the ‘ode23s’ solver was used to solve the coupled system of the PDEs with the PHCS, since the PHCS is stiff.

To discretize in space various methods can be used such as finite difference, finite volume, and finite element [71]. The finite difference method is chosen since this method is relatively simple and sufficient for the one-dimensional case considered. A reference used for the implementation of the method of lines is a book by Schiesser and Griffiths [72].

14.8.2 Finite difference scheme

The equations of motion (14.12) and (14.13) are both non-linear. There is no generalized numerical scheme that can solve every type of non-linear PDE. This means a trial-and-error approach is needed to obtain a numerical scheme that works. For a numerical solver the key things to know are if it has stability and if it converges [73]. Convergence means if the numerical solution converges to an analytical solution when the grid in time and space is refined. Stability means the solution does not grow un-bounded in time.

The equations of motion (14.12) and (14.13) both involve first and second derivatives with respect to the spatial coordinate z. The terms involving first derivatives with respect to z are convective and the terms involving second derivatives are diffusive. The convective property means the variable is convected along the spatial coordinate from left to right if the coordinate system starts on the left. For this type of physics an upwind finite difference scheme is more suitable than a centered finite difference scheme. This is because this takes into account the direction the information is being propagated in, whereas the centered difference scheme uses information from both directions [73]. It is better to use a higher order finite difference (FD) approximation than first order, since first order FD can give numerical diffusion due to severe truncation of the Taylor series.

A 4th order biased upwind discretization was used to obtain the first derivative. This was successively applied to obtain the second derivative. Schiesser [71] provides various codes for obtaining first and second derivatives using various order centered and upwind methods. With these codes a trial-and-error approach in the finite difference scheme could be done relatively quickly.

14.8.3 Stability and convergence

Despite trying various finite difference schemes the results eventually became unstable in time. This is likely due to the non-linear coupled terms in the equations of motion. To make the results more stable, artificial viscosity was added [74]. This was done by adding the term:

$$\nu_w \frac{\partial^2 w}{\partial z^2} \tag{14.24}$$

to the right-hand side of (14.12) and the term:

$$\nu_u \frac{\partial^2 u}{\partial z^2} \tag{14.25}$$

to the right-hand side of (14.13), where ν_w and ν_u are artificial viscosities. This dissipation of the variables gave better stability although this influences the physics of the problem. The solution is not accurate and becomes closer to the correct solution when the constants ν_w and ν_u go to zero. However, the solution is useful since it is relatively stable and has values that are reasonable physically, but the accuracy is limited. It is better to avoid using artificial viscosity and trying a different discretization especially adapted to non-linear PDEs should be tried. Furthermore, the convergence of the solutions was not verified. This is because the artificial viscosity will always make the solution inaccurate so having convergence is not believed to be meaningful.

14.8.4 Coupling to PHCS

The input to the PHCS model is the longitudinal displacement of the rod at the end of the rod, $u(z = L, t)$, a function of time. This replaces the z_d input in (14.26) to get (14.27):

$$\ddot{z}_1 = \frac{1}{(M_{\text{hook,payload}} + A_{\text{hook,payload}})} \left[P_{\text{p1}} A_{\text{p}} - P_{\text{p2}} A_{\text{p}} + F_{\text{water}} - F_{\text{water}} + \rho_{\text{water}} V_{\text{d}} g \right. \\ \left. - M_{\text{hook,payload}} g - \frac{1}{2} \rho_{\text{water}} C_{\text{d,hook,payload}} D_{\text{hook,payload}} |\dot{z}_1| \dot{z}_1 - k_{\text{d}} (z_1 - z_{\text{d}}) \right] \tag{14.26}$$

$$\ddot{z}_1 = \frac{1}{(M_{\text{hook,payload}} + A_{\text{hook,payload}})} \left[P_{\text{p1}} A_{\text{p}} - P_{\text{p2}} A_{\text{p}} + F_{\text{water}} - F_{\text{water}} + \rho_{\text{water}} V_{\text{d}} g \right. \\ \left. - M_{\text{hook,payload}} g - \frac{1}{2} \rho_{\text{water}} C_{\text{d,hook,payload}} D_{\text{hook,payload}} |\dot{z}_1| \dot{z}_1 - k_{\text{d}} (z_1 - u(z = L, t)) \right] \tag{14.27}$$

For coupling the rope and PHCS, the boundary conditions discussed in section 14.6 of $\frac{\partial w}{\partial z}(z = L, t)$ and $\frac{\partial u}{\partial z}(z = L, t)$ need to be considered. These two boundary conditions are functions of the acceleration at the rope tip and the hook/payload mass, which is the inertia of the hook/payload mass. In reality, since the rope tip is attached to the piston of the PHCS cylinder the effect of the PHCS on the rope includes the dynamics from the pressure forces acting on the piston inside the cylinder. Since this effect is excluded, this limits the amount of coupling between the rope and PHCS. Nevertheless, the inertia of the hook/payload mass likely dominates the dynamics at this location and is the more important information to consider.

14.9 Results

The effect of the continuous Dyneema rope model relative to the discrete Dyneema rope model used to obtain results in chapter 11 is investigated. The goal of the sensitivity study is to investigate the effect of the damping of Dyneema rope motion due to the large water depths on the hook/payload motion. Thus, the performance of the PHCS is not as important as the motion of the hook/payload motion. The SDA gives a direct measure of the motion of the hook/payload motion so is used.

The SDA as a function of period for H=2.5m and regular input is shown in Figure 14.2a from section 11.5.1. The same results but using the continuous model of the Dyneema rope is shown in Figure 14.2b. The effect of using the continuous model of the Dyneema rope is to reduce the magnitude of the SDA. This is most noticeable at close to the natural periods. In Figure 14.2a there are peaks for 1000m water depth at 5s and 12s. As mentioned earlier these peaks are due to there being natural periods close to 5s and 12s. With the continuous rope model in Figure 14.2b the peaks are not there. This is likely due to the natural periods not existing anymore at these periods due to the different rope model used. Furthermore, the Dyneema rope motion is reduced due to taking into account the damping due to the water. Since the hook/payload is directly coupled to the Dyneema rope then this should result in a reduced hook/payload motion thus smaller SDA.

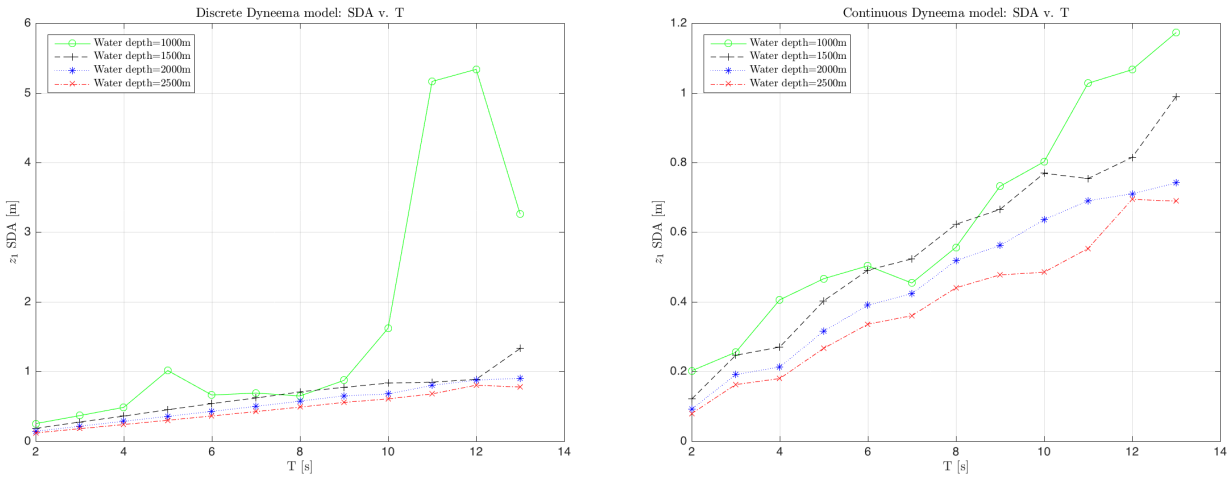

(a) Discrete

(b) Continuous

Figure 14.2

14.10 Conclusion

The sensitivity study of replacing the discrete Dyneema rope model with a continuous model shows that the SDA is reduced for the water depths and periods considered. This shows that the damping at large water depths has an important effect on reducing the motions of the Dyneema rope.

15 Conclusion

In the introduction of the report the main research objective of the project was given as:

The main research objective is to make a design of a modular and removable deep-water hybrid heave compensation system for an offshore crane installed on a monohull heavy lift vessel. This is accomplished by identifying and then assessing designs of heave compensation systems and selecting a design. The hybrid heave compensation system is modelled as a numerical time-domain model.

In this chapter, a summary is given in section 15.1 of the steps taken towards achieving the main research objective. The results are discussed in section 15.2. Discussion is made on the modelling choices in this project in section 15.3. Recommendations for further work are given in section 15.4. Finally, a summary of the contributions of this project is given in section 15.5.

15.1 Summary

In chapter 2, a literature review was done to mainly review existing active heave compensation methods. This formed a theoretical basis for the project. In chapter 3, a multi-criteria analysis was done to choose a HHCS concept. In chapter 4, the available numerical vessel model was described. To obtain the crane-tip motions from the vessel model a crane-tip model was needed, this was described in chapter 5. In chapter 6, the PHCS part of the HHCS was investigated by first introducing the PHCS cylinder. In chapter 7, this cylinder was used to create the entire PHCS. First, one accumulator was used and this was tested with the throttle, orifice, and Darcy-Weisbach type flow restrictors. The throttle and orifice were used further since the Darcy-Weisbach system had poor performance. Two accumulators were used in the PHCS and this was tested with the throttle and orifice. After trying these different flow restrictors, the final flow restrictor chosen was the orifice. This model was further improved by including fluid inertia in the model to remove un-physical behavior such as instantaneous changes in pressure and hydraulic oil flow-rate. The initial pressures and volumes of the PHCS were sized for a natural frequency outside of realistic wave frequencies in chapter 8. This was done to avoid the PHCS being excited through resonance by any realistic sea-state. The natural frequencies of the PHCS were identified in chapter 9. In chapter 10, the natural frequencies were verified by looking at the frequency and time response of the PHCS. The performance of the PHCS was assessed in chapter 11. In chapter 12, the PHCS was combined with the crane-tip and vessel model and the influence of this coupling assessed. The AHCS was designed in chapter 13 and combined with the PHCS to form the HHCS. The HHCS was coupled

with the crane-tip and vessel model to see the effect of activating the active part on the response of the system. In chapter 14, the Dyneema rope was modelled as a continuous structural element to account for damping due to water. This was done as a sensitivity study to compare with the results of modelling the rope as a discrete mass.

15.2 Results

Firstly, the results from chapter 11 are described since this gives the performance of the PHCS by itself. It was found for the design conditions of 8s period, 2.5m wave height, and 2500m water depth that the PHCS works with reasonable performance. Decreasing the water depth can result in an amplification of the hook/payload motion due to the natural periods of the system being shifted. This is due to the natural period being inversely proportional to rope stiffness. Thus, it is important to take this into account when designing a PHCS. The natural periods of the PHCS in design conditions showed a large amplification of motion at the larger natural periods, as would be expected. For the smaller natural periods, the larger frequency of motion enables the damping present to drain energy, avoiding a large amplification of motion.

Secondly, the results from chapter 12 of the coupled PHCS model are described to show the impact of coupling with the vessel. There was a negligible effect on the vessel of using the PHCS. The influence on the PHCS is that the wave motions transferred to the crane-tip are attenuated due to the vessel and crane. This means the PHCS sees a smaller z_{in} input signal compared to when the PHCS operates by itself.

Thirdly, the results from chapter 13 of the coupled HHCS model are described to show the effect of activating the active part of the HHCS. This answers the main research question mentioned in the introduction in section 1.3:

How important is the change in natural period from when the active heave compensation system is disabled to when the active heave compensation is enabled on resonance?

Activating the AHCS does not lead to a change in natural period that influences the resonance behavior. Therefore, the change in natural period is not important on resonance. It was found that the controller can result in pre-existing resonance motion to be amplified, depending on which natural period of the PHCS is considered. Thus, the controller design is a key part of the HHCS and careful controller design is needed when using HHC systems in practice.

The influence of water depth on the performance of the PHCS, C-PHCS, and C-HHCS is shown in Figure 15.1. The performance is measured by the compensation rate β where 0% is no compensation and 100% is complete compensation. With decreasing water depth the following occurs; the PHCS has decreasing β, the C-PHCS has greater decreasing β, and the C-HHCS has the greatest decreasing β. A possible explanation for decreasing β with decreasing water depth is that there is a smaller mass of Dyneema/steel rope with decreasing water depth. This smaller mass produces larger movements of the Dyneema/steel rope for a given input acceleration since the ropes have less inertia. Since the hook/payload is directly coupled to the Dyneema rope an increase in Dyneema rope motion results in an increase in hook/payload motion, leading to lower β.

It is expected the C-HHCS has the greatest decrease in β with decreasing water depth since the controller parameters are optimized for a certain water depth, 2500m. If the C-HHCS operates at another water depth than 2500m it is reasonable the performance worsens. In reality, if the controller parameters are optimized for each water depth than at smaller water depths the performance should be greater than at larger water depths, with everything else being equal. This is because at smaller water depths the motions of the rope takes less time to propagate between the crane-tip and hook/payload. This is because the motion is governed by physics similar to that of waves, as mentioned in chapter 14.

This means the control action of the controller has less delay which generally leads to better performance.

The design requirement in section 3.2 of compensation for 2.5m of heave motion within 8 seconds was not satisfied. This was likely due to the relatively simple controller design used. Commercial systems use more advanced methods that would likely be able to satisfy this design requirement. These methods were not made available for this thesis by Bosch Rexroth, a company Jumbo Maritime is working with for the AHCS. So it was necessary for the author to come up with a controller design leading to the simple controller design used.

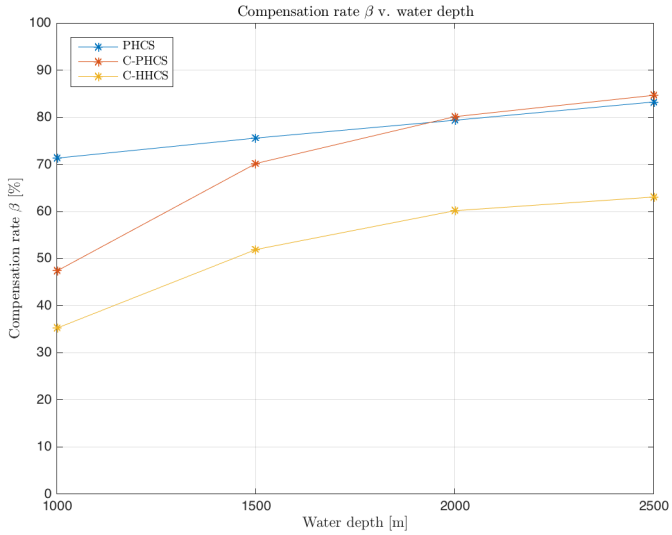

Figure 15.1: Compensation rate β as a function of water depth, for H=2.5m and T=8s

15.3 Discussion

To produce the models in this project various simplifications and assumptions were needed. These are discussed.

For the PHCS cylinder the assumptions used are described in section 6.2. To size the pressure system further assumptions were used in section 8.2.1. To obtain the equations of motion of the PHCS various assumptions were used, given in section 7.5.

A key simplification is that the added mass and water drag on the PHCS and hook/payload are included but neglected for the Dyneema and steel rope. Furthermore, the steel and Dyneema rope are assumed to only move in the vertical direction. If both these simplifications for the steel and Dyneema rope are undone then they would move transversely. This transverse motion would be damped by the damping present for the long lengths of rope considered. This would result in smaller transverse motions of the ropes and consequently smaller heave motions of the ropes. In the sensitivity study in chapter 14 this was considered and resulted in smaller motions of the hook/payload mass. This means that the damping from water has an effect at large water depths.

The added mass for the PHC cylinder and hook/payload mass is taken from the added mass at infinite frequency. The added mass is actually frequency dependent and is generally lower for lower frequencies meaning the added mass would likely be smaller if this frequency dependence was accounted for. This would generate larger motions meaning the results obtained are under-predicting the motions.

A key assumption for the PHCS cylinder is that the accumulators undergo adiabatic and reversible

processes. The adiabatic assumption is close to reality since the gas in the accumulators experiences quick compression and expansion meaning there is little time for heat to escape. However, the reversible assumption means there are no losses in energy due to friction. This implies the accumulators act more efficiently than in reality. Since the accumulators store energy there is more energy stored allowing for more effective heave compensation. This means the performance is better than possible in reality.

15.4 Recommendations

In this project it was assumed there is no current. When a current exists vortex-induced vibration can occur. This means the rope moves in a direction transverse to the current due to a modified pressure distribution around the rope. There would be coupling into the vertical plane which would affect the heave motion of the ropes and thus the hook/payload. This is why vortex-induced vibration could be examined in future work since it can amplify the motion of the hook/payload.

The inclusion of a roll-reduction system could be done which reduces the roll of the vessel since this is a large contributor to the heave motion of the crane-tip. If this system operates in parallel to the HHCS it is likely more effective heave compensation can be achieved. Since the roll-reduction system is also an active system it is important to design the controller parameters to take into account the HHCS, to ensure an effective choice of parameters.

The HHCS and vessel model could be combined into a state-space system. Using this state-space system, the transfer functions of the system can be obtained and the open-loop performance can be found. This will give the gain and phase margins of the coupled system which is likely more accurate than the gain and phase margins obtained in this project.

The PID controller design could be investigated further. This can be done by using the state-space system of the combined HHCS and vessel model. Alternatively, more advanced controller design using an optimization procedure can be used to design the controller. Furthermore, the time-delay existing between the winch and the hook/payload from the large water depths could be taken into account, in a similar way to work by Kuchler and Sawodny [34].

For solving the coupled PDEs for the continuous model of the rope different numerical schemes could be attempted. Using artificial viscosity it not an ideal method due to the inaccuracies this introduces. More advanced numerical schemes especially adapted to non-linear PDEs can be attempted.

15.5 Contributions

The main contribution of this work is a numerical time-domain model of a hybrid heave compensation system coupled with a crane-tip and vessel model. A further model is the passive heave compensation model using a continuous Dyneema rope model instead of a discrete Dyneema rope model.

List of Figures

2.1 A schematic of the primary control method [10] . . . 6
2.2 A schematic of the secondary control method [10] . . . 7
2.3 A schematic of the LAHCS [14] . . . 8
2.4 A diagram from Bosch Rexroth showing the key differences between PHC and AHC systems [16] . . . 9
2.5 A diagram of the three coupled masses, for definitions of the variables see the paper by Korde [22] . . . 11
2.6 A schematic of an AHCS using an electro-hydraulic system being driven by a double rod actuator, for definitions of the variables see the paper by Do and Pan [26] . . . 12
2.7 Crane model from Sawodny et al., for definitions of the variables see the paper by Sawodny et al. [34] . . . 14

3.1 Ideal modelling and simulation process [38] . . . 17
3.2 Concept 1: using a roll reduction system . . . 19
3.3 Concept 2: the linear active heave compensation system . . . 19
3.4 Concept 3: electric winch at the top of the crane and a passive cylinder integrated with the hook . . . 20

4.1 Six degrees of freedom for three axes with the origin at the center of gravity [41] . . . 24

5.1 Coordinate system [41] . . . 30
5.2 RAO for 6 degrees of freedom [41] . . . 31
5.3 Vertical crane-tip motion in the top sub-plot in blue with vessel heave in red, in the bottom sub-plot the vessel roll is shown . . . 32

6.1 Schematic of the system . . . 33

7.1 Schematic of the PHCS . . . 39
7.2 In the literature this system is referred to as the plunger cylinder [51] . . . 39
7.3 Schematic of the PHCS with two accumulators . . . 40
7.4 In the literature this system is referred to as the double-acting cylinder [51] . . . 41
7.5 Variables for the initial conditions of the pressure system of the PHCS . . . 50
7.6 Design iteration loop shown [38] . . . 54
7.7 Throttle: rms reduction ratio as function of accumulator volume . . . 55
7.8 Orifice: rms reduction ratio as function of accumulator volume . . . 56
7.9 Schematic of the PHCS with two accumulators and orifices, fluid inertia is included in the model . . . 58
7.10 Time-series for z_1, z_{phc}, z_{c}, and z_{d} are shown . . . 60

8.1 A diagram of the PHCS with just accumulators . . . 62
8.2 A diagram showing the variables defined in Table 8.1 . . . 63
8.3 For piston-head diameter $d_{\mathrm{p,tot}} = 0.3$m the natural frequency of the accumulator system is given as a function of the lower accumulator initial pressure $P_1 = P_{\mathrm{a1,1}}$. The horizontal line corresponds to the design natural frequency. . . . 66
8.4 A schematic for the upper case . . . 68
8.5 A schematic for the lower case . . . 69
8.6 . . . 69

9.1 A diagram of the LAM . . . 72
9.2 A diagram of the RLAM . . . 72
9.3 A diagram of the ORLAM . . . 73

10.1 Base case, for the LAM . . . 80
10.2 Base case, time-response of P_{a3} and P_{a1} . . . 81
10.3 Base case, bode plot for z_1, the RLAM. . . . 82
10.4 Time-series for z_1 for five input frequencies . . . 84

11.1 Pierson-Moskowitz spectrum discretized with 582 frequency bins . . . 88
11.2 Pierson-Moskowitz spectrum discretized with 10 frequency bins . . . 89
11.3 SDA: Irregular and regular input results . . . 93
11.4 . . . 95
11.5 . . . 96
11.6 . . . 97
11.7 z_1 (hook and payload motion) and z_{in} (crane-tip motion), top sub-plot shows data for time from 0s to 500s. There is some transient behavior initially, as would be expected. The bottom sub-plot shows the full simulation time from 0s to 1800s. . . . 98
11.8 . . . 100
11.9 Compensation rate: Irregular and regular input results . . . 101
11.10 R ratio: Irregular and regular input results . . . 103
11.11 Irregular and regular input results . . . 108
11.12 Irregular and regular input results . . . 110
11.13 Irregular and regular input results . . . 113
11.14 Irregular and regular input results . . . 114
11.15 Irregular and regular input results . . . 115
11.16 Irregular and regular input results . . . 116
11.17 Irregular and regular input results . . . 117

12.1 C-PHCS: T=8s, the first 500s are a ramp-up period for the vessel model and are removed from the analysis . . . 120
12.2 PHCS: T=12.34s, the first 500s are removed to be consistent with the figures above . . . 121
12.3 C-PHCS: The first 500s are a ramp-up period for the vessel model and are not included in the analysis . . . 122
12.4 Coupled refers to the C-PHCS and uncoupled refers to the PHCS only . . . 123

13.1 Scenario [3] . . . 125
13.2 . . . 125
13.3 . . . 127
13.4 PID controller with plant [67] . . . 127
13.5 Winch . . . 130
13.6 Closed loop control block diagram . . . 133
13.7 Open loop model . . . 134
13.8 C-HHCS: Motion results (8s period) . . . 137

13.9 C-HHCS: The first 500s are a ramp-up period for the vessel model and are not included in the analysis . . . 138
13.10 . . . 140
13.11 . . . 141
13.12 Motion results (8s period) . . . 142

14.1 Coordinate system . . . 145
14.2 . . . 151

15.1 Compensation rate β as a function of water depth, for H=2.5m and T=8s . . . 154

A.1 Cylinder control volume . . . 169
A.2 Packet control volume . . . 169
A.3 Check the spring stopper works . . . 180
A.4 Throttle: rms reduction ratio as function of accumulator volume . . . 182
A.5 Throttle: pressure time series . . . 183
A.6 Throttle: time series for key degrees of freedom . . . 183
A.7 Bottom accumulator, note that $Q_{\mathrm{a}} = Q_{\mathrm{r}}$ . . . 184
A.8 Upper accumulator, note that $Q_{\mathrm{a,u}} = Q_{\mathrm{r,2}}$ . . . 186
A.9 A schematic for the upper case . . . 205
A.10 A schematic for the lower case . . . 207
A.11 Upper case, for the LAM . . . 216
A.12 Lower case, for the LAM . . . 217
A.13 Upper case, time-response of P_{a3} and P_{a1} . . . 218
A.14 Lower case, time-response of P_{a3} and P_{a1} . . . 218
A.15 Upper case, bode plot for z_1, the RLAM. . . . 220
A.16 Lower case, bode plot for z_1, the RLAM. . . . 220
A.17 Time-series for z_1 for five input frequencies . . . 222
A.18 Time-series for z_1 for five input frequencies . . . 223
A.19 z_1, $\dot{z}_1$, z_{phc}, $\dot{z}_{\mathrm{phc}}$ time series . . . 238
A.20 z_{c}, $\dot{z}_{\mathrm{c}}$, z_{d}, $\dot{z}_{\mathrm{d}}$ time series . . . 239
A.21 P_{p1}, Q_{r},V_{in},P_{p2} time series . . . 239
A.22 $Q_{\mathrm{r,2}}$, $V_{\mathrm{in,u}}$, z_{in} time series . . . 240
A.23 z_1 time series . . . 240

List of Tables

3.1 The multi-criteria analysis . . . 21

5.1 Definitions of variables . . . 29
5.2 Inputs and outputs of the crane model . . . 31

6.1 Mass data . . . 35

7.1 Added mass $A = \rho C_{\mathrm{A}} V_{\mathrm{R}}$ for vertical direction of motion . . . 42
7.2 Variables . . . 49
7.3 Initial conditions for the pressure system . . . 50
7.4 Initial conditions for the motions . . . 50
7.5 State variables and physical variables . . . 51
7.6 Eigenvalues and natural frequencies . . . 53

8.1 Base case, the variables are shown in Figure 8.2 . . . 62
8.2 Key variables . . . 63
8.3 Key variable values, lower accumulator . . . 67
8.4 Key variable values, upper accumulator . . . 67
8.5 Base case . . . 68

9.1 LAM: base case eigenvalues, natural frequencies, natural periods . . . 73
9.2 Upper case eigenvalues, natural frequencies, natural periods . . . 74
9.3 Lower case eigenvalues, natural frequencies, natural periods . . . 74
9.4 Natural frequency for the different cases . . . 74
9.5 RLAM: base case eigenvalues, natural frequencies, natural periods . . . 75
9.6 ORLAM: base case eigenvalues, natural frequencies, natural periods . . . 76
9.7 Natural frequency for the different cases . . . 78

10.1 Three cases, frequency and magnitude for P_{a3} . . . 80
10.2 Three cases, frequency and magnitude for P_{a1} . . . 81
10.3 Frequency and magnitudes for peaks in Figure 10.3 (RLAM) . . . 83
10.4 Base case, natural frequencies for the ORLAM with percent differences of values in Table 10.3 . . . 83
10.5 Natural frequencies and periods for the base case . . . 85

11.1 For $H_{1/3}$ =0.5m, the maximum wave height observed and the theoretical maximum wave height for various simulation times . . . 91
11.2 Natural periods for 1000m water depth as function of increased steel rope stiffness . . . 95
11.3 Natural periods for 1000m water depth as function of increased Dyneema rope stiffness . 96

11.4 Natural periods for [2500, 2000, 1500, 1000]m water depths 98
11.5 SDA, R, and β as a function of Hs, for Tp=8s, for water depth of 2500m 105
11.6 SDA, R, and β as a function of Tp, for Hs=2.5m, for water depth of 2500m 105
11.7 SDA, R, and β as a function of H, for T=8s, for water depth of 2500m 106
11.8 SDA, R, and β as a function of T, for H=2.5m, for water depth of 2500m 106
11.9 SDA, R, and β for regular and irregular input, for water depth of 2500m 106
11.10 Base case, natural periods for the ORLAM 107
11.11 Irregular input: SDA, R, and β as a function of Tp, for Hs=2.5m, for water depth of 2500m 111
11.12 Regular input: SDA, R, and β as a function of T, for H=2.5m, for water depth of 2500m 111

12.1 Difference between PHCS and C-PHCS 119

13.1 System parameters 132
13.2 Eigenvalues, natural frequencies, natural periods 136
13.3 Gain and phase margins 137
13.4 Summary of data from C-PHCS, C-HHCS 138

A.1 Time when spring stops acting as a function of spring stiffness value 179
A.2 q variables 189
A.3 q variables 203
A.4 Upper case, key variable values for the lower accumulator, variables with * changed relative to the base case 206
A.5 Upper case, key variable values for the upper accumulator, variables with * changed relative to the base case 206
A.6 Upper case, variables with * are changed relative to the base case 207
A.7 Lower case, key variable values for the lower accumulator, variables with * changed relative to the base case 208
A.8 Lower case, key variable values for the upper accumulator, variables with * changed relative to the base case 209
A.9 Lower case, variables with * are changed relative to the base case 209
A.10 q variables 211
A.11 Upper case eigenvalues, natural frequencies, natural periods 213
A.12 Lower case eigenvalues, natural frequencies, natural periods 213
A.13 Upper case: Eigenvalues, natural frequencies 214
A.14 Lower case: Eigenvalues, natural frequencies 215
A.15 Frequency and magnitudes for peaks in Figure A.15 (RLAM) 219
A.16 Upper case, natural frequencies for the ORLAM with percent differences of values in Table A.15 219
A.17 Frequency and magnitudes for peaks in Figure A.16 (RLAM) 219
A.18 Lower case, natural frequencies for the ORLAM with percent differences of values in Table A.17 220
A.19 Upper case, natural frequencies 221
A.20 Lower case, natural frequencies 221
A.21 q variables 225

References

[1] Big Lift, "Installation loading arms: active heave compensation on Happy-D type vessels," http://www.bigliftshipping.com/projects/petrochemical-power-lng/installation-loading-arms, 2015.

[2] P. Belenfant, "Active heave compensation comes of age," http://www.oedigital.com/production/workover/item/670-active-heave-compensation-comes-of-age-subsea, Jan 2012.

[3] N. Mannigel, "Unexpected crane active heave compensation (AHC) behavior during deepwater deployments," Subsea 7, Tech. Rep. 2 December 2015, 2015.

[4] J. Woodacre, R. Bauer, and R. Irani, "A review of vertical motion heave compensation systems," *Ocean Engineering*, vol. 104, pp. 140–154, 2015. [Online]. Available: http://linkinghub.elsevier.com/retrieve/pii/S0029801815001729

[5] A. Southerland, "Mechanical systems for ocean engineering," *Naval Engineers Journal*, pp. 63–74, 1970.

[6] Bosch Rexroth, "Active heave compensation," https://www.boschrexroth.com/en/xc/industries/machinery-applications-and-engineering/offshore/products-and-solutions/heave-compensation/active-heave-compensation/index, 2015.

[7] IHC Hytop. Integrated heave compensator. http://www.ihchytop.com/products-systems/motion-compensation/.

[8] Bosch Rexroth, "Secondary active heave compensator," http://www.boschrexroth.com/en/xc/industries/machinery-applications-and-engineering/offshore/products-and-solutions/heave-compensation/active-heave-compensation/secondary-active-heave-compensator/index.

[9] Bosch Rexroth, "Primary active heave compensator," http://www.boschrexroth.com/en/xc/industries/machinery-applications-and-engineering/offshore/products-and-solutions/heave-compensation/active-heave-compensation/primary-active-heave-compensator/index.

[10] K. Holm, "Master thesis, industrial economics for offshore crane concepts for subsea operations - core competence," University of Stavanger, Stavanger, Tech. Rep.

[11] Norwegian Deck Machinery, "Active heave compensated winches," http://www.ndm.no/products/marine/active-heave-compensated-winches.

[12] Bosch Rexroth, "Secondary-controlled drives compensate for sea swells," Tech. Rep.

[13] Bosch Rexroth, "Linear active heave compensator," http://www.boschrexroth.com/en/xc/industries/machinery-applications-and-engineering/offshore/products-and-solutions/heave-compensation/active-heave-compensation/linear-active-heave-compensator/index.

[14] B. Biemans and A. Ooijen, "Active heave compensation system Jumbo shipping 500mT AHC," Bosch Rexroth, Tech. Rep., 2014.

[15] O. Bergem, "Cranemaster calculation sheet (css) engineering guide," http://www.cranemaster.no/file/engineering-guide-ccs.pdf, Jan 2015.

[16] Bosch Rexroth, "Passive heave compensation," http://www.boschrexroth.com/en/xc/industries/machinery-applications-and-engineering/offshore/products-and-solutions/heave-compensation/index.

[17] Cranemaster, "Technical product sheet cm1-21t-1000-a," http://www.cranemaster.no/file/datasheetcm1-21t-1000-a.pdf, Feb 2014.

[18] Cranemaster, "Overview - cranemaster - passive heave compensation - shock absorbers," http://www.cranemaster.no/cranemaster-products.

[19] B. W. Nam, S. Y. Hong, Y. S. Kim, and J. W. Kim, "Effects of passive and active heave compensators on deepwater lifting operation," *International Journal of Offshore and Polar Engineering*, vol. 23, no. 1, pp. 33–37, 2013.

[20] V. D. Angelis, "Comparison study of electric, electro-hydraulic, and hydraulic drive science winches," European Research Vessel Operators Meeting, Tech. Rep., 2009.

[21] Y. Chu, F. Sanfilippo, V. Asoy, and H. Zhang, "An effective heave compensation and anti-sway control approach for offshore hydraulic crane operations," *2014 IEEE International Conference on Mechatronics and Automation*, pp. 1282–1287, 2014. [Online]. Available: http://www.scopus.com/inward/record.url?eid=2-s2.0-84906972232{&}partnerID=tZOtx3y1

[22] U. A. Korde, "Active heave compensation on drill-ships in irregular waves," *Ocean Engineering*, vol. 25, no. 7, pp. 541–561, 1998. [Online]. Available: http://www.sciencedirect.com/science/article/B6V4F-3T02WMM-4/2/41082ad5914defb64cbbef218426b373

[23] K. Ogata, *System dynamics*. Prentice-Hall, Englewood Cliffs, NJ, 1978, pp. 456-459.

[24] L. Meirovitch, *Elements of Vibration Analysis*, 2nd, Ed. McGraw-Hill, New York, NY, 1986, chapters 3-6.

[25] S. Liu and L. Li, "Control performance simulation on heave compensation system of deep-sea mining based on dynamic vibration absorber," *2010 International Conference on Digital Manufacturing & Automation*, no. 50675226, pp. 441–445, 2010. [Online]. Available: http://ieeexplore.ieee.org/lpdocs/epic03/wrapper.htm?arnumber=5701192

[26] K. D. Do and J. Pan, "Nonlinear control of an active heave compensation system," *Ocean Engineering*, vol. 35, pp. 558–571, 2008.

[27] T. A. Johansen, T. I. Fossen, S. I. Sagatun, and F. G. Nielsen, "Wave synchronizing crane control during water entry in offshore moonpool operations - experimental results," *IEEE Journal of Oceanic Engineering*, vol. 28, no. 4, pp. 720–728, 2003.

[28] S. I. S. Bjørn Skaare, Olav Egeland, "Adaptive wave synchronization for lowering of crane load," *Proc. 8th IFACConf. Manoeuvering Control Mar. Crafts*, p. 197 to 202, 2003, girona, Spain.

[29] B. Skaare and O. Egeland, "Parallel force/position crane control in marine operations," *Oceanic Engineering, IEEE Journal of*, vol. 31, no. 3, pp. 599–613, 2006. [Online]. Available: http://ieeexplore.ieee.org/xpls/abs{_}all.jsp?arnumber=4089046

[30] T. A. Johansen, T. I. Fossen, S. I. Sagatun, and F. G. Nielsen, "Wave synchronizing crane control during water entry in offshore moonpool operations," *Proc. IEEE Int. Conf. Control Appl.*, pp. 174–179, 2002.

[31] B. Skaare and O. Egeland, "Force control of a load through the splash zone," in *Control applications in marine systems 2004 (CAMS 2004): a proceedings volume from the IFAC conference, Ancona, Italy, 7-9 July 2004*. Elsevier Science, 2005, p. 215.

[32] S. I. Sagatun, T. I. Fossen, and K.-P. Lindegaard, "Inertance control of underwater installations," in *Proceedings of the 5th IFAC Conference on Control Application in Marine Systems (CAMS'01)*, 2001.

[33] S. I. Sagatun, "Active control of underwater installation," *IEEE Transactions on Control Systems Technology*, vol. 10, no. 5, pp. 743–748, 2002. [Online]. Available: http://ieeexplore.ieee.org/lpdocs/epic03/wrapper.htm?arnumber=1028129

[34] S. Küchler and O. Sawodny, "Nonlinear control of an active heave compensation system with time-delay," *Ocean Engineering*, vol. 35, pp. 558–571, 2008.

[35] Q. Yuan, "Actively damped heave compensation (ADHC) system," in *2010 American Control Conference*, 2010, pp. 1544–1549.

[36] R. S. Nicoll, B. J. Buckham, and F. R. Driscoll, "Optimization of a direct drive active heave compensator," *ISOPE*, vol. 8, pp. 241–248, 2008.

[37] K. van der Heiden, "Personal communication," Verbal, December 2015.

[38] L. G. Birta and G. Arbez, *Modelling and simulation: exploring dynamic system behaviour*, 2013. [Online]. Available: http://link.springer.com/10.1007/978-1-4471-2783-3

[39] J. van Heijst, "Improvement of the workability of monohull heavy lift vessels during lifting operations by reducing roll motion," Delft University of Technology, MSc thesis, Tech. Rep., 2015.

[40] WAMIT, "Technical description," http://www.wamit.com/techdescription.htm, 2016.

[41] J. M. J. Journee and W. W. Massie, *Offshore hydromechanics*, 1st ed. Delft University of Technology, 2001.

[42] J. Sverdrup-thygeson, "Modeling and simulation of an active hydraulic heave compensation system for offshore cranes," 2007.

[43] Lloyd's Register, "Certificate of test and thorough examination of wire rope runner."

[44] Det Norske Veritas, "Recommended practice DNV-RP-H103: modelling and analysis of marine operations," no. April, 2011.

[45] W. Koo and J. D. Kim, "Simplified formulas of heave added mass coefficients at high frequency for various two-dimensional bodies in a finite water depth," *International Journal of Naval Architecture and Ocean Engineering*, vol. 7, no. 1, pp. 1–13, 2015.

[46] J. N. Delmas, "Investigation AHC installation J-type: status update August 2015 Jumbo Maritime," 2015.

[47] Cranemaster, "Cranemaster products," http://www.cranemaster.no/cranemaster-products, date accessed: 02/02/16.

[48] J. Ni, S. Liu, M. Wang, X. Hu, and Y. Dai, "The simulation research on passive heave compensation system for deep sea mining," pp. 5111–5116, 2009.

[49] Lankhorst Ropes, "LankoDeep rope," 2015. [Online]. Available: http://www.lankhorstropes.com

[50] Lankhorst Ropes, "LankoForce rope," 2013. [Online]. Available: http://www.lankhorstropes.com

[51] W. Bauer, *Spring and damping characteristics of hydropneumatic suspension systems.* Berlin: Springer-Verlag, 2011.

[52] J. Newman, *Marine hydrodynamics*, 1977.

[53] M. J. Purcell, N. C. Forrester, and W. Hole, "Bobbing crane heave compensation for the deep towed fiber optic survey system," 1994.

[54] G. Rega and S. Sorokin, "Asymptotic analysis of linear/nonlinear vibrations of suspended cables under heavy fluid loading," *IUTAM Symposium on Fluid-Structure Interaction in Ocean Engineering*, 2008. [Online]. Available: http://link.springer.com/content/pdf/10.1007/978-1-4020-8630-4{_}19.pdf

[55] W. Borutzky, B. Barnard, and J. Thoma, "An orifice flow model for laminar and turbulent conditions," vol. 10, pp. 141–152, 2002.

[56] MathWorks, "Choose an ode solver," http://nl.mathworks.com/help/matlab/math/choose-an-ode-solver.html.

[57] P. Lau, "Calculation of flow rate from differential pressure devices- orifice plates," http://www.ematem.org/Dokumente/2008_lau_calculat.pdf, August 2008.

[58] P. Drexler, H. Faatz, F. Feicht, H. Geis, J. Morlok, E. Wiesmann, A. Krielen, N. Achten, and M. Reik, *Planning and design of hydraulic power systems, the hydraulic trainer, volume 3*. Bosch Rexroth AG, 2003.

[59] L. H. Holthuijsen, *Waves in oceanic and coastal waters*. Cambridge: Cambridge University Press, 2007.

[60] A. Jarquin-Laguna and C. Keijdener, "Introduction to computational dynamics for offshore structures: W6.L1&2: environmental loading," Delft. NL, 2015.

[61] S. Steen, "Experimental methods in marine hydrodynamics: statistical analysis," 2015. [Online]. Available: http://astorplast.no/wp-content/uploads/AppendixStatisticalAnalysis.pdf

[62] F. R. Driscoll, M. Nahon, and R. G. Lueck, "A comparison of ship-mounted and cage-mounted passive heave compensation systems," *Journal of Offshore Mechanics and Arctic Engineering*, vol. 122, no. 3, p. 214, 2000. [Online]. Available: http://link.aip.org/link/JMOEEX/v122/i3/p214/s1{&}Agg=doi

[63] WAFO-group, *WAFO - A MATLAB toolbox for analysis of random waves and loads - a tutorial*, Math. Stat., Center for Math. Sci., Lund Univ., Lund, Sweden, 2000. [Online]. Available: http://www.maths.lth.se/matstat/wafo

[64] F. Richards, "Motors for efficiency: permanent-magnet, reluctance, and induction motors compared," http://machinedesign.com/motorsdrives/motors-efficiency-permanent-magnet-reluctance-and-induction-motors-compared, April 2013, date accessed: 18 Jan 2016.

[65] S. Peterson, "How to choose the right control method for VFDs," 2014. [Online]. Available: http://machinedesign.com/motorsdrives/how-choose-right-control-method-vfds

[66] Y. X. Su, D. Sun, and B. Y. Duan, "Design of an enhanced nonlinear PID controller," *Mechatronics*, vol. 15, no. 8, pp. 1005–1024, 2005.

[67] University of Michigan, "Introduction: Pid controller design," http://ctms.engin.umich.edu/CTMS/index.php?example=Introduction&section=ControlPID.

[68] K. Ogata, *Modern control engineering*, 5th ed. Upper Saddle River: Prentice Hall, 2010.

[69] J. B. Herbich, *Developments in offshore engineering - wave phenomena and offshore topics*. Elsevier, 1999. [Online]. Available: http://app.knovel.com/hotlink/toc/id:kpDOEWPOT6/developments-in-offshore/developments-in-offshore

[70] G. W. Griffiths, "Linear and nonlinear waves," http://www.scholarpedia.org/article/Linear_and_nonlinear_waves#The_linear_wave_equation, 2009.

[71] W. Schiesser, *The numerical method of lines: integration of partial differential equations.* San Diego: Academic Press, 1991.

[72] W. Schiesser and G. W. Griffiths, *A compendium of partial differential equation models: method of lines analysis with MATLAB.* Cambridge: Cambridge University Press, 2009.

[73] R. Fedkiw, "Mathematical methods for fluids, solids and interfaces lecture notes," 2009. [Online]. Available: http://web.stanford.edu/class/cs205b/lectures/lecture9.pdf

[74] B. Gustafsson, *High order difference methods for time dependent PDE.* Berlin: Springer-Verlag, 2008.

[75] R. F. Gans, *Engineering dynamics: from the Lagrangian to simulation.* New York: Springer, 2013.

Appendices

A

A.1 Euler-Lagrange method

The Euler-Lagrange approach uses the Euler-Lagrange equation defined by:

$$\frac{\mathrm{d}}{\mathrm{d}t}\left(\frac{\partial L}{\partial \dot{q}^k}\right) - \frac{\partial L}{\partial q^k} = Q_{NPk} \tag{A.1}$$

Where Q_{NPk} refers to the generalized forces and subscript NP means from non-potential sources. L is the Lagrangian. k indicates the number of the degree of freedom considered. q represents the variable for the degree of freedom. (A.1) is applied to each coordinate so there will be as many equations as coordinates [75].

The degrees of freedom are $z_\mathrm{c} = q^1$,

z_c	q^1
z_d	q^2
z_phc	q^3
z_1	q^4
z_in	q^5

The kinetic energy part of the Lagrangian is

$$T = \frac{1}{2}M_\mathrm{c}\dot{z}_\mathrm{c}^2 + \frac{1}{2}M_\mathrm{d}\dot{z}_\mathrm{d}^2 + \frac{1}{2}M_\mathrm{hook,payload}\dot{z}_1^2 + \frac{1}{2}M_\mathrm{phc}\dot{z}_\mathrm{phc}^2 \tag{A.2}$$

The potential energy part of the Lagrangian is

$$V = \frac{1}{2}k_\mathrm{d}(z_\mathrm{in} - z_\mathrm{d})^2 + \frac{1}{2}k_\mathrm{d}(z_\mathrm{d} - z_1)^2 + \frac{1}{2}k_\mathrm{c}(z_\mathrm{in} - z_\mathrm{c})^2 + \frac{1}{2}k_\mathrm{c}(z_\mathrm{c} - z_\mathrm{phc})^2 \tag{A.3}$$

Thus

$$\begin{aligned} L = T - V = \frac{1}{2}M_\mathrm{c}\dot{z}_\mathrm{c}^2 + \frac{1}{2}M_\mathrm{d}\dot{z}_\mathrm{d}^2 + \frac{1}{2}M_\mathrm{hook,payload}\dot{z}_1^2 + \frac{1}{2}M_\mathrm{phc}\dot{z}_\mathrm{phc}^2 \\ -\left(\frac{1}{2}k_\mathrm{d}(z_\mathrm{in} - z_\mathrm{d})^2 + \frac{1}{2}k_\mathrm{d}(z_\mathrm{d} - z_1)^2 + \frac{1}{2}k_\mathrm{c}(z_\mathrm{in} - z_\mathrm{c})^2 + \frac{1}{2}k_\mathrm{c}(z_\mathrm{c} - z_\mathrm{phc})^2\right) \end{aligned} \tag{A.4}$$

For $k = 1$, $q^1 = z_\mathrm{c}$ the equation of motion, with $Q_{NP,1} = 0$

$$\frac{\mathrm{d}}{\mathrm{d}t}\left(\frac{\partial L}{\partial \dot{q}^1}\right) - \frac{\partial L}{\partial q^1} = 0 \tag{A.5}$$

$$\frac{\mathrm{d}}{\mathrm{d}t}\left(\frac{\partial L}{\partial \dot{q}^1}\right) = \frac{\partial L}{\partial q^1} \tag{A.6}$$

$$\frac{\mathrm{d}}{\mathrm{d}t}\left(\frac{\partial L}{\partial \dot{z}_\mathrm{c}}\right) = \frac{\partial L}{\partial z_\mathrm{c}} \tag{A.7}$$

$$\begin{aligned} \frac{\mathrm{d}}{\mathrm{d}t}\Bigg(\frac{\partial}{\partial \dot{z}_\mathrm{c}}\Big[\frac{1}{2}M_\mathrm{c}\dot{z}_\mathrm{c}^2 + \frac{1}{2}M_\mathrm{d}\dot{z}_\mathrm{d}^2 + \frac{1}{2}M_\mathrm{hook,payload}\dot{z}_1^2 + \frac{1}{2}M_\mathrm{phc}\dot{z}_\mathrm{phc}^2 \\ -\Big\{\frac{1}{2}k_\mathrm{d}(z_\mathrm{in} - z_\mathrm{d})^2 + \frac{1}{2}k_\mathrm{d}(z_\mathrm{d} - z_1)^2 + \frac{1}{2}k_\mathrm{c}(z_\mathrm{in} - z_\mathrm{c})^2 + \frac{1}{2}k_\mathrm{c}(z_\mathrm{c} - z_\mathrm{phc})^2\Big\}\Big]\Bigg) \\ = \frac{\partial}{\partial z_\mathrm{c}}\Big[\frac{1}{2}M_\mathrm{c}\dot{z}_\mathrm{c}^2 + \frac{1}{2}M_\mathrm{d}\dot{z}_\mathrm{d}^2 + \frac{1}{2}M_\mathrm{hook,payload}\dot{z}_1^2 + \frac{1}{2}M_\mathrm{phc}\dot{z}_\mathrm{phc}^2 \\ -\Big\{\frac{1}{2}k_\mathrm{d}(z_\mathrm{in} - z_\mathrm{d})^2 + \frac{1}{2}k_\mathrm{d}(z_\mathrm{d} - z_1)^2 + \frac{1}{2}k_\mathrm{c}(z_\mathrm{in} - z_\mathrm{c})^2 + \frac{1}{2}k_\mathrm{c}(z_\mathrm{c} - z_\mathrm{phc})^2\Big\}\Big] \end{aligned} \tag{A.8}$$

Using the product rule of calculus

$$\frac{\mathrm{d}}{\mathrm{d}t}\left(\frac{2}{2}M_{\mathrm{c}}\dot{z}_{\mathrm{c}}\frac{\partial \dot{z}_{\mathrm{c}}}{\partial \dot{z}_{\mathrm{c}}}\right) = \frac{\partial}{\partial z_{\mathrm{c}}}\Big[-\Big\{\frac{1}{2}k_{\mathrm{c}}(z_{\mathrm{in}}-z_{\mathrm{c}})^2+\frac{1}{2}k_{\mathrm{c}}(z_{\mathrm{c}}-z_{\mathrm{phc}})^2\Big\}\Big] \tag{A.9}$$

$$\frac{\mathrm{d}}{\mathrm{d}t}\left(M_{\mathrm{c}}\dot{z}_{\mathrm{c}}\frac{\partial \dot{z}_{\mathrm{c}}}{\partial \dot{z}_{\mathrm{c}}}\right) = -\Big\{\frac{2}{2}k_{\mathrm{c}}(z_{\mathrm{in}}-z_{\mathrm{c}})\frac{\partial(z_{\mathrm{in}}-z_{\mathrm{c}})}{\partial z_{\mathrm{c}}}+\frac{2}{2}k_{\mathrm{c}}(z_{\mathrm{c}}-z_{\mathrm{phc}})\frac{\partial(z_{\mathrm{c}}-z_{\mathrm{phc}})}{\partial z_{\mathrm{c}}}\Big\} \tag{A.10}$$

$$\frac{\mathrm{d}}{\mathrm{d}t}\left(\frac{2}{2}M_{\mathrm{c}}\dot{z}_{\mathrm{c}}(1)\right) = -\Big\{\frac{2}{2}k_{\mathrm{c}}(z_{\mathrm{in}}-z_{\mathrm{c}})(-1)(1)+\frac{2}{2}k_{\mathrm{c}}(z_{\mathrm{c}}-z_{\mathrm{phc}})(1)(1)\Big\} \tag{A.11}$$

$$(M_{\mathrm{c}})\ddot{z}_{\mathrm{c}} = k_{\mathrm{c}}(z_{\mathrm{in}}-z_{\mathrm{c}})+k_{\mathrm{c}}(z_{\mathrm{phc}}-z_{\mathrm{c}}) \tag{A.12}$$

The steps in equations (A.5) to (A.12) are repeated for the other degrees of freedom, z_{d} and z_{phc}. Similar to z_{c} no external forces are assumed since quadratic damping due to water is ignored. These steps are omitted for brevity, the results are:

$$(M_{\mathrm{d}})\ddot{z}_{\mathrm{d}} = k_{\mathrm{d}}(z_{\mathrm{in}}-z_{\mathrm{d}})+k_{\mathrm{d}}(z_1-z_{\mathrm{d}}) \tag{A.13}$$

$$(M_{\mathrm{phc}}+A_{\mathrm{phc}})\ddot{z}_{\mathrm{phc}} = k_{\mathrm{c}}(z_{\mathrm{c}}-z_{\mathrm{phc}}) \tag{A.14}$$

For z_1 there are external forces these are the force generated by the pressure difference on the piston head, the water pressure force which is cancelled out, the buoyancy force, and the gravity weight force. Using (A.1)

$$\frac{\mathrm{d}}{\mathrm{d}t}\Big(\frac{\partial L}{\partial \dot{q}^4}\Big)-\frac{\partial L}{\partial q^4} = Q_{NP,4} \tag{A.15}$$

$$\frac{\mathrm{d}}{\mathrm{d}t}\Big(\frac{\partial L}{\partial \dot{z}_1}\Big) = \frac{\partial L}{\partial z_1}+Q_{NP,z_1} \tag{A.16}$$

With

$$Q_{NP,z_1} = P_{\mathrm{p1}}A_{\mathrm{p}}-P_{\mathrm{p2}}A_{\mathrm{p}}+F_{\mathrm{water}}-F_{\mathrm{water}}+\rho_{\mathrm{water}}V_{\mathrm{d}}g-M_{\mathrm{hook,payload}}g-\frac{1}{2}\rho_{\mathrm{water}}C_{\mathrm{d,hook}}D_{\mathrm{hook,payload}}|\dot{z}_1|\dot{z}_1 \tag{A.17}$$

This gives:

$$(M_{\mathrm{hook,payload}}+A_{\mathrm{hook,payload}})\ddot{z}_1 = k_{\mathrm{d}}(z_{\mathrm{d}}-z_1)+Q_{NP,z_1} \tag{A.18}$$

$$\begin{aligned}(M_{\mathrm{hook,payload}}+A_{\mathrm{hook,payload}})\ddot{z}_1 = \\ k_{\mathrm{d}}(z_{\mathrm{d}}-z_1)+P_{\mathrm{p1}}A_{\mathrm{p}}-P_{\mathrm{p2}}A_{\mathrm{p}}+F_{\mathrm{water}}-F_{\mathrm{water}}+\rho_{\mathrm{water}}V_{\mathrm{d}}g-M_{\mathrm{hook,payload}}g \\ -\frac{1}{2}\rho_{\mathrm{water}}C_{\mathrm{d,hook}}D_{\mathrm{hook,payload}}|\dot{z}_1|\dot{z}_1\end{aligned} \tag{A.19}$$

In summary the equations of motion are:

$$\begin{aligned}(M_{\mathrm{hook,payload}}+A_{\mathrm{hook,payload}})\ddot{z}_1 = \\ k_{\mathrm{d}}(z_{\mathrm{d}}-z_1)+P_{\mathrm{p1}}A_{\mathrm{p}}-P_{\mathrm{p2}}A_{\mathrm{p}}+F_{\mathrm{water}}-F_{\mathrm{water}}+\rho_{\mathrm{water}}V_{\mathrm{d}}g-M_{\mathrm{hook,payload}}g \\ -\frac{1}{2}\rho_{\mathrm{water}}C_{\mathrm{d,hook}}D_{\mathrm{hook,payload}}|\dot{z}_1|\dot{z}_1\end{aligned} \tag{A.20}$$

$$(M_{\mathrm{phc}}+A_{\mathrm{phc}})\ddot{z}_{\mathrm{phc}} = k_{\mathrm{c}}(z_{\mathrm{c}}-z_{\mathrm{phc}}) \tag{A.21}$$

$$(M_{\mathrm{c}})\ddot{z}_{\mathrm{c}} = k_{\mathrm{c}}(z_{\mathrm{in}}-z_{\mathrm{c}})+k_{\mathrm{c}}(z_{\mathrm{phc}}-z_{\mathrm{c}}) \tag{A.22}$$

$$(M_{\mathrm{d}})\ddot{z}_{\mathrm{d}} = k_{\mathrm{d}}(z_{\mathrm{in}}-z_{\mathrm{d}})+k_{\mathrm{d}}(z_1-z_{\mathrm{d}}) \tag{A.23}$$

These are identical to those obtained using the displacement method, verifying the original equations are correct.

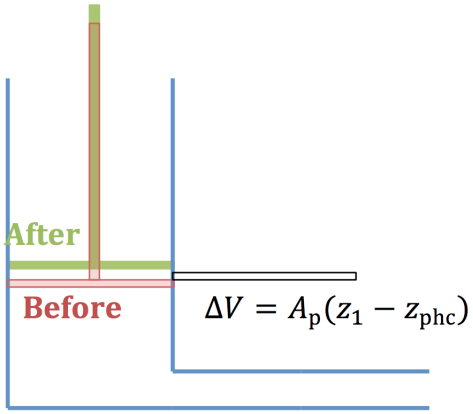

Figure A.1: Cylinder control volume

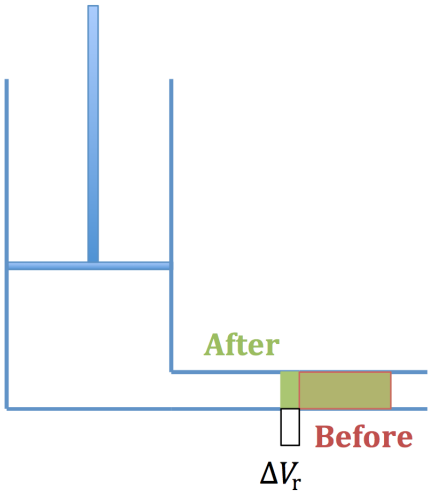

Figure A.2: Packet control volume

A.2 Derivation of equation (7.36)

Since the fluid is oil it has a high bulk modulus so an approach to take is to use the bulk modulus relationship

$$-K\Delta V = V\Delta P \tag{A.24}$$

Applying (A.24) taking the cylinder as the control volume, see Figure A.1, a positive increase in volume is upwards, for a given pressure change ΔP

$$-K\Big(A_p(z_1 - z_{phc})\Big) = V_1\Delta P \tag{A.25}$$

Applying (A.24) taking a packet of volume in the pipe as the control volume, see Figure A.2, a positive increase in volume is leftwards, for the same given pressure change ΔP

$$-K\Delta V_r = V_2\Delta P \tag{A.26}$$

Adding together (A.25) and (A.26)
Taking a packet of volume in the pipe as the control volume

$$-K\Delta V_r - K\Big(A_p(z_1 - z_{phc})\Big) = V_1\Delta P + V_2\Delta P \tag{A.27}$$

$$-K\Delta V_r - K\Big(A_p(z_1 - z_{phc})\Big) = (V_1 + V_2)\Delta P \tag{A.28}$$

Defining $V = V_1 + V_2$

$$- K\Delta V_{\mathrm{r}} - K\Big(A_{\mathrm{p}}(z_1 - z_{\mathrm{phc}})\Big) = (V)\Delta P \tag{A.29}$$

Taking infinitesimally small pressure change and using the time derivative operator $\frac{\mathrm{d}}{\mathrm{d}t}$ on both sides of (A.29)

$$\frac{\mathrm{d}}{\mathrm{d}t}\left[- K\Delta V_{\mathrm{r}} - K\Big(A_{\mathrm{p}}(z_1 - z_{\mathrm{phc}})\Big)\right] = (V)\frac{\mathrm{d}P}{\mathrm{d}t} \tag{A.30}$$

$$(V)\frac{\mathrm{d}P}{\mathrm{d}t} = \frac{\mathrm{d}}{\mathrm{d}t}\left[- K\Delta V_{\mathrm{r}} - K\Big(A_{\mathrm{p}}(z_1 - z_{\mathrm{phc}})\Big)\right] \tag{A.31}$$

$$(V)\frac{\mathrm{d}P}{\mathrm{d}t} = \frac{\mathrm{d}}{\mathrm{d}t}\left[- K\Big(A_{\mathrm{p}}(z_1 - z_{\mathrm{phc}})\Big) - K\Delta V_{\mathrm{r}}\right] \tag{A.32}$$

$$(V)\frac{\mathrm{d}P}{\mathrm{d}t} = K\left[- \Big(A_{\mathrm{p}}\frac{\mathrm{d}}{\mathrm{d}t}(z_1 - z_{\mathrm{phc}})\Big) - \frac{\mathrm{d}}{\mathrm{d}t}(\Delta V_{\mathrm{r}})\right] \tag{A.33}$$

Defining $q_r = \frac{\mathrm{d}}{\mathrm{d}t}(\Delta V_{\mathrm{r}})$, $\dot{z}_1 = \frac{\mathrm{d}}{\mathrm{d}t}(z_1)$, $\dot{z}_{\mathrm{phc}} = \frac{\mathrm{d}}{\mathrm{d}t}(z_{\mathrm{phc}})$, $V = V_{\mathrm{p1,1}}$, and $\dot{P}_{\mathrm{p1}} = \frac{\mathrm{d}P}{\mathrm{d}t}$, gives

$$\dot{P}_{\mathrm{p1}} = \frac{K}{V_{\mathrm{p1,1}}}\Big[- A_{\mathrm{p}}(\dot{z}_1 - \dot{z}_{\mathrm{phc}}) - q_r\Big] \tag{A.34}$$

(A.34) is the same as equation (7.36), this concludes the derivation.

A.3 Derivation of linearized state-space equations

Need to get everything in the form of a linear, time-invariant system [68]

$$\dot{\mathbf{q}}(t) = \mathbf{A}\mathbf{q}(t) + \mathbf{B}\mathbf{u}(t) \tag{A.35}$$

$$\dot{\mathbf{y}}(t) = \mathbf{C}\mathbf{q}(t) + \mathbf{D}\mathbf{u}(t) \tag{A.36}$$

A.3.1 Hook and payload equation of motion

The non-linear hook and payload equation of motion is shown in (A.37):

$$\begin{aligned} (M_{\text{hook,payload}} + A_{\text{hook,payload}})\ddot{z}_1 = \\ P_{\text{p1}}A_{\text{p}} - P_{\text{p2}}A_{\text{p}} + F_{\text{water}} - F_{\text{water}} + \rho_{\text{water}}V_{\text{d}}g \\ -M_{\text{hook,payload}}g - \frac{1}{2}\rho_{\text{water}}C_{\text{d,hook,payload}}D_{\text{hook,payload}}|\dot{z}_1|\dot{z}_1 - k_{\text{d}}(z_1 - z_{\text{d}}) \end{aligned} \tag{A.37}$$

(A.37) needs to be linearized. This is done using the Taylor series approach given by steps given by [68]. Where:

$$y = f(x) \tag{A.38}$$

with operating condition around $\bar{x}$ gives

$$y = f(\bar{x}) + \frac{\mathrm{d}f}{\mathrm{d}x}(x - \bar{x}) + \frac{1}{2!}\frac{\mathrm{d}^2 f}{\mathrm{d}x^2}(x - \bar{x})^2 + ... \tag{A.39}$$

Derivatives such as $\frac{\mathrm{d}f}{\mathrm{d}x}$ are evaluated at $x = \bar{x}$, if the variation $x - \bar{x}$ is small then higher-order terms in $x - \bar{x}$ can be neglected, resulting in

$$y = \bar{y} + K(x - \bar{x}) \tag{A.40}$$

with:

$$\bar{y} = f(\bar{x}) \tag{A.41}$$

and:

$$K = \frac{\mathrm{d}f}{\mathrm{d}x}|_{x=\bar{x}} \tag{A.42}$$

which gives a linear relationship between y and x.
Linearizing (A.37) with (A.40). The only thing to linearize is:

$$\frac{1}{2}\rho_{\text{water}}C_{\text{d,hook,payload}}D_{\text{hook,payload}}|\dot{z}_1|\dot{z}_1 \tag{A.43}$$

the magnitude operator is removed otherwise there would be a time-dependent coefficient in the state-space matrices, which violates the assumption of a time-invariant system. Thus, linearize:

$$y = f(\dot{z}_1) = \frac{1}{2}\rho_{\text{water}}C_{\text{d,hook,payload}}D_{\text{hook,payload}}(\dot{z}_1)^2 \tag{A.44}$$

It is chosen to linearize at the operating point $\dot{z}_1 = x_{\text{bar}}$. This gives:

$$\bar{y} = \frac{1}{2}\rho_{\text{water}}C_{\text{d,hook,payload}}D_{\text{hook,payload}}(x_{\text{bar}})^2 \tag{A.45}$$

Applying the chain rule

$$\frac{\mathrm{d}f}{\mathrm{d}\dot{z}_1} = \frac{2}{2}\rho_{\text{water}}C_{\text{d,hook,payload}}D_{\text{hook,payload}}(\dot{z}_1)\frac{\mathrm{d}\dot{z}_1}{\mathrm{d}\dot{z}_1} = \rho_{\text{water}}C_{\text{d,hook,payload}}D_{\text{hook,payload}}(\dot{z}_1) \tag{A.46}$$

Evaluating at $\dot{z}_1 = x_{\text{bar}}$, this gives

$$K = \frac{\mathrm{d}f}{\mathrm{d}\dot{z}_1}|_{\dot{z}_1=x_{\text{bar}}} = \rho_{\text{water}}C_{\text{d,hook,payload}}D_{\text{hook,payload}}(x_{\text{bar}}) \tag{A.47}$$

Thus the linearized equation is

$$y = \left[\frac{1}{2}\rho_{\text{water}}C_{\text{d,hook,payload}}D_{\text{hook,payload}}(x_{\text{bar}})^2+\rho_{\text{water}}C_{\text{d,hook,payload}}D_{\text{hook,payload}}(x_{\text{bar}})(\dot{z}_1-x_{\text{bar}})\right] \quad \text{(A.48)}$$

Using this form in (A.37)

$$(M_{\text{hook,payload}} + A_{\text{hook,payload}})\ddot{z}_1 = P_{\text{p1}}A_{\text{p}} - P_{\text{p2}}A_{\text{p}} + F_{\text{water}} - F_{\text{water}} + \rho_{\text{water}}V_{\text{d}}g - M_{\text{hook,payload}}g$$
$$-\left[\frac{1}{2}\rho_{\text{water}}C_{\text{d,hook,payload}}D_{\text{hook,payload}}(x_{\text{bar}})^2 + \rho_{\text{water}}C_{\text{d,hook,payload}}D_{\text{hook,payload}}(x_{\text{bar}})(\dot{z}_1 - x_{\text{bar}})\right] - k_{\text{d}}(z_1 - z_{\text{d}}) \quad \text{(A.49)}$$

$$(M_{\text{hook,payload}} + A_{\text{hook,payload}})\dot{q}_2 = P_{\text{p1}}A_{\text{p}} - P_{\text{p2}}A_{\text{p}} + F_{\text{water}} - F_{\text{water}} + \rho_{\text{water}}V_{\text{d}}g - M_{\text{hook,payload}}g$$
$$-\left[\frac{1}{2}\rho_{\text{water}}C_{\text{d,hook,payload}}D_{\text{hook,payload}}(x_{\text{bar}})^2 + \rho_{\text{water}}C_{\text{d,hook,payload}}D_{\text{hook,payload}}(x_{\text{bar}})(q_2 - x_{\text{bar}})\right] - k_{\text{d}}(q_1 - q_7) \quad \text{(A.50)}$$

$$(M_{\text{hook,payload}} + A_{\text{hook,payload}})\dot{q}_2 = P_{\text{p1}}A_{\text{p}} - P_{\text{p2}}A_{\text{p}} + F_{\text{water}} - F_{\text{water}} + \rho_{\text{water}}V_{\text{d}}g - M_{\text{hook,payload}}g$$
$$-\left[-\frac{1}{2}\rho_{\text{water}}C_{\text{d,hook,payload}}D_{\text{hook,payload}}(x_{\text{bar}})^2 + \rho_{\text{water}}C_{\text{d,hook,payload}}D_{\text{hook,payload}}(x_{\text{bar}})(q_2)\right] - k_{\text{d}}(q_1 - q_7) \quad \text{(A.51)}$$

Defining F_{external} for the constant terms:

$$F_{\text{external}} = F_{\text{water}} - F_{\text{water}} + \rho_{\text{water}}V_{\text{d}}g - M_{\text{hook,payload}}g + \frac{1}{2}\rho_{\text{water}}C_{\text{d,hook,payload}}D_{\text{hook,payload}}(x_{\text{bar}})^2 \quad \text{(A.52)}$$

Substituting F_{external} into (A.51) gives:

$$\dot{q}_2 = \frac{1}{(M_{\text{hook,payload}} + A_{\text{hook,payload}})}\Big(q_{11}A_{\text{p}} - q_9A_{\text{p}} + F_{\text{external}} - \rho_{\text{water}}C_{\text{d,hook,payload}}D_{\text{hook,payload}}(x_{\text{bar}})(q_2) - k_{\text{d}}(q_1 - q_7)\Big) \quad \text{(A.53)}$$

To shorten the equation $(M_{\text{hook,payload}} + A_{\text{hook,payload}})$ is defined as $\alpha_{\text{hook,payload}}$:

$$\alpha_{\text{hook,payload}} = (M_{\text{hook,payload}} + A_{\text{hook,payload}}) \quad \text{(A.54)}$$

Substituting in $\alpha_{\text{hook,payload}}$ gives:

$$\dot{q}_2 = \frac{1}{(\alpha_{\text{hook,payload}})}\Big(q_{11}A_{\text{p}} - q_9A_{\text{p}} + F_{\text{external}} - \rho_{\text{water}}C_{\text{d,hook,payload}}D_{\text{hook,payload}}(x_{\text{bar}})(q_2) - k_{\text{d}}(q_1 - q_7)\Big) \quad \text{(A.55)}$$

$\rho_{\text{water}}C_{\text{d,hook,payload}}D_{\text{hook,payload}}(x_{\text{bar}})$ is defined as $\beta_{\text{hook,payload}}$

$$\beta_{\text{hook,payload}} = \rho_{\text{water}}C_{\text{d,hook,payload}}D_{\text{hook,payload}}(x_{\text{bar}}) \quad \text{(A.56)}$$

Substituting in $\beta_{\text{hook,payload}}$ gives:

$$\dot{q}_2 = \frac{1}{(\alpha_{\text{hook,payload}})}\Bigg(q_{11}A_{\text{p}} - q_9 A_{\text{p}} + F_{\text{external}} - \beta_{\text{hook,payload}}(q_2) - k_{\text{d}}(q_1 - q_7)\Bigg) \tag{A.57}$$

A.3.2 PHCS equation of motion

The non-linear PHCS equation of motion is shown in (A.58):

$$(M_{\text{phc}} + A_{\text{phc}})\ddot{z}_{\text{phc}} = -k_{\text{c}}(z_{\text{phc}} - z_{\text{c}}) - \frac{1}{2}\rho_{\text{water}} C_{\text{d,phc}} D_{\text{phc}} |\dot{z}_{\text{phc}}| \dot{z}_{\text{phc}} \tag{A.58}$$

Following the same steps as in appendix A.3.1, the function to linearize is:

$$y = f(\dot{z}_{\text{phc}}) = \frac{1}{2}\rho_{\text{water}} C_{\text{d,phc}} D_{\text{phc}} (\dot{z}_{\text{phc}})^2 \tag{A.59}$$

The linearization point is $\dot{z}_{\text{phc}} = x_{\text{bar,phc}}$.

$$y = \Big[\frac{1}{2}\rho_{\text{water}} C_{\text{d,phc}} D_{\text{phc}} (x_{\text{bar,phc}})^2 + \rho_{\text{water}} C_{\text{d,phc}} D_{\text{phc}} (x_{\text{bar,phc}})(\dot{z}_{\text{phc}} - x_{\text{bar,phc}})\Big] \tag{A.60}$$

Substitute (A.60) into (A.58). Collect like terms.

$$(M_{\text{phc}}+A_{\text{phc}})\ddot{z}_{\text{phc}} = -k_{\text{c}}(z_{\text{phc}}-z_{\text{c}}) - \Big[\frac{1}{2}\rho_{\text{water}} C_{\text{d,phc}} D_{\text{phc}} (x_{\text{bar,phc}})^2 + \rho_{\text{water}} C_{\text{d,phc}} D_{\text{phc}} (x_{\text{bar,phc}})(\dot{z}_{\text{phc}} - x_{\text{bar,phc}})\Big] \tag{A.61}$$

$$(M_{\text{phc}} + A_{\text{phc}})\ddot{z}_{\text{phc}} = -k_{\text{c}}(z_{\text{phc}} - z_{\text{c}}) - \Big[-\frac{1}{2}\rho_{\text{water}} C_{\text{d,phc}} D_{\text{phc}} (x_{\text{bar,phc}})^2 + \rho_{\text{water}} C_{\text{d,phc}} D_{\text{phc}} (x_{\text{bar,phc}})(\dot{z}_{\text{phc}})\Big] \tag{A.62}$$

Substitute in state-space variables.

$$\dot{q}_4 = \frac{1}{(M_{\text{phc}} + A_{\text{phc}})}\Bigg(-k_{\text{c}}(q_3 - q_5) - \Big[-\frac{1}{2}\rho_{\text{water}} C_{\text{d,phc}} D_{\text{phc}} (x_{\text{bar,phc}})^2 + \rho_{\text{water}} C_{\text{d,phc}} D_{\text{phc}} (x_{\text{bar,phc}})(q_4)\Big]\Bigg) \tag{A.63}$$

$$\dot{q}_4 = \frac{1}{(M_{\text{phc}} + A_{\text{phc}})}\Bigg(-k_{\text{c}}(q_3 - q_5) + \frac{1}{2}\rho_{\text{water}} C_{\text{d,phc}} D_{\text{phc}} (x_{\text{bar,phc}})^2 - \rho_{\text{water}} C_{\text{d,phc}} D_{\text{phc}} (x_{\text{bar,phc}})(q_4)\Bigg) \tag{A.64}$$

Defining $F_{\text{external,2}}$ for the constant terms:

$$F_{\text{external,2}} = \frac{1}{2}\rho_{\text{water}} C_{\text{d,phc}} D_{\text{phc}} (x_{\text{bar,phc}})^2 \tag{A.65}$$

Substituting $F_{\text{external,2}}$ into (A.64) gives:

$$\dot{q}_4 = \frac{1}{(M_{\text{phc}} + A_{\text{phc}})}\Bigg(-k_{\text{c}}(q_3 - q_5) + F_{\text{external,2}} - \rho_{\text{water}} C_{\text{d,phc}} D_{\text{phc}} (x_{\text{bar,phc}})(q_4)\Bigg) \tag{A.66}$$

To shorten the equation $(M_{\text{phc}} + A_{\text{phc}})$ is defined as α_{phc}

$$\alpha_{\text{phc}} = (M_{\text{phc}} + A_{\text{phc}}) \tag{A.67}$$

Substituting in α_{phc} gives:

$$\dot{q}_4 = \frac{1}{(\alpha_{\text{phc}})}\Bigg(-k_{\text{c}}(q_3 - q_5) + F_{\text{external,2}} - \rho_{\text{water}} C_{\text{d,phc}} D_{\text{phc}} (x_{\text{bar,phc}})(q_4)\Bigg) \tag{A.68}$$

A.3.3 Steel rope

$$(M_c)\ddot{z}_c = -k_c(z_c - z_{in}) - k_c(z_c - z_{phc}) \tag{A.69}$$

$$(M_c)\ddot{z}_c + k_c z_c + k_c z_c = k_c z_{in} + k_c z_{phc} \tag{A.70}$$

$$(M_c)\ddot{z}_c + 2k_c z_c = k_c z_{in} + k_c z_{phc} \tag{A.71}$$

$$(M_c)\ddot{z}_c + 2k_c z_c = k_c z_{in} + k_c z_{phc} \tag{A.72}$$

Substitute in state-space variables:

$$\dot{q}_6 = \frac{1}{M_c}\Big[- 2k_c q_5 + k_c z_{in} + k_c q_3\Big] \tag{A.73}$$

A.3.4 Dyneema rope

$$(M_d)\ddot{z}_d = -k_d(z_d - z_{in}) - k_d(z_d - z_1) \tag{A.74}$$

$$\ddot{z}_d = \frac{1}{M_d}\Big[- 2k_d z_d + k_d z_{in} + k_d z_1\Big] \tag{A.75}$$

$$\dot{q}_8 = \frac{1}{M_d}\Big[- 2k_d q_7 + k_d z_{in} + k_d q_1\Big] \tag{A.76}$$

A.3.5 Upper chamber of cylinder and upper accumulator

A.3.5.1 Fluid flow between upper chamber of cylinder and upper accumulator

$$Q_{r,2} = \frac{\pi d_{f,2}^4}{128\mu l_2}(P_{p2} - P_{a3}) \tag{A.77}$$

Defining the constant coefficient γ:

$$\gamma = \frac{\pi d_{f,2}^4}{128\mu l_2} \tag{A.78}$$

Substituting in γ into (A.77):

$$Q_{r,2} = \gamma(q_9 - q_{10}) \tag{A.79}$$

A.3.5.2 Upper chamber of cylinder

$$\dot{P}_{p2} = \frac{K}{V_{p2,1}}[-A_p(\dot{z}_{phc} - \dot{z}_1) - Q_{r,2}] \tag{A.80}$$

Substituting in state variables and (A.79) for $Q_{r,2}$:

$$\dot{q}_9 = \frac{K}{V_{p2,1}}[-A_p(q_4 - q_2) - \gamma(q_9 - q_{10})\Big] \tag{A.81}$$

A.3.5.3 Upper accumulator

$$\dot{P}_{a3} = \frac{P_{a3,1} n Q_{r,2}}{V_{a3,1}} \tag{A.82}$$

Substituting in state variables and (A.79) for $Q_{r,2}$:

$$\dot{q}_{10} = \frac{P_{a3,1} n \gamma(q_9 - q_{10})}{V_{a3,1}} \tag{A.83}$$

A.3.6 Lower chamber of cylinder and lower accumulator

A.3.6.1 Fluid flow between lower chamber of cylinder and lower accumulator

$$Q_{\mathrm{r}} = \frac{\pi d_{\mathrm{f}}^4}{128\mu l}(P_{\mathrm{p1}} - P_{\mathrm{a1}}) \tag{A.84}$$

Defining the constant coefficient ϕ:

$$\phi = \frac{\pi d_{\mathrm{f}}^4}{128\mu l} \tag{A.85}$$

Substituting in ϕ into (A.84):

$$Q_{\mathrm{r}} = \phi(q_{11} - q_{12}) \tag{A.86}$$

A.3.6.2 Lower chamber of cylinder

$$\dot{P}_{\mathrm{p1}} = \frac{K}{V_{\mathrm{p1},1}}\Big[- A_{\mathrm{p}}(\dot{z}_1 - \dot{z}_{\mathrm{phc}}) - Q_r\Big] \tag{A.87}$$

Substituting in state variables and (A.86) for Q_{r}:

$$\dot{q}_{11} = \frac{K}{V_{\mathrm{p1},1}}\Big[- A_{\mathrm{p}}(q_2 - q_4) - \phi(q_{11} - q_{12})\Big] \tag{A.88}$$

A.3.6.3 Lower accumulator

$$\dot{P}_{\mathrm{a1}} = \frac{P_{\mathrm{a1},1} n Q_r}{V_{\mathrm{a1},1}} \tag{A.89}$$

Substituting in state variables and (A.86) for Q_{r}:

$$\dot{q}_{12} = \frac{P_{\mathrm{a1},1} n \phi(q_{11} - q_{12})}{V_{\mathrm{a1},1}} \tag{A.90}$$

A.3.7 State-space equations

The state-space equations are given in the form of (A.91) and (A.92):

$$\dot{\mathbf{q}}(t) = \mathbf{A}\mathbf{q}(t) + \mathbf{B}\mathbf{u}(t) \tag{A.91}$$

$$\dot{\mathbf{y}}(t) = \mathbf{C}\mathbf{q}(t) + \mathbf{D}\mathbf{u}(t) \tag{A.92}$$

The vectors are shown in (A.93). The matrices are shown in (A.94) and (A.95)

$$\dot{\mathbf{q}}(t) = \begin{bmatrix} \dot{q}_1 \\ \dot{q}_2 \\ \dot{q}_3 \\ \dot{q}_4 \\ \dot{q}_5 \\ \dot{q}_6 \\ \dot{q}_7 \\ \dot{q}_8 \\ \dot{q}_9 \\ \dot{q}_{10} \\ \dot{q}_{11} \\ \dot{q}_{12} \end{bmatrix}, \mathbf{q}(t) = \begin{bmatrix} q_1 \\ q_2 \\ q_3 \\ q_4 \\ q_5 \\ q_6 \\ q_7 \\ q_8 \\ q_9 \\ q_{10} \\ q_{11} \\ q_{12} \end{bmatrix}, \mathbf{u}(t) = \begin{bmatrix} F_{\mathrm{external}} \\ F_{\mathrm{external},2} \\ z_{\mathrm{in}} \end{bmatrix}, \dot{\mathbf{y}}(t) = \begin{bmatrix} y_1 \\ y_3 \\ y_5 \\ y_7 \\ y_9 \\ y_{10} \\ y_{11} \\ y_{12} \end{bmatrix} \tag{A.93}$$

$$\mathbf{A} = \begin{bmatrix}
0 & 1 & 0 & 0 & 0 & 0 & 0 & 0 & 0 & 0 & 0 & 0 \\
-\frac{k_{\mathrm{d}}}{\alpha_{\mathrm{hook,payload}}} & -\frac{\beta_{\mathrm{hook,payload}}}{\alpha_{\mathrm{hook,payload}}} & 0 & 0 & 0 & 0 & \frac{k_{\mathrm{d}}}{\alpha_{\mathrm{hook,payload}}} & 0 & \frac{-A_{\mathrm{p}}}{\alpha_{\mathrm{hook,payload}}} & 0 & \frac{A_{\mathrm{p}}}{\alpha_{\mathrm{hook,payload}}} & 0 \\
0 & 0 & 0 & 1 & 0 & 0 & 0 & 0 & 0 & 0 & 0 & 0 \\
0 & 0 & -\frac{k_{\mathrm{c}}}{\alpha_{\mathrm{phc}}} & \frac{-\rho_{\mathrm{water}} C_{\mathrm{d,phc}} D_{\mathrm{phc}} x_{\mathrm{bar,phc}}}{\alpha_{\mathrm{phc}}} & \frac{k_{\mathrm{c}}}{\alpha_{\mathrm{phc}}} & 0 & 0 & 0 & 0 & 0 & 0 & 0 \\
0 & 0 & 0 & 0 & 0 & 1 & 0 & 0 & 0 & 0 & 0 & 0 \\
0 & 0 & \frac{k_{\mathrm{c}}}{M_{\mathrm{c}}} & 0 & \frac{-2k_{\mathrm{c}}}{M_{\mathrm{c}}} & 0 & 0 & 0 & 0 & 0 & 0 & 0 \\
0 & 0 & 0 & 0 & 0 & 0 & 1 & 0 & 0 & 0 & 0 & 0 \\
\frac{k_{\mathrm{d}}}{M_{\mathrm{d}}} & 0 & 0 & 0 & 0 & 0 & \frac{-2k_{\mathrm{d}}}{M_{\mathrm{d}}} & 0 & 0 & 0 & 0 & 0 \\
0 & \frac{KA_p}{V_{\mathrm{p2,1}}} & 0 & -\frac{KA_p}{V_{\mathrm{p2,1}}} & 0 & 0 & 0 & 0 & -\gamma\frac{K}{V_{\mathrm{p2,1}}} & \gamma\frac{K}{V_{\mathrm{p2,1}}} & 0 & 0 \\
0 & 0 & 0 & 0 & 0 & 0 & 0 & 0 & \frac{P_{\mathrm{a3,1}} n\gamma}{V_{\mathrm{a3,1}}} & -\frac{P_{\mathrm{a3,1}} n\gamma}{V_{\mathrm{a3,1}}} & 0 & 0 \\
0 & -\frac{KA_{\mathrm{p}}}{V_{\mathrm{p1,1}}} & 0 & \frac{KA_{\mathrm{p}}}{V_{\mathrm{p1,1}}} & 0 & 0 & 0 & 0 & 0 & 0 & -\frac{K\phi}{V_{\mathrm{p1,1}}} & \frac{K\phi}{V_{\mathrm{p1,1}}} \\
0 & 0 & 0 & 0 & 0 & 0 & 0 & 0 & 0 & 0 & \frac{P_{\mathrm{a1,1}} n\phi}{V_{\mathrm{a1,1}}} & -\frac{P_{\mathrm{a1,1}} n\phi}{V_{\mathrm{a1,1}}}
\end{bmatrix} \tag{A.94}$$

$$\mathbf{B} = \begin{bmatrix}
0 & 0 & 0 \\
\frac{1}{\alpha_{\mathrm{hook,payload}}} & 0 & 0 \\
0 & 0 & 0 \\
0 & \frac{1}{\alpha_{\mathrm{phc}}} & 0 \\
0 & 0 & 0 \\
0 & 0 & \frac{k_{\mathrm{c}}}{M_{\mathrm{c}}} \\
0 & 0 & 0 \\
0 & 0 & \frac{k_{\mathrm{d}}}{M_{\mathrm{d}}} \\
0 & 0 & 0 \\
0 & 0 & 0 \\
0 & 0 & 0 \\
0 & 0 & 0
\end{bmatrix}, \mathbf{C} = \begin{bmatrix}
1 & 0 & 0 & 0 & 0 & 0 & 0 & 0 & 0 & 0 & 0 & 0 \\
0 & 0 & 1 & 0 & 0 & 0 & 0 & 0 & 0 & 0 & 0 & 0 \\
0 & 0 & 0 & 0 & 1 & 0 & 0 & 0 & 0 & 0 & 0 & 0 \\
0 & 0 & 0 & 0 & 0 & 0 & 1 & 0 & 0 & 0 & 0 & 0 \\
0 & 0 & 0 & 0 & 0 & 0 & 0 & 0 & 1 & 0 & 0 & 0 \\
0 & 0 & 0 & 0 & 0 & 0 & 0 & 0 & 0 & 1 & 0 & 0 \\
0 & 0 & 0 & 0 & 0 & 0 & 0 & 0 & 0 & 0 & 1 & 0 \\
0 & 0 & 0 & 0 & 0 & 0 & 0 & 0 & 0 & 0 & 0 & 1
\end{bmatrix}, \mathbf{D} = \begin{bmatrix}
0 & 0 & 0 \\
0 & 0 & 0 \\
0 & 0 & 0 \\
0 & 0 & 0 \\
0 & 0 & 0 \\
0 & 0 & 0 \\
0 & 0 & 0 \\
0 & 0 & 0
\end{bmatrix} \tag{A.95}$$

$$
\begin{bmatrix} \dot{q}_1 \\ \dot{q}_2 \\ \dot{q}_3 \\ \dot{q}_4 \\ \dot{q}_5 \\ \dot{q}_6 \\ \dot{q}_7 \\ \dot{q}_8 \\ \dot{q}_9 \\ \dot{q}_{10} \\ \dot{q}_{11} \\ \dot{q}_{12} \end{bmatrix}
=
\begin{bmatrix}
0 & 1 & 0 & 0 & 0 & 0 & 0 & 0 & 0 & 0 & 0 & 0 \\
-\frac{k_\mathrm{d}}{\alpha_\mathrm{hook,payload}} & -\frac{\beta_\mathrm{hook,payload}}{\alpha_\mathrm{hook,payload}} & 0 & 0 & 0 & 0 & \frac{k_\mathrm{d}}{\alpha_\mathrm{hook,payload}} & 0 & \frac{-A_\mathrm{p}}{\alpha_\mathrm{hook,payload}} & 0 & \frac{A_\mathrm{p}}{\alpha_\mathrm{hook,payload}} & 0 \\
0 & 0 & 0 & 1 & 0 & 0 & 0 & 0 & 0 & 0 & 0 & 0 \\
0 & 0 & -\frac{k_\mathrm{c}}{\alpha_\mathrm{phc}} & \frac{-\rho_\mathrm{water} C_\mathrm{d,phc} D_\mathrm{phc} x_\mathrm{bar,phc}}{\alpha_\mathrm{phc}} & \frac{k_\mathrm{c}}{\alpha_\mathrm{phc}} & 0 & 0 & 0 & 0 & 0 & 0 & 0 \\
0 & 0 & 0 & 0 & 0 & 1 & 0 & 0 & 0 & 0 & 0 & 0 \\
0 & 0 & \frac{k_\mathrm{c}}{M_\mathrm{c}} & 0 & \frac{-2k_\mathrm{c}}{M_\mathrm{c}} & 0 & 0 & 0 & 0 & 0 & 0 & 0 \\
0 & 0 & 0 & 0 & 0 & 0 & 0 & 1 & 0 & 0 & 0 & 0 \\
\frac{k_\mathrm{d}}{M_\mathrm{d}} & 0 & 0 & 0 & 0 & 0 & \frac{-2k_\mathrm{d}}{M_\mathrm{d}} & 0 & 0 & 0 & 0 & 0 \\
0 & \frac{KA_p}{V_\mathrm{p2,1}} & 0 & -\frac{KA_p}{V_\mathrm{p2,1}} & 0 & 0 & 0 & 0 & -\gamma\frac{K}{V_\mathrm{p2,1}} & \gamma\frac{K}{V_\mathrm{p2,1}} & 0 & 0 \\
0 & 0 & 0 & 0 & 0 & 0 & 0 & 0 & \frac{P_\mathrm{a3,1} n\gamma}{V_\mathrm{a3,1}} & -\frac{P_\mathrm{a3,1} n\gamma}{V_\mathrm{a3,1}} & 0 & 0 \\
0 & -\frac{KA_\mathrm{p}}{V_\mathrm{p1,1}} & 0 & \frac{KA_\mathrm{p}}{V_\mathrm{p1,1}} & 0 & 0 & 0 & 0 & 0 & 0 & -\frac{K\phi}{V_\mathrm{p1,1}} & \frac{K\phi}{V_\mathrm{p1,1}} \\
0 & 0 & 0 & 0 & 0 & 0 & 0 & 0 & 0 & 0 & \frac{P_\mathrm{a1,1} n\phi}{V_\mathrm{a1,1}} & -\frac{P_\mathrm{a1,1} n\phi}{V_\mathrm{a1,1}}
\end{bmatrix}
\begin{bmatrix} q_1 \\ q_2 \\ q_3 \\ q_4 \\ q_5 \\ q_6 \\ q_7 \\ q_8 \\ q_9 \\ q_{10} \\ q_{11} \\ q_{12} \end{bmatrix}
\tag{A.96}
$$

$$+\begin{bmatrix} 0 & 0 & 0 \\ \frac{1}{\alpha_{\text{hook,payload}}} & 0 & 0 \\ 0 & 0 & 0 \\ 0 & \frac{1}{\alpha_{\text{phc}}} & 0 \\ 0 & 0 & 0 \\ 0 & 0 & \frac{k_{\text{c}}}{M_{\text{c}}} \\ 0 & 0 & 0 \\ 0 & 0 & \frac{k_{\text{d}}}{M_{\text{d}}} \\ 0 & 0 & 0 \\ 0 & 0 & 0 \\ 0 & 0 & 0 \\ 0 & 0 & 0 \end{bmatrix} \begin{bmatrix} F_{\text{external}} \\ F_{\text{external,2}} \\ z_{\text{in}} \end{bmatrix} \tag{A.97}$$

$$\begin{bmatrix} y_1 \\ y_3 \\ y_5 \\ y_7 \\ y_9 \\ y_{10} \\ y_{11} \\ y_{12} \end{bmatrix} = \begin{bmatrix} 1 & 0 & 0 & 0 & 0 & 0 & 0 & 0 & 0 & 0 & 0 & 0 \\ 0 & 0 & 1 & 0 & 0 & 0 & 0 & 0 & 0 & 0 & 0 & 0 \\ 0 & 0 & 0 & 0 & 1 & 0 & 0 & 0 & 0 & 0 & 0 & 0 \\ 0 & 0 & 0 & 0 & 0 & 0 & 1 & 0 & 0 & 0 & 0 & 0 \\ 0 & 0 & 0 & 0 & 0 & 0 & 0 & 0 & 1 & 0 & 0 & 0 \\ 0 & 0 & 0 & 0 & 0 & 0 & 0 & 0 & 0 & 1 & 0 & 0 \\ 0 & 0 & 0 & 0 & 0 & 0 & 0 & 0 & 0 & 0 & 1 & 0 \\ 0 & 0 & 0 & 0 & 0 & 0 & 0 & 0 & 0 & 0 & 0 & 1 \end{bmatrix} \begin{bmatrix} q_1 \\ q_2 \\ q_3 \\ q_4 \\ q_5 \\ q_6 \\ q_7 \\ q_8 \\ q_9 \\ q_{10} \\ q_{11} \\ q_{12} \end{bmatrix} + \begin{bmatrix} 0 & 0 & 0 \\ 0 & 0 & 0 \\ 0 & 0 & 0 \\ 0 & 0 & 0 \\ 0 & 0 & 0 \\ 0 & 0 & 0 \\ 0 & 0 & 0 \\ 0 & 0 & 0 \end{bmatrix} \begin{bmatrix} F_{\text{external}} \\ F_{\text{external,2}} \\ z_{\text{in}} \end{bmatrix} \tag{A.98}$$

A.4 Throttle

A.4.1 Preliminary results

V_{p2} and P_{p2} are in phase which is not physical. If the upper cylinder volume shrinks the pressure should increase. This can be attributed to the rod's position (z_1) being unbounded, in the sense that it ignores the confines of the cylinder and is able to go through the cylinder top. Spring stoppers are added to improve the behavior.

A.4.2 Spring stoppers

It is aimed to answer the question what effect do the spring stoppers have and what spring stiffness is necessary to achieve this effect?

The answer to this question is repeated below: So 6e8N/m is used as a value going forward since the stoppers should not be used in normal operation.

Spring stoppers are added to the inside of the cylinder at the top and bottom. If the piston-head reaches the spring stopper a force is applied in the opposite direction. The spring stiffness first is 5e3N/m. The result of using these stiffness is not noticeable, the spring stiffness is increased across a range. Stiffness values from 5e1N/m to 5e10N/m were examined to determine when the spring stoppers become effective, see Table A.1. From 5e7N/m to 5e8N/m the volume is no longer negative, below this the volume is negative. At 5e8N/m the stopper springs are activated much more than for 5e7N/m and below. For 5e7N/m, z_1 oscillates around a mean of 6m this is a similar pattern for all stiffnesses below this. For 5e8N/m z_1 oscillates around 1m and this trend continues for higher stiffnesses. 5e8N/m is used as a value going forward since the response is reasonable and the stoppers should not be used in normal operation in any case.

In fact the spring stiffeners are a last resort. These should only be used for a rogue wave condition and should not be expected to be used in normal operation. It is better to adjust the stiffness of the system which is governed by accumulator size, this will be manipulated in appendix A.4.3.

Table A.1: Time when spring stops acting as a function of spring stiffness value

ks [N/m]	Time when spring stops [s]
5e1	9
5e2	9
5e3	9
5e4	9
5e5	7
5e6	9
5e7	9
5e8	75
6e8	never stops
5e9	never stops
5e10	never stops

A.4.2.1 Verify spring stopper working

To verify the spring stopper works the graph of (z_1-z_{phc}) is examined, see Figure A.3. The difference between z_1 and z_{phc} becomes smaller which is expected since the spring pushes the hook+payload mass downwards making z_1 smaller and since z_1 was just larger than z_{phc} the immediate effect is to make the relative distance smaller. The difference converges to 1.5m which is logical since the spring is active

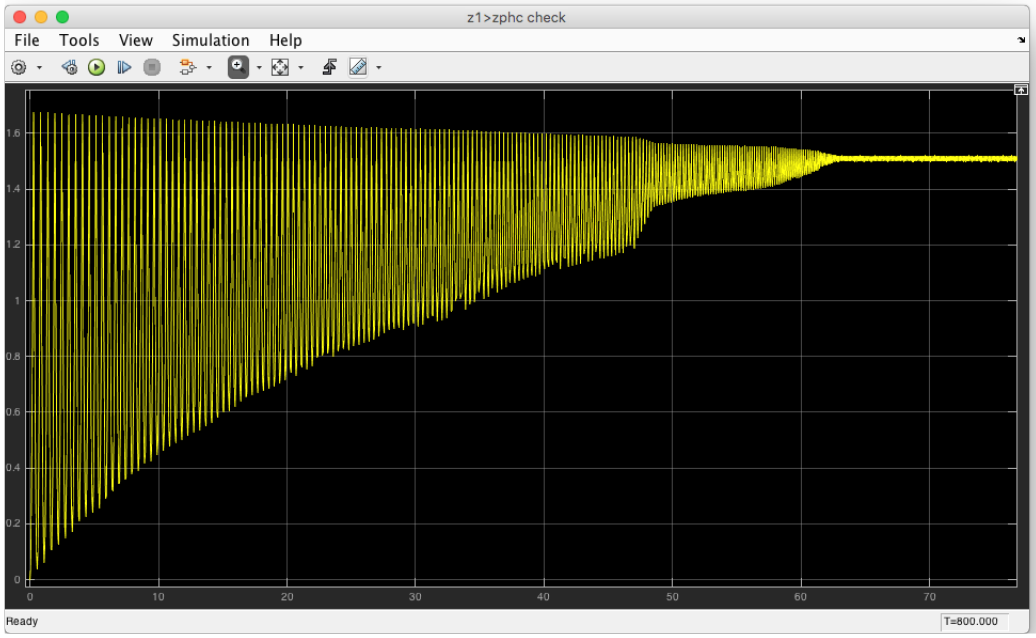

Figure A.3: Check the spring stopper works

when 1.5m<(z_1-z_{phc})<1.7m. What this means is the spring is acting with a downwards force but due to the motion of the system z_1 is naturally pushed to be greater than z_{phc} so the spring is reached again soon after a downwards force is applied. The fact that the bottom spring is never touched reinforces this.

A.4.3 Accumulator volume influence on stiffness

It is desired to answer the question
What accumulator volume (in first and second accumulator) is suitable to prevent the piston from hitting the stopper springs?

The answer to this question: there was no accumulator volume found suitable to prevent the piston from hitting the stopper springs, the system should be further investigated and designed such that in normal operation the piston doesn't hit the stopper springs, thus the stopper springs are there for emergencies only

Increasing the accumulator volume so far does not prevent the top of the cylinder being hit, from small values to unrealistically large values of accumulator volume, the stopper spring at the top still acts. It is decided to use the orifice type damper.

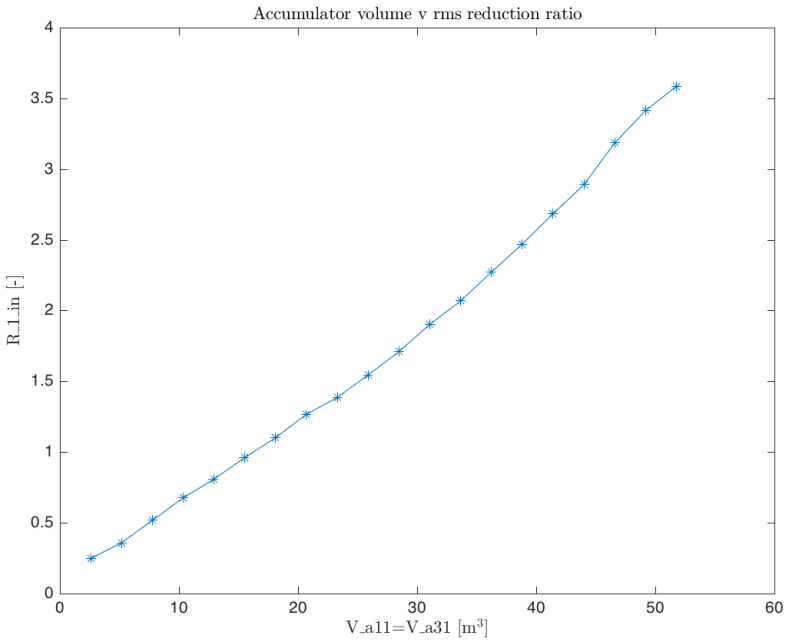

Figure A.4: Throttle: rms reduction ratio as function of accumulator volume

A.5 Throttle again

A.5.1 Accumulator volume effect on effectiveness

The question to be answered: What is the effect of increasing accumulator volume on effectiveness of the passive heave compensator, measured by the rms reduction ratio R?

The effect of the accumulator volume is investigated. A sinusoidal heave input for z_{in} is used. Various V_a11_factors are tried ([1:1:20]). A larger accumulator volume should provide better attenuation of z_1 motion, this means the rms reduction ratio R is lower. See Figure A.4. The R value increases since there is a large oscillation in z_1 for the first approximately 20s that lowers in amplitude thereafter. This is not the expected behavior of the system. With increasing accumulator volume, the initial amplitude of z_1 increases, see Figure A.6. The large oscillation is due to the large amplitude pressure signals that occur initially, shown in Figure A.5 for V_a31=V_a11=25.9m^3. In contrast the amplitude of the pressure signals are smaller for the orifice system for the same time period and accumulator volume. The pressures control the movement of the piston which in turn controls the movement of the payload. An explanation for the large pressure amplitude is that the throttle type system is quite sensitive to the pipe diameter and pipe length. Thus it is likely the combination of pipe diameter and pipe length is not suitable. Adding the fact that the overall design with 2 accumulators is more complicated, the influence of the correct pipe diameter and pipe length may be critical. The throttle is not investigated further since the orifice system has more promising results.

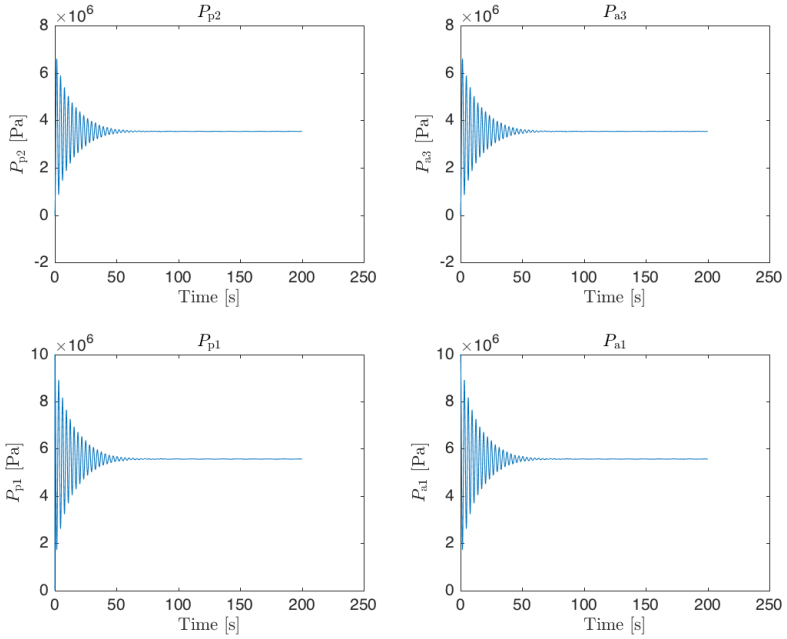

Figure A.5: Throttle: pressure time series

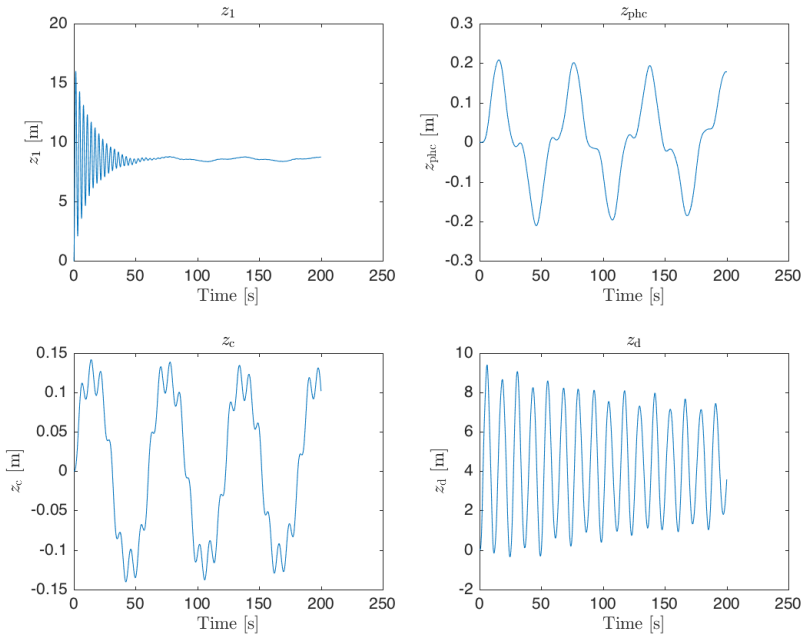

Figure A.6: Throttle: time series for key degrees of freedom

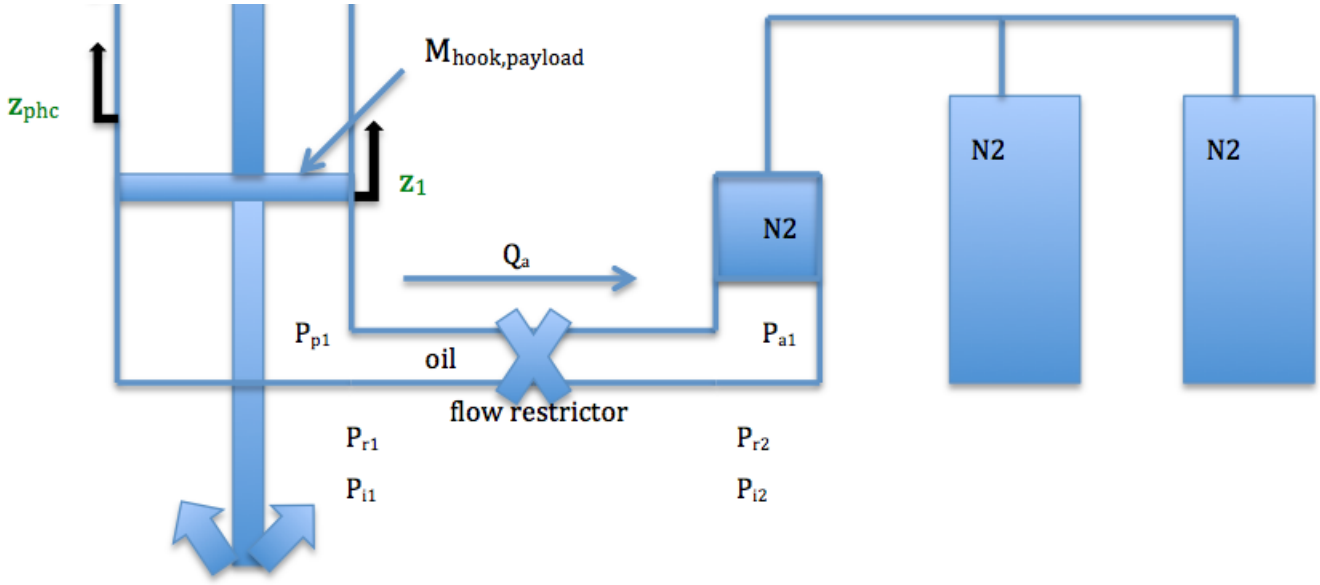

Figure A.7: Bottom accumulator, note that $Q_{\mathrm{a}} = Q_{\mathrm{r}}$

A.6 Bottom accumulator

A.6.1 Non-linear equations: bottom accumulator

The system is shown in Figure A.7 with relevant parameters defined here. There are two pressure drops, one is inertial pressure drop:

$$\Delta P_i = P_{\mathrm{i1}} - P_{\mathrm{i2}} \tag{A.99}$$

the other is resistive pressure drop due to the orifice:

$$\Delta P_r = P_{\mathrm{r1}} - P_{\mathrm{r2}} \tag{A.100}$$

The relationship between hydraulic fluid flow rate and pressure drop for the orifice is in equation (A.101)

$$Q_{\mathrm{a}} = C_{\mathrm{discharge}} A \sqrt{\frac{2}{\rho_{\mathrm{oil}}} |\Delta P_r|} \mathrm{sign}(\Delta P_r) \tag{A.101}$$

Where $C_{\mathrm{discharge}}$ is the discharge coefficient and Q_{a} is the volume flow rate of hydraulic fluid through the orifice and to the accumulator. Note that $Q_{\mathrm{a}} = Q_{\mathrm{r}}$.
Using (7.59) the equation for inertia of the fluid is given by (A.102)

$$\rho_{\mathrm{oil}} \frac{L}{A} \dot{Q}_{\mathrm{a}} = \Delta P_i \tag{A.102}$$

The total pressure drop ΔP_{tot} is given by the sum of the inertial and resistive pressure drop

$$\Delta P_{\mathrm{tot}} = \Delta P_i + \Delta P_r \tag{A.103}$$

Now there are 3 equations (A.101) (A.102) (A.103) with 4 unknowns $(Q_{\mathrm{a}}, \Delta P_r, \Delta P_i, \Delta P_{\mathrm{tot}})$. In the current state it is not possible to solve the system since at least one more equation is needed.
Refer to the system in Figure A.7. Using (7.58) the pressure, P_{p1}, in the lower chamber of the cylinder is given by (A.104).

$$\dot{P}_{\mathrm{p1}} = \frac{K}{V_{\mathrm{p1,1}}} \Big[- A_{\mathrm{p}} (\dot{z}_1 - \dot{z}_{\mathrm{phc}}) - Q_{\mathrm{a}} \Big] \tag{A.104}$$

Where K is the bulk modulus of the hydraulic oil, $V_{\mathrm{p1,1}}$ is the initial volume, A_{p} is the area of the piston-head, z_1 is the displacement of the mass of the hook and payload, z_{phc} is the displacement of the

mass of the PHC cylinder.
The pressure in the accumulator, P_{a1}, is obtained from the isentropic relationship:

$$P_1 V_1^n = P_0 V_0^n \tag{A.105}$$

this is applied to the lower accumulator

$$P_{a1} V_{a1}^n = P_{a1,1} V_{a1,1}^n \tag{A.106}$$

where $P_{a1,1}$ is the initial pressure, $V_{a1,1}$ is the initial volume and n is the gas constant and $V_{a1}(t)$ and $P_{a1}(t)$ are functions of time, re-arranging for P_{a1}

$$P_{a1} = P_{a1,1}\Big(\frac{V_{a1,1}}{V_{a1}}\Big)^n \tag{A.107}$$

In equation (A.107) V_{a1} is given by

$$V_{a1} = V_{a1,1} - \int Q_a \mathrm{d}t \tag{A.108}$$

Defining $V_{in} = \int Q_a \mathrm{d}t$ equivalently $\dot{V}_{in} = Q_a$ and substituting into (A.108)

$$V_{a1} = V_{a1,1} - V_{in} \tag{A.109}$$

Substituting (A.109) into (A.107)

$$P_{a1} = P_{a1,1}\Big(\frac{V_{a1,1}}{V_{a1,1} - V_{in}}\Big)^n \tag{A.110}$$

Physically the total pressure drop in (A.103) is equal to the difference of the pressures P_{p1} and P_{a1} from (A.104) and (A.110)

$$\Delta P_{tot} = P_{p1} - P_{a1} \tag{A.111}$$

The other pressure drops, $\Delta P_i, \Delta P_r$, in (A.103) are needed. (A.101) is rearranged for ΔP_r

$$\Delta P_r = \frac{\mathrm{sign}(Q_a) Q_a^2}{(C_{discharge} A)^2} \frac{\rho_{oil}}{2} \tag{A.112}$$

ΔP_i is obtained from (A.102). Substituting (A.102) (A.112) and (A.111) into (A.103) gives

$$P_{p1} - P_{a1} = \rho_{oil} \frac{L}{A} \dot{Q}_a + \frac{\mathrm{sign}(Q_a) Q_a^2}{(C_{discharge} A)^2} \frac{\rho_{oil}}{2} \tag{A.113}$$

re-arranging for $\dot{Q}_a$

$$\dot{Q}_a = \frac{A}{\rho_{oil} L}\Big[P_{p1} - P_{a1} - \frac{\mathrm{sign}(Q_a) Q_a^2}{(C_{discharge} A)^2} \frac{\rho_{oil}}{2}\Big] \tag{A.114}$$

A.6.1.1 Final non-linear equations: bottom accumulator

Final equations, 3 differential equations (A.115) (A.116) (A.117) and 1 algebraic equation (A.118) for 4 unknowns P_{p1}, Q_a, V_{in}, and P_{a1} so the system is closed. $\dot{z}_1$ and $\dot{z}_{phc}$ are known as inputs. Constants are K, $V_{p1,1}$, A_p, $P_{a1,1}$, $V_{a1,1}$, A, ρ_{oil}, L, $C_{discharge}$. These equations are solved numerically for the time-domain simulations.

$$\dot{P}_{p1} = \frac{K}{V_{p1,1}}\Big[- A_p(\dot{z}_1 - \dot{z}_{phc}) - Q_a\Big] \tag{A.115}$$

$$\dot{Q}_a = \frac{A}{\rho_{oil} L}\Big[P_{p1} - P_{a1} - \frac{\mathrm{sign}(Q_a) Q_a^2}{(C_{discharge} A)^2} \frac{\rho_{oil}}{2}\Big] \tag{A.116}$$

$$\dot{V}_{in} = Q_a \tag{A.117}$$

$$P_{a1} = P_{a1,1}\Big(\frac{V_{a1,1}}{V_{a1,1} - V_{in}}\Big)^n \tag{A.118}$$

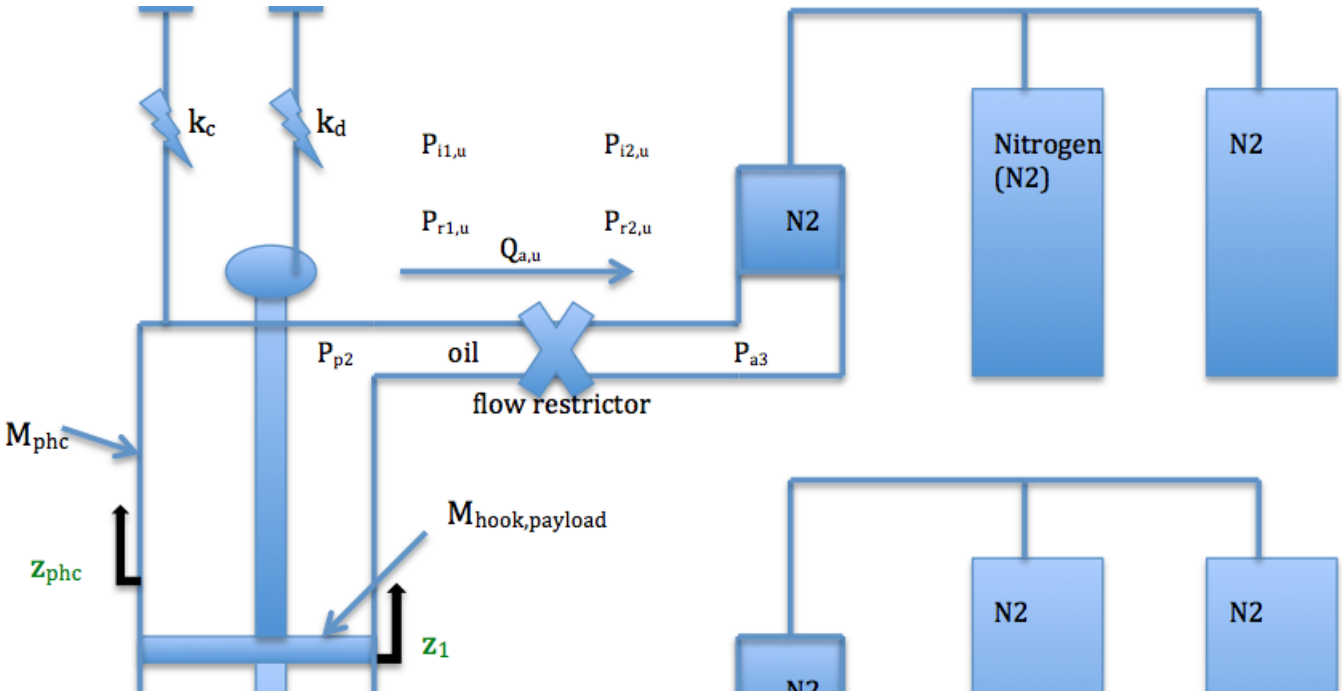

Figure A.8: Upper accumulator, note that $Q_{\mathrm{a,u}} = Q_{\mathrm{r,2}}$

A.7 Upper accumulator

A.7.1 Non-linear equations: upper accumulator

The system is shown in Figure A.8. There are two pressure drops, one is inertial pressure drop:

$$\Delta P_{i,u} = P_{\mathrm{i1,u}} - P_{\mathrm{i2,u}} \tag{A.119}$$

the other is resistive pressure drop due to the orifice:

$$\Delta P_{r,u} = P_{\mathrm{r1,u}} - P_{\mathrm{r2,u}} \tag{A.120}$$

The relationship between hydraulic fluid flow rate and pressure drop for the orifice is in equation (A.121).

$$Q_{\mathrm{a,u}} = C_{\mathrm{discharge}} A \sqrt{\frac{2}{\rho_{\mathrm{oil}}} |\Delta P_{r,u}|} \mathrm{sign}(\Delta P_{r,u}) \tag{A.121}$$

Where $Q_{\mathrm{a,u}}$ is the volume flow rate of hydraulic fluid through the orifice and to the upper accumulator. Note that $Q_{\mathrm{a,u}} = Q_{\mathrm{r,2}}$.

Re-arranging (A.121) for $\Delta P_{\mathrm{r,u}}$

$$\Delta P_{r,u} = \frac{\mathrm{sign}(Q_{\mathrm{a,u}}) Q_{\mathrm{a,u}}^2}{(C_{\mathrm{discharge}} A)^2} \frac{\rho_{\mathrm{oil}}}{2} \tag{A.122}$$

The inertial pressure drop is given by (A.123)

$$\rho_{\mathrm{oil}} \frac{L}{A} \dot{Q}_{\mathrm{a,u}} = \Delta P_{i,u} \tag{A.123}$$

(A.103) applied to the upper accumulator gives (A.124)

$$\Delta P_{\mathrm{tot,upper}} = \Delta P_{i,u} + \Delta P_{r,u} \tag{A.124}$$

With $\Delta P_{\mathrm{tot,upper}}$ given by Figure A.8 as

$$\Delta P_{\mathrm{tot,upper}} = P_{\mathrm{p2}} - P_{\mathrm{a3}} \tag{A.125}$$

Substituting (A.125) (A.123) (A.122) into (A.124)

$$P_{\mathrm{p2}} - P_{\mathrm{a3}} = \rho_{\mathrm{oil}} \frac{L}{A} \dot{Q}_{\mathrm{a,u}} + \frac{\mathrm{sign}(Q_{\mathrm{a,u}}) Q_{\mathrm{a,u}}^2}{(C_{\mathrm{discharge}} A)^2} \frac{\rho_{\mathrm{oil}}}{2} \tag{A.126}$$

re-arranging for $\dot{Q}_{\mathrm{a,u}}$

$$\dot{Q}_{\mathrm{a,u}} = \frac{A}{\rho_{\mathrm{oil}} L} \left[P_{\mathrm{p2}} - P_{\mathrm{a3}} - \frac{\mathrm{sign}(Q_{\mathrm{a,u}}) Q_{\mathrm{a,u}}^2}{(C_{\mathrm{discharge}} A)^2} \frac{\rho_{\mathrm{oil}}}{2} \right] \tag{A.127}$$

The upper cylinder is attached to an accumulator. The pressure in the upper cylinder is P_{p2} and the pressure in the accumulator is P_{a3}. A differential equation for the pressure in the upper cylinder is found using (7.58) in (A.128)

$$\dot{P}_{\mathrm{p2}} = \frac{K}{V_{\mathrm{p2,1}}} [-A_{\mathrm{p}} (\dot{z}_{\mathrm{phc}} - \dot{z}_1) - Q_{\mathrm{a,u}}] \tag{A.128}$$

Where $V_{\mathrm{p2,1}}$ is the initial volume. Volume flow rate $Q_{\mathrm{a,u}}$ is positive left to right so a positive volume flow rate is generated by P_{p2} being greater than P_{a3}.

Using the isentropic relationship an expression for P_{a3} is given by

$$P_{\mathrm{a3}} = P_{\mathrm{a3,1}} \left(\frac{V_{\mathrm{a3,1}}}{V_{\mathrm{a3}}} \right)^n \tag{A.129}$$

Where $V_{a3,1}$ is the initial volume, $P_{a3,1}$ is the initial pressure, and V_{a3} is given by (A.130)

$$V_{a3} = V_{a3,1} - \int Q_{a,u} dt \tag{A.130}$$

Defining $V_{in,u} = \int Q_{a,u} dt$ equivalently $\dot{V}_{in,u} = Q_{a,u}$, substituting this into (A.130)

$$V_{a3} = V_{a3,1} - V_{in,u} \tag{A.131}$$

Substituting (A.131) into (A.129) gives an equation for P_{a3}, (A.132)

$$P_{a3} = P_{a3,1}\left(\frac{V_{a3,1}}{V_{a3,1} - V_{in,u}}\right)^n \tag{A.132}$$

A.7.1.1 Final non-linear equations: upper accumulator

Final equations, 3 differential equations (A.133) (A.134) (A.135) and 1 algebraic equation (A.136) for 4 unknowns P_{p2}, $Q_{a,u}$, $V_{in,u}$, and P_{a3} so the system is closed. $\dot{z}_1$ and $\dot{z}_{phc}$ are known as inputs. Constants are K, $V_{p2,1}$, A_p, $P_{a3,1}$, $V_{a3,1}$, A, ρ_{oil}, L, $C_{discharge}$. These equations are solved numerically for time-domain simulations.

$$\dot{P}_{p2} = \frac{K}{V_{p2,1}}[-A_p(\dot{z}_{phc} - \dot{z}_1) - Q_{a,u}] \tag{A.133}$$

$$\dot{Q}_{a,u} = \frac{A}{\rho_{oil} L}\left[P_{p2} - P_{a3} - \frac{\text{sign}(Q_{a,u}) Q_{a,u}^2}{(C_{discharge} A)^2}\frac{\rho_{oil}}{2}\right] \tag{A.134}$$

$$\dot{V}_{in,u} = Q_{a,u} \tag{A.135}$$

$$P_{a3} = P_{a3,1}\left(\frac{V_{a3,1}}{V_{a3,1} - V_{in,u}}\right)^n \tag{A.136}$$

A.8 Non-linear equations

The non-linear equations that will be put into state-space form are repeated from previous sections below.

From (7.8)

$$\begin{aligned}\ddot{z}_1 = \frac{1}{(M_{hook,payload} + A_{hook,payload})} \\ \Big[P_{p1}A_p - P_{p2}A_p + F_{water} - F_{water} + \rho_{water} V_d g \\ -M_{hook,payload} g - \frac{1}{2}\rho_{water} C_{d,hook,payload} D_{hook,payload} |\dot{z}_1| \dot{z}_1 - k_d(z_1 - z_d)\Big]\end{aligned} \tag{A.137}$$

From (7.12)

$$\ddot{z}_{phc} = \frac{1}{(M_{phc} + A_{phc})}\left[- k_c(z_{phc} - z_c) - \frac{1}{2}\rho_{water} C_{d,phc} D_{phc} |\dot{z}_{phc}| \dot{z}_{phc}\right] \tag{A.138}$$

From (7.15)

$$\ddot{z}_c = \frac{1}{(M_c)}\left[- k_c(z_c - z_{in}) - k_c(z_c - z_{phc})\right] \tag{A.139}$$

From (7.18)

$$\ddot{z}_d = \frac{1}{(M_d)}\left[- k_d(z_d - z_{in}) - k_d(z_d - z_1)\right] \tag{A.140}$$

From (7.62)

$$\dot{P}_{\mathrm{p1}} = \frac{K}{V_{\mathrm{p1,1}}}\Big[- A_{\mathrm{p}}(\dot{z}_1 - \dot{z}_{\mathrm{phc}}) - Q_{\mathrm{r}}\Big] \tag{A.141}$$

From (7.63)

$$\dot{Q}_{\mathrm{r}} = \frac{A}{\rho_{\mathrm{oil}} L}\Big[P_{\mathrm{p1}} - P_{\mathrm{a1}} - \frac{\mathrm{sign}(Q_{\mathrm{r}})Q_{\mathrm{r}}^2}{(C_{\mathrm{discharge}}A)^2}\frac{\rho_{\mathrm{oil}}}{2}\Big] \tag{A.142}$$

From (7.64)

$$\dot{V}_{\mathrm{in}} = Q_{\mathrm{r}} \tag{A.143}$$

From (7.65)

$$P_{\mathrm{a1}} = P_{\mathrm{a1,1}}\Big(\frac{V_{\mathrm{a1,1}}}{V_{\mathrm{a1,1}} - V_{\mathrm{in}}}\Big)^n \tag{A.144}$$

From (7.66)

$$\dot{P}_{\mathrm{p2}} = \frac{K}{V_{\mathrm{p2,1}}}[-A_{\mathrm{p}}(\dot{z}_{\mathrm{phc}} - \dot{z}_1) - Q_{\mathrm{r,2}}] \tag{A.145}$$

From (7.67)

$$\dot{Q}_{\mathrm{r,2}} = \frac{A}{\rho_{\mathrm{oil}} L}\Big[P_{\mathrm{p2}} - P_{\mathrm{a3}} - \frac{\mathrm{sign}(Q_{\mathrm{r,2}})Q_{\mathrm{r,2}}^2}{(C_{\mathrm{discharge}}A)^2}\frac{\rho_{\mathrm{oil}}}{2}\Big] \tag{A.146}$$

From (7.68)

$$\dot{V}_{\mathrm{in,u}} = Q_{\mathrm{r,2}} \tag{A.147}$$

From (7.69)

$$P_{\mathrm{a3}} = P_{\mathrm{a3,1}}\Big(\frac{V_{\mathrm{a3,1}}}{V_{\mathrm{a3,1}} - V_{\mathrm{in,u}}}\Big)^n \tag{A.148}$$

A.9 Non-linear state-space equations

The chosen state-space variables are shown in Table A.2.

Table A.2: q variables

state variable	original variable
q_1	z_1
q_2	$\dot{z}_1$
q_3	z_{phc}
q_4	$\dot{z}_{\mathrm{phc}}$
q_5	z_{c}
q_6	$\dot{z}_{\mathrm{c}}$
q_7	z_{d}
q_8	$\dot{z}_{\mathrm{d}}$
q_9	P_{p1}
q_{10}	Q_{r}
q_{11}	V_{in}
q_{12}	P_{p2}
q_{13}	$Q_{\mathrm{r,2}}$
q_{14}	$V_{\mathrm{in,u}}$

The state-space equations are obtained by substituting in the state variables in Table A.2 into the equations in section A.8. These equations are solved numerically for the time-domain simulations.

$$\dot{q}_1 = q_2 \tag{A.149}$$

From (A.137)

$$\begin{aligned}\dot{q}_2 = \frac{1}{(M_{\text{hook,payload}} + A_{\text{hook,payload}})} \\ \Big[q_9 A_\text{p} - q_{12} A_\text{p} + F_\text{water} - F_\text{water} + \rho_\text{water} V_\text{d} g \\ -M_{\text{hook,payload}} g - \frac{1}{2}\rho_\text{water} C_{\text{d,hook,payload}} D_{\text{hook,payload}} |q_2| q_2 - k_\text{d}(q_1 - q_7)\Big]\end{aligned} \tag{A.150}$$

$$\dot{q}_3 = q_4 \tag{A.151}$$

From (A.138)

$$\dot{q}_4 = \frac{1}{(M_\text{phc} + A_\text{phc})}\Big[- k_\text{c}(q_3 - q_5) - \frac{1}{2}\rho_\text{water} C_{\text{d,phc}} D_\text{phc} |q_4| q_4\Big] \tag{A.152}$$

$$\dot{q}_5 = q_6 \tag{A.153}$$

From (A.139)

$$\dot{q}_6 = \frac{1}{(M_\text{c})}\Big[- k_\text{c}(q_5 - z_\text{in}) - k_\text{c}(q_5 - q_3)\Big] \tag{A.154}$$

$$\dot{q}_7 = q_8 \tag{A.155}$$

From (A.140)

$$\dot{q}_8 = \frac{1}{(M_\text{d})}\Big[- k_\text{d}(q_7 - z_\text{in}) - k_\text{d}(q_7 - q_1)\Big] \tag{A.156}$$

From (A.141)

$$\dot{q}_9 = \frac{K}{V_{\text{p1,1}}}\Big[- A_p(q_2 - q_4) - q_{10}\Big] \tag{A.157}$$

From (A.142) and (A.144)

$$\dot{q}_{10} = \frac{A}{\rho_\text{oil} L}\Big[q_9 - P_{\text{a1,1}}\Big(\frac{V_{\text{a1,1}}}{V_{\text{a1,1}} - q_{11}}\Big)^n - \frac{\text{sign}(q_{10}) q_{10}^2}{(C_\text{discharge} A)^2}\frac{\rho_\text{oil}}{2}\Big] \tag{A.158}$$

From (A.143)

$$\dot{q}_{11} = q_{10} \tag{A.159}$$

From (A.145)

$$\dot{q}_{12} = \frac{K}{V_{\text{p2,1}}}[-A_\text{p}(q_4 - q_2) - q_{13}] \tag{A.160}$$

From (A.146) and (A.148)

$$\dot{q}_{13} = \frac{A}{\rho_\text{oil} L}\Big[q_{12} - P_{\text{a3,1}}\Big(\frac{V_{\text{a3,1}}}{V_{\text{a3,1}} - q_{14}}\Big)^n - \frac{\text{sign}(q_{13}) q_{13}^2}{(C_\text{discharge} A)^2}\frac{\rho_\text{oil}}{2}\Big] \tag{A.161}$$

From (A.147)

$$\dot{q}_{14} = q_{13} \tag{A.162}$$

P_a1 and P_a3 are not state variables and are obtained from a non-linear combination of the state variables.

A.10 Non-linear state-space equations simplified

A.10.1 $\dot{q}_1$

$$\dot{q}_1 = q_2 \tag{A.163}$$

A.10.2 $\dot{q}_2$

From (A.137)

$$\begin{aligned}\dot{q}_2 = \frac{1}{(M_{\text{hook,payload}} + A_{\text{hook,payload}})} \\ \Big[q_9 A_{\text{p}} - q_{12} A_{\text{p}} + F_{\text{water}} - F_{\text{water}} + \rho_{\text{water}} V_{\text{d}} g \\ -M_{\text{hook,payload}} g - \frac{1}{2}\rho_{\text{water}} C_{\text{d,hook,payload}} D_{\text{hook,payload}} |q_2| q_2 - k_{\text{d}}(q_1 - q_7)\Big]\end{aligned} \tag{A.164}$$

Defining

$$\zeta_2 = M_{\text{hook,payload}} + A_{\text{hook,payload}} \tag{A.165}$$

$$\eta_2 = F_{\text{water}} - F_{\text{water}} + \rho_{\text{water}} V_{\text{d}} g - M_{\text{hook,payload}} g \tag{A.166}$$

$$\theta_2 = \frac{1}{2}\rho_{\text{water}} C_{\text{d,hook,payload}} D_{\text{hook,payload}} \tag{A.167}$$

Finally,

$$\begin{aligned}\dot{q}_2 = \frac{1}{\zeta_2} \\ \Big[q_9 A_{\text{p}} - q_{12} A_{\text{p}} + \eta_2 - \theta_2 \text{sign}(q_2) q_2^2 - k_{\text{d}}(q_1 - q_7)\Big]\end{aligned} \tag{A.168}$$

A.10.3 $\dot{q}_3$

$$\dot{q}_3 = q_4 \tag{A.169}$$

A.10.4 $\dot{q}_4$

From (A.138)

$$\dot{q}_4 = \frac{1}{(M_{\text{phc}} + A_{\text{phc}})}\Big[- k_{\text{c}}(q_3 - q_5) - \frac{1}{2}\rho_{\text{water}} C_{\text{d,phc}} D_{\text{phc}} |q_4| q_4\Big] \tag{A.170}$$

Defining

$$\zeta_4 = M_{\text{phc}} + A_{\text{phc}} \tag{A.171}$$

$$\eta_4 = \frac{1}{2}\rho_{\text{water}} C_{\text{d,phc}} D_{\text{phc}} \tag{A.172}$$

Finally,

$$\dot{q}_4 = \frac{1}{\zeta_4}\Big[- k_{\text{c}}(q_3 - q_5) - \eta_4 \text{sign}(q_4) q_4^2\Big] \tag{A.173}$$

A.10.5 $\dot{q}_5$

$$\dot{q}_5 = q_6 \tag{A.174}$$

A.10.6 $\dot{q}_6$

From (A.139)

$$\dot{q}_6 = \frac{1}{(M_c)}\Big[- k_c(q_5 - z_{in}) - k_c(q_5 - q_3)\Big] \tag{A.175}$$

A.10.7 $\dot{q}_7$

$$\dot{q}_7 = q_8 \tag{A.176}$$

A.10.8 $\dot{q}_8$

From (A.140)

$$\dot{q}_8 = \frac{1}{(M_d)}\Big[- k_d(q_7 - z_{in}) - k_d(q_7 - q_1)\Big] \tag{A.177}$$

A.10.9 $\dot{q}_9$

From (A.141)

$$\dot{q}_9 = \frac{K}{V_{p1,1}}\Big[- A_p(q_2 - q_4) - q_{10}\Big] \tag{A.178}$$

A.10.10 $\dot{q}_{10}$

From (A.142) and (A.144)

$$\dot{q}_{10} = \frac{A}{\rho_{oil}L}\Big[q_9 - P_{a1,1}\Big(\frac{V_{a1,1}}{V_{a1,1} - q_{11}}\Big)^n - \frac{\text{sign}(q_{10})q_{10}^2}{(C_{discharge}A)^2}\frac{\rho_{oil}}{2}\Big] \tag{A.179}$$

Defining

$$\zeta_{10} = \frac{A}{\rho_{oil}L} \tag{A.180}$$

$$\eta_{10} = \frac{\text{sign}(q_{10})}{(C_{discharge}A)^2}\frac{\rho_{oil}}{2} \tag{A.181}$$

Finally,

$$\dot{q}_{10} = \zeta_{10}\Big[q_9 - P_{a1,1}\Big(\frac{V_{a1,1}}{V_{a1,1} - q_{11}}\Big)^n - \eta_{10}q_{10}^2\Big] \tag{A.182}$$

A.10.11 $\dot{q}_{11}$

From (A.143)

$$\dot{q}_{11} = q_{10} \tag{A.183}$$

A.10.12 $\dot{q}_{12}$

From (A.145)

$$\dot{q}_{12} = \frac{K}{V_{p2,1}}[-A_p(q_4 - q_2) - q_{13}] \tag{A.184}$$

A.10.13 $\dot{q}_{13}$

From (A.146) and (A.148)

$$\dot{q}_{13} = \frac{A}{\rho_{\text{oil}} L}\left[q_{12} - P_{\text{a3,1}}\left(\frac{V_{\text{a3,1}}}{V_{\text{a3,1}} - q_{14}}\right)^{n} - \frac{\text{sign}(q_{13}) q_{13}^2}{(C_{\text{discharge}} A)^2}\frac{\rho_{\text{oil}}}{2}\right] \tag{A.185}$$

Defining

$$\zeta_{13} = \frac{A}{\rho_{\text{oil}} L} \tag{A.186}$$

$$\eta_{13} = \frac{\text{sign}(q_{13})}{(C_{\text{discharge}} A)^2}\frac{\rho_{\text{oil}}}{2} \tag{A.187}$$

Finally,

$$\dot{q}_{13} = \zeta_{13}\left[q_{12} - P_{\text{a3,1}}\left(\frac{V_{\text{a3,1}}}{V_{\text{a3,1}} - q_{14}}\right)^{n} - \eta_{13} q_{13}^2\right] \tag{A.188}$$

A.10.14 $\dot{q}_{14}$

From (A.147)

$$\dot{q}_{14} = q_{13} \tag{A.189}$$

P_{a1} and P_{a3} are not state variables and are obtained from a non-linear combination of the state variables.

A.11 Linearized state-space equations

The state-space equations with non-linear terms are linearized in appendices A.11.1, A.11.2, A.11.3, and A.11.4.

A.11.1 Linearizing $\dot{q}_2$

The equation for $\dot{q}_2$ given by (A.150) is repeated in (A.190)

$$\begin{aligned}\dot{q}_2 = \frac{1}{(M_{\text{hook,payload}} + A_{\text{hook,payload}})} \\ \Big[q_9 A_\text{p} - q_{12} A_\text{p} + F_\text{water} - F_\text{water} + \rho_\text{water} V_\text{d} g \\ -M_{\text{hook,payload}} g - \frac{1}{2}\rho_\text{water} C_{\text{d,hook,payload}} D_{\text{hook,payload}} |q_2| q_2 - k_\text{d}(q_1 - q_7)\Big]\end{aligned} \tag{A.190}$$

The non-linear term is identified with $j(q_2)$

$$\begin{aligned}\dot{q}_2 = \frac{1}{(M_{\text{hook,payload}} + A_{\text{hook,payload}})} \\ \Big[q_9 A_\text{p} - q_{12} A_\text{p} + F_\text{water} - F_\text{water} + \rho_\text{water} V_\text{d} g \\ -M_{\text{hook,payload}} g - j(q_2) - k_\text{d}(q_1 - q_7)\Big]\end{aligned} \tag{A.191}$$

The non-linear term in (A.191) is $j(q_2)$

$$j(q_2) = \frac{1}{2}\rho_\text{water} C_{\text{d,hook,payload}} D_{\text{hook,payload}} |q_2| q_2 \tag{A.192}$$

$$j(q_2) = \frac{1}{2}\rho_\text{water} C_{\text{d,hook,payload}} D_{\text{hook,payload}} \text{sign}(q_2) q_2^2 \tag{A.193}$$

$j^{'}(q_2)$ is found by applying the chain rule

$$j^{'}(q_2) = \frac{1}{2}\rho_\text{water} C_{\text{d,hook,payload}} D_{\text{hook,payload}} \text{sign}(q_2) 2 q_2 \frac{\text{d}q_2}{\text{d}q_2} \tag{A.194}$$

$$j^{'}(q_2) = \rho_\text{water} C_{\text{d,hook,payload}} D_{\text{hook,payload}} \text{sign}(q_2) q_2 \tag{A.195}$$

Applying the first order Taylor series with linearization point q_2^*

$$j(q_2) = j(q_2^*) + j^{'}(q_2^*)(q_2 - q_2^*) \tag{A.196}$$

Substituting in $j^{'}(q_2^*)$ from (A.195)

$$j(q_2) = j(q_2^*) + \rho_\text{water} C_{\text{d,hook,payload}} D_{\text{hook,payload}} \text{sign}(q_2^*) q_2^* (q_2 - q_2^*) \tag{A.197}$$

Substituting in $j(q_2^*)$ from (A.193) gives the linearized equation (A.198) for $j(q_2)$

$$j(q_2) = \frac{1}{2}\rho_\text{water} C_{\text{d,hook,payload}} D_{\text{hook,payload}} \text{sign}(q_2^*) q_2^{*2} + \rho_\text{water} C_{\text{d,hook,payload}} D_{\text{hook,payload}} \text{sign}(q_2^*) q_2^* (q_2 - q_2^*) \tag{A.198}$$

Inserting the linearized term $j(q_2)$ from (A.198) into (A.191) gives (A.199), the linearized equation for $\dot{q}_2$

$$\dot{q}_2 = \frac{1}{(M_{\text{hook,payload}} + A_{\text{hook,payload}})}\Bigg[q_9 A_{\text{p}} - q_{12} A_{\text{p}} + F_{\text{water}} - F_{\text{water}} + \rho_{\text{water}} V_{\text{d}} g - M_{\text{hook,payload}} g - \Bigg\{\frac{1}{2}\rho_{\text{water}} C_{\text{d,hook,payload}} D_{\text{hook,payload}} \text{sign}(q_2^*) q_2^{*2} + \rho_{\text{water}} C_{\text{d,hook,payload}} D_{\text{hook,payload}} \text{sign}(q_2^*) q_2^* (q_2 - q_2^*)\Bigg\} - k_{\text{d}}(q_1 - q_7)\Bigg] \tag{A.199}$$

A.11.2 Linearizing $\dot{q}_4$

The equation for $\dot{q}_4$ given by (A.152) is repeated in (A.200)

$$\dot{q}_4 = \frac{1}{(M_{\text{phc}} + A_{\text{phc}})}\Bigg[- k_{\text{c}}(q_3 - q_5) - \frac{1}{2}\rho_{\text{water}} C_{\text{d,phc}} D_{\text{phc}} |q_4| q_4\Bigg] \tag{A.200}$$

The non-linear term is identified with $k(q_4)$

$$\dot{q}_4 = \frac{1}{(M_{\text{phc}} + A_{\text{phc}})}\Bigg[- k_{\text{c}}(q_3 - q_5) - k(q_4)\Bigg] \tag{A.201}$$

The non-linear term in (A.201) is $k(q_4)$

$$k(q_4) = \frac{1}{2}\rho_{\text{water}} C_{\text{d,phc}} D_{\text{phc}} |q_4| q_4 \tag{A.202}$$

$$k(q_4) = \frac{1}{2}\rho_{\text{water}} C_{\text{d,phc}} D_{\text{phc}} \text{sign}(q_4) q_4^2 \tag{A.203}$$

$k^{'}(q_4)$ is found by applying the chain rule

$$k^{'}(q_4) = \frac{1}{2}\rho_{\text{water}} C_{\text{d,phc}} D_{\text{phc}} \text{sign}(q_4) 2 q_4 \frac{\text{d}q_4}{\text{d}q_4} \tag{A.204}$$

$$k^{'}(q_4) = \rho_{\text{water}} C_{\text{d,phc}} D_{\text{phc}} \text{sign}(q_4) q_4 \tag{A.205}$$

Applying the first order Taylor series with linearization point q_4^*

$$k(q_4) = k(q_4^*) + k^{'}(q_4^*)(q_4 - q_4^*) \tag{A.206}$$

Substituting in $k^{'}(q_4^*)$ from (A.205)

$$k(q_4) = k(q_4^*) + \rho_{\text{water}} C_{\text{d,phc}} D_{\text{phc}} \text{sign}(q_4^*) q_4^* (q_4 - q_4^*) \tag{A.207}$$

Substituting in $k(q_4^*)$ from (A.203) gives the linearized equation (A.208) for $k(q_4)$

$$k(q_4) = \frac{1}{2}\rho_{\text{water}} C_{\text{d,phc}} D_{\text{phc}} \text{sign}(q_4^*) q_4^{*2} + \rho_{\text{water}} C_{\text{d,phc}} D_{\text{phc}} \text{sign}(q_4^*) q_4^* (q_4 - q_4^*) \tag{A.208}$$

Inserting the linearized term $k(q_4)$ from (A.208) into (A.201) gives (A.209), the linearized equation for $\dot{q}_4$

$$\dot{q}_4 = \frac{1}{(M_{\text{phc}} + A_{\text{phc}})}\Bigg[-k_{\text{c}}(q_3 - q_5) - \Bigg\{\frac{1}{2}\rho_{\text{water}} C_{\text{d,phc}} D_{\text{phc}} \text{sign}(q_4^*) q_4^{*2} + \rho_{\text{water}} C_{\text{d,phc}} D_{\text{phc}} \text{sign}(q_4^*) q_4^* (q_4 - q_4^*)\Bigg\}\Bigg] \tag{A.209}$$

A.11.3 Linearizing $\dot{q}_{10}$

The equation for $\dot{q}_{10}$ given by (A.158) is repeated in (A.210)

$$\dot{q}_{10} = \frac{A}{\rho_{\text{oil}} L}\Big[q_9 - P_{\text{a1,1}}\Big(\frac{V_{\text{a1,1}}}{V_{\text{a1,1}} - q_{11}}\Big)^n - \frac{\text{sign}(q_{10}) q_{10}^2}{(C_{\text{discharge}} A)^2}\frac{\rho_{\text{oil}}}{2}\Big] \tag{A.210}$$

The non-linear terms are identified with $f(q_{11})$ and $g(q_{10})$

$$\dot{q}_{10} = \frac{A}{\rho_{\text{oil}} L}\Big[q_9 - f(q_{11}) - g(q_{10})\Big] \tag{A.211}$$

The first non-linear term in (A.211) is $f(q_{11})$

$$f(q_{11}) = P_{\text{a1,1}}\Big(\frac{V_{\text{a1,1}}}{V_{\text{a1,1}} - q_{11}}\Big)^n \tag{A.212}$$

$f^{'}(q_{11})$ is found by applying the chain rule

$$f^{'}(q_{11}) = P_{\text{a1,1}} V_{\text{a1,1}}^n (-n)(V_{\text{a1,1}} - q_{11})^{-n-1}(-\frac{\text{d}q_{11}}{\text{d}q_{11}}) \tag{A.213}$$

$$f^{'}(q_{11}) = n P_{\text{a1,1}} V_{\text{a1,1}}^n (V_{\text{a1,1}} - q_{11})^{-n-1} \tag{A.214}$$

Applying the first order Taylor series with linearization point q_{11}^*

$$f(q_{11}) = f(q_{11}^*) + f^{'}(q_{11}^*)(q_{11} - q_{11}^*) \tag{A.215}$$

Substituting in $f^{'}(q_{11}^*)$ from (A.214)

$$f(q_{11}) = f(q_{11}^*) + n P_{\text{a1,1}} V_{\text{a1,1}}^n (V_{\text{a1,1}} - q_{11}^*)^{-n-1}(q_{11} - q_{11}^*) \tag{A.216}$$

Substituting in $f(q_{11}^*)$ from (A.212) gives the linearized equation (A.217) for $f(q_{11})$

$$f(q_{11}) = P_{\text{a1,1}}\Big(\frac{V_{\text{a1,1}}}{V_{\text{a1,1}} - q_{11}^*}\Big)^n + n P_{\text{a1,1}} V_{\text{a1,1}}^n (V_{\text{a1,1}} - q_{11}^*)^{-n-1}(q_{11} - q_{11}^*) \tag{A.217}$$

The second non-linear term in (A.211) is $g(q_{10})$

$$g(q_{10}) = \frac{\text{sign}(q_{10}) q_{10}^2}{(C_{\text{discharge}} A)^2}\frac{\rho_{\text{oil}}}{2} \tag{A.218}$$

$g^{'}(q_{10})$ is found by applying the chain rule

$$g^{'}(q_{10}) = \frac{\rho_{\text{oil}}}{2}\frac{\text{sign}(q_{10}) 2 q_{10}}{(C_{\text{discharge}} A)^2}\frac{\text{d}q_{10}}{\text{d}q_{10}} \tag{A.219}$$

$$g^{'}(q_{10}) = \frac{\rho_{\text{oil}} \text{sign}(q_{10}) q_{10}}{(C_{\text{discharge}} A)^2} \tag{A.220}$$

Applying the first order Taylor series with linearization point q_{10}^*

$$g(q_{10}) = g(q_{10}^*) + g^{'}(q_{10}^*)(q_{10} - q_{10}^*) \tag{A.221}$$

Substituting in $g^{'}(q_{10}^*)$ from (A.220)

$$g(q_{10}) = g(q_{10}^*) + \frac{\rho_{\text{oil}} \text{sign}(q_{10}^*) q_{10}^*}{(C_{\text{discharge}} A)^2}(q_{10} - q_{10}^*) \tag{A.222}$$

Substituting in $g(q_{10})$ from (A.218) gives the linearized equation (A.223) for $g(q_{10})$

$$g(q_{10}) = \frac{\text{sign}(q_{10}^*) q_{10}^{*2}}{(C_{\text{discharge}} A)^2}\frac{\rho_{\text{oil}}}{2} + \frac{\rho_{\text{oil}} \text{sign}(q_{10}^*) q_{10}^*}{(C_{\text{discharge}} A)^2}(q_{10} - q_{10}^*) \tag{A.223}$$

Inserting the linearized terms $f(q_{11})$ from (A.217) and $g(q_{10})$ from (A.223) into (A.211) gives (A.224)

$$\begin{aligned}\dot{q}_{10} = \frac{A}{\rho_{\text{oil}} L}\Bigg[q_9 - \Bigg\{P_{\text{a1,1}}\Big(\frac{V_{\text{a1,1}}}{V_{\text{a1,1}} - q_{11}^*}\Big)^n + n P_{\text{a1,1}} V_{\text{a1,1}}^n (V_{\text{a1,1}} - q_{11}^*)^{-n-1}(q_{11} - q_{11}^*)\Bigg\} \\ - \Bigg\{\frac{\text{sign}(q_{10}^*) q_{10}^{*2}}{(C_{\text{discharge}} A)^2}\frac{\rho_{\text{oil}}}{2} + \frac{\rho_{\text{oil}} \text{sign}(q_{10}^*) q_{10}^*}{(C_{\text{discharge}} A)^2}(q_{10} - q_{10}^*)\Bigg\}\Bigg]\end{aligned} \tag{A.224}$$

A.11.4 Linearizing $\dot{q}_{13}$

The equation for $\dot{q}_{13}$ given by (A.161) is repeated in (A.225)

$$\dot{q}_{13} = \frac{A}{\rho_{\text{oil}} L}\Big[q_{12} - P_{\text{a3,1}}\Big(\frac{V_{\text{a3,1}}}{V_{\text{a3,1}} - q_{14}}\Big)^n - \frac{\text{sign}(q_{13}) q_{13}^2}{(C_{\text{discharge}} A)^2}\frac{\rho_{\text{oil}}}{2}\Big] \tag{A.225}$$

The non-linear terms are identified with $h(q_{14})$ and $i(q_{13})$

$$\dot{q}_{13} = \frac{A}{\rho_{\text{oil}} L}\Big[q_{12} - h(q_{14}) - i(q_{13})\Big] \tag{A.226}$$

The first non-linear term in (A.226) is $h(q_{14})$

$$h(q_{14}) = P_{\text{a3,1}}\Big(\frac{V_{\text{a3,1}}}{V_{\text{a3,1}} - q_{14}}\Big)^n \tag{A.227}$$

$h^{'}(q_{14})$ is found by applying the chain rule

$$h^{'}(q_{14}) = P_{\text{a3,1}} V_{\text{a3,1}}^n (-n)(V_{\text{a3,1}} - q_{14})^{-n-1}(-\frac{\text{d}q_{14}}{\text{d}q_{14}}) \tag{A.228}$$

$$h^{'}(q_{14}) = n P_{\text{a3,1}} V_{\text{a3,1}}^n (V_{\text{a3,1}} - q_{14})^{-n-1} \tag{A.229}$$

Applying the first order Taylor series with linearization point q_{14}^*

$$h(q_{14}) = h(q_{14}^*) + h^{'}(q_{14}^*)(q_{14} - q_{14}^*) \tag{A.230}$$

Substituting in $h^{'}(q_{14}^*)$ from (A.229)

$$h(q_{14}) = h(q_{14}^*) + n P_{\text{a3,1}} V_{\text{a3,1}}^n (V_{\text{a3,1}} - q_{14}^*)^{-n-1}(q_{14} - q_{14}^*) \tag{A.231}$$

Substituting in $h(q_{14})$ from (A.227) gives the linearized equation (A.232) for $h(q_{14})$

$$h(q_{14}) = P_{\text{a3,1}}\Big(\frac{V_{\text{a3,1}}}{V_{\text{a3,1}} - q_{14}^*}\Big)^n + n P_{\text{a3,1}} V_{\text{a3,1}}^n (V_{\text{a3,1}} - q_{14}^*)^{-n-1}(q_{14} - q_{14}^*) \tag{A.232}$$

The second non-linear term in (A.226) is $i(q_{13})$

$$i(q_{13}) = \frac{\text{sign}(q_{13}) q_{13}^2}{(C_{\text{discharge}} A)^2}\frac{\rho_{\text{oil}}}{2} \tag{A.233}$$

$i^{'}(q_{13})$ is found by applying the chain rule

$$i^{'}(q_{13}) = \frac{\rho_{\text{oil}}}{2}\frac{\text{sign}(q_{13}) 2 q_{13}}{(C_{\text{discharge}} A)^2}\frac{\text{d}q_{13}}{\text{d}q_{13}} \tag{A.234}$$

$$i^{'}(q_{13}) = \frac{\rho_{\text{oil}} \text{sign}(q_{13}) q_{13}}{(C_{\text{discharge}} A)^2} \tag{A.235}$$

Applying the first order Taylor series with linearization point q_{13}^*

$$i(q_{13}) = i(q_{13}^*) + i^{'}(q_{13}^*)(q_{13} - q_{13}^*) \tag{A.236}$$

Substituting in $i^{'}(q_{13}^*)$ from (A.235)

$$i(q_{13}) = i(q_{13}^*) + \frac{\rho_{\text{oil}} \text{sign}(q_{13}^*) q_{13}^*}{(C_{\text{discharge}} A)^2}(q_{13} - q_{13}^*) \tag{A.237}$$

Substituting in $i(q_{13}^*)$ from (A.233) gives the linearized equation

$$i(q_{13}) = \frac{\text{sign}(q_{13}^*) q_{13}^{*2}}{(C_{\text{discharge}} A)^2}\frac{\rho_{\text{oil}}}{2} + \frac{\rho_{\text{oil}} \text{sign}(q_{13}^*) q_{13}^*}{(C_{\text{discharge}} A)^2}(q_{13} - q_{13}^*) \tag{A.238}$$

Inserting the linearized terms $h(q_{14})$ from (A.232) and $i(q_{13})$ from (A.238) into (A.226) gives (A.239)

$$\begin{aligned}\dot{q}_{13} = \frac{A}{\rho_{\text{oil}} L}\Bigg[q_{12} - \Bigg\{P_{\text{a3,1}}\Big(\frac{V_{\text{a3,1}}}{V_{\text{a3,1}} - q_{14}^*}\Big)^n + n P_{\text{a3,1}} V_{\text{a3,1}}^n (V_{\text{a3,1}} - q_{14}^*)^{-n-1}(q_{14} - q_{14}^*)\Bigg\} \\ - \Bigg\{\frac{\text{sign}(q_{13}^*) q_{13}^{*2}}{(C_{\text{discharge}} A)^2}\frac{\rho_{\text{oil}}}{2} + \frac{\rho_{\text{oil}} \text{sign}(q_{13}^*) q_{13}^*}{(C_{\text{discharge}} A)^2}(q_{13} - q_{13}^*)\Bigg\}\Bigg]\end{aligned} \tag{A.239}$$

A.12 Resulting linear state-space equations

The linearized state-space equations are shown below.

A.12.1 $\dot{q}_1$

$$\dot{q}_1 = q_2 \tag{A.240}$$

A.12.2 $\dot{q}_2$

$$\dot{q}_2 = \frac{1}{(M_{\text{hook,payload}} + A_{\text{hook,payload}})} \Bigg[q_9 A_{\text{p}} - q_{12} A_{\text{p}} + F_{\text{water}} - F_{\text{water}} + \rho_{\text{water}} V_{\text{d}} g - M_{\text{hook,payload}} g$$
$$- \left\{ \frac{1}{2} \rho_{\text{water}} C_{\text{d,hook,payload}} D_{\text{hook,payload}} \text{sign}(q_2^*) q_2^{*2} + \rho_{\text{water}} C_{\text{d,hook,payload}} D_{\text{hook,payload}} \text{sign}(q_2^*) q_2^* (q_2 - q_2^*) \right\}$$
$$- k_{\text{d}} (q_1 - q_7) \Bigg] \tag{A.241}$$

Defining

$$F_{\text{external,1}} = F_{\text{water}} - F_{\text{water}} + \rho_{\text{water}} V_{\text{d}} g - M_{\text{hook,payload}} g \tag{A.242}$$

$$\alpha_2 = (M_{\text{hook,payload}} + A_{\text{hook,payload}}) \tag{A.243}$$

$$\beta_2 = \frac{1}{2} \rho_{\text{water}} C_{\text{d,hook,payload}} D_{\text{hook,payload}} \text{sign}(q_2^*) q_2^{*2} \tag{A.244}$$

$$\gamma_2 = \rho_{\text{water}} C_{\text{d,hook,payload}} D_{\text{hook,payload}} \text{sign}(q_2^*) q_2^* \tag{A.245}$$

gives (A.246)

$$\dot{q}_2 = \frac{1}{\alpha_2} \Bigg[q_9 A_{\text{p}} - q_{12} A_{\text{p}} + F_{\text{external,1}}$$
$$- \left\{ \beta_2 + \gamma_2 (q_2 - q_2^*) \right\}$$
$$- k_{\text{d}} (q_1 - q_7) \Bigg] \tag{A.246}$$

$$\dot{q}_2 = \frac{1}{\alpha_2} \Bigg[q_9 A_{\text{p}} - q_{12} A_{\text{p}} + F_{\text{external,1}}$$
$$- \beta_2 - \gamma_2 q_2 + \gamma_2 q_2^*$$
$$- k_{\text{d}} q_1 + k_{\text{d}} q_7 \Bigg] \tag{A.247}$$

Collecting the constant terms and defining

$$F_{\text{U,2}} = F_{\text{external,1}} - \beta_2 + \gamma_2 q_2^* \tag{A.248}$$

Finally,

$$\dot{q}_2 = \frac{1}{\alpha_2} \Bigg[q_9 A_{\text{p}} - q_{12} A_{\text{p}}$$
$$- \gamma_2 q_2$$
$$- k_{\text{d}} q_1 + k_{\text{d}} q_7 + F_{\text{U,2}} \Bigg] \tag{A.249}$$

A.12.3 $\dot{q}_3$

$$\dot{q}_3 = q_4 \tag{A.250}$$

A.12.4 $\dot{q}_4$

$$\dot{q}_4 = \frac{1}{(M_{\text{phc}} + A_{\text{phc}})}\left[-k_{\text{c}}(q_3 - q_5) - \left\{\frac{1}{2}\rho_{\text{water}} C_{\text{d,phc}} D_{\text{phc}} \text{sign}(q_4^*) q_4^{*2} + \rho_{\text{water}} C_{\text{d,phc}} D_{\text{phc}} \text{sign}(q_4^*) q_4^* (q_4 - q_4^*)\right\}\right] \tag{A.251}$$

Defining

$$\alpha_4 = (M_{\text{phc}} + A_{\text{phc}}) \tag{A.252}$$

$$\beta_4 = \frac{1}{2}\rho_{\text{water}} C_{\text{d,phc}} D_{\text{phc}} \text{sign}(q_4^*) q_4^{*2} \tag{A.253}$$

$$\gamma_4 = \rho_{\text{water}} C_{\text{d,phc}} D_{\text{phc}} \text{sign}(q_4^*) q_4^* \tag{A.254}$$

gives (A.255)

$$\dot{q}_4 = \frac{1}{\alpha_4}\left[-k_{\text{c}}(q_3 - q_5) - \left\{\beta_4 + \gamma_4(q_4 - q_4^*)\right\}\right] \tag{A.255}$$

$$\dot{q}_4 = \frac{1}{\alpha_4}\left[-k_{\text{c}}(q_3 - q_5) - \beta_4 - \gamma_4 q_4 + \gamma_4 q_4^*\right] \tag{A.256}$$

Collecting the constant terms and defining

$$F_{\text{U},4} = -\beta_4 + \gamma_4 q_4^* \tag{A.257}$$

Finally,

$$\dot{q}_4 = \frac{1}{\alpha_4}\left[-k_{\text{c}}(q_3 - q_5) - \gamma_4 q_4 + F_{\text{U},4}\right] \tag{A.258}$$

A.12.5 $\dot{q}_5$

$$\dot{q}_5 = q_6 \tag{A.259}$$

A.12.6 $\dot{q}_6$

$$\dot{q}_6 = \frac{1}{(M_{\text{c}})}\left[-k_{\text{c}}(q_5 - z_{\text{in}}) - k_{\text{c}}(q_5 - q_3)\right] \tag{A.260}$$

Collecting like terms

$$\dot{q}_6 = \frac{1}{M_{\text{c}}}\left[k_{\text{c}} q_3 - 2k_{\text{c}} q_5 + k_{\text{c}} z_{\text{in}}\right] \tag{A.261}$$

A.12.7 $\dot{q}_7$

$$\dot{q}_7 = q_8 \tag{A.262}$$

A.12.8 $\dot{q}_8$

$$\dot{q}_8 = \frac{1}{(M_{\text{d}})}\left[-k_{\text{d}}(q_7 - z_{\text{in}}) - k_{\text{d}}(q_7 - q_1)\right] \tag{A.263}$$

Collecting like terms

$$\dot{q}_8 = \frac{1}{M_{\text{d}}}\left[k_{\text{d}} q_1 - 2k_{\text{d}} q_7 + k_{\text{d}} z_{\text{in}}\right] \tag{A.264}$$

A.12.9 $\dot{q}_9$

$$\dot{q}_9 = \frac{K}{V_{\mathrm{p1,1}}}\Big[- A_p(q_2 - q_4) - q_{10}\Big] \tag{A.265}$$

A.12.10 $\dot{q}_{10}$

$$\begin{aligned}\dot{q}_{10} = \frac{A}{\rho_{\mathrm{oil}} L}\Bigg[q_9 - \Bigg\{P_{\mathrm{a1,1}}\Big(\frac{V_{\mathrm{a1,1}}}{V_{\mathrm{a1,1}} - q_{11}^*}\Big)^n + nP_{\mathrm{a1,1}}V_{\mathrm{a1,1}}^n(V_{\mathrm{a1,1}} - q_{11}^*)^{-n-1}(q_{11} - q_{11}^*)\Bigg\} \\ -\Bigg\{\frac{\mathrm{sign}(q_{10}^*)q_{10}^{*2}}{(C_{\mathrm{discharge}}A)^2}\frac{\rho_{\mathrm{oil}}}{2} + \frac{\rho_{\mathrm{oil}}\mathrm{sign}(q_{10}^*)q_{10}^*}{(C_{\mathrm{discharge}}A)^2}(q_{10} - q_{10}^*)\Bigg\}\Bigg]\end{aligned} \tag{A.266}$$

Defining

$$\beta_{10} = P_{\mathrm{a1,1}}\Big(\frac{V_{\mathrm{a1,1}}}{V_{\mathrm{a1,1}} - q_{11}^*}\Big)^n \tag{A.267}$$

$$\gamma_{10} = nP_{\mathrm{a1,1}}V_{\mathrm{a1,1}}^n(V_{\mathrm{a1,1}} - q_{11}^*)^{-n-1} \tag{A.268}$$

$$\delta_{10} = \frac{\mathrm{sign}(q_{10}^*)q_{10}^{*2}}{(C_{\mathrm{discharge}}A)^2}\frac{\rho_{\mathrm{oil}}}{2} \tag{A.269}$$

$$\epsilon_{10} = \frac{\rho_{\mathrm{oil}}\mathrm{sign}(q_{10}^*)q_{10}^*}{(C_{\mathrm{discharge}}A)^2} \tag{A.270}$$

$$\begin{aligned}\dot{q}_{10} = \frac{A}{\rho_{\mathrm{oil}} L}\Bigg[q_9 - \Big\{\beta_{10} + \gamma_{10}(q_{11} - q_{11}^*)\Big\} \\ -\Big\{\delta_{10} + \epsilon_{10}(q_{10} - q_{10}^*)\Big\}\Bigg]\end{aligned} \tag{A.271}$$

$$\begin{aligned}\dot{q}_{10} = \frac{A}{\rho_{\mathrm{oil}} L}\Big[q_9 - \beta_{10} - \gamma_{10}q_{11} + \gamma_{10}q_{11}^* \\ -\delta_{10} - \epsilon_{10}q_{10} + \epsilon_{10}q_{10}^*\Big]\end{aligned} \tag{A.272}$$

Collecting the constant terms and defining

$$F_{\mathrm{U},10} = -\beta_{10} + \gamma_{10}q_{11}^* - \delta_{10} + \epsilon_{10}q_{10}^* \tag{A.273}$$

Finally,

$$\begin{aligned}\dot{q}_{10} = \frac{A}{\rho_{\mathrm{oil}} L}\Big[q_9 - \gamma_{10}q_{11} \\ -\epsilon_{10}q_{10} + F_{\mathrm{U},10}\Big]\end{aligned} \tag{A.274}$$

A.12.11 $\dot{q}_{11}$

$$\dot{q}_{11} = q_{10} \tag{A.275}$$

A.12.12 $\dot{q}_{12}$

$$\dot{q}_{12} = \frac{K}{V_{\mathrm{p2,1}}}[-A_{\mathrm{p}}(q_4 - q_2) - q_{13}] \tag{A.276}$$

A.12.13 $\dot{q}_{13}$

$$\dot{q}_{13} = \frac{A}{\rho_{\text{oil}} L}\Bigg[q_{12} - \Bigg\{P_{\text{a3,1}}\Big(\frac{V_{\text{a3,1}}}{V_{\text{a3,1}} - q_{14}^*}\Big)^n + nP_{\text{a3,1}}V_{\text{a3,1}}^n(V_{\text{a3,1}} - q_{14}^*)^{-n-1}(q_{14} - q_{14}^*)\Bigg\} - \Bigg\{\frac{\text{sign}(q_{13}^*)q_{13}^{*2}}{(C_{\text{discharge}}A)^2}\frac{\rho_{\text{oil}}}{2} + \frac{\rho_{\text{oil}}\text{sign}(q_{13}^*)q_{13}^*}{(C_{\text{discharge}}A)^2}(q_{13} - q_{13}^*)\Bigg\}\Bigg] \tag{A.277}$$

Defining

$$\beta_{13} = P_{\text{a3,1}}\Big(\frac{V_{\text{a3,1}}}{V_{\text{a3,1}} - q_{14}^*}\Big)^n \tag{A.278}$$

$$\gamma_{13} = nP_{\text{a3,1}}V_{\text{a3,1}}^n(V_{\text{a3,1}} - q_{14}^*)^{-n-1} \tag{A.279}$$

$$\delta_{13} = \frac{\text{sign}(q_{13}^*)q_{13}^{*2}}{(C_{\text{discharge}}A)^2}\frac{\rho_{\text{oil}}}{2} \tag{A.280}$$

$$\epsilon_{13} = \frac{\rho_{\text{oil}}\text{sign}(q_{13}^*)q_{13}^*}{(C_{\text{discharge}}A)^2} \tag{A.281}$$

$$\dot{q}_{13} = \frac{A}{\rho_{\text{oil}} L}\Bigg[q_{12} - \Big\{\beta_{13} + \gamma_{13}(q_{14} - q_{14}^*)\Big\} - \Big\{\delta_{13} + \epsilon_{13}(q_{13} - q_{13}^*)\Big\}\Bigg] \tag{A.282}$$

$$\dot{q}_{13} = \frac{A}{\rho_{\text{oil}} L}\Big[q_{12} - \beta_{13} - \gamma_{13}q_{14} + \gamma_{13}q_{14}^* - \delta_{13} - \epsilon_{13}q_{13} + \epsilon_{13}q_{13}^*\Big] \tag{A.283}$$

Collecting the like terms and defining

$$F_{\text{U,13}} = -\beta_{13} + \gamma_{13}q_{14}^* - \delta_{13} + \epsilon_{13}q_{13}^* \tag{A.284}$$

Finally,

$$\dot{q}_{13} = \frac{A}{\rho_{\text{oil}} L}\Big[q_{12} - \gamma_{13}q_{14} - \epsilon_{13}q_{13} + F_{\text{U,13}}\Big] \tag{A.285}$$

A.12.14 $\dot{q}_{14}$

$$\dot{q}_{14} = q_{13} \tag{A.286}$$

A.12.15 A matrix from linearized state-space equations

The state-space equations are re-arranged into matrix form, shown in (A.287). What is important is the **A** matrix which is extracted from (A.287) and shown in (A.288). From (A.288) the eigenvalues can be

determined.

$$\begin{bmatrix}\dot{q}_1\\ \dot{q}_2\\ \dot{q}_3\\ \dot{q}_4\\ \dot{q}_5\\ \dot{q}_6\\ \dot{q}_7\\ \dot{q}_8\\ \dot{q}_9\\ \dot{q}_{10}\\ \dot{q}_{11}\\ \dot{q}_{12}\\ \dot{q}_{13}\\ \dot{q}_{14}\end{bmatrix} = \begin{bmatrix} 0 & 1 & 0 & 0 & 0 & 0 & 0 & 0 & 0 & 0 & 0 & 0 & 0 & 0\\ \frac{-k_\mathrm{d}}{\alpha_2} & \frac{-\gamma_2}{\alpha_2} & 0 & 0 & 0 & 0 & \frac{k_\mathrm{d}}{\alpha_2} & 0 & \frac{A_\mathrm{p}}{\alpha_2} & 0 & 0 & \frac{-A_\mathrm{p}}{\alpha_2} & 0 & 0\\ 0 & 0 & 0 & 1 & 0 & 0 & 0 & 0 & 0 & 0 & 0 & 0 & 0 & 0\\ 0 & 0 & \frac{-k_\mathrm{c}}{\alpha_4} & \frac{-\gamma_4}{\alpha_4} & \frac{k_\mathrm{c}}{\alpha_4} & 0 & 0 & 0 & 0 & 0 & 0 & 0 & 0 & 0\\ 0 & 0 & 0 & 0 & 0 & 1 & 0 & 0 & 0 & 0 & 0 & 0 & 0 & 0\\ 0 & 0 & \frac{k_\mathrm{c}}{M_\mathrm{c}} & 0 & \frac{-2k_\mathrm{c}}{M_\mathrm{c}} & 0 & 0 & 0 & 0 & 0 & 0 & 0 & 0 & 0\\ 0 & 0 & 0 & 0 & 0 & 0 & 0 & 1 & 0 & 0 & 0 & 0 & 0 & 0\\ \frac{k_\mathrm{d}}{M_\mathrm{d}} & 0 & 0 & 0 & 0 & 0 & \frac{-2k_\mathrm{d}}{M_\mathrm{d}} & 0 & 0 & 0 & 0 & 0 & 0 & 0\\ 0 & \frac{-KA_\mathrm{p}}{V_{\mathrm{p}1,1}} & 0 & \frac{KA_\mathrm{p}}{V_{\mathrm{p}1,1}} & 0 & 0 & 0 & 0 & 0 & \frac{-K}{V_{\mathrm{p}1,1}} & 0 & 0 & 0 & 0\\ 0 & 0 & 0 & 0 & 0 & 0 & 0 & 0 & \frac{A}{\rho_\mathrm{oil}L} & \frac{-A\epsilon_{10}}{\rho_\mathrm{oil}L} & \frac{-A\gamma_{10}}{\rho_\mathrm{oil}L} & 0 & 0 & 0\\ 0 & 0 & 0 & 0 & 0 & 0 & 0 & 0 & 0 & 1 & 0 & 0 & 0 & 0\\ 0 & \frac{KA_\mathrm{p}}{V_{\mathrm{p}2,1}} & 0 & \frac{-KA_\mathrm{p}}{V_{\mathrm{p}2,1}} & 0 & 0 & 0 & 0 & 0 & 0 & 0 & 0 & \frac{-K}{V_{\mathrm{p}2,1}} & 0\\ 0 & 0 & 0 & 0 & 0 & 0 & 0 & 0 & 0 & 0 & 0 & \frac{A}{\rho_\mathrm{oil}L} & \frac{-A\epsilon_{13}}{\rho_\mathrm{oil}L} & \frac{-A\gamma_{13}}{\rho_\mathrm{oil}L}\\ 0 & 0 & 0 & 0 & 0 & 0 & 0 & 0 & 0 & 0 & 0 & 0 & 1 & 0\end{bmatrix}\begin{bmatrix}q_1\\ q_2\\ q_3\\ q_4\\ q_5\\ q_6\\ q_7\\ q_8\\ q_9\\ q_{10}\\ q_{11}\\ q_{12}\\ q_{13}\\ q_{14}\end{bmatrix} +$$

$$\begin{bmatrix} 0 & 0 & 0 & 0 & 0\\ \frac{1}{\alpha_2} & 0 & 0 & 0 & 0\\ 0 & 0 & 0 & 0 & 0\\ 0 & \frac{1}{\alpha_4} & 0 & 0 & 0\\ 0 & 0 & 0 & 0 & 0\\ 0 & 0 & \frac{k_\mathrm{c}}{M_\mathrm{c}} & 0 & 0\\ 0 & 0 & 0 & 0 & 0\\ 0 & 0 & \frac{k_\mathrm{d}}{M_\mathrm{d}} & 0 & 0\\ 0 & 0 & 0 & 0 & 0\\ 0 & 0 & 0 & \frac{A}{\rho_\mathrm{oil}L} & 0\\ 0 & 0 & 0 & 0 & 0\\ 0 & 0 & 0 & 0 & 0\\ 0 & 0 & 0 & 0 & \frac{A}{\rho_\mathrm{oil}L}\\ 0 & 0 & 0 & 0 & 0\end{bmatrix}\begin{bmatrix}F_{\mathrm{U},2}\\ F_{\mathrm{U},4}\\ z_\mathrm{in}\\ F_{\mathrm{U},10}\\ F_{\mathrm{U},13}\end{bmatrix} \tag{A.287}$$

$$\mathbf{A} = \begin{bmatrix} 0 & 1 & 0 & 0 & 0 & 0 & 0 & 0 & 0 & 0 & 0 & 0 & 0 & 0\\ \frac{-k_\mathrm{d}}{\alpha_2} & \frac{-\gamma_2}{\alpha_2} & 0 & 0 & 0 & 0 & \frac{k_\mathrm{d}}{\alpha_2} & 0 & \frac{A_\mathrm{p}}{\alpha_2} & 0 & 0 & \frac{-A_\mathrm{p}}{\alpha_2} & 0 & 0\\ 0 & 0 & 0 & 1 & 0 & 0 & 0 & 0 & 0 & 0 & 0 & 0 & 0 & 0\\ 0 & 0 & \frac{-k_\mathrm{c}}{\alpha_4} & \frac{-\gamma_4}{\alpha_4} & \frac{k_\mathrm{c}}{\alpha_4} & 0 & 0 & 0 & 0 & 0 & 0 & 0 & 0 & 0\\ 0 & 0 & 0 & 0 & 0 & 1 & 0 & 0 & 0 & 0 & 0 & 0 & 0 & 0\\ 0 & 0 & \frac{k_\mathrm{c}}{M_\mathrm{c}} & 0 & \frac{-2k_\mathrm{c}}{M_\mathrm{c}} & 0 & 0 & 0 & 0 & 0 & 0 & 0 & 0 & 0\\ 0 & 0 & 0 & 0 & 0 & 0 & 0 & 1 & 0 & 0 & 0 & 0 & 0 & 0\\ \frac{k_\mathrm{d}}{M_\mathrm{d}} & 0 & 0 & 0 & 0 & 0 & \frac{-2k_\mathrm{d}}{M_\mathrm{d}} & 0 & 0 & 0 & 0 & 0 & 0 & 0\\ 0 & \frac{-KA_\mathrm{p}}{V_{\mathrm{p}1,1}} & 0 & \frac{KA_\mathrm{p}}{V_{\mathrm{p}1,1}} & 0 & 0 & 0 & 0 & 0 & \frac{-K}{V_{\mathrm{p}1,1}} & 0 & 0 & 0 & 0\\ 0 & 0 & 0 & 0 & 0 & 0 & 0 & 0 & \frac{A}{\rho_\mathrm{oil}L} & \frac{-A\epsilon_{10}}{\rho_\mathrm{oil}L} & \frac{-A\gamma_{10}}{\rho_\mathrm{oil}L} & 0 & 0 & 0\\ 0 & 0 & 0 & 0 & 0 & 0 & 0 & 0 & 0 & 1 & 0 & 0 & 0 & 0\\ 0 & \frac{KA_\mathrm{p}}{V_{\mathrm{p}2,1}} & 0 & \frac{-KA_\mathrm{p}}{V_{\mathrm{p}2,1}} & 0 & 0 & 0 & 0 & 0 & 0 & 0 & 0 & \frac{-K}{V_{\mathrm{p}2,1}} & 0\\ 0 & 0 & 0 & 0 & 0 & 0 & 0 & 0 & 0 & 0 & 0 & \frac{A}{\rho_\mathrm{oil}L} & \frac{-A\epsilon_{13}}{\rho_\mathrm{oil}L} & \frac{-A\gamma_{13}}{\rho_\mathrm{oil}L}\\ 0 & 0 & 0 & 0 & 0 & 0 & 0 & 0 & 0 & 0 & 0 & 0 & 1 & 0\end{bmatrix} \tag{A.288}$$

A.13 Equations of motion for the LAM

A.13.1 EOM

A.13.1.1 1 mass

$$\begin{aligned}(M_{\text{hook,payload}})\ddot{z}_2 = \\ P_{\text{a1}}A_{\text{p}} - P_{\text{a3}}A_{\text{p}} + F_{\text{water}} - F_{\text{water}} + \rho_{\text{water}}V_{\text{d}}g \\ -M_{\text{hook,payload}}g\end{aligned} \tag{A.289}$$

Where $M_{\text{hook,payload}}$ is the mass of the hook and payload, z_2 is the displacement of the hook and payload, P_{a1} is the pressure in the lower accumulator, P_{a3} is the pressure in the upper accumulator, A_{p} is the area of the piston-head the pressures act on, F_{water} is the force of water pressure on the top and bottom of the cylinder that cancels out, ρ_{water} is the water density, V_{d} is the volume of displaced fluid, and g is gravitational acceleration.

A.13.1.2 2 pressures

The pressure in the lower accumulator is given by (A.290)

$$\dot{P}_{\text{a1}} = \frac{P_{\text{a1,1}}nQ_{\text{a1}}}{V_{\text{a1,1}}} \tag{A.290}$$

Where P_{a1} is the pressure in the lower accumulator, $P_{\text{a1,1}}$ is the initial pressure in the lower accumulator, n is the gas constant, Q_{a1} is the volume flow-rate with respect to the lower accumulator, and $V_{\text{a1,1}}$ is the initial volume in the lower accumulator.

$$Q_{\text{a1}} = -A_{\text{p}}(\dot{z}_2) \tag{A.291}$$

Where Q_{a1} is the volume flow-rate with respect to the lower accumulator, A_{p} is the area of the piston-head, and $\dot{z}_2$ is the velocity of the piston-head.

The pressure in the upper accumulator is given by (A.292)

$$\dot{P}_{\text{a3}} = \frac{P_{\text{a3,1}}nQ_{\text{a3}}}{V_{\text{a3,1}}} \tag{A.292}$$

Where P_{a3} is the pressure in the upper accumulator, $P_{\text{a3,1}}$ is the initial pressure in the upper accumulator, n is the gas constant, Q_{a3} is the volume flow-rate with respect to the upper accumulator, and $V_{\text{a3,1}}$ is the initial volume in the upper accumulator.

$$Q_{\text{a3}} = A_{\text{p}}(\dot{z}_2) \tag{A.293}$$

Where Q_{a3} is the volume flow-rate with respect to the upper accumulator, A_{p} is the area of the piston-head, $\dot{z}_2$ is the velocity of the piston-head.

A.13.1.3 State space system

See (A.294) and (A.295) for the state-space system corresponding to equations (A.289), (A.290), (A.292). The state variables are shown in Table A.3.

Table A.3: q variables

State variable	Physical variable
q_1	P_{a3}
q_2	z_2
q_3	$\dot{z}_2 = \dot{q}_2$
q_4	P_{a1}

$$\begin{bmatrix}\dot{q}_1\\ \dot{q}_2\\ \dot{q}_3\\ \dot{q}_4\end{bmatrix} = \begin{bmatrix} 0 & 0 & \frac{P_{\mathrm{a3},1} n A_{\mathrm{p}}}{V_{\mathrm{a3},1}} & 0 \\ 0 & 0 & 1 & 0 \\ -\frac{A_{\mathrm{p}}}{(M_{\mathrm{hook,payload}})} & 0 & 0 & \frac{A_{\mathrm{p}}}{(M_{\mathrm{hook,payload}})} \\ 0 & 0 & \frac{-P_{\mathrm{a1},1} n A_{\mathrm{p}}}{V_{\mathrm{a1},1}} & 0 \end{bmatrix} \begin{bmatrix} q_1\\ q_2\\ q_3\\ q_4 \end{bmatrix} + \begin{bmatrix} 0 \\ 0 \\ \frac{1}{M_{\mathrm{hook,payload}}} \\ 0 \end{bmatrix} \left[F_{\mathrm{external}}\right] \tag{A.294}$$

$$\begin{bmatrix} y_1\\ y_2\\ y_4 \end{bmatrix} = \begin{bmatrix} 1 & 0 & 0 & 0 \\ 0 & 1 & 0 & 0 \\ 0 & 0 & 0 & 1 \end{bmatrix} \begin{bmatrix} q_1\\ q_2\\ q_3\\ q_4 \end{bmatrix} + \begin{bmatrix} 0 \\ 0 \\ 0 \\ 0 \end{bmatrix} \left[F_{\mathrm{external}}\right] \tag{A.295}$$

A.14 Working out upper/lower case initial conditions for section 8.2

A.14.1 Upper case initial conditions

The upper case is where the piston-head is 10% of the maximum stroke length from the top of the cylinder, the top position. See Figure A.9. This means the piston-head is displaced $L_{\text{upper,case}} = 0.4L_{\text{max,stroke}}$ upwards from the middle of the cylinder. The change in the system is referenced relative to the base case. This change in volume is

$$\Delta V_{\text{upper,case}} = L_{\text{upper,case}}(0.25\pi d_{\text{p,tot}}^2) \tag{A.296}$$

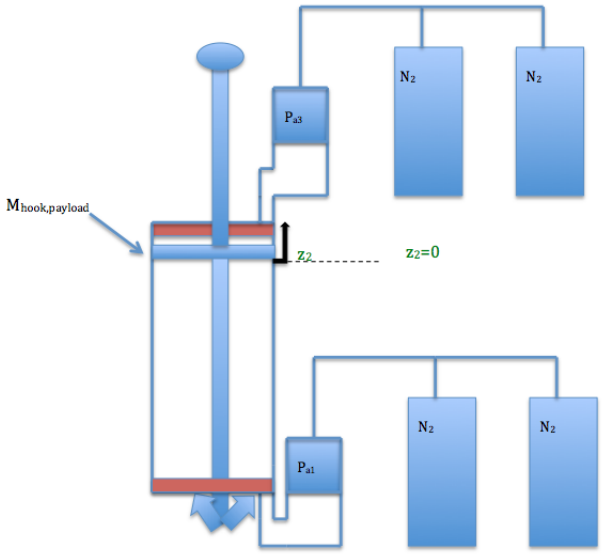

Figure A.9: A schematic for the upper case

A.14.1.1 Lower accumulator dimensions

The effect on the system is that the lower accumulator will have an increased initial volume relative to the base case

$$V_{\text{a1,1,UC}} = V_{\text{a1,1}} + \Delta V_{\text{upper,case}} \tag{A.297}$$

where $V_{\text{a1,1}}$ is for the base case.
V_1 is defined as the initial volume:

$$V_1 = V_{\text{a1,1,UC}} \tag{A.298}$$

Since the initial volume is specified the initial pressure P_1 will change. The useful volume ΔV has changed. ΔV is calculated using (8.3) as a function of $d_{\text{p,tot}}$ and L_{useful}. For the lower accumulator:

$$L_{\text{useful}} = 0.9L_{\text{max,stroke}} \tag{A.299}$$

Since ΔV has changed then V_0 must change. V_0 is a function of ΔV, P_0, P_1, and P_2. It is assumed P_2 and V_2 are the same as for the base case since these correspond to the maximum pressure state. Using:

$$P_1 V_1^n = P_2 V_2^n \tag{A.300}$$

P_1 can be found. As mentioned before:

$$P_0 = 0.9P_1 \tag{A.301}$$

Then V_0 can be found. See Table A.4 for the calculated values.

Table A.4: Upper case, key variable values for the lower accumulator, variables with * changed relative to the base case

Variable	Unit	value
$*P_0$	[N/m^2]	1.0856e+07
$*P_1$	[N/m^2]	1.2062e+07
P_2	[N/m^2]	6e7
$*\frac{P_2}{P_0}$	[-]	5.5268
$*V_0$	[m^3]	0.3017
$*V_1$	[m^3]	0.2798
V_2	[m^3]	0.0890
$*\Delta V$	[m^3]	0.1909

A.14.1.2 Upper accumulator dimensions

The upper accumulator will have a decreased initial volume relative to the base case

$$V_{\text{a3,1,UC}} = V_{\text{a3,1}} - \Delta V_{\text{upper,case}} \tag{A.302}$$

where $V_{\text{a3,1}}$ is for the base case.
V_1 is defined as the initial volume:

$$V_1 = V_{\text{a3,1,UC}} \tag{A.303}$$

Since the initial volume is specified the initial pressure P_1 will change. The useful volume ΔV has changed. ΔV is calculated using (8.3) as a function of $d_{\text{p,tot}}$ and L_{useful}. For the upper accumulator:

$$L_{\text{useful}} = 0.1 L_{\text{max,stroke}} \tag{A.304}$$

Since ΔV has changed then V_0 must change. V_0 is a function of ΔV, P_0, P_1, and P_2. It is assumed P_2 and V_2 are the same since these are the maximum states. Using:

$$P_1 V_1^n = P_2 V_2^n \tag{A.305}$$

P_1 can be found. As mentioned before:

$$P_0 = 0.9 P_1 \tag{A.306}$$

Then V_0 can be found. See Table A.5 for the calculated values.

Table A.5: Upper case, key variable values for the upper accumulator, variables with * changed relative to the base case

Variable	Unit	value
$*P_0$	[N/m^2]	2.0631e+06
$*P_1$	[N/m^2]	2.2924e+06
P_2	[N/m^2]	3.3065e+06
$*\frac{P_2}{P_0}$	[-]	1.6027
$*V_0$	[m^3]	0.0993
$*V_1$	[m^3]	0.0921
V_2	[m^3]	0.0709
$*\Delta V$	[m^3]	0.0212

A.14.1.3 Upper case dimensions

Values from Table A.5 and Table A.4 are summarized in Table A.6 for the upper case.

Table A.6: Upper case, variables with * are changed relative to the base case

Variable	Value	Unit	Note
$PS_{PHC,lower}$	1.0856e+07	[N/m^2]	Charge pressure, lower accumulator
$PS_{PHC,upper}$	2.0631e+06	[N/m^2]	Charge pressure, upper accumulator
$d_{p,tot}$	0.3	[m]	Diameter of piston-head
$P_{\Delta p}$	1.9081e+07	[N/m^2]	Difference in pressure across piston-head required to hold payload and hook in water
$*P_{a1,1}$	1.2062e+07	[N/m^2]	Initial pressure in the lower accumulator
$*P_{a3,1}$	2.2924e+06	[N/m^2]	Initial pressure in the upper accumulator
$*V_{a1,1}$	0.2798	[m^3]	Initial volume in lower accumulator
$*V_{a3,1}$	0.0921	[m^3]	Initial volume in upper accumulator
$*\omega_{z_1}$	1.7689	[rad/s]	Natural frequency of accumulator system
$\omega_{z_{1,design}}$	2.0944	[rad/s]	Designed natural frequency
$*\epsilon$	15.5	[%]	Percent error of natural frequency, relative to design
Base case ω_{z_1}	2.2269	[rad/s]	Natural frequency of accumulator system

A.14.2 Lower case initial conditions

The lower case is where the piston-head is at 10% $L_{max,stroke}$ above the bottom of the cylinder. See Figure A.10. This means the piston-head is displaced $L_{lower,case} = 0.4L_{max,stroke}$ downwards from the middle of the cylinder. The change in the system is referenced relative to the base case. This change in volume is

$$\Delta V_{lower,case} = L_{lower,case}(0.25\pi d_{p,tot}^2) \tag{A.307}$$

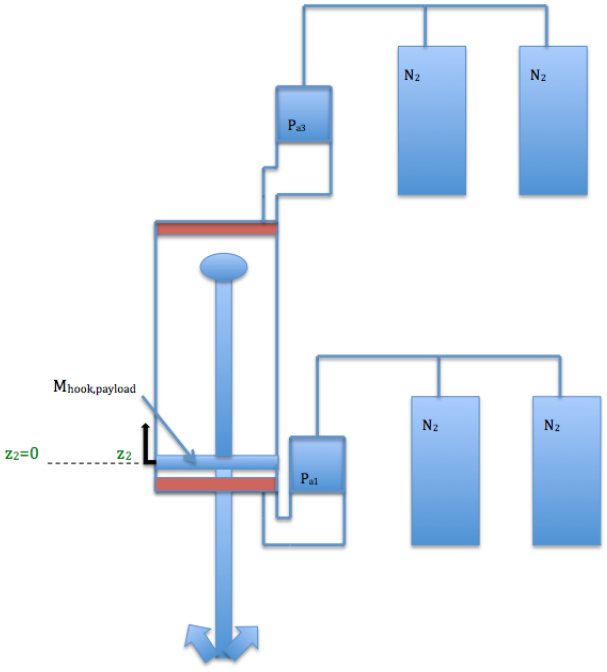

Figure A.10: A schematic for the lower case

A.14.2.1 Lower accumulator dimensions

The effect on the system is that the lower accumulator will have a decreased initial volume relative to the base case

$$V_{\text{a1,1,LC}} = V_{\text{a1,1}} - \Delta V_{\text{lower,case}} \tag{A.308}$$

where $V_{\text{a1,1}}$ is for the base case.
V_1 is defined as the initial volume:

$$V_1 = V_{\text{a1,1,LC}} \tag{A.309}$$

Since the initial volume is specified the initial pressure P_1 will change. The useful volume ΔV has changed. ΔV is calculated using (8.3) as a function of $d_{\text{p,tot}}$ and L_{useful}. For the lower accumulator:

$$L_{\text{useful}} = 0.1 L_{\text{max,stroke}} \tag{A.310}$$

Since ΔV has changed then V_0 must change. V_0 is a function of ΔV, P_0, P_1, and P_2. It is assumed P_2 and V_2 are the same since these are the maximum states. Using:

$$P_1 V_1^n = P_2 V_2^n \tag{A.311}$$

P_1 can be found. As mentioned before:

$$P_0 = 0.9 * P_1 \tag{A.312}$$

Now V_0 can be found. See Table A.7 for the calculated values.

Table A.7: Lower case, key variable values for the lower accumulator, variables with * changed relative to the base case

Variable	Unit	value
$*P_0$	[N/m^2]	4.0032e+07
$*P_1$	[N/m^2]	4.4480e+07
P_2	[N/m^2]	6e7
$*\frac{P_2}{P_0}$	[-]	1.4988
$*V_0$	[m^3]	0.1188
$*V_1$	[m^3]	0.1102
V_2	[m^3]	0.0890
$*\Delta V$	[m^3]	0.0212

A.14.2.2 Upper accumulator dimensions

The upper accumulator will have an increased initial volume relative to the base case.

$$V_{\text{a3,1,LC}} = V_{\text{a3,1}} + \Delta V_{\text{lower,case}} \tag{A.313}$$

where $V_{\text{a3,1}}$ is for the base case.
V_1 is defined as the initial volume $V_1 = V_{\text{a3,1,LC}}$. Since the initial volume is specified the initial pressure P_1 will change. The useful volume ΔV has changed. ΔV is calculated using (8.3) as a function of $d_{\text{p,tot}}$ and L_{useful}. For the upper accumulator:

$$L_{\text{useful}} = 0.9 L_{\text{max,stroke}} \tag{A.314}$$

Since ΔV has changed then V_0 must change. V_0 is a function of ΔV, P_0, P_1, and P_2. It is assumed P_2 and V_2 are the same since these are the maximum states. Using:

$$P_1 * V_1^n = P_2 * V_2^n \tag{A.315}$$

P_1 can be found. As mentioned before:

$$P_0 = 0.9 * P_1 \tag{A.316}$$

Now V_0 can be found. See Table A.8 for the calculated values.

Table A.8: Lower case, key variable values for the upper accumulator, variables with * changed relative to the base case

Variable	Unit	value
$*P_0$	[N/m^2]	4.7807e+05
$*P_1$	[N/m^2]	5.3119e+05
P_2	[N/m^2]	3.3065e+06
$*\frac{P_2}{P_0}$	[-]	6.9163
$*V_0$	[m^3]	0.2822
$*V_1$	[m^3]	0.2618
V_2	[m^3]	0.0709
$*\Delta V$	[m^3]	0.1909

A.14.2.3 Lower case dimensions

Values from Table A.8 and Table A.7 are summarized in Table A.9 for the lower case.

Table A.9: Lower case, variables with * are changed relative to the base case

Variable	Value	Unit	Note
$PS_{PHC,lower}$	4.0032e+07	[N/m^2]	Charge pressure, lower accumulator
$PS_{PHC,upper}$	4.7807e+05	[N/m^2]	Charge pressure, upper accumulator
$d_{p,tot}$	0.3	[m]	Diameter of piston-head
$P_{\Delta p}$	1.9081e+07	[N/m^2]	Difference in pressure across piston-head required to hold payload and hook in water
$*P_{a1,1}$	4.4480e+07	[N/m^2]	Initial pressure in the lower accumulator
$*P_{a3,1}$	5.3119e+05	[N/m^2]	Initial pressure in the upper accumulator
$*V_{a1,1}$	0.1102	[m^3]	Initial volume in lower accumulator
$*V_{a3,1}$	0.2618	[m^3]	Initial volume in upper accumulator
$*\omega_{z_1}$	4.3213	[rad/s]	Natural frequency of accumulator system
$\omega_{z_{1,design}}$	2.0944	[rad/s]	Designed natural frequency
$*\epsilon$	106.3	[%]	Percent error of natural frequency of accumulator system, relative to design
Base case ω_{z_1}	2.2269	[rad/s]	Natural frequency of accumulator system

A.15 Natural frequencies, the RLAM

For the equations of motion and the state-space system.

A.15.1 EOM

A.15.1.1 4 masses

The equation of motion (EOM) for the hook and payload is shown.

$$\begin{aligned}(M_{\text{hook,payload}})\ddot{z}_1 = \\ P_{\text{a1}}A_{\text{p}} - P_{\text{a3}}A_{\text{p}} + F_{\text{water}} - F_{\text{water}} + \rho_{\text{water}}V_{\text{d}}g \\ -M_{\text{hook,payload}}g - k_{\text{d}}(z_1 - z_{\text{d}})\end{aligned} \tag{A.317}$$

The EOM for the cylinder is shown.

$$(M_{\text{phc}})\ddot{z}_{\text{phc}} = -k_{\text{c}}(z_{\text{phc}} - z_{\text{c}}) \tag{A.318}$$

The EOM for the steel rope is shown.

$$(M_{\text{c}})\ddot{z}_{\text{c}} = -k_{\text{c}}(z_{\text{c}} - z_{\text{in}}) - k_{\text{c}}(z_{\text{c}} - z_{\text{phc}}) \tag{A.319}$$

The EOM for the Dyneema is shown.

$$(M_{\text{d}})\ddot{z}_{\text{d}} = -k_{\text{d}}(z_{\text{d}} - z_{\text{in}}) - k_{\text{d}}(z_{\text{d}} - z_1) \tag{A.320}$$

A.15.1.2 2 pressures

Assumptions

- Isentropic process

The pressure in the lower accumulator is given by (A.321)

$$\dot{P}_{\text{a1}} = \frac{P_{\text{a1,1}}nQ_{\text{r,1}}}{V_{\text{a1,1}}} \tag{A.321}$$

$$Q_{\text{r,1}} = A_{\text{p}}(\dot{z}_{\text{phc}} - \dot{z}_1) \tag{A.322}$$

The pressure in the upper accumulator is given by (A.323)

$$\dot{P}_{\text{a3}} = \frac{P_{\text{a3,1}}nQ_{\text{r,3}}}{V_{\text{a3,1}}} \tag{A.323}$$

$$Q_{\text{r,3}} = A_{\text{p}}(\dot{z}_1 - \dot{z}_{\text{phc}}) \tag{A.324}$$

A.15.1.3 State space system

See (A.325) and (A.326) for the state-space system corresponding to equations (A.317), (A.318), (A.319), (A.320), (A.321), and (A.323). The state variables are shown in Table A.10.

Table A.10: q variables

State variable	Physical variable
q_1	z_1
q_2	$\dot{z}_1 = \dot{q}_1$
q_3	z_{phc}
q_4	$\dot{z}_{\text{phc}} = \dot{q}_3$
q_5	z_c
q_6	$\dot{z}_c = \dot{q}_5$
q_7	z_d
q_8	$\dot{z}_d = \dot{q}_7$
q_9	P_{a1}
q_{10}	P_{a3}

$$\begin{bmatrix}\dot{q}_1\\ \dot{q}_2\\ \dot{q}_3\\ \dot{q}_4\\ \dot{q}_5\\ \dot{q}_6\\ \dot{q}_7\\ \dot{q}_8\\ \dot{q}_9\\ \dot{q}_{10}\end{bmatrix} = \begin{bmatrix} 0 & 1 & 0 & 0 & 0 & 0 & 0 & 0 & 0 & 0 \\ -\frac{k_\mathrm{d}}{M_\mathrm{hook,payload}} & 0 & 0 & 0 & 0 & 0 & \frac{k_\mathrm{d}}{M_\mathrm{hook,payload}} & 0 & \frac{A_\mathrm{p}}{M_\mathrm{hook,payload}} & -\frac{A_\mathrm{p}}{M_\mathrm{hook,payload}} \\ 0 & 0 & 0 & 1 & 0 & 0 & 0 & 0 & 0 & 0 \\ 0 & 0 & -\frac{k_c}{M_\mathrm{phc}} & 0 & \frac{k_c}{M_\mathrm{phc}} & 0 & 0 & 0 & 0 & 0 \\ 0 & 0 & 0 & 0 & 0 & 1 & 0 & 0 & 0 & 0 \\ 0 & 0 & \frac{k_\mathrm{c}}{M_\mathrm{c}} & 0 & \frac{-2k_\mathrm{c}}{M_\mathrm{c}} & 0 & 0 & 0 & 0 & 0 \\ 0 & 0 & 0 & 0 & 0 & 0 & 0 & 1 & 0 & 0 \\ \frac{k_\mathrm{d}}{M_\mathrm{d}} & 0 & 0 & 0 & 0 & 0 & \frac{-2k_\mathrm{d}}{M_\mathrm{d}} & 0 & 0 & 0 \\ 0 & -\frac{P_{\mathrm{a1},1} n A_\mathrm{p}}{V_{\mathrm{a1},1}} & 0 & \frac{P_{\mathrm{a1},1} n A_\mathrm{p}}{V_{\mathrm{a1},1}} & 0 & 0 & 0 & 0 & 0 & 0 \\ 0 & \frac{P_{\mathrm{a3},1} n A_\mathrm{p}}{V_{\mathrm{a3},1}} & 0 & -\frac{P_{\mathrm{a3},1} n A_\mathrm{p}}{V_{\mathrm{a3},1}} & 0 & 0 & 0 & 0 & 0 & 0 \end{bmatrix} \begin{bmatrix}q_1\\ q_2\\ q_3\\ q_4\\ q_5\\ q_6\\ q_7\\ q_8\\ q_9\\ q_{10}\end{bmatrix} + \begin{bmatrix} 0 & 0 \\ \frac{1}{M_\mathrm{hook,payload}} & 0 \\ 0 & 0 \\ 0 & 0 \\ 0 & 0 \\ 0 & \frac{k_\mathrm{c}}{M_\mathrm{c}} \\ 0 & 0 \\ 0 & \frac{k_\mathrm{d}}{M_\mathrm{d}} \\ 0 & 0 \\ 0 & 0 \end{bmatrix} \begin{bmatrix} F_\mathrm{external} \\ z_\mathrm{in} \end{bmatrix} \tag{A.325}$$

$$\begin{bmatrix}y_1\\ y_3\\ y_5\\ y_7\\ y_9\\ y_{10}\end{bmatrix} = \begin{bmatrix} 1 & 0 & 0 & 0 & 0 & 0 & 0 & 0 & 0 & 0 \\ 0 & 0 & 1 & 0 & 0 & 0 & 0 & 0 & 0 & 0 \\ 0 & 0 & 0 & 0 & 1 & 0 & 0 & 0 & 0 & 0 \\ 0 & 0 & 0 & 0 & 0 & 0 & 1 & 0 & 0 & 0 \\ 0 & 0 & 0 & 0 & 0 & 0 & 0 & 0 & 1 & 0 \\ 0 & 0 & 0 & 0 & 0 & 0 & 0 & 0 & 0 & 1 \end{bmatrix} \begin{bmatrix}q_1\\ q_2\\ q_3\\ q_4\\ q_5\\ q_6\\ q_7\\ q_8\\ q_9\\ q_{10}\end{bmatrix} + \begin{bmatrix} 0 & 0 \\ 0 & 0 \\ 0 & 0 \\ 0 & 0 \\ 0 & 0 \\ 0 & 0 \end{bmatrix} \begin{bmatrix} F_\mathrm{external} \\ z_\mathrm{in} \end{bmatrix} \tag{A.326}$$

A.15.2 Upper case natural frequencies

See Table A.11

Table A.11: Upper case eigenvalues, natural frequencies, natural periods

Eigenvalue λ	Natural frequency ω_n [rad/s]	Natural period [s]
0	0	inf
0	0	inf
0.1079i	0.1079	58.2316
-0.1079i	0.1079	58.2316
0.4095i	0.4095	15.3436
-0.4095i	0.4095	15.3436
0.5088i	0.5088	12.3490
-0.5088i	0.5088	12.3490
1.7723i	1.7723	3.5452
-1.7723i	1.7723	3.5452

A.15.3 Lower case natural frequencies

See Table A.12

Table A.12: Lower case eigenvalues, natural frequencies, natural periods

Eigenvalue λ	Natural frequency ω_n [rad/s]	Natural period [s]
0	0	inf
0	0	inf
0.1079i	0.1079	58.2316
-0.1079i	0.1079	58.2316
0.4095i	0.4095	15.3436
-0.4095i	0.4095	15.3436
0.5093i	0.5093	12.3369
-0.5093i	0.5093	12.3369
4.3226i	4.3226	1.4536
-4.3226i	4.3226	1.4536

A.16 Upper/lower case for the ORLAM

A.16.1 Upper case natural frequencies

See Table A.13 for the natural frequencies when the piston-head is in the upper position. Comparison with Table 9.6 shows that the second, third, and fourth largest natural frequencies are the same. This is reasonable since these natural frequencies are due to the steel rope, Dyneema, and cylinder respectively. So they should be independent of piston-head position. The fifth largest natural frequency, 1.7558rad/s, is due to the hook/payload mass and is different from the base case natural frequency, 2.2020rad/s. This is expected since the hook/payload mass natural frequency is a function of piston-head position.

Table A.13: Upper case: Eigenvalues, natural frequencies

Eigenvalue λ	Natural frequency ω_n [rad/s]	Natural frequency [Hz]	Natural period [s]
0	0	0	inf
0	0	0	inf
-9.6626e-5 - 0.1035i	0.1035	0.0165	60.7071
-9.6626e-5 + 0.1035i	0.1035	0.0165	60.7071
-4.5410e-4 - 0.3070i	0.3070	0.0489	20.4664
-4.5410e-4 + 0.3070i	0.3070	0.0489	20.4664
-5.1028e-8 - 0.5090i	0.5090	0.0810	12.3442
-5.1028e-8 + 0.5090i	0.5090	0.0810	12.3442
-2.8155e-4 - 1.7558i	1.7558	0.2794	3.5785
-2.8155e-4 + 1.7558i	1.7558	0.2794	3.5785
-2.4370e-2 - 301.86i	301.86	48.0420	0.0208
-2.4370e-2 + 301.86i	301.86	48.0420	0.0208
-2.4136e-2 - 303.37i	303.37	48.2822	0.0207
-2.4136e-2 + 303.37i	303.37	48.2822	0.0207

A.16.2 Lower case natural frequencies

See Table A.14. Comparison with Table 9.6 shows that the second, third, and fourth largest natural frequencies are nearly the same. This is reasonable since these natural frequencies are due to the steel rope, Dyneema, and cylinder respectively. So they should be independent of piston-head position. The fifth largest natural frequency, 4.2060rad/s, is due to the hook/payload mass and is different from the base case natural frequency, 2.2020rad/s. This is expected since the hook/payload mass natural frequency is a function of piston-head position.

Table A.14: Lower case: Eigenvalues, natural frequencies

Eigenvalue λ	Natural frequency ω_n [rad/s]	Natural frequency [Hz]	Natural period [s]
0	0	0	inf
0	0	0	inf
-9.6626e-5 - 0.1035i	0.1035	0.0165	60.7071
-9.6626e-5 + 0.1035i	0.1035	0.0165	60.7071
-4.5410e-4 - 0.3070i	0.3070	0.0489	20.4664
-4.5410e-4 + 0.3070i	0.3070	0.0489	20.4664
-1.3034e-9 - 0.5093i	0.5093	0.0811	12.3369
-1.3034e-9 + 0.5093i	0.5093	0.0811	12.3369
-2.7410e-4 - 4.2060i	4.2060	0.6694	1.4939
-2.7410e-4 + 4.2060i	4.2060	0.6694	1.4939
-2.4279e-2 - 302.04i	302.04	48.0713	0.0208
-2.4279e-2 - 302.04i	302.04	48.0713	0.0208
-2.4234e-2 - 308.26i	308.26	49.0609	0.0204
-2.4234e-2 + 308.26i	308.26	49.0609	0.0204

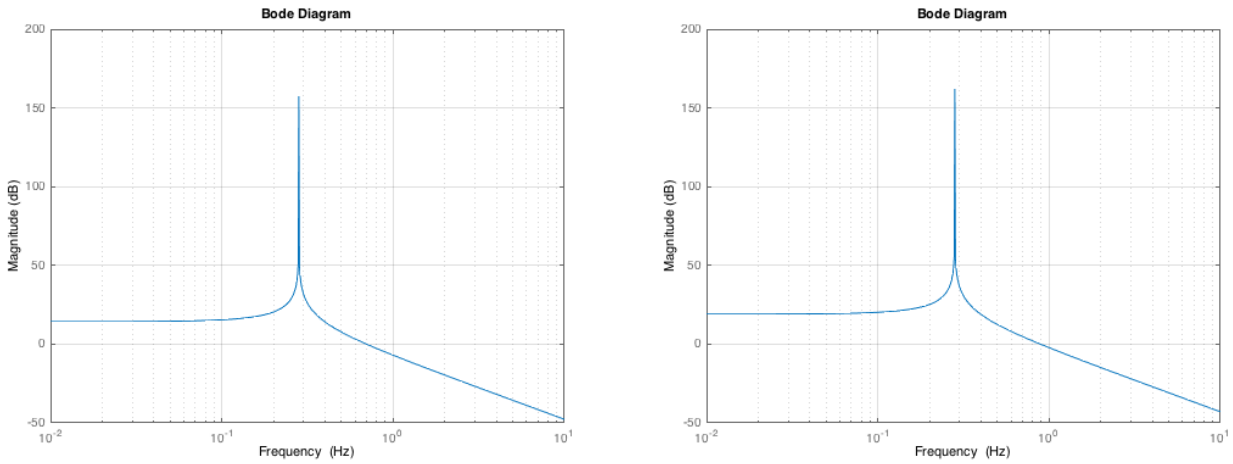

(a) Bode plot for P_{a3}, peak at 0.282Hz

(b) Bode plot for P_{a1}, peak at 0.282Hz

Figure A.11: Upper case, for the LAM

A.17 Frequency response of pressures, upper/lower case initial conditions

A.17.1 Upper case

A.17.1.1 The LAM

In Figures A.11a and A.11b the frequency response for the LAM (from Figure 9.1) is shown for the upper case initial conditions. There is only one peak at 0.282Hz.

A.17.1.2 The ORLAM

For the ORLAM in appendix A.16.1 in Table A.13. The closest natural frequency is 0.2794Hz which has a 0.9% difference with 0.282Hz. These natural frequencies are almost the same.

A.17.2 Lower case

A.17.2.1 The LAM

In Figures A.12a and A.12b the frequency response for the LAM (from Figure 9.1) is shown for the lower case initial conditions. There is only one peak at 0.688Hz.

A.17.2.2 The ORLAM

For the ORLAM in appendix A.16.2 in Table A.14. The closest natural frequency is 0.6694Hz which has a 2.7% difference with 0.688Hz. These natural frequencies are almost the same.

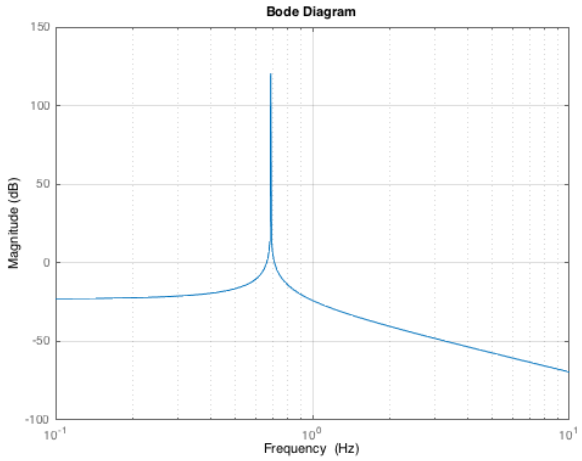

(a) Bode plot for $P_{\mathrm{a}3}$, peak at 0.688Hz

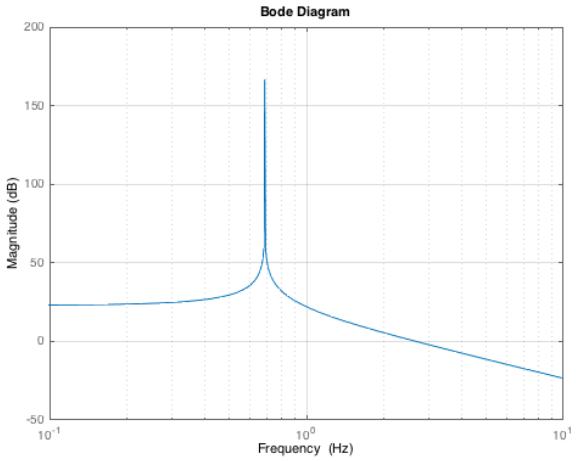

(b) Bode plot for $P_{\mathrm{a}1}$, peak at 0.688Hz

Figure A.12: Lower case, for the LAM

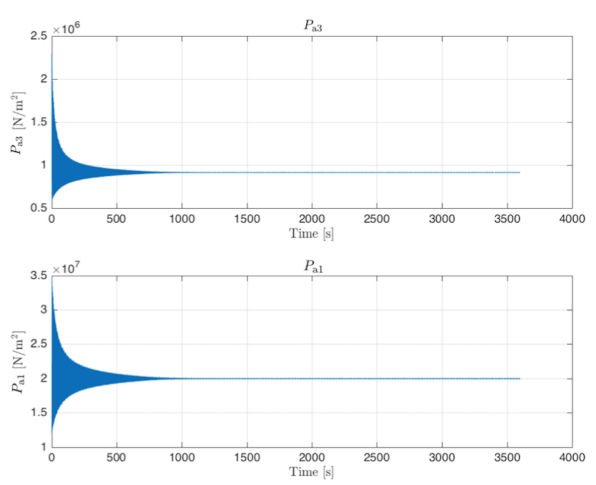

(a) Using the NLORLAM, input frequency is the design wave frequency of 0.125Hz

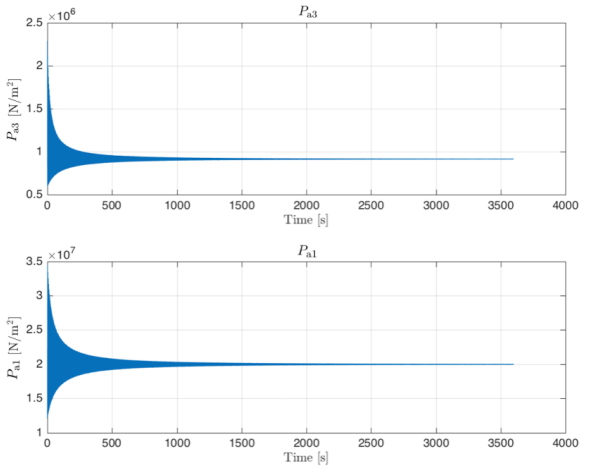

(b) Using the NLORLAM, input frequency is the natural frequency of 0.2794Hz

Figure A.13: Upper case, time-response of P_{a3} and P_{a1}

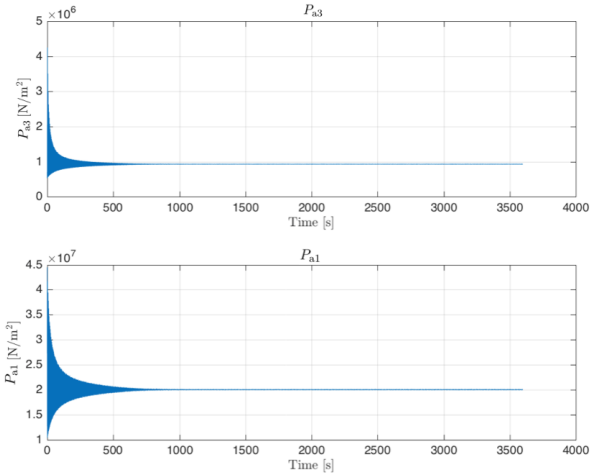

(a) Using the NLORLAM, input frequency is the design wave frequency of 0.125Hz

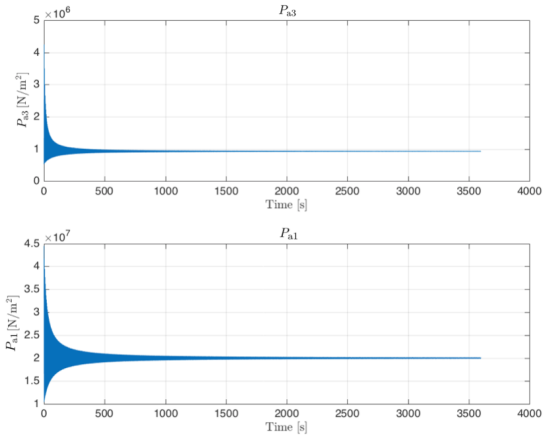

(b) Using the NLORLAM, input frequency is the natural frequency of 0.6694Hz

Figure A.14: Lower case, time-response of P_{a3} and P_{a1}

A.18 Time response of pressures, upper/lower case initial conditions

A.18.1 Upper case

Figure A.13a shows the pressures P_{a1} and P_{a3} for the design wave condition. Figure A.13b shows the pressures using an input frequency of 0.2794Hz the same as the frequency in appendix A.17.1.2.

A.18.2 Lower case

Figure A.14a shows the pressures P_{a1} and P_{a3} for the design wave condition. Figure A.14b shows the pressures using an input frequency of 0.6694Hz the same as the frequency in appendix A.17.2.2.

A.19 Frequency response of hook/payload motion, upper/lower case initial conditions

A.19.1 Upper case

See Figure A.15 for the frequency response of the hook displacement with respect to a harmonic crane tip motion, for the upper case. The frequency and magnitude of peaks is shown in Table A.15.

For the ORLAM in section A.16.1 in Table A.13 the closest natural frequencies are extracted and put into Table A.16. The percent differences with the corresponding values in Table A.15 are shown in Table A.16. Most of the percent differences are low as would be expected since they are supposed to be the same natural frequencies.

Table A.15: Frequency and magnitudes for peaks in Figure A.15 (RLAM)

Frequency [Hz]	Magnitude [dB]
0.0172	144
0.0652	121
0.081	89
0.282	56.7

Table A.16: Upper case, natural frequencies for the ORLAM with percent differences of values in Table A.15

Frequency [Hz]	% difference
0.0165	4.2
0.0489	25.1
0.0810	0
0.2794	0.9

A.19.2 Lower case

See Figure A.16 for the frequency response of the hook displacement with respect to a harmonic crane tip motion, for the lower case. The frequency and magnitude of peaks is shown in Table A.17.

For the ORLAM in section A.16.2 in Table A.14 the closest natural frequencies are extracted and put into Table A.18. The percent differences with the corresponding values in Table A.17 are shown in Table A.18. Most of the percent differences are low as would be expected since they are supposed to be the same natural frequencies.

Table A.17: Frequency and magnitudes for peaks in Figure A.16 (RLAM)

Frequency [Hz]	Magnitude [dB]
0.0172	141
0.0652	121
0.0811	201
0.688	26.1

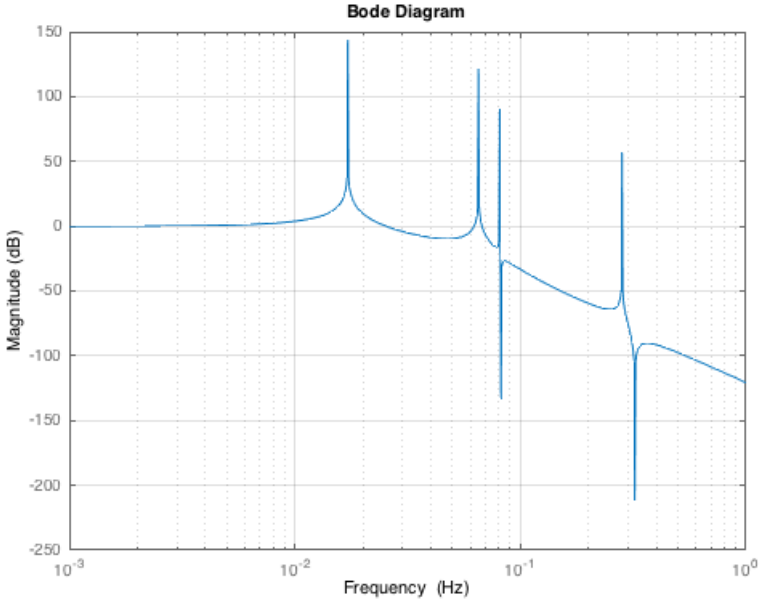

Figure A.15: Upper case, bode plot for z_1, the RLAM.

Table A.18: Lower case, natural frequencies for the ORLAM with percent differences of values in Table A.17

Frequency [Hz]	% difference
0.0165	4.2
0.0489	25.1
0.0811	0.1
0.6694	2.7

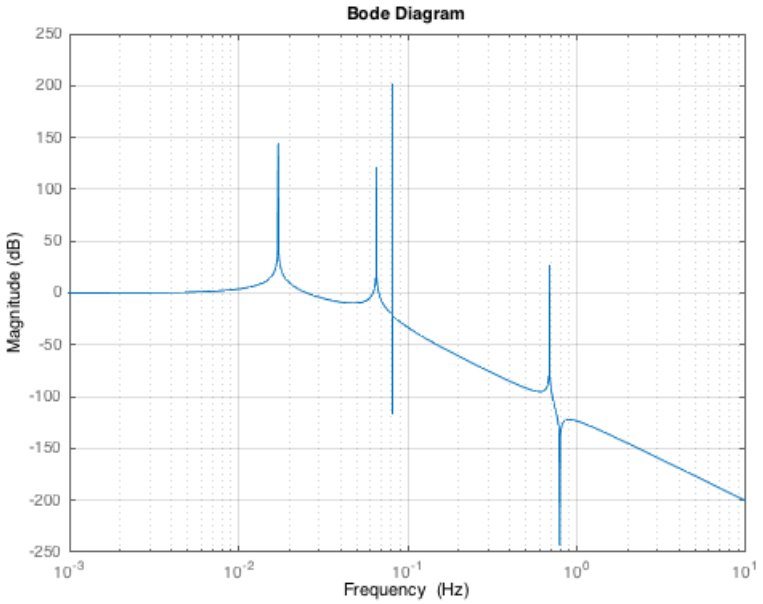

Figure A.16: Lower case, bode plot for z_1, the RLAM.

A.20 Time response of hook/payload motion, upper/lower case initial conditions

A.20.1 Upper case

The four frequencies found in the frequency response in Table A.16 are used as input frequencies to verify the frequency response, the table is repeated in Table A.19.

Table A.19: Upper case, natural frequencies

Frequency [Hz]	% difference
0.0165	4.2
0.0489	25.1
0.0810	0
0.2794	0.9

For 0.0165Hz see Figure A.17b, there is a large amplification of the maximum crest-to-trough value of z_1 relative to the design wave condition in Figure A.17a.

For 0.0489Hz see Figure A.17c, the maximum crest-to-trough value of z_1 is larger relative to the case of the design wave condition.

For 0.0810Hz see Figure A.17d, the maximum crest-to-trough value of z_1 is larger than in the case of the design wave condition and increases in time. As mentioned in section 10.5.1 this is most likely due to an interaction with the accumulators.

For 0.2794Hz see Figure A.17e, the maximum crest-to-trough value of z_1 is approximately the same as the case of the design wave condition. The high frequency leads to damping have a greater effect which is why the crest-to-trough value of z_1 decreases in time.

A.20.2 Lower case

The four frequencies found in the frequency response in Table A.18 are used as input frequencies to verify the frequency response, the table is repeated in Table A.20.

Table A.20: Lower case, natural frequencies

Frequency [Hz]	% difference
0.0165	4.2
0.0489	25.1
0.0811	0.1
0.6694	2.7

For 0.0165Hz see Figure A.18b, there is a large amplification of maximum crest-to-trough value of z_1 relative to the design wave condition in Figure A.18a.

For 0.0489Hz see Figure A.18c, the maximum crest-to-trough value of z_1 is larger relative to the case of the design wave condition.

For 0.0811Hz see Figure A.18d , the maximum crest-to-trough value of z_1 is higher than the case of the design wave condition. In time, the crest-to-trough value of z_1 grows. As mentioned in

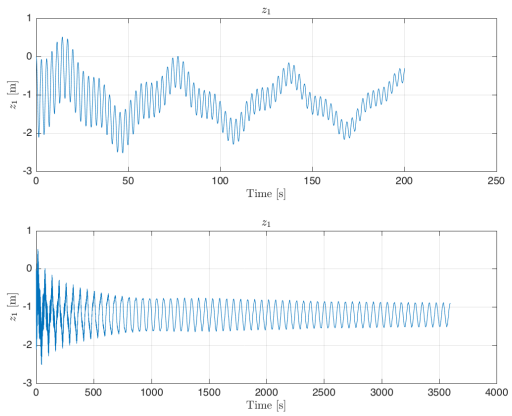

(a) Using the NLORLAM, input frequency is the design wave frequency of 0.125Hz

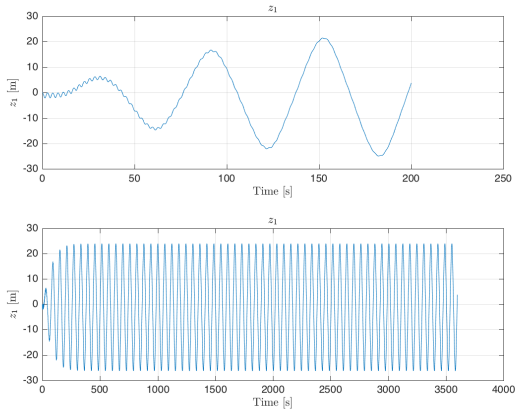

(b) Using the NLORLAM, input frequency is the natural frequency of 0.0165Hz

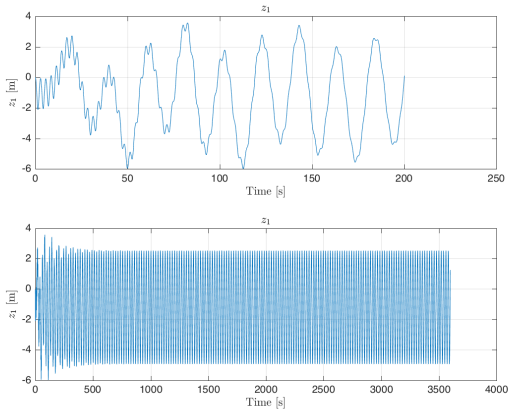

(c) Using the NLORLAM, input frequency is the natural frequency of 0.0489Hz

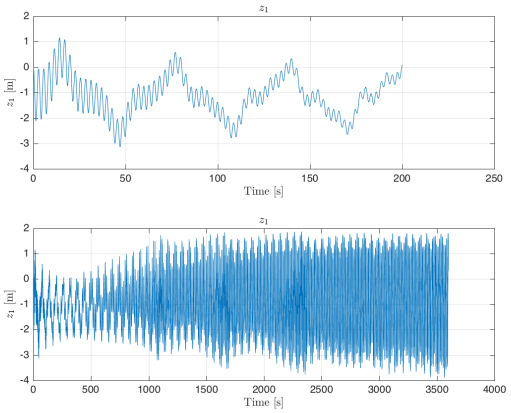

(d) Using the NLORLAM, input frequency is the natural frequency of 0.0810Hz

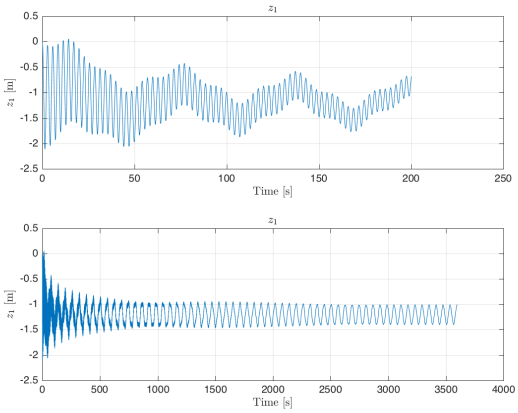

(e) Using the NLORLAM, input frequency is the natural frequency of 0.2794 Hz

Figure A.17: Time-series for z_1 for five input frequencies

section 10.5.1 this is most likely due to an interaction with the accumulators.

For 0.6694Hz see Figure A.18e , the maximum crest-to-trough value of z_1 is approximately the same as in the case of the design wave condition. In time the crest-to-trough value of z_1 diminishes due to the frequency being relatively larger which enables the damping in the system to have a larger influence.

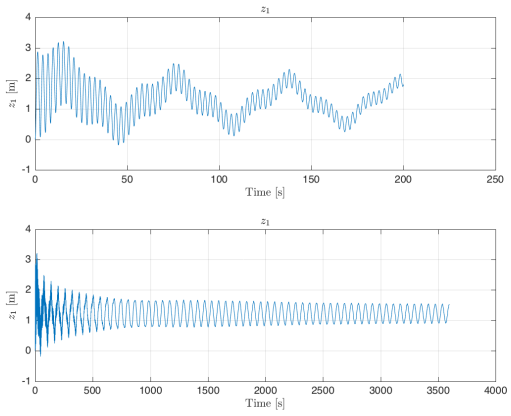

(a) Using the NLORLAM, input frequency is the design wave frequency of 0.125Hz

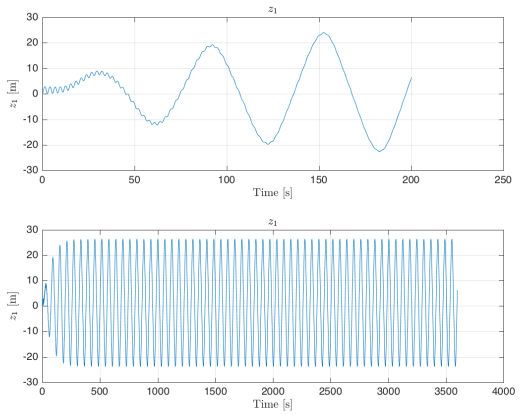

(b) Using the NLORLAM, input frequency is the natural frequency of 0.0165Hz

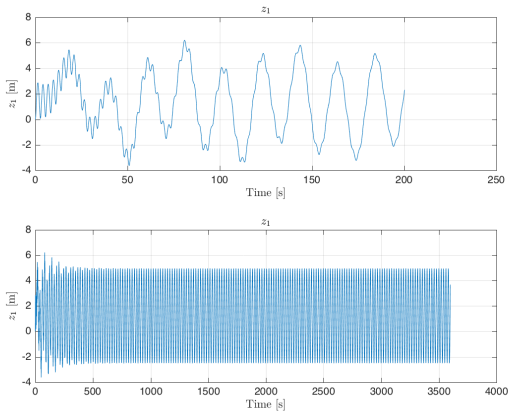

(c) Using the NLORLAM, input frequency is the natural frequency of 0.0489Hz

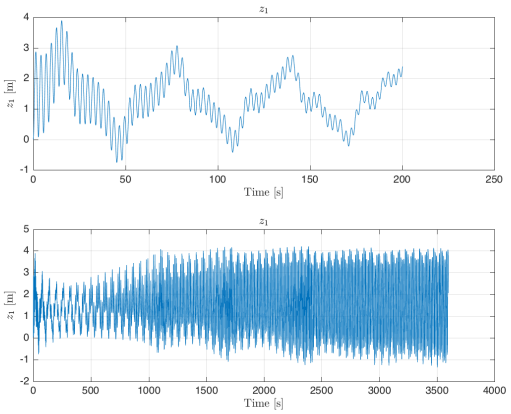

(d) Using the NLORLAM, input frequency is the natural frequency of 0.0811Hz

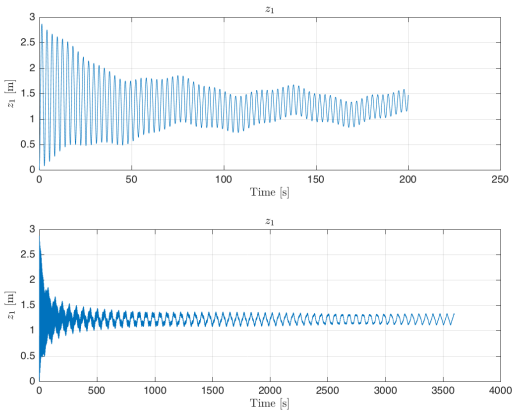

(e) Using the NLORLAM, input frequency is the natural frequency of 0.6694Hz

Figure A.18: Time-series for z_1 for five input frequencies

A.21 HHCS equations

A.21.1 PHCS equations

From appendix (A.8) the non-linear PHCS equations are repeated below. However, the equation for z_1 (A.137) is modified to take into account the AHCS. (A.137) is modified to (A.327) by replacing z_{d} with $z_{\mathrm{d,p}}$

$$\ddot{z}_1 = \frac{1}{(M_{\mathrm{hook,payload}} + A_{\mathrm{hook,payload}})} \Big[P_{\mathrm{p1}} A_{\mathrm{p}} - P_{\mathrm{p2}} A_{\mathrm{p}} + F_{\mathrm{water}} - F_{\mathrm{water}} + \rho_{\mathrm{water}} V_{\mathrm{d}} g - M_{\mathrm{hook,payload}} g - \frac{1}{2} \rho_{\mathrm{water}} C_{\mathrm{d,hook,payload}} D_{\mathrm{hook,payload}} |\dot{z}_1| \dot{z}_1 - k_{\mathrm{d}}(z_1 - z_{\mathrm{d,p}}) \Big] \tag{A.327}$$

$$\ddot{z}_{\mathrm{phc}} = \frac{1}{(M_{\mathrm{phc}} + A_{\mathrm{phc}})} \Big[- k_{\mathrm{c}}(z_{\mathrm{phc}} - z_{\mathrm{c}}) - \frac{1}{2} \rho_{\mathrm{water}} C_{\mathrm{d,phc}} D_{\mathrm{phc}} |\dot{z}_{\mathrm{phc}}| \dot{z}_{\mathrm{phc}} \Big] \tag{A.328}$$

$$\ddot{z}_{\mathrm{c}} = \frac{1}{(M_{\mathrm{c}})} \Big[- k_{\mathrm{c}}(z_{\mathrm{c}} - z_{\mathrm{in}}) - k_{\mathrm{c}}(z_{\mathrm{c}} - z_{\mathrm{phc}}) \Big] \tag{A.329}$$

(A.140) was modified by replacing z_{d} with $z_{\mathrm{d,p}}$ to form (A.330)

$$\ddot{z}_{\mathrm{d,p}} = \frac{1}{(M_{\mathrm{d}})} \Big[k_{\mathrm{d}}(-z_{\mathrm{d,p}} + z_{\mathrm{in}} - z_{\mathrm{d,a}}) - k_{\mathrm{d}}(z_{\mathrm{d,p}} - z_1) \Big] \tag{A.330}$$

$$\dot{P}_{\mathrm{p1}} = \frac{K}{V_{\mathrm{p11}}} \Big[- A_{\mathrm{p}}(\dot{z}_1 - \dot{z}_{\mathrm{phc}}) - Q_{\mathrm{r}} \Big] \tag{A.331}$$

$$\dot{Q}_{\mathrm{r}} = \frac{A}{\rho_{\mathrm{oil}} L} \Big[P_{\mathrm{p1}} - P_{\mathrm{a1}} - \frac{\mathrm{sign}(Q_{\mathrm{r}}) Q_{\mathrm{r}}^2}{(C_{\mathrm{discharge}} A)^2} \frac{\rho_{\mathrm{oil}}}{2} \Big] \tag{A.332}$$

$$\dot{V}_{\mathrm{in}} = Q_{\mathrm{r}} \tag{A.333}$$

$$P_{\mathrm{a1}} = P_{\mathrm{a1,1}} \Big(\frac{V_{\mathrm{a1,1}}}{V_{\mathrm{a1,1}} - V_{\mathrm{in}}} \Big)^n \tag{A.334}$$

$$\dot{P}_{\mathrm{p2}} = \frac{K}{V_{\mathrm{p21}}} [-A_{\mathrm{p}}(\dot{z}_{\mathrm{phc}} - \dot{z}_1) - Q_{\mathrm{r,2}}] \tag{A.335}$$

$$\dot{Q}_{\mathrm{r,2}} = \frac{A}{\rho_{\mathrm{oil}} L} \Big[P_{\mathrm{p2}} - P_{\mathrm{a3}} - \frac{\mathrm{sign}(Q_{\mathrm{r,2}}) Q_{\mathrm{r,2}}^2}{(C_{\mathrm{discharge}} A)^2} \frac{\rho_{\mathrm{oil}}}{2} \Big] \tag{A.336}$$

$$\dot{V}_{\mathrm{in,u}} = Q_{\mathrm{r,2}} \tag{A.337}$$

$$P_{\mathrm{a3}} = P_{\mathrm{a3,1}} \Big(\frac{V_{\mathrm{a3,1}}}{V_{\mathrm{a3,1}} - V_{\mathrm{in,u}}} \Big)^n \tag{A.338}$$

A.21.2 AHCS equations

Repeating (13.24) from section 13.4.1

$$\ddot{\phi}_{\mathrm{w}} = \frac{T_{\mathrm{e,max}} d + \Big(k_{\mathrm{d}}(z_{\mathrm{in}} - z_{\mathrm{d,p}} - z_{\mathrm{d,a}}) \Big) r_{\mathrm{w}} - \mathrm{sign}(\dot{\phi}_{\mathrm{w}}) \Big(\frac{2 T_{\mathrm{e,max}}}{0.05 \dot{z}_{\mathrm{d,a,max}}} (|\dot{\phi}_{\mathrm{w}} r_{\mathrm{w}}| - \dot{z}_{\mathrm{d,a,max}}) \Big) - B_{\mathrm{w}} \dot{\phi}_{\mathrm{w}}}{J_{\mathrm{w}}} \tag{A.339}$$

A.21.3 Including PI controller, open loop

The only difference is that (A.339) is replaced with (13.44) from section 13.5.3

$$\ddot{\phi}_{\mathrm{w}} = \frac{T_{\mathrm{e,max}}\Big([k_{\mathrm{p},1}+k_{\mathrm{i},1}]r_1(t) - k_{\mathrm{i},1}r_1(0) + [k_{\mathrm{p},2}+k_{\mathrm{i},2}]r_2(t) - k_{\mathrm{i},2}r_2(0)\Big) + \Big(k_{\mathrm{d}}(z_{\mathrm{in}} - z_{\mathrm{d,p}} - z_{\mathrm{d,a}})\Big)r_{\mathrm{w}}}{J_{\mathrm{w}}} + \frac{-\mathrm{sign}(\dot{\phi}_{\mathrm{w}})\Big(\frac{2T_{\mathrm{e,max}}}{0.05\dot{z}_{\mathrm{d,a,max}}}(|\dot{\phi}_{\mathrm{w}}r_{\mathrm{w}}| - \dot{z}_{\mathrm{d,a,max}})\Big) - B_{\mathrm{w}}\dot{\phi}_{\mathrm{w}}}{J_{\mathrm{w}}} \tag{A.340}$$

A.22 Non-linear HHCS state-space equations

The chosen state-space variables are shown in Table A.21.

Table A.21: q variables

state variable	original variable
q_1	z_1
q_2	$\dot{z}_1$
q_3	z_{phc}
q_4	$\dot{z}_{\mathrm{phc}}$
q_5	z_c
q_6	$\dot{z}_c$
q_7	$z_{\mathrm{d,p}}$
q_8	$\dot{z}_{\mathrm{d,p}}$
q_9	P_{p1}
q_{10}	Q_{r}
q_{11}	V_{in}
q_{12}	P_{p2}
q_{13}	$Q_{\mathrm{r,2}}$
q_{14}	$V_{\mathrm{in,u}}$
q_{15}	ϕ_{w}
q_{16}	$\dot{\phi}_{\mathrm{w}}$

A.22.1 Non-linear PHCS state-space equations

The state-space equations for the PHCS were found in appendix A.10, they are repeated below.

A.22.1.1 $\dot{q}_1$

$$\dot{q}_1 = q_2 \tag{A.341}$$

A.22.1.2 $\dot{q}_2$

(A.342) was modified to take into account the AHCS using (A.327), so use (A.342)

$$\dot{q}_2 = \frac{1}{\zeta_2} \left[q_9 A_\mathrm{p} - q_{12} A_\mathrm{p} + \eta_2 - \theta_2 \mathrm{sign}(q_2) q_2^2 - k_\mathrm{d}(q_1 - q_7) \right] \tag{A.342}$$

A.22.1.3 $\dot{q}_3$

$$\dot{q}_3 = q_4 \tag{A.343}$$

A.22.1.4 $\dot{q}_4$

$$\dot{q}_4 = \frac{1}{\zeta_4} \left[- k_\mathrm{c}(q_3 - q_5) - \eta_4 \mathrm{sign}(q_4) q_4^2 \right] \tag{A.344}$$

A.22.1.5 $\dot{q}_5$

$$\dot{q}_5 = q_6 \tag{A.345}$$

A.22.1.6 $\dot{q}_6$

$$\dot{q}_6 = \frac{1}{(M_\mathrm{c})} \left[- k_\mathrm{c}(q_5 - z_\mathrm{in}) - k_\mathrm{c}(q_5 - q_3) \right] \tag{A.346}$$

A.22.1.7 $\dot{q}_7$

$$\dot{q}_7 = q_8 \tag{A.347}$$

A.22.1.8 $\dot{q}_8$

(A.348) was modified to take into account the AHCS using (A.330)

$$\dot{q}_8 = \frac{1}{(M_\mathrm{d})} \left[k_\mathrm{d}(-q_7 + z_\mathrm{in} - q_{15} r_\mathrm{w}) - k_\mathrm{d}(q_7 - q_1) \right] \tag{A.348}$$

A.22.1.9 $\dot{q}_9$

$$\dot{q}_9 = \frac{K}{V_\mathrm{p11}} \left[- A_p(q_2 - q_4) - q_{10} \right] \tag{A.349}$$

A.22.1.10 $\dot{q}_{10}$

$$\dot{q}_{10} = \zeta_{10} \left[q_9 - P_\mathrm{a1,1} \left(\frac{V_\mathrm{a1,1}}{V_\mathrm{a1,1} - q_{11}} \right)^n - \eta_{10} q_{10}^2 \right] \tag{A.350}$$

A.22.1.11 $\dot{q}_{11}$

$$\dot{q}_{11} = q_{10} \tag{A.351}$$

A.22.1.12 $\dot{q}_{12}$

$$\dot{q}_{12} = \frac{K}{V_\mathrm{p21}} [-A_\mathrm{p}(q_4 - q_2) - q_{13}] \tag{A.352}$$

A.22.1.13 $\dot{q}_{13}$

$$\dot{q}_{13} = \zeta_{13}\Big[q_{12} - P_{\mathrm{a3,1}}\Big(\frac{V_{\mathrm{a3,1}}}{V_{\mathrm{a3,1}} - q_{14}}\Big)^{n} - \eta_{13}q_{13}^{2}\Big] \tag{A.353}$$

A.22.1.14 $\dot{q}_{14}$

$$\dot{q}_{14} = q_{13} \tag{A.354}$$

A.22.2 Non-linear AHCS state-space equations

A.22.2.1 $\dot{q}_{15}$

$$\dot{q}_{15} = q_{16} \tag{A.355}$$

A.22.2.2 $\dot{q}_{16}$

Putting (A.339) into state-space form

$$\dot{q}_{16} = \frac{T_{\mathrm{e,max}} d + \Big(k_{\mathrm{d}}(z_{\mathrm{in}} - q_7 - q_{15} r_{\mathrm{w}})\Big) r_{\mathrm{w}} - \mathrm{sign}(q_{16}) \Big(\frac{2T_{\mathrm{e,max}}}{0.05 \dot{z}_{\mathrm{d,a,max}}} (|q_{16} r_{\mathrm{w}}| - \dot{z}_{\mathrm{d,a,max}})\Big) - B_{\mathrm{w}} q_{16}}{J_{\mathrm{w}}} \tag{A.356}$$

A.22.2.3 Including PI controller open loop

Putting (A.340) into state-space form gives (A.357). (A.357) replaces (A.356).

$$\begin{aligned} \dot{q}_{16} = \\ \frac{T_{\mathrm{e,max}} \Big([k_{\mathrm{p},1} + k_{\mathrm{i},1}] r_1(t) - k_{\mathrm{i},1} r_1(0) + [k_{\mathrm{p},2} + k_{\mathrm{i},2}] r_2(t) - k_{\mathrm{i},2} r_2(0) \Big) + \Big(k_{\mathrm{d}}(z_{\mathrm{in}} - q_7 - q_{15} r_{\mathrm{w}})\Big) r_{\mathrm{w}}}{J_{\mathrm{w}}} + \\ \frac{-\mathrm{sign}(q_{16}) \Big(\frac{2T_{\mathrm{e,max}}}{0.05 \dot{z}_{\mathrm{d,a,max}}} (|q_{16} r_{\mathrm{w}}| - \dot{z}_{\mathrm{d,a,max}})\Big) - B_{\mathrm{w}} q_{16}}{J_{\mathrm{w}}} \end{aligned} \tag{A.357}$$

A.23 Linear HHCS state-space equations

A.23.1 Linear PHCS state-space equations

The linearized PHCS equations from section (A.12) are repeated below.

A.23.1.1 $\dot{q}_1$

$$\dot{q}_1 = q_2 \tag{A.358}$$

A.23.1.2 $\dot{q}_2$

$$\begin{aligned} \dot{q}_2 = \frac{1}{\alpha_2} \Big[& q_9 A_{\mathrm{p}} - q_{12} A_{\mathrm{p}} \\ & -\gamma_2 q_2 \\ & -k_{\mathrm{d}} q_1 + k_{\mathrm{d}} q_7 + F_{\mathrm{U},2} \Big] \end{aligned} \tag{A.359}$$

A.23.1.3 $\dot{q}_3$

$$\dot{q}_3 = q_4 \tag{A.360}$$

A.23.1.4 $\dot{q}_4$

$$\dot{q}_4 = \frac{1}{\alpha_4} \Big[-k_{\mathrm{c}}(q_3 - q_5) - \gamma_4 q_4 + F_{\mathrm{U},4} \Big] \tag{A.361}$$

A.23.1.5 $\dot{q}_5$

$$\dot{q}_5 = q_6 \tag{A.362}$$

A.23.1.6 $\dot{q}_6$

$$\dot{q}_6 = \frac{1}{M_\mathrm{c}}\Big[k_\mathrm{c}q_3 - 2k_\mathrm{c}q_5 + k_\mathrm{c}z_\mathrm{in}\Big] \tag{A.363}$$

A.23.1.7 $\dot{q}_7$

$$\dot{q}_7 = q_8 \tag{A.364}$$

A.23.1.8 $\dot{q}_8$

Using (A.348) gives (A.365)

$$\dot{q}_8 = \frac{1}{(M_\mathrm{d})}\Big[k_\mathrm{d}q_1 - 2k_\mathrm{d}q_7 - k_\mathrm{d}r_\mathrm{w}q_{15} + k_\mathrm{d}z_\mathrm{in}\Big] \tag{A.365}$$

A.23.1.9 $\dot{q}_9$

$$\dot{q}_9 = \frac{K}{V_\mathrm{p11}}\Big[-A_p(q_2 - q_4) - q_{10}\Big] \tag{A.366}$$

A.23.1.10 $\dot{q}_{10}$

$$\dot{q}_{10} = \frac{A}{\rho_\mathrm{oil}L}\Big[q_9 - \gamma_{10}q_{11} - \epsilon_{10}q_{10} + F_{\mathrm{U},10}\Big] \tag{A.367}$$

A.23.1.11 $\dot{q}_{11}$

$$\dot{q}_{11} = q_{10} \tag{A.368}$$

A.23.1.12 $\dot{q}_{12}$

$$\dot{q}_{12} = \frac{K}{V_\mathrm{p21}}[-A_\mathrm{p}(q_4 - q_2) - q_{13}] \tag{A.369}$$

A.23.1.13 $\dot{q}_{13}$

$$\dot{q}_{13} = \frac{A}{\rho_\mathrm{oil}L}\Big[q_{12} - \gamma_{13}q_{14} - \epsilon_{13}q_{13} + F_{\mathrm{U},13}\Big] \tag{A.370}$$

A.23.1.14 $\dot{q}_{14}$

$$\dot{q}_{14} = q_{13} \tag{A.371}$$

A.23.2 Linear AHCS state-space equations

The AHCS state-space equations are always linear and are the same as in appendix A.22.2. They are repeated here.

A.23.2.1 $\dot{q}_{15}$

$$\dot{q}_{15} = q_{16} \tag{A.372}$$

A.23.2.2 $\dot{q}_{16}$

$$\dot{q}_{16} = \frac{T_{\mathrm{e,max}} d + \Big(k_{\mathrm{d}}(z_{\mathrm{in}} - q_7 - q_{15} r_{\mathrm{w}})\Big) r_{\mathrm{w}} - \mathrm{sign}(q_{16}) \Big(\frac{2T_{\mathrm{e,max}}}{0.05 \dot{z}_{\mathrm{d,a,max}}} (|q_{16} r_{\mathrm{w}}| - \dot{z}_{\mathrm{d,a,max}})\Big) - B_{\mathrm{w}} q_{16}}{J_{\mathrm{w}}} \tag{A.373}$$

Expanding

$$\dot{q}_{16} = \frac{T_{\mathrm{e,max}} d + r_{\mathrm{w}} k_{\mathrm{d}}(z_{\mathrm{in}} - q_7 - q_{15} r_{\mathrm{w}}) - \mathrm{sign}(q_{16}) \Big(\frac{2T_{\mathrm{e,max}}}{0.05 \dot{z}_{\mathrm{d,a,max}}} (|q_{16} r_{\mathrm{w}}| - \dot{z}_{\mathrm{d,a,max}})\Big) - B_{\mathrm{w}} q_{16}}{J_{\mathrm{w}}} \tag{A.374}$$

Removing $\mathrm{sign}(q_{16})$ and the absolute value sign

$$\dot{q}_{16} = \frac{T_{\mathrm{e,max}} d + r_{\mathrm{w}} k_{\mathrm{d}} z_{\mathrm{in}} - r_{\mathrm{w}} k_{\mathrm{d}} q_7 - r_{\mathrm{w}}^2 k_{\mathrm{d}} q_{15} - \frac{2T_{\mathrm{e,max}}}{0.05 \dot{z}_{\mathrm{d,a,max}}} q_{16} r_{\mathrm{w}} + \frac{2T_{\mathrm{e,max}}}{0.05 \dot{z}_{\mathrm{d,a,max}}} \dot{z}_{\mathrm{d,a,max}} - B_{\mathrm{w}} q_{16}}{J_{\mathrm{w}}} \tag{A.375}$$

Defining

$$F_{\mathrm{R},16} = \frac{2T_{\mathrm{e,max}}}{0.05 \dot{z}_{\mathrm{d,a,max}}} \dot{z}_{\mathrm{d,a,max}} \tag{A.376}$$

Inserting $F_{\mathrm{R},16}$ and collecting like terms

$$\dot{q}_{16} = \frac{T_{\mathrm{e,max}} d + r_{\mathrm{w}} k_{\mathrm{d}} z_{\mathrm{in}} - r_{\mathrm{w}} k_{\mathrm{d}} q_7 - r_{\mathrm{w}}^2 k_{\mathrm{d}} q_{15} + q_{16}(-\frac{2T_{\mathrm{e,max}}}{0.05 \dot{z}_{\mathrm{d,a,max}}} r_{\mathrm{w}} - B_{\mathrm{w}}) + F_{\mathrm{R},16}}{J_{\mathrm{w}}} \tag{A.377}$$

For matrices see section A.23.3

A.23.2.3 Including PI controller open loop

Repeating (A.357)

$$\dot{q}_{16} = \frac{T_{\mathrm{e,max}} \Big([k_{\mathrm{p},1} + k_{\mathrm{i},1}] r_1(t) - k_{\mathrm{i},1} r_1(0) + [k_{\mathrm{p},2} + k_{\mathrm{i},2}] r_2(t) - k_{\mathrm{i},2} r_2(0)\Big) + \Big(k_{\mathrm{d}}(z_{\mathrm{in}} - q_7 - q_{15} r_{\mathrm{w}})\Big) r_{\mathrm{w}}}{J_{\mathrm{w}}} + \frac{-\mathrm{sign}(q_{16}) \Big(\frac{2T_{\mathrm{e,max}}}{0.05 \dot{z}_{\mathrm{d,a,max}}} (|q_{16} r_{\mathrm{w}}| - \dot{z}_{\mathrm{d,a,max}})\Big) - B_{\mathrm{w}} q_{16}}{J_{\mathrm{w}}} \tag{A.378}$$

Simplifying

$$\dot{q}_{16} = \frac{T_{\mathrm{e,max}}[k_{\mathrm{p},1} + k_{\mathrm{i},1}] r_1(t) - T_{\mathrm{e,max}} k_{\mathrm{i},1} r_1(0) + T_{\mathrm{e,max}}[k_{\mathrm{p},2} + k_{\mathrm{i},2}] r_2(t) - T_{\mathrm{e,max}} k_{\mathrm{i},2} r_2(0) + r_{\mathrm{w}} k_{\mathrm{d}}(z_{\mathrm{in}} - q_7 - q_{15} r_{\mathrm{w}})}{J_{\mathrm{w}}} + \frac{-\mathrm{sign}(q_{16}) \frac{2T_{\mathrm{e,max}}}{0.05 \dot{z}_{\mathrm{d,a,max}}} (|q_{16} r_{\mathrm{w}}| - \dot{z}_{\mathrm{d,a,max}}) - B_{\mathrm{w}} q_{16}}{J_{\mathrm{w}}} \tag{A.379}$$

The sign(q_{16}) term is removed since it creates a time-dependent coefficient. The abs function is removed since it does not work for the state-space system with constant coefficients.
For readability new constants are defined for (A.379)

$$\xi_{16} = T_{\mathrm{e,max}}[k_{\mathrm{p},1} + k_{\mathrm{i},1}] \tag{A.380}$$

$$o_{16} = T_{\mathrm{e,max}} k_{\mathrm{i},1} r_1(0) \tag{A.381}$$

$$\pi_{16} = T_{\mathrm{e,max}}[k_{\mathrm{p},2} + k_{\mathrm{i},2}] \tag{A.382}$$

$$\rho_{16} = T_{\mathrm{e,max}} k_{\mathrm{i},2} r_2(0) \tag{A.383}$$

$$\sigma_{16} = \frac{2T_{\mathrm{e,max}}}{0.05\dot{z}_{\mathrm{d,a,max}}} \tag{A.384}$$

Substituting in the new constants.

$$\begin{aligned}\dot{q}_{16} = \\ \frac{\xi_{16} r_1(t) - o_{16} + \pi_{16} r_2(t) - \rho_{16} + r_{\mathrm{w}} k_{\mathrm{d}}(z_{\mathrm{in}} - q_7 - q_{15} r_{\mathrm{w}})}{J_{\mathrm{w}}} + \\ \frac{-\sigma_{16}(q_{16} r_{\mathrm{w}} - \dot{z}_{\mathrm{d,a,max}}) - B_{\mathrm{w}} q_{16}}{J_{\mathrm{w}}}\end{aligned} \tag{A.385}$$

Collecting like terms

$$\begin{aligned}\dot{q}_{16} = \\ \frac{\xi_{16} r_1(t) + \pi_{16} r_2(t) - o_{16} - \rho_{16} + \sigma_{16}\dot{z}_{\mathrm{d,a,max}} + r_{\mathrm{w}} k_{\mathrm{d}} z_{\mathrm{in}} - r_{\mathrm{w}} k_{\mathrm{d}} q_7 - r_{\mathrm{w}}^2 k_{\mathrm{d}} q_{15}}{J_{\mathrm{w}}} + \\ \frac{q_{16}(-\sigma_{16} r_{\mathrm{w}} - B_{\mathrm{w}})}{J_{\mathrm{w}}}\end{aligned} \tag{A.386}$$

Defining the constant terms as

$$F_{\mathrm{Q},16} = -o_{16} - \rho_{16} + \sigma_{16}\dot{z}_{\mathrm{d,a,max}} \tag{A.387}$$

Substituting

$$\begin{aligned}\dot{q}_{16} = \\ \frac{\xi_{16} r_1(t) + \pi_{16} r_2(t) + F_{\mathrm{Q},16} + r_{\mathrm{w}} k_{\mathrm{d}} z_{\mathrm{in}} - r_{\mathrm{w}} k_{\mathrm{d}} q_7 - r_{\mathrm{w}}^2 k_{\mathrm{d}} q_{15}}{J_{\mathrm{w}}} + \\ \frac{q_{16}(-\sigma_{16} r_{\mathrm{w}} - B_{\mathrm{w}})}{J_{\mathrm{w}}}\end{aligned} \tag{A.388}$$

For matrices see section A.23.4.

A.23.3 A, B, C, D matrices

The outputs of interest are $y_1 = z_1 = q_1$ and $y_2 = F_{\mathrm{d}} = k_{\mathrm{d}}(z_{\mathrm{in}} - z_{\mathrm{d,p}} - z_{\mathrm{d,a}}) = k_{\mathrm{d}}(z_{\mathrm{in}} - q_7 - q_{15} r_{\mathrm{w}})$. The state-space equations are re-arranged into matrix form, shown in (A.389) and (A.390).

$$
\begin{bmatrix} \dot{q}_1 \\ \dot{q}_2 \\ \dot{q}_3 \\ \dot{q}_4 \\ \dot{q}_5 \\ \dot{q}_6 \\ \dot{q}_7 \\ \dot{q}_8 \\ \dot{q}_9 \\ \dot{q}_{10} \\ \dot{q}_{11} \\ \dot{q}_{12} \\ \dot{q}_{13} \\ \dot{q}_{14} \\ \dot{q}_{15} \\ \dot{q}_{16} \end{bmatrix} =
\begin{bmatrix}
0 & 1 & 0 & 0 & 0 & 0 & 0 & 0 & 0 & 0 & 0 & 0 & 0 & 0 & 0 & 0 \\
\frac{-k_\mathrm{d}}{\alpha_2} & \frac{-\gamma_2}{\alpha_2} & 0 & 0 & 0 & 0 & \frac{k_\mathrm{d}}{\alpha_2} & 0 & \frac{A_\mathrm{p}}{\alpha_2} & 0 & 0 & \frac{-A_\mathrm{p}}{\alpha_2} & 0 & 0 & 0 & 0 \\
0 & 0 & 0 & 1 & 0 & 0 & 0 & 0 & 0 & 0 & 0 & 0 & 0 & 0 & 0 & 0 \\
0 & 0 & \frac{-k_\mathrm{c}}{\alpha_4} & \frac{-\gamma_4}{\alpha_4} & \frac{k_\mathrm{c}}{\alpha_4} & 0 & 0 & 0 & 0 & 0 & 0 & 0 & 0 & 0 & 0 & 0 \\
0 & 0 & 0 & 0 & 0 & 1 & 0 & 0 & 0 & 0 & 0 & 0 & 0 & 0 & 0 & 0 \\
0 & 0 & \frac{k_\mathrm{c}}{M_\mathrm{c}} & 0 & \frac{-2k_\mathrm{c}}{M_\mathrm{c}} & 0 & 0 & 0 & 0 & 0 & 0 & 0 & 0 & 0 & 0 & 0 \\
0 & 0 & 0 & 0 & 0 & 0 & 0 & 1 & 0 & 0 & 0 & 0 & 0 & 0 & 0 & 0 \\
\frac{k_\mathrm{d}}{M_\mathrm{d}} & 0 & 0 & 0 & 0 & 0 & \frac{-2k_\mathrm{d}}{M_\mathrm{d}} & 0 & 0 & 0 & 0 & 0 & 0 & 0 & \frac{-k_\mathrm{d} r_\mathrm{w}}{M_\mathrm{d}} & 0 \\
0 & \frac{-KA_\mathrm{p}}{V_\mathrm{p11}} & 0 & \frac{KA_\mathrm{p}}{V_\mathrm{p11}} & 0 & 0 & 0 & 0 & 0 & \frac{-K}{V_\mathrm{p11}} & 0 & 0 & 0 & 0 & 0 & 0 \\
0 & 0 & 0 & 0 & 0 & 0 & 0 & 0 & \frac{A}{\rho_\mathrm{oil} L} & \frac{-A\epsilon_{10}}{\rho_\mathrm{oil} L} & \frac{-A\gamma_{10}}{\rho_\mathrm{oil} L} & 0 & 0 & 0 & 0 & 0 \\
0 & 0 & 0 & 0 & 0 & 0 & 0 & 0 & 0 & 1 & 0 & 0 & 0 & 0 & 0 & 0 \\
0 & \frac{KA_\mathrm{p}}{V_\mathrm{p21}} & 0 & \frac{-KA_\mathrm{p}}{V_\mathrm{p21}} & 0 & 0 & 0 & 0 & 0 & 0 & 0 & 0 & \frac{-K}{V_\mathrm{p21}} & 0 & 0 & 0 \\
0 & 0 & 0 & 0 & 0 & 0 & 0 & 0 & 0 & 0 & 0 & \frac{A}{\rho_\mathrm{oil} L} & \frac{-A\epsilon_{13}}{\rho_\mathrm{oil} L} & \frac{-A\gamma_{13}}{\rho_\mathrm{oil} L} & 0 & 0 \\
0 & 0 & 0 & 0 & 0 & 0 & 0 & 0 & 0 & 0 & 0 & 0 & 1 & 0 & 0 & 0 \\
0 & 0 & 0 & 0 & 0 & 0 & 0 & 0 & 0 & 0 & 0 & 0 & 0 & 0 & 0 & 1 \\
0 & 0 & 0 & 0 & 0 & 0 & \frac{-r_\mathrm{w} k_\mathrm{d}}{J_\mathrm{w}} & 0 & 0 & 0 & 0 & 0 & 0 & 0 & \frac{-r_\mathrm{w}^2 k_\mathrm{d}}{J_\mathrm{w}} & \frac{(-\frac{2T_\mathrm{e,max}}{0.05 \dot{z}_\mathrm{d,a,max}} r_\mathrm{w} - B_\mathrm{w})}{J_\mathrm{w}}
\end{bmatrix}
\begin{bmatrix} q_1 \\ q_2 \\ q_3 \\ q_4 \\ q_5 \\ q_6 \\ q_7 \\ q_8 \\ q_9 \\ q_{10} \\ q_{11} \\ q_{12} \\ q_{13} \\ q_{14} \\ q_{15} \\ q_{16} \end{bmatrix}
+
\begin{bmatrix}
0 & 0 & 0 & 0 & 0 & 0 & 0 \\
\frac{1}{\alpha_2} & 0 & 0 & 0 & 0 & 0 & 0 \\
0 & 0 & 0 & 0 & 0 & 0 & 0 \\
0 & \frac{1}{\alpha_4} & 0 & 0 & 0 & 0 & 0 \\
0 & 0 & 0 & 0 & 0 & 0 & 0 \\
0 & 0 & \frac{k_\mathrm{c}}{M_\mathrm{c}} & 0 & 0 & 0 & 0 \\
0 & 0 & 0 & 0 & 0 & 0 & 0 \\
0 & 0 & \frac{k_\mathrm{d}}{M_\mathrm{d}} & 0 & 0 & 0 & 0 \\
0 & 0 & 0 & 0 & 0 & 0 & 0 \\
0 & 0 & 0 & \frac{A}{\rho_\mathrm{oil} L} & 0 & 0 & 0 \\
0 & 0 & 0 & 0 & 0 & 0 & 0 \\
0 & 0 & 0 & 0 & 0 & 0 & 0 \\
0 & 0 & 0 & 0 & \frac{A}{\rho_\mathrm{oil} L} & 0 & 0 \\
0 & 0 & 0 & 0 & 0 & 0 & 0 \\
0 & 0 & 0 & 0 & 0 & 0 & 0 \\
0 & 0 & \frac{r_\mathrm{w} k_\mathrm{d}}{J_\mathrm{w}} & 0 & 0 & \frac{1}{J_\mathrm{w}} & \frac{T_\mathrm{e,max}}{J_\mathrm{w}}
\end{bmatrix}
\begin{bmatrix} F_{\mathrm{U},2} \\ F_{\mathrm{U},4} \\ z_{\mathrm{in}(t)} \\ F_{\mathrm{U},10} \\ F_{\mathrm{U},13} \\ F_{\mathrm{R},16} \\ d(t) \end{bmatrix}
\tag{A.389}
$$

$$\begin{bmatrix} y_1 \\ y_2 \end{bmatrix} = \begin{bmatrix} 1 & 0 & 0 & 0 & 0 & 0 & 0 & 0 & 0 & 0 & 0 & 0 & 0 & 0 & 0 & 0 \\ 0 & 0 & 0 & 0 & 0 & 0 & -k_{\mathrm{d}} & 0 & 0 & 0 & 0 & 0 & 0 & 0 & -k_{\mathrm{d}} r_{\mathrm{w}} & 0 \end{bmatrix} \begin{bmatrix} q_1 \\ q_2 \\ q_3 \\ q_4 \\ q_5 \\ q_6 \\ q_7 \\ q_8 \\ q_9 \\ q_{10} \\ q_{11} \\ q_{12} \\ q_{13} \\ q_{14} \\ q_{15} \\ q_{16} \end{bmatrix} + \begin{bmatrix} 0 & 0 & 0 & 0 & 0 & 0 & 0 \\ 0 & 0 & k_{\mathrm{d}} & 0 & 0 & 0 & 0 \end{bmatrix} \begin{bmatrix} F_{\mathrm{U},2} \\ F_{\mathrm{U},4} \\ z_{\mathrm{in}(t)} \\ F_{\mathrm{U},10} \\ F_{\mathrm{U},13} \\ F_{\mathrm{R},16} \\ d(t) \end{bmatrix} \tag{A.390}$$

A.23.4 Open loop A, B, C, D matrices

The outputs of interest are $y_1 = z_1 = q_1$ and $y_2 = F_\mathrm{d} = k_\mathrm{d}(z_\mathrm{in} - z_\mathrm{d,p} - z_\mathrm{d,a}) = k_\mathrm{d}(z_\mathrm{in} - q_7 - q_{15} r_\mathrm{w})$. The state-space equations are re-arranged into matrix form, shown in (A.391) and (A.392).

$$
\begin{bmatrix} \dot{q}_1 \\ \dot{q}_2 \\ \dot{q}_3 \\ \dot{q}_4 \\ \dot{q}_5 \\ \dot{q}_6 \\ \dot{q}_7 \\ \dot{q}_8 \\ \dot{q}_9 \\ \dot{q}_{10} \\ \dot{q}_{11} \\ \dot{q}_{12} \\ \dot{q}_{13} \\ \dot{q}_{14} \\ \dot{q}_{15} \\ \dot{q}_{16} \end{bmatrix} =
\begin{bmatrix}
0 & 1 & 0 & 0 & 0 & 0 & 0 & 0 & 0 & 0 & 0 & 0 & 0 & 0 & 0 & 0 \\
\frac{-k_{\mathrm{d}}}{\alpha_2} & \frac{-\gamma_2}{\alpha_2} & 0 & 0 & 0 & 0 & \frac{k_{\mathrm{d}}}{\alpha_2} & 0 & \frac{A_{\mathrm{p}}}{\alpha_2} & 0 & 0 & \frac{-A_{\mathrm{p}}}{\alpha_2} & 0 & 0 & 0 & 0 \\
0 & 0 & 0 & 1 & 0 & 0 & 0 & 0 & 0 & 0 & 0 & 0 & 0 & 0 & 0 & 0 \\
0 & 0 & \frac{-k_{\mathrm{c}}}{\alpha_4} & \frac{-\gamma_4}{\alpha_4} & \frac{k_{\mathrm{c}}}{\alpha_4} & 0 & 0 & 0 & 0 & 0 & 0 & 0 & 0 & 0 & 0 & 0 \\
0 & 0 & 0 & 0 & 0 & 1 & 0 & 0 & 0 & 0 & 0 & 0 & 0 & 0 & 0 & 0 \\
0 & 0 & \frac{k_{\mathrm{c}}}{M_{\mathrm{c}}} & 0 & \frac{-2k_{\mathrm{c}}}{M_{\mathrm{c}}} & 0 & 0 & 0 & 0 & 0 & 0 & 0 & 0 & 0 & 0 & 0 \\
0 & 0 & 0 & 0 & 0 & 0 & 0 & 1 & 0 & 0 & 0 & 0 & 0 & 0 & 0 & 0 \\
\frac{k_{\mathrm{d}}}{M_{\mathrm{d}}} & 0 & 0 & 0 & 0 & 0 & \frac{-2k_{\mathrm{d}}}{M_{\mathrm{d}}} & 0 & 0 & 0 & 0 & 0 & 0 & 0 & \frac{-k_{\mathrm{d}}r_{\mathrm{w}}}{M_{\mathrm{d}}} & 0 \\
0 & \frac{-KA_{\mathrm{p}}}{V_{\mathrm{p}11}} & 0 & \frac{KA_{\mathrm{p}}}{V_{\mathrm{p}11}} & 0 & 0 & 0 & 0 & \frac{-K}{V_{\mathrm{p}11}} & 0 & 0 & 0 & 0 & 0 & 0 & 0 \\
0 & 0 & 0 & 0 & 0 & 0 & 0 & 0 & \frac{A}{\rho_{\mathrm{oil}}L} & \frac{-A\epsilon_{10}}{\rho_{\mathrm{oil}}L} & \frac{-A\gamma_{10}}{\rho_{\mathrm{oil}}L} & 0 & 0 & 0 & 0 & 0 \\
0 & 0 & 0 & 0 & 0 & 0 & 0 & 0 & 0 & 1 & 0 & 0 & 0 & 0 & 0 & 0 \\
0 & \frac{KA_{\mathrm{p}}}{V_{\mathrm{p}21}} & 0 & \frac{-KA_{\mathrm{p}}}{V_{\mathrm{p}21}} & 0 & 0 & 0 & 0 & 0 & 0 & 0 & 0 & \frac{-K}{V_{\mathrm{p}21}} & 0 & 0 & 0 \\
0 & 0 & 0 & 0 & 0 & 0 & 0 & 0 & 0 & 0 & 0 & \frac{A}{\rho_{\mathrm{oil}}L} & \frac{-A\epsilon_{13}}{\rho_{\mathrm{oil}}L} & \frac{-A\gamma_{13}}{\rho_{\mathrm{oil}}L} & 0 & 0 \\
0 & 0 & 0 & 0 & 0 & 0 & 0 & 0 & 0 & 0 & 0 & 0 & 1 & 0 & 0 & 0 \\
0 & 0 & 0 & 0 & 0 & 0 & 0 & 0 & 0 & 0 & 0 & 0 & 0 & 0 & 0 & 1 \\
0 & 0 & 0 & 0 & 0 & 0 & \frac{-r_{\mathrm{w}}k_{\mathrm{d}}}{J_{\mathrm{w}}} & 0 & 0 & 0 & 0 & 0 & 0 & 0 & \frac{-r_{\mathrm{w}}^2k_{\mathrm{d}}}{J_{\mathrm{w}}} & \frac{(-\sigma_{16}r_{\mathrm{w}}-B_{\mathrm{w}})}{J_{\mathrm{w}}}
\end{bmatrix}
\begin{bmatrix} q_1 \\ q_2 \\ q_3 \\ q_4 \\ q_5 \\ q_6 \\ q_7 \\ q_8 \\ q_9 \\ q_{10} \\ q_{11} \\ q_{12} \\ q_{13} \\ q_{14} \\ q_{15} \\ q_{16} \end{bmatrix}
$$

$$
+
\begin{bmatrix}
0 & 0 & 0 & 0 & 0 & 0 & 0 & 0 \\
\frac{1}{\alpha_2} & 0 & 0 & 0 & 0 & 0 & 0 & 0 \\
0 & 0 & 0 & 0 & 0 & 0 & 0 & 0 \\
0 & \frac{1}{\alpha_4} & 0 & 0 & 0 & 0 & 0 & 0 \\
0 & 0 & 0 & 0 & 0 & 0 & 0 & 0 \\
0 & 0 & \frac{k_{\mathrm{c}}}{M_{\mathrm{c}}} & 0 & 0 & 0 & 0 & 0 \\
0 & 0 & 0 & 0 & 0 & 0 & 0 & 0 \\
0 & 0 & \frac{k_{\mathrm{d}}}{M_{\mathrm{d}}} & 0 & 0 & 0 & 0 & 0 \\
0 & 0 & 0 & 0 & 0 & 0 & 0 & 0 \\
0 & 0 & 0 & \frac{A}{\rho_{\mathrm{oil}}L} & 0 & 0 & 0 & 0 \\
0 & 0 & 0 & 0 & 0 & 0 & 0 & 0 \\
0 & 0 & 0 & 0 & 0 & 0 & 0 & 0 \\
0 & 0 & 0 & 0 & \frac{A}{\rho_{\mathrm{oil}}L} & 0 & 0 & 0 \\
0 & 0 & 0 & 0 & 0 & 0 & 0 & 0 \\
0 & 0 & 0 & 0 & 0 & 0 & 0 & 0 \\
0 & 0 & \frac{r_{\mathrm{w}}k_{\mathrm{d}}}{J_{\mathrm{w}}} & 0 & 0 & \frac{1}{J_{\mathrm{w}}} & \frac{\xi_{16}}{J_{\mathrm{w}}} & \frac{\pi_{16}}{J_{\mathrm{w}}}
\end{bmatrix}
\begin{bmatrix} F_{\mathrm{U},2} \\ F_{\mathrm{U},4} \\ z_{\mathrm{in}(t)} \\ F_{\mathrm{U},10} \\ F_{\mathrm{U},13} \\ F_{\mathrm{Q},16} \\ r_1(t) \\ r_2(t) \end{bmatrix}
\tag{A.391}
$$

$$\begin{bmatrix} y_1 \\ y_2 \end{bmatrix} = \begin{bmatrix} 1 & 0 & 0 & 0 & 0 & 0 & 0 & 0 & 0 & 0 & 0 & 0 & 0 & 0 & 0 & 0 \\ 0 & 0 & 0 & 0 & 0 & 0 & -k_{\mathrm{d}} & 0 & 0 & 0 & 0 & 0 & 0 & 0 & -k_{\mathrm{d}} r_{\mathrm{w}} & 0 \end{bmatrix} \begin{bmatrix} q_1 \\ q_2 \\ q_3 \\ q_4 \\ q_5 \\ q_6 \\ q_7 \\ q_8 \\ q_9 \\ q_{10} \\ q_{11} \\ q_{12} \\ q_{13} \\ q_{14} \\ q_{15} \\ q_{16} \end{bmatrix} + \begin{bmatrix} 0 & 0 & 0 & 0 & 0 & 0 & 0 & 0 \\ 0 & 0 & k_{\mathrm{d}} & 0 & 0 & 0 & 0 & 0 \end{bmatrix} \begin{bmatrix} F_{\mathrm{U},2} \\ F_{\mathrm{U},4} \\ z_{\mathrm{in}(t)} \\ F_{\mathrm{U},10} \\ F_{\mathrm{U},13} \\ F_{\mathrm{Q},16} \\ r_1(t) \\ r_2(t) \end{bmatrix} \tag{A.392}$$

A.24 Verifying Simulink results with MATLAB results

To verify that Simulink is correctly solving the system of equations the equations were implemented in MATLAB and ode23s was used to solve the equations. ode23s was used in MATLAB and Simulink since the problem is stiff. Another stiff solver, ode15s, was tried in MATLAB and Simulink. For MATLAB and Simulink, ode15s gives the same result as ode23s when using relative tolerance (RelTol) of 1e-7 but if use RelTol=1e-3 then there is a difference in result between ode15s and ode23s (in MATLAB and Simulink). For MATLAB and Simulink tried ode15s with RelTol=1e-7 gives essentially the same result as ode23s with 1e-3. This means ode23s is more effective for this problem since a lower relative tolerance is needed to have the same result.

To verify the results, ode23s with RelTol=1e-3 (default value) for MATLAB and Simulink was used. See Figures A.19, A.20, A.21, and A.22 for the results. The input signal z_{in} is the same for MATLAB and Simulink, shown in Figure A.22. The design condition is used, period of 8s and amplitude of 1.25m. The results match essentially exactly. This is shown in Figure A.23 where the time-series for z_1 from 624s to 625s is enlarged, showing a small difference between MATLAB and Simulink results. Since the results from MATLAB and Simulink are nearly the same it is reasoned Simulink solves the equations correctly meaning Simulink and MATLAB can be used equivalently.

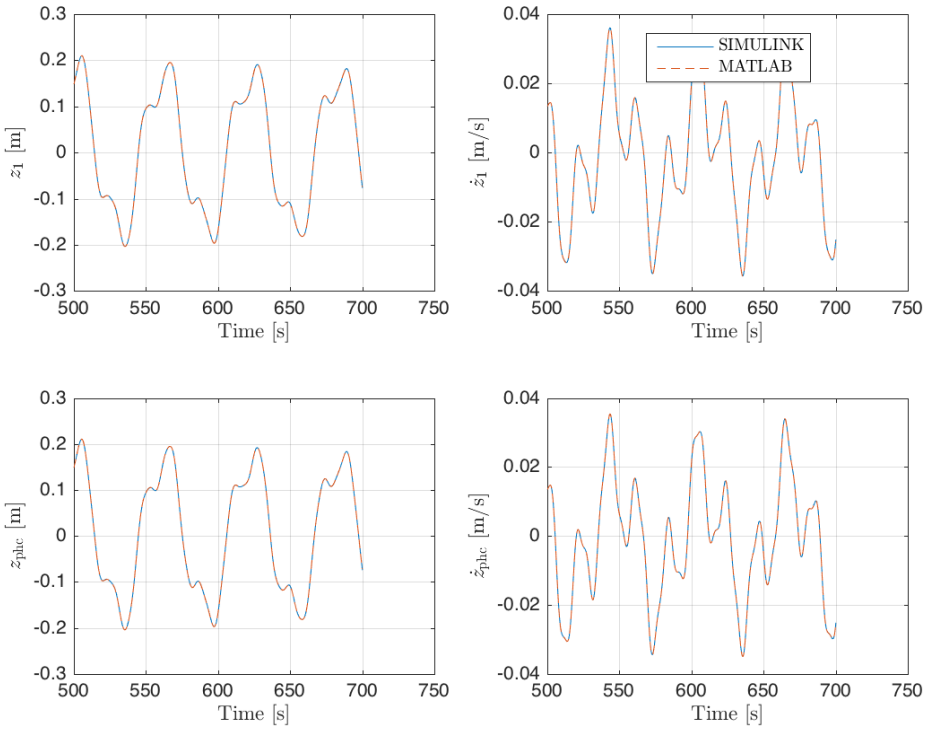

Figure A.19: z_1, $\dot{z}_1$, z_{phc}, $\dot{z}_{\text{phc}}$ time series

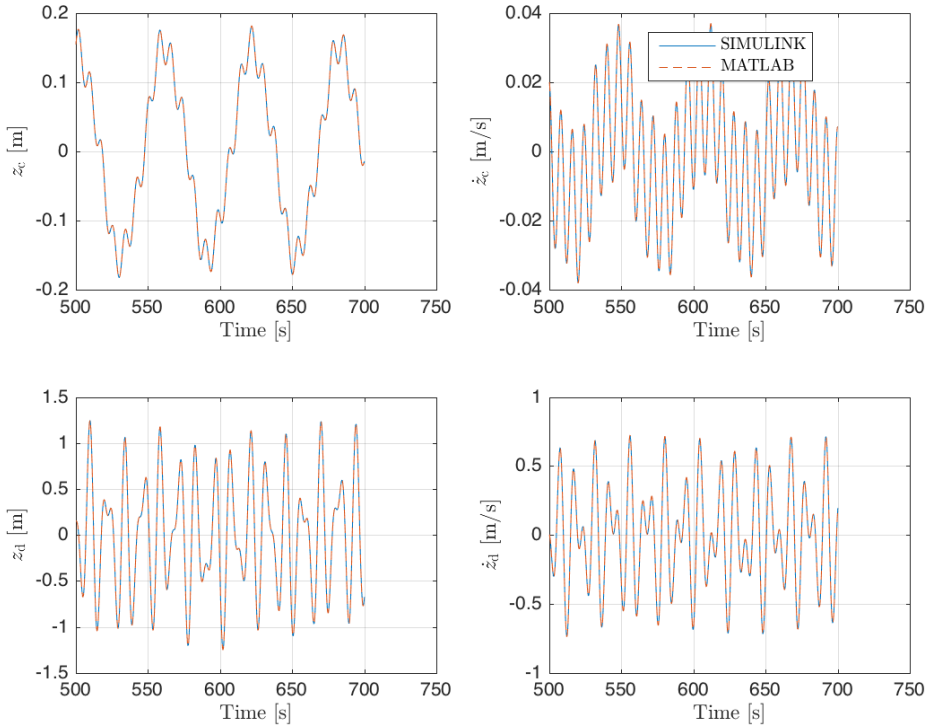

Figure A.20: z_c, $\dot{z}_c$, z_d, $\dot{z}_d$ time series

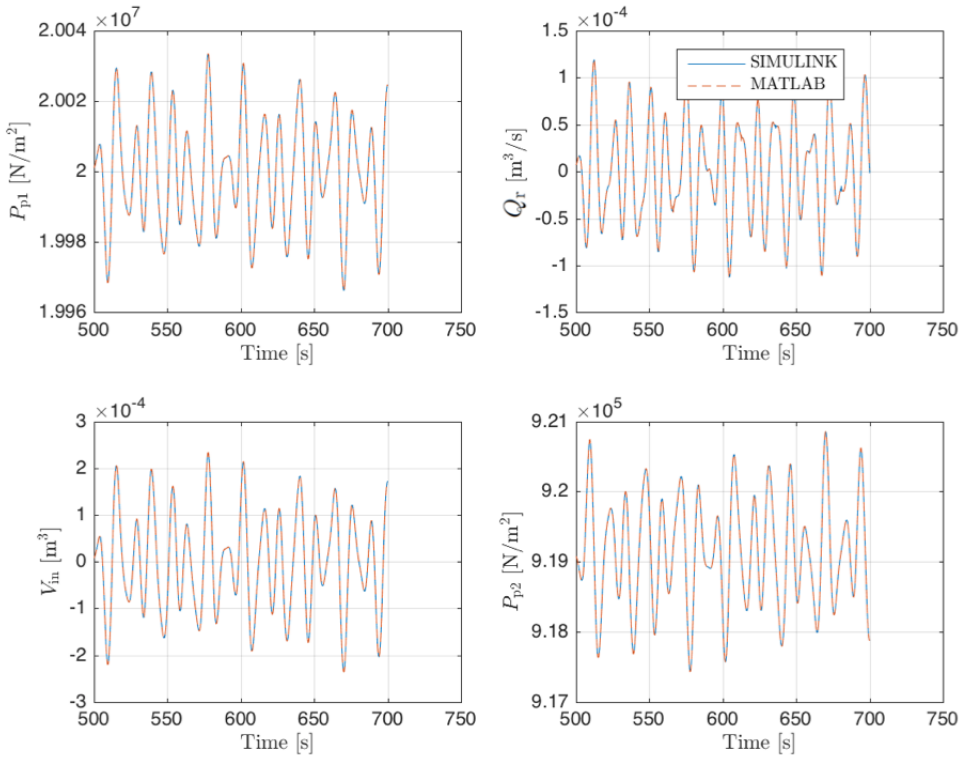

Figure A.21: P_{p1}, Q_r,V_{in},P_{p2} time series

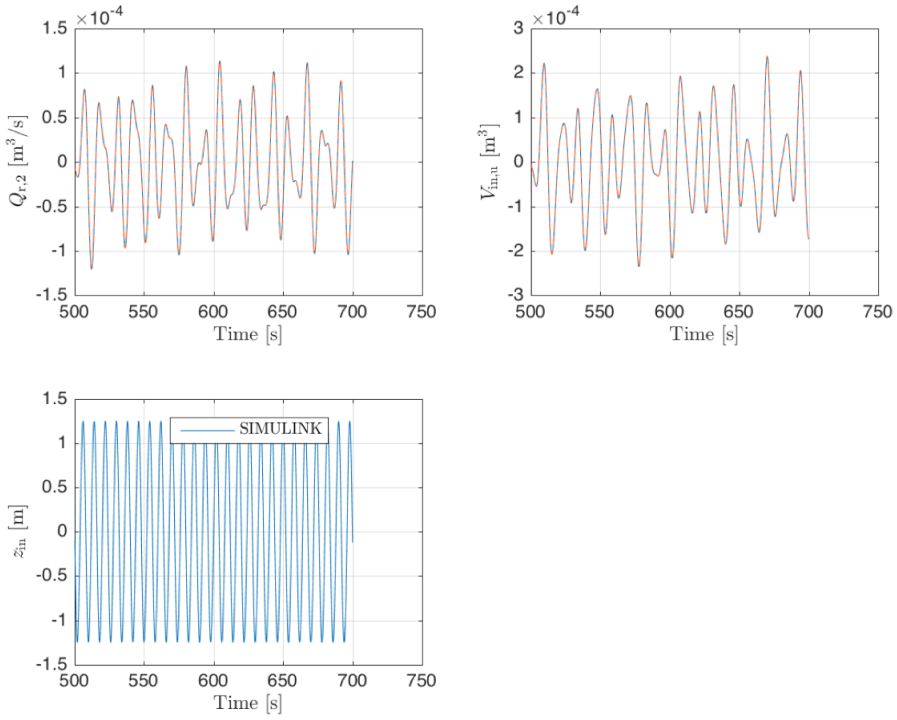

Figure A.22: $Q_{\mathrm{r},2}$, $V_{\mathrm{in,u}}$, z_{in} time series

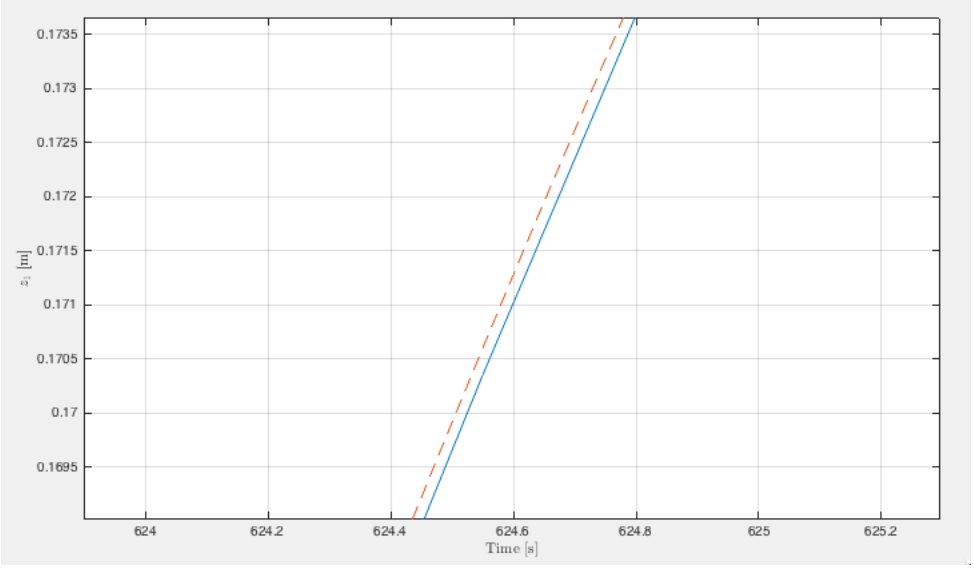

Figure A.23: z_1 time series